INFORMATION TO USERS

This manuscript has been reproduced from the microfilm master. UMI films the text directly from the original or copy submitted. Thus, some thesis and dissertation copies are in typewriter face, while others may be from any type of computer printer.

The quality of this reproduction is dependent upon the quality of the copy submitted. Broken or indistinct print, colored or poor quality illustrations and photographs, print bleedthrough, substandard margins, and improper alignment can adversely affect reproduction.

In the unlikely event that the author did not send UMI a complete manuscript and there are missing pages, these will be noted. Also, if unauthorized copyright material had to be removed, a note will indicate the deletion.

Oversize materials (e.g., maps, drawings, charts) are reproduced by sectioning the original, beginning at the upper left-hand corner and continuing from left to right in equal sections with small overlaps.

ProQuest Information and Learning
300 North Zeeb Road, Ann Arbor, MI 48106-1346 USA
800-521-0600

Université d'Ottawa • University of Ottawa

NEW CONCEPTS IN DESIGN OF OLEFIN METATHESIS CATALYSTS

By

DINO AMOROSO

Thesis submitted to the
Faculty of Graduate and Postdoctoral Studies
University of Ottawa
In partial fulfillment of the requirements for the degree of

Doctor of Philosophy

Ottawa-Carleton Chemistry Institute
University of Ottawa
Ottawa, Ontario
Canada

ABSTRACT

Treatment of compounds with general formula $RuCl_2(PP)(PPh_3)$ (PP = dppb (**3a**); binap (**3b**); dcypb (**3c**)) or $[RuCl_2(PP)]_2$ (PP = dppb (**4**); dcypb (**5**)) with $PhCHN_2$ generates alkylidene complexes of the type $RuCl_2(PP)(CHPh)$ (**2a-c**), the first such systems to exhibit high ROMP activity *without* halide or phosphine abstraction. Low polymer polydispersity is found in ring-opening metathesis polymerization (ROMP) of norbornene via these catalysts. Investigations into the role of dissociated PPh_3 show that free phosphine acts as a poison, dramatically retarding the rate of polymerization via **3** relative to catalysts derived from **4** or **5**. Chelate retention is suggested by the narrow polydispersities and increased cis olefin content of the polymers obtained, and is consistent with the detrimental effects of phosphine scavenger.

Reaction of $RuCl_2(PPh_3)_3$ with bis(dicyclohexyl)-1,4-phosphinobutane (dcypb) under N_2 gives access to PPh_3-free $RuCl(dcypb)(\mu\text{-}Cl)_3Ru(dcypb)(N_2)$ **5** in which the presence of N_2 and dative chloride bridges stabilize two equivalents of "$RuCl_2(dcypb)$". Under Ar or vacuum atmosphere, decomposition occurs via Ru-promoted dehydrogenation of the dcypb ligand, while reaction with chlorinated solvents rapidly yields paramagnetic $RuCl(dcypb)(\mu\text{-}Cl)_3RuCl(dcypb)$ **6**. However, the N_2-stabilized species **5** is easily handled under N_2 in non-chlorinated solvents, giving an ideal entry point into Ru-dcypb chemistry. The N_2 ligand within **5** is readily displaced under H_2 or CO atmosphere, yielding $RuCl(dcypb)(\mu\text{-}Cl)_3Ru(dcypb)(H_2)$ **6** or $RuCl_2(dcypb)(CO)_2$, the latter as a mixture of *ccc* (**8**) and *tcc* (**9**) isomers. Interestingly, the CO ligands can be

displaced, and the symmetrical dimer $RuCl(dcypb)(CO)(\mu\text{-}Cl)_2RuCl(dcypb)(CO)$ **10** is formed by decarbonylation of **8/9** on prolonged storage under N_2.

The incorporation of the stable silylene ligand 1,3-di-*tert*-butyl-1,3,2-diazasilol-2-ylidene (SiL^N_2) in to the ligand scaffold of a metathesis catalyst was undertaken to probe its utility as a phosphine mimic. Reaction of $[(dcypb)ClRu(\mu\text{-}Cl)_3Ru(dcypb)(N_2)]$ **(5)** with 4 equivalents of the silylene yields coordinatively unsaturated $RuCl(\eta^3\text{-}dcypb)(SiL^N_2)$ **(12)**. Complex **12** is a rare example of a trans-spanning diphosphine complex, this geometry resulting from an unprecedented attack of the metal on the tetramethylene ligand backbone. Reaction of **12** with H_2 containing trace H_2O yields siloxane dimer $[L^N_2Si(H)]_2O$ **(13)** and the ruthenium hydride $[(dcypb)(H)Ru(\mu\text{-}Cl)_2(\mu\text{-}H)Ru(dcypb)(H_2)]$ **(14)**. Displacement of silylene from **12** is facile: treatment with 1 atm of CO affords free SiL^N_2, accompanied by $RuCl(\eta^3\text{-}dcypb)(CO)_2$ as a mixture of three isomers **(16-18)**.

Decomposition pathways within "$RuCl_2(PP)(CHR)$" type systems were investigated. Reaction of $RuCl(dcypb)(\mu\text{-}Cl)_3Ru(dcypb)(N_2)$ **5** with an excess of *tert*-butylacetylene at ambient temperatures yields dinuclear monovinylidene $RuCl(dcypb)(\mu\text{-}Cl)_3Ru(dcypb)(L)$ (**19**, L = C=CHBu^t), rather than the expected, mononuclear $RuCl_2(dcypb)(L)$. Attempted synthesis of an allenylidene derivative via the corresponding reaction with 1,1-diphenyl-2-propyn-1-ol halts at the stage of hydroxyvinylidene **20a** (L = $C{=}CC(OH)Ph_2$). Heating suspensions of **20a** induces the dehydration of the hydroxyvinylidene yielding the dinuclear monoallenylidene **20b** (L = $C{=}C{=}CPh_2$) While formation of these dinuclear products may be an artifact of low solubility, the monoalkylidene analog **21** (L = $CHCH{=}CMe_2$) is obtained on treating

soluble $RuH(dcypb)(\mu\text{-}Cl)_2(\mu\text{-}H)Ru(dcypb)(H_2)$ **14** with 3-methyl-3-chloro-1-butyne. Formation of perchloro **21** implies facile homodimerization of initially-formed $RuCl_2(dcypb)(CHCH{=}CMe_2)$, with expulsion of one alkylidene ligand. The organic coupling product, 1,1,6,6-tetramethyl-1,3,5-hexatriene, is observed by ^1H NMR. A minor product in this synthesis is proposed to be $RuCl(dcypb)(\mu\text{-}Cl)_2(\mu_2,\eta^1\text{–}CHCH{=}CMe_2)RuCl(dcypb)$ **22**. The low activity of **19** and **20** in ring-opening metathesis polymerization of norbornene is attributable to their low solubility, but that of **21/22** points toward the stability of the face-bridged dimeric structure. The low activity and facile formation of **21/22** reveals an important decomposition pathway for mononuclear alkylidene species of type **2**, with potential relevance to related chlororuthenium systems of type $RuCl_2(PR_3)_2(CHR')$ **1**, including Grubbs' catalyst.

Reaction of $RuCl_2(PPh_3)_3$ with dicyclohexylphosphinoxylene (dcpx) in the presence of base (NEt_3) affords the pincer complex $RuCl(dcpx)PPh_3{\bullet}PPh_3$ **24**$\bullet PPh_3$. As a result of the steric crowding at ruthenium, **24**$\bullet PPh_3$ does not react with $PhCHN_2$, *tert*-butylacetylene or 1,1-diphenyl-2-propyn-1-ol. Bound PPh_3 could be displaced by CO, however, yielding the bis-CO adduct $RuCl(dcpx)(CO)_2$ **25**. Reaction of **24**$\bullet PPh_3$ with one equivalent of KHB^sBu_3 gives hydride pincer $RuH(dcpx)PPh_3(N_2)$ (**26a/b**) as a mixture of isomers. Exposure of **26a/b** to 1 atm of H_2 affords the analogous, isomeric dihydrogen adducts $RuH(dcpx)PPh_3(H_2)$ (**27a/b**). Unexpectedly, reaction of **26a/b** with 3-chloro-3-methyl-1-butyne regenerates $RuCl(dcpx)(PPh_3)$ (**24**), with coproduction of 3-methyl-buta-1,2-diene. Treatment of $RuCl_2(PPh_3)_2(CHCHC(CH_3)_2)$ with an equivalent of dcpx affords η^2-pincer complex $RuCl_2(dcpx')(CHCHC(CH_3)_2)$ **28**. Complex **28** displays modest activity in the ROMP of norbornene until activated by abstraction of a chloride

ligand cis to alkylidene, on which exceptional activity is observed. Complexes 24•PPh_3 and 26a/b are found to be highly active in the transfer hydrogenation of benzophenone.

TABLE OF CONTENTS

TABLE OF COMPOUND NUMBERS

Number	Compound
1	$RuCl_2(PR_3)_2(CHR')$
1a	R = Cy
1b	R = Ph
2	$RuCl_2(PP)(CHR)$
2a	PP = dppb; R = Ph
2b	PP = binap; R = Ph
2c	PP = dcypb; R = Ph
2d	PP = dtbpm; R = $CHCHC(CH_3)_2$
2e	PP = dcypb; R = $CHCHC(CH_3)_2$
3	$RuCl_2(PP)(PPh_3)$
3a	PP = dppb
3b	PP = binap
3c	PP = dcypb
4	$[RuCl(dppb)]_2(\mu\text{-}Cl)_2(\mu\text{-}H_2O)$
5	$RuCl(dcypb)(\mu\text{-}Cl)_3Ru(dcypb)(N_2)$
6	$RuCl(dcypb)(\mu\text{-}Cl)_3RuCl(dcypb)$
7	$RuCl(dcypb)(\mu\text{-}Cl)_3Ru(dcypb)(H_2)$
8	*ccc*-$RuCl_2(dcypb)(CO)_2$
9	*tcc*-$RuCl_2(dcypb)(CO)_2$
10	$RuCl(dcypb)(CO)(\mu\text{-}Cl)_2RuCl(dcypb)(CO)$
11	$RuCl(dcypb)(\mu\text{-}Cl)_3Ru(dcypb)(CO)$
12	$RuCl(\eta^3\text{-}dcypb)(SiL^N{}_2)$
13	$[L^N{}_2Si(H)]_2O$
14	$[Ru(H)(dcypb)(\mu\text{-}Cl)_2(\mu\text{-}H)Ru(dcypb)(H_2)]$
15	$[Ru(H)(dcypb)(\mu\text{-}Cl)_3Ru(dcypb)(N_2)]$
16	$RuCl(\eta^3\text{-}dcypb)(CO)_2$*

17	$RuCl(\eta^3\text{-dcypb})(CO)_2$*
18	$RuCl(\eta^3\text{-dcypb})(CO)_2$*
19	$RuCl(dcypb)(\mu\text{-}Cl)_3Ru(dcypb)[C{=}CH(Bu^t)]$
20a	$RuCl(dcypb)(\mu\text{-}Cl)_3Ru(dcypb)[C{=}CHC(OH)Ph_2]$
20b	$RuCl(dcypb)(\mu\text{-}Cl)_3Ru(dcypb)[C{=}C{=}CPh_2]$
21	$RuCl(dcypb)(\mu\text{-}Cl)_3Ru(dcypb)[CHCHC(CH_3)_2]$
22	$RuCl(dcypb)(\mu\text{-}Cl)_2(\mu\text{-}CHCHC(CH_3)_2)RuCl(dcypb)$
23	**21/22 + halogenated solvent**
24	$RuCl(dcpx)PPh_3{\cdot}PPh_3$
25	$RuCl(dcpx)(CO)_2$
26a	$RuH(dcpx)PPh_3(N_2)$**
26b	$RuH(dcpx)PPh_3(N_2)$**
27a	$RuH(dcpx)PPh_3(H_2)$**
27b	$RuH(dcpx)PPh_3(H_2)$**
28	$RuCl_2(dcpx')(CHCHC(CH_3)_2)$
29	$RuCl(dtbpx)(C(CH_3)C_3H_7)]$
i	1,1-Diphenyl-2-Diazomethyl-Ethene
ii	1-Naphthyldiazomethane
iii	2-Naphthyldiazomethane
iv	Trimethylsilyldiazomethane

*one of three isomers; ** one of two isomers

LIST OF TABLES

LIST OF FIGURES

LIST OF ABBREVIATIONS

Å	angstrom
atm	atmosphere (1 atm = 760 mmHg, 101.3 kPa, 1.01 bar)
binap	rac 2,2'-bis(diphenylphosphino)-1,1'-binaphthyl
br	broad
c-	cis
$^{13}C\{^{1}H\}$	proton-decoupled carbon-13 (nmr)
chiraphos	2,3-bis(diphenylphosphino)butane
Cp*	pentamethylcyclopentadienyl, η^5-$C_5(CH_3)_5$
CP/MAS	Cross Polarization Magic Angle Spinning
d	doublet
dcpx	$[2,6\text{-}(Cy_2PCH_2)C_6H_3]^-$
dcpx'	$[1,3\text{-}(Cy_2PCH_2)C_6H_4]$
dcypb	1,4-bis(dicyclohexylphosphino)butane
DEPT	Distortionless Enhancement by Polarization Transfer
dppx	$[2,6\text{-}(Ph_2PCH_2)C_6H_3]^-$
dtbpm	bis(di-*tert*-butylphosphino)methane, $^tBu_2PCH_2P^tBu_2$
dtbpe	bis(di-*tert*-butylphosphino)ethane, $^tBu_2PCH_2CH_2P^tBu_2$
dmso	dimethylsulfoxide
dppb	1,4-bis(diphenylphosphino)butane
dppe	1,2-bis(diphenylphosphino)ethane
eV	electron Volts (1 eV = 27.2 hartree)

EXSY	Exchange Spectroscopy
GPC	Gel Permeation Chromatography
HMBC	Heteronuclear Multiple Bond Coherence
HMQC	Heteronuclear Multiple Quantum Coherence
HOMO	Highest Occupied Molecular Orbital
Hz	Hertz, cycles per second
INEPT	Insensitive Nuclei Enhancement by Polarization Transfer
IR	Infrared
J	coupling constant, in Hz
L	ligand
LUMO	Lowest Unoccupied Molecular Orbital
M	central metal atom in a complex
m	multiplet (nmr)
m	meta
NMR	Nuclear Magnetic Resonance
nbe	norbornene
nbd	norbornadiene
o	ortho
ORTEP	Oak Ridge Thermal Ellipsoid Projection
$^{31}P\{^{1}H\}$	proton-decoupled phophorus-31 (nmr)
PP	ditertiary phosphine
q	quartet (nmr)
RT	room temperature

s	singlet (nmr)
$^{29}Si\{^{1}H\}$	proton-decoupled silicon-29 (nmr)
SiL^{N}_{2}	1,3-di-*tert*-butyl-1,3,2-diazasilol-2-ylidene
t	triplet (nmr)
tert-, ^{t}	tertiary
t	trans
T_1	longitudinal relaxation time
TMS-OTf	trimethylsilyl trifluoromethanesulfonate
XRD	X-Ray Diffraction
δ	chemical shift (in ppm)
ν	frequency (in cm^{-1})
η	descriptor for hapticity
μ	descriptor for bridging

ACKNOWLEDGEMENTS

I must first thank my supervisor, Prof. Deryn Fogg for her unrelenting enthusiasm and uncanny ability to motivate. I am very much indebted to the members of this research group, past and present, for their camaraderie and more importantly their tolerance. I would particularly like to thank Samantha Drouin, Jennifer Snelgrove and Fojan Zamanian whose friendship has been invaluable. The cooperation of Prof. Robert West (University of Wisconsin, Madison), Prof. Michael Haaf (Elizabethtown College, PA), Prof. Dmitry Gusev (Wilfrid Laurier University) and Prof. Douglas Stephan (University of Windsor) in various collaborations is acknowledged with thanks.

Dr. Glenn Facey of the NMR Laboratory is thanked for his assistance and genuine interest. The assistance of Dr. Glenn Yap of the X-ray Laboratory with the crystallographic analyses is acknowledged. The support of the various members of the chemistry department is also acknowledged. The many useful discussions with Prof. Sandro Gambarotta and Prof. Alain St. Amant are very much appreciated.

I would also like to thank Bradley Barnes, Jason McAdoo, Jay Conrad, Nick "Papagiorgio", Omar Bouh, Pat Bazinet, Rachel Mainville-Dale, Steve Foley, and Yuwen Liu whose friendship made time pass quickly. I must also thank my family (including extended members) for their endless support and encouragement, especially the local support of my sister, Teresa. Most importantly, I must thank Rachel whose patience and devotion made all of this possible.

CONTRIBUTIONS TO RESEARCH

D. Amoroso and D. E. Fogg, "Ring-Opening Metathesis Polymerization via Ruthenium Complexes of Chelating Diphosphines", *Macromolecules*, 2000, 33, 2815.

D. Amoroso, G. P. A. Yap and D. E. Fogg, "The Life, Death, and ROMP Activity of Ruthenium Complexes Containing the Basic Chelating Diphosphine Bis(dicyclohexyl)-1,4-phosphinobutane", *Can. J. Chem.* (special issue in honour of Brian James), 2001, 79, 958.

D. Amoroso, M. Haaf, G.P.A. Yap, R. West, D. E. Fogg, "A Stable Silylene in a Reactive Environment: Synthesis, Reactivity, and Silicon Extrusion Chemistry of a Coordinatively Unsaturated Ruthenium Silylene Complex Containing Chloride and η^3-P-C-P Ligands" *Organometallics*, 2002, 21, 534.

S. D. Drouin, D. Amoroso, G. P. A. Yap and D. E. Fogg, "Multifunctional Ruthenium Catalysts: A Novel Polyhydride Complex Containing the Basic, Chelating Diphosphine Bis(dicyclohexyl)-1,4-phosphinobutane, and Its Application to Hydrogenation and Murai Catalysis" *Organometallics*, 2002, 21, 1042.

D. Amoroso, G. P. A. Yap and D. E. Fogg, "Deactivation of Chlororuthenium Metathesis Catalysts: Facile Formation of Face-Bridged Dimers" *Organometallics*, in press.

D. E. Fogg*, D. Amoroso, S. D. Drouin, J. L. Snelgrove, J. C. Conrad, F. Zamanian, "Ligand Manipulation and Design for Ruthenium Metathesis and Tandem Metathesis-Hydrogenation Catalysis" *J. Mol. Catal.*, accepted.

D. Amoroso, J. L. Snelgrove, Jay Conrad, Glenn P. A. Yap, and Deryn E. Fogg, "Versatile, Efficient Routes to Metathesis Catalysts Based On Phenoxide as a Hydride Equivalent", *Advanced Synthesis & Catalysis*, accepted.

D. Amoroso, D. Gusev, G. P. A. Yap, D. E. Fogg, "A New Class of Metathesis-Active Ru Alkylidene Complexes Containing Pincer Ligands" *Organometallics*, in preparation.

D. Amoroso, J. Conrad, J. Snelgrove, G.P.A. Yap, D. E. Fogg*, "A Four-Coordinate Ruthenium Complex Containing a σ-Phenoxide Ligand: What Determines s- vs p-Coordination?", *JACS*, in preparation.

S. D. Drouin, D. Amoroso, Glenn P. A. Yap, and Deryn E. Fogg, "Dinuclear Hydridochlorocarbonyl Ruthenium Complexes Containing a Bulky Diphosphine Ligand: Formation and Equilibration of Edge-Sharing and Face-Sharing Bioctahedra." *Organometallics*, in preparation.

CHAPTER 1

Introduction

1.1. The Olefin Metathesis Reaction

Olefin metathesis, though simple in concept, has emerged as a powerful and versatile route to both organic and polymeric materials.[1,2] The process can be very generally described as the interchange of carbon atoms between a pair of double bonds (see Figure 1.1, reaction A). The versatility of the process is evident upon consideration of the many possible variations in the nature of the olefin substrate.

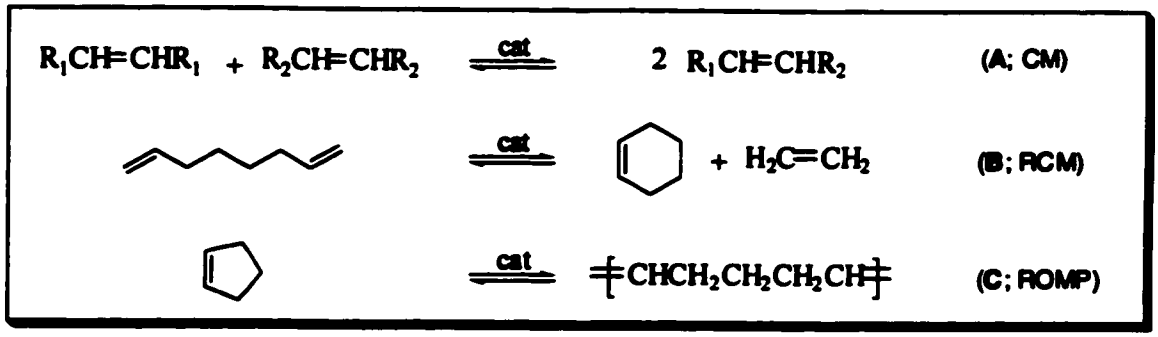

Figure 1.1. Overview of olefin metathesis reactions.

The three general classes of olefin metathesis reactions are represented in Figure 1.1. Reaction A represents cross-metathesis (CM), or exchange across the double bond of two different olefins. This process effectively "scrambles" the substituents of the parent

olefins. In the case where each parent olefin bears two different substituents (i.e. heterodisubstituted olefins), a statistical distribution of all possible combinations is normally obtained.

Ring-closing metathesis (RCM; reaction **B**) is perhaps the most widely used metathesis reaction by synthetic organic chemists.[1] In this reaction, formation of a cyclic olefin is achieved with concomitant elimination of ethylene. RCM has been used to prepare complex ring structures bearing a range of functional groups and heteroatoms.[2] While the reaction shown represents intramolecular metathesis, an intermolecular variant can also occur, referred to as acyclic diene metathesis (ADMET; Figure 1.2). ADMET reactions are related to RCM in that the reaction is accompanied by extrusion of ethylene, however ADMET yields a polymeric, rather than a cyclic, product.

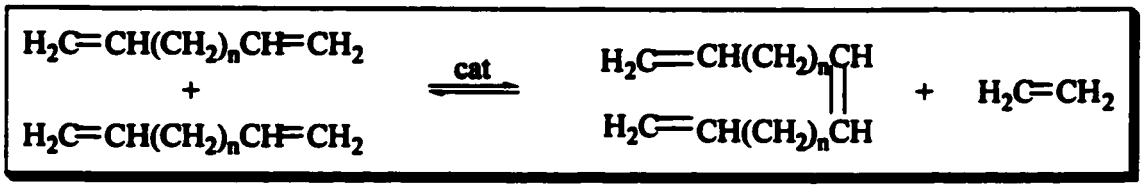

Figure 1.2. Acyclic diene metathesis (ADMET).

The third class of olefin metathesis reaction, ring-opening metathesis polymerization (ROMP), is represented by reaction **C** in Figure 1.1. In this reaction, a cycloolefin is effectively "opened" across the double bond, and these olefinic sites are linked to a growing chain of similarly ring-opened olefins. The equilibrium can be driven in favor of the products via judicious choice of substrate. Particularly common is the use of highly strained cyclic monomers, for which the reaction is driven by relief of ring

strain, and the polymerization is essentially irreversible. It is for this reason that bicyclic monomers such as norbornene (nbe), norbornadiene (nbd) and their derivatives dominate the ROMP literature. (The relative ease of synthesis of such monomers via Diels-Alder reactions also makes them attractive as substrates.) In other, more reversible, metathesis reactions, the equilibrium can be manipulated by appropriate choice of reaction conditions (i.e. substrate concentration, pressure etc.).

The catalysts employed to induce metathesis reactions are normally transition metal complexes. Many such complexes effect metathesis in the absence of additives, although in some instances cocatalysts (e.g. $EtAlCl_2$, TMS-OTf) and/or promoters (eg. O_2, $h\nu$) are required.[2] Irrespective of the process or the nature of the catalyst, the mechanism of olefin metathesis is always the same: transition-metal alkylidene complexes initiate and propagate the reaction. The involvement of these key intermediates was first postulated by Herisson and Chauvin in 1971.[3] Since then, ample evidence has been presented to support their proposed mechanism (Figure 1.3).[2] This involves 2+2 addition of a metal alkylidene to an olefin to form a metallacyclobutane intermediate, which can then undergo retro-addition. Productive metathesis yields a new (propagating) alkylidene. Non-productive or degenerate metathesis can also occur, regenerating the parent alkylidene and olefin.

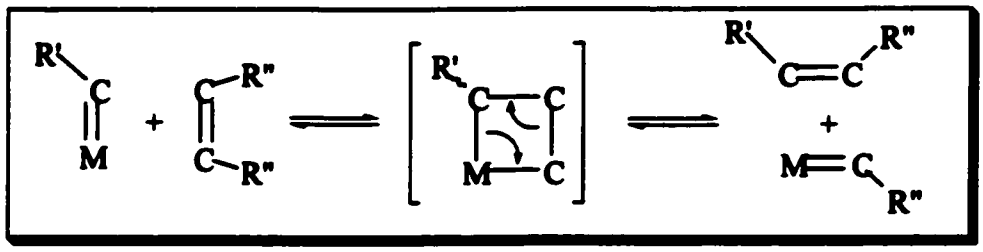

Figure 1.3. Mechanism of olefin metathesis.

Always of concern in metathesis reactions is the rate at which the catalyst attacks the olefinic bonds in the targeted products. This is especially true in ROMP reactions, in which attack of the catalyst on the polymer chain results in formation of cyclic oligomers. This process (termed "backbiting") can occur concurrently with ROMP, or after polymerization is complete. Backbiting increases the molecular weight distribution of the polymer, giving rise to polydisperse materials, and thus undermining precise specification of polymer properties. Such processes are common for catalyst systems containing sterically unregulated active sites, which can exhibit high activity, but typically at the cost of discrimination between monomer and polymer olefinic sites. Structurally well-defined transition-metal alkylidene complexes, in contrast, offer routes to polymer materials with precisely specified molecular weights and polydispersities. Living polymerization is also attainable, as well as (in Mo catalysis) control over polymer stereochemistry or tacticity.

1.2. Stereochemistry in ROMP

Stereochemical control in ROMP of simple, unsubstituted olefins (Figure 1.1 C) is expressed in its simplest form as specification of the cis/trans geometry of the olefinic units in the polymer backbone. More complex stereochemical consequences arise from the relative orientation of the chiral centers. For polynorbornene or its symmetrically substituted derivatives, tacticity is defined by the sequence of configurations of the *pairs* of methine carbon atoms on adjacent C_5 rings. Analysis of the tacticity of such polymers thus requires consideration of at least two consecutive repeat units, or dyads (Figure 1.4), though higher sequences are also readily treated. Thus, -RS-RS-RS- represents an isotactic sequence, while -RS-SR-RS- represents a syndiotactic sequence. *Meso* (*m*) dyads are related by a symmetry element that bisects the C=C bond between two C_5 rings. This may be a mirror plane (cis linkages), or an inversion center (trans linkages); in either case the dyad is isotactic. In *racemic* (*r*) dyads, a C_2 axis relates the both cis and trans linkages, which are thus syndiotactic.

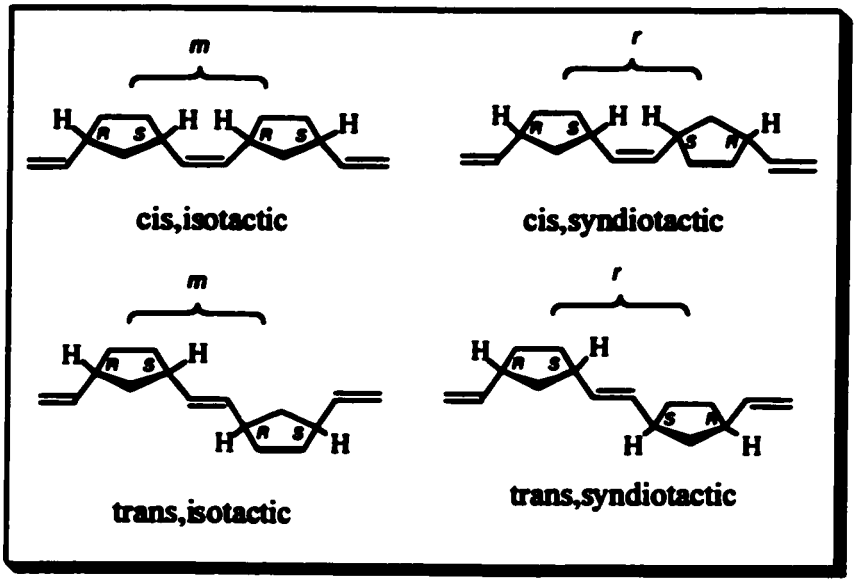

Figure 1.4. The four stereoregular structures for polynorbornene.

Identical structural possibilities obtain for polymers of 5,6-symmetrically disubstituted norbornenes. For the unsymmetrically disubstituted derivatives (Figure 1.5; $R_1 \neq R_2$), further possibilities are presented at the dyad level as head-to-head, head-to-tail or tail-to-tail structures. Finally, the possibility of *syn* or *anti* isomerism may also exist (that is, the relative orientation of the substituents R_1 and R_2 may vary).

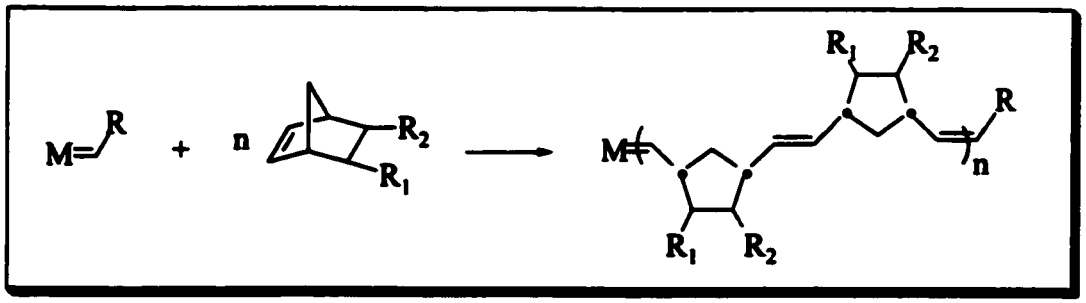

Figure 1.5. ROMP of 5,6-disubstituted norbornenes. (• denotes a chiral center.)

Production of all-cis syndiotactic and all-trans isotactic polymers is believed to proceed via "enantiomorphic site control", involving interaction of a chiral metal complex with substrate.[2] Rigorously-designed catalysts capable of exerting rigorous control over the stereochemical features summarized above thus afford a key means of specifying polymer microstructure, and hence polymer properties. (It should be noted, however, that the utility of catalyst design is limited if a chain-end control mechanism prevails, in which case the chirality of the adjacent repeat unit(s) controls the stereochemistry of propagation.)

1.3. Current State of Ruthenium-Catalyzed Olefin Metathesis

Though many transition-metal complexes catalyze olefin metathesis, few hold as much promise as those of ruthenium. The functional-group tolerance of the late transition metals, as well as their greater stability toward oxygen and moisture, makes these systems highly attractive. The ability to perform metathesis on functionalized substrates which normally poison the more Lewis acidic early metal catalyst systems (e.g. Mo or W) renders accessible a range of organic and polymeric materials previously unattainable. Furthermore, the robustness of the late metals lifts the requirement for rigorously anhydrous and anaerobic conditions a prerequisite found for early-metal systems. In fact, ruthenium catalyzed olefin metathesis has been reported in alcoholic and aqueous media (although at the expense of catalyst lifetime and polymer polydispersity).[4,5]

The catalytic versatility of ruthenium makes Ru-based systems highly desirable from the perspective of tandem catalyses. Such processes, coupling metathesis with

hydrogenation or other catalytic manifolds, are attractive for their power and efficiency. Complexes of ruthenium have found utility in processes including hydrogenation and oxidation (i.e. epoxidation, aziridination and dehalogenation), nucleophilic addition to carbon-carbon and carbon-heteroatom bonds, Kharasch addition, atom-transfer radical polymerization, cyclopropanation and all types of metathesis reactions.[6]

Despite the potential of ruthenium systems in olefin metathesis, the development of well-defined ruthenium alkylidene complexes has only recently been undertaken. Initially studies focused on structurally ill-defined catalysts derived from simple precursors such as $RuCl_3$•hydrate[4,5,7] or $Ru(H_2O)_6(tos)_2$ (tos = *p*-toluenesulfonate).[8,9] It was not until Grubbs' isolation of the first ruthenium alkylidene complex $RuCl_2(PPh_3)_2(CHCHCPh_2)$[10] in 1992, via reaction of $RuCl_2(PPh_3)_3$ with diphenylcyclopropene, that a better understanding of the nature of ruthenium catalysts was formed. This compound was found to initiate polymerization rapidly, and to polymerize norbornene in a living manner.[11] Subsequent increases in the bulk and basicity of the phosphine ligands resulted in dramatic increases in activity; for example, $RuCl_2(PCy_3)_2(CHCHCPh_2)$ was found to be active for ROMP of low-strain cyclic monomers as well as acyclic olefins.[12]

The difficulty of preparing diphenylcyclopropene led to development of an alternate route to installation of the alkylidene. Reaction of $RuCl_2(PPh_3)_3$ with diazoalkanes ($R'CHN_2$) affords products of general formula $RuCl_2(PR_3)_2(CHR')$ (R = Cy , **1a**; R = Ph, **1b**).[13,14] Related alkylidenes were proposed as the metathesis-active species generated on addition of diazoalkanes to $[RuCl_2(p\text{-cymene})]_2$.[15] Systems of type **1** (particularly benzylidene derivative **1a**, R' = Ph) proved highly active in ROMP, yielding

polymers with very narrow polydispersities.[14] Detailed mechanistic investigations which demonstrated that metathesis via these catalyst systems proceeds primarily by dissociation of one phosphine ligand. (An associative mechanism is also operative, however its contribution was found to be insignificant to the overall activity.)[16] A further, significant expansion in synthetic capabilities emerged from the development of Ru hydride complexes as precursors to alkylidene complexes, via reaction with propargyl chlorides.[17]

The catalyst systems described above, though well-understood and highly active, do not offer any stereochemical control over the products of the metathesis reaction. This limitation contrasts sharply with the exceptional stereochemical control attainable in metathesis via early-metal systems. Given the key importance of stereoselective ROMP in determining polymer properties, as well as the enormous potential of asymmetric RCM via robust, functional-group tolerant catalysts, it is startling that the general design of ruthenium metathesis catalysts has not been broadened to incorporate stereochemical control.

The few modifications reported (Figure 1. 6) have done little to increase the scope of the reaction. Incorporation of Schiff bases[18] (A) or tris(pyrazolylborate)[19] (B) into the ligand set resulted in decreased metathesis activity, attributed to hindered ligand dissociation. Heterobimetallic[20] (C) and pyridine-coordinated[21] (D) catalyst systems were characterized by high activity (due to the increased lability of the hetero-metal and pyridine respectively) but decreased stability. Complex **E** is noteworthy for its coordinative unsaturation, and the incorporation of alkoxides (instead of halogen) as anionic ligands. The resulting deviation from the square pyramidal geometry ubiquitous

in the five-coordinate Ru systems (vide infra) had little effect, with only moderate activity being attained even at elevated temperatures.[22]

The chelate complexes F,[23] G,[24] and H,[24] catalyze ROMP of norbornene with generally modest activity, for reasons we discuss in detail in Chapter 4. In the case of F, the polymer products exhibit polymodal molecular weight distributions, consistent with the presence of several active species.

Systems of type 2 (of which several variants have been reported[25-31]; see Chapter 4) represent a more significant step toward improved selectivity without a serious decline in activity. In these systems, we consider that the incorporation of chelating ligands serves to prevent dissociation, augmenting steric definition at the metal center during metathesis. This is a logical step toward incorporating stereoselectivity into ruthenium catalyst systems. Alkylidenes of type 2 (i.e. $RuCl_2(PP)(CHR)$) which incorporate chelating diphosphines with one-[27-29], two-[30,31] and four-methylene[25,26] bridges have been reported. Those based on both one- and two-carbon bridged diphosphines do not catalyze metathesis unless a halogen scavenger is added. Such rigid systems offer only a modest gain in definition of the active site relative to systems of type 1. In systems of four-carbon bridged diphosphines (reported in this thesis) no ligand dissociation/abstraction is required for high activity (Chapter 4). "Proof of principle" is provided by the increased steric definition using $RuCl_2$(binap)(CHR) (**2b**), which yields higher cis-olefin content relative to all other Ru systems described above.

The most recent addition to the family of ruthenium metathesis catalysts incorporates stable, N-heterocyclic carbenes.[32] The catalyst systems reported are essentially identical to those of type 1, except that one[33-35] or both[36,37] of the phosphine

ligands are replaced by carbene ligands. The former systems, in particular, are remarkably active. However as with other catalyst systems of type 1, there is no stereochemical control over the reaction products.

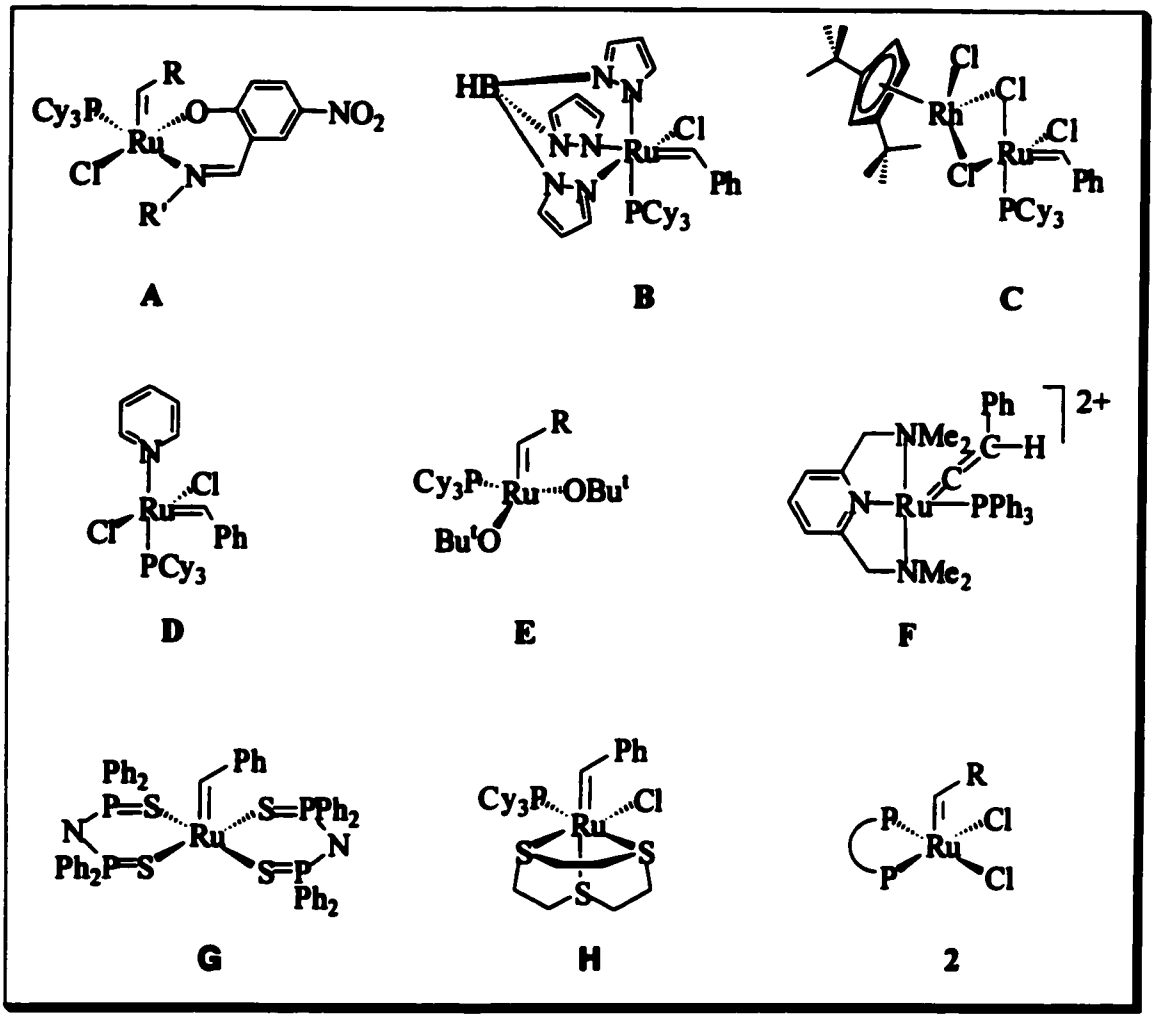

Figure 1. 6. Overview of ligand sets employed in Ru metathesis catalysts.

1.4. Approach

The goal of this research is to gain insight into the design features required for

development of stereoselective Ru metathesis catalysts. While catalyst activity and stereoselectivity is readily screened by either ROMP or RCM, ROMP was preferred as a means of simultaneously assessing catalyst lifetime and homogeneity, about which RCM is much less informative. Thus, polymer polydispersities provide valuable insight into catalyst homogeneity, while catalyst stability can be judged from molecular weight data and the "livingness" of polymerization.

The inability of catalysts of type 1 to effect stereochemically controlled metathesis is unsurprising, given the limited definition of the active site (cf. the catalyst precursor). The requirement for phosphine dissociation (Figure 1.7) means that propagation occurs at a four-coordinate, presumably fluxional, active site. Thus, a system in which ligand dissociation is not required seemed an obvious starting point for development of stereoselective catalyst systems. Our studies focused on preparation of novel Ru alkylidenes, containing sterically demanding ligand scaffolds that are retained during metathesis.

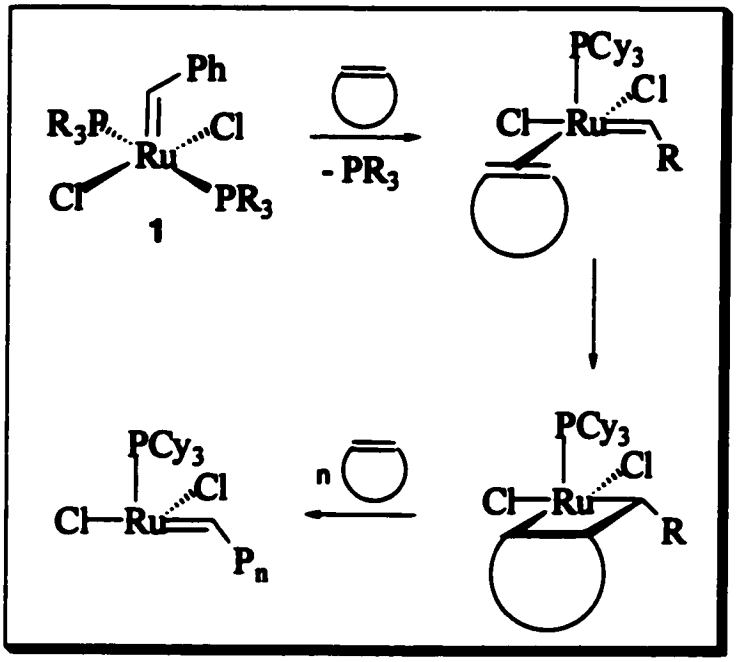

Figure 1. 7. Olefin metathesis via $RuCl_2(PR_3)_2(CHPh)$ 1.

The potential for systems containing chelating diphosphines becomes apparent upon consideration of the mechanism outlined in Figure 1.8. Metathesis via a sterically defined, five-coordinate species (hence a six-coordinate transition state) is expected to offer significantly improved control over product stereochemistry. The potential versatility of this approach is underscored by the large pool of readily accessible chelating diphosphines, and their track record in asymmetric catalysis.

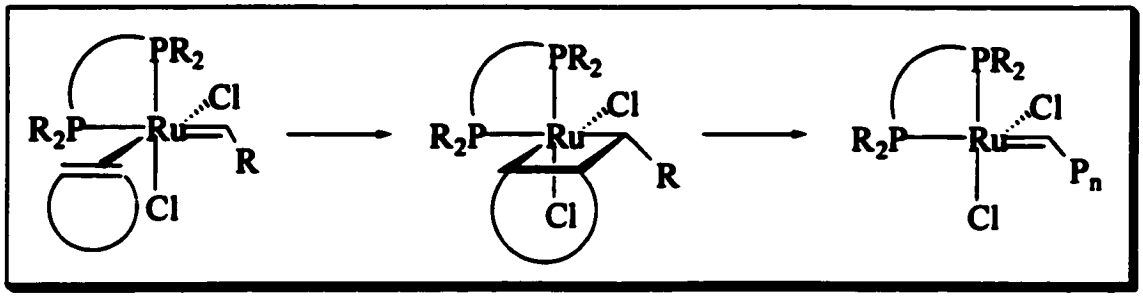

Figure 1. 8. Olefin metathesis via $RuCl_2(PP)(CHPh)$.

Also relevant to the proposed design is the use of alternative, non-halide anionic ligands. Modification of the anionic sites was deferred until the steric congestion of the active site could be evaluated from the catalyst activity and selectivity data. We considered, however, that while systems of type **2** provide an excellent point of origin for our studies, incorporation of sterically tunable pseudohalides into the ligand scaffolds might ultimately be required.

1.5. Scope of this Thesis

This thesis describes the synthesis of a series of ruthenium alkylidene complexes containing chelating diphosphines, and their application to the ring-opening metathesis polymerization of norbornene. Detailed experimental procedures are outlined in Chapter 2. Chapter 3 describes the chemistry of the dinuclear ruthenium complex RuCl(dcypb)(μ-Cl)$_3$Ru(dcypb)(N_2) (**5**), and its utility as a precursor to highly active, alkyldiphosphine catalysts. Chapter 4 describes the in situ synthesis and ROMP activity of $RuCl_2$(PP)(CHPh) (**2a-c**; **a**, PP = dppb; **b**, PP = binap; **c**, PP = dcypb), and the limitations associated with this methodology. The potential of a stable silylene, 1,3-di-*tert*-butyl-1,3,2-diazasilol-2-ylidene (SiL^N_2), as a phosphine mimic is described in Chapter 5. Chapter 6 identifies a key deactivation pathway for catalysts of type **2**, describing the facile formation and low catalytic activity of face-bridged RuCl(dcypb)(μ-Cl)$_3$Ru(dcypb)[CHCHC(CH_3)$_2$] (**21**). Detailed in Chapter 7 is the preparation of ruthenium complexes based on the pincer ligand dicyclohexylphosphinoxylene (dcpx)

and their application to olefin methathesis and transfer hydrogenation. General conclusions and recommendations for future work are given in Chapter 8.

1.6. References

1) Recent reviews: (a) Trnka, T. M.; Grubbs, R. H. *Acc. Chem. Res.* **2001**, 34, 18. (b) Jørgensen, M.; Hadwiger, P.; Madsen, R.; Stütz, A. E.; Wrodnigg, T. M. *Curr. Org. Chem.* **2000**, 4, 565. (c) Roy, R.; Das, S. K. *J. Chem. Soc., Chem. Commun.* **2000**, 519. (d) Buchmeiser, M. R. *Chem. Rev.* **2000**, 100, 1565. (e) Fürstner, A. *Angew. Chem. Int. Ed. Engl.* **2000**, 39, 3012. (f) Wright, D. *Org. Chem.* **1999**, 3, 211. (g) Randall, M. L.; Snapper, M. L. *J. Mol. Catal.* **1998**, 133, 29. (h) Ivin, K. J. *J. Mol. Catal.* **1998**, 133, 1. (i) Armstrong, S. K. *Perkin Trans. 1* **1998**, 371. (j) Grubbs, R. H.; Chang, S. *Tetrahedron* **1998**, 54, 4413. (k) Schuster, M.; Blechert, S. *Angew. Chem., Int. Ed. Engl.* **1997**, 36, 2036.

2) Ivin, K. J.; Mol, J. C. *Olefin Metathesis and Metathesis Polymerization*; Academic Press: New York, 1997.

3) Herisson, J.-L.; Chauvin, Y. *Makromol. Chem.* **1971**, *141*, 161.

4) Michelotti, F. W.; Keaveney, W. P. *J. Polym. Sci* **1965**, *A3*, 895.

5) Rinehart, R. E.; Smith, H. P. *Polym. Lett.* **1965**, *3*, 1049.

6) Recent reviews: (a) General Ru-catalysis: Naota, T.; Takaya, H.; Murahashi, S.-I. *Chem. Rev.* **1998**, *98*, 2599; (b) C-C bond activation: Mitsudo, T.-A.; Kondo, T. *Synlett.* **2001**, 309; (c) Kharasch and atom transfer radical polymerization: Simal, F.; Demonceau, A.; Noels, A. F. *Recent Res. Dev. Org. Chem.* **1999**, *3 (Pt. 2)*, 455; (d) Biomimetic oxidations: Murahashi, S.-I.; Naruyoshi., K. In *Biomimetic Oxidations Catalyzed by Transition Metal Complexes*; Meunier, B., Ed.; Imperial College Press: London, 2000, p. 563; (e) Lewis Acid and Base Catalysis: Murahashi, S. I.; Takaya, H.

Acc. Chem. Res. **2000**, *33*, 225; (f) Olefin cyclopropanation and metathesis: Noels, A. F.; Demonceau, A.; Jan, D. *Russ. Chem. Bull.* **1999**, *48*, 1206; (g) Oxidation of alcohols: Friedrich, H. B. *Platinum Met. Rev.* **1999**, *43*, 94. (h) Epoxidation and aziridination of alkenes: Che, C.-M.; Yu, W.-Y. *Pure Appl. Chem.* **1999**, *71*, 281; (i) Oxidative dehalogenation of organics: Bressan, M.; d'Alessandro; Liberatore, L.; Morvillo, A. *Coord. Chem. Rev.* **1999**, *185-186*, 385; (j) Murai coupling: Murai, S.; Kakiuchi, F.; Sekine, S.; Tanaka, Y.; Kamatani, A.; Sonoda, M.; Chatani, N. *Nature* **1993**, *366*, 529; (k) Asymmetric reduction of ketones: Noyori, R.; Ohkuma, T. *Angew. Chem. Int. Ed. Engl.* **2001**, *40*, 40. (l) Copolymerization of aromatic ketones and 1,3-divinyltetramethyldisiloxane: Weber, W. P.; Guo, H.; Kepler, C. L.; Londergan, T. M.; Lu, P.; Paulsaari, J.; Sargent, J. R.; Tapsak, M. A.; Wang, G. *ACS Symp. Ser.* **2000**, *729*, 433. (m) C-C bond formation: Trost, B. M.; Toste, D.; Pinkerton, A. B. *Chem. Rev.* **2001**, *101*, 2067.

7) Novak, B. M.; Grubbs, R. H. *J. Am. Chem. Soc.* **1988**, *110*, 960.

8) Novak, B. M.; Grubbs, R. H. *J. Am. Chem. Soc.* **1988**, *110*, 7542.

9) Hillmyer, M. A.; Lepetit, C.; McGrath, D. V.; Novak, B. M.; Grubbs, R. H. *Macromolecules* **1992**, *25*, 3345.

10) Nguyen, S. T.; Johnson, L. K.; Grubbs, R. H.; Ziller, J. W. *J. Am. Chem. Soc.* **1992**, *114*, 3974.

11) Wu, Z.; Benedicto, A. D.; Grubbs, R. H. *Macromolecules* **1993**, *26*, 4975.

12) Nguyen, S. T.; Johnson, L. K.; Grubbs, R. H.; Ziller, J. W. *J. Am. Chem. Soc.* **1993**, *115*, 9858.

13) Schwab, P.; France, M. B.; Ziller, J. W.; Grubbs, R. H. *Angew. Chem. Int. Ed. Engl.* **1995**, *34*, 2039.

14) Schwab, P.; Grubbs, R. H.; Ziller, J. W. *J. Am. Chem. Soc.* **1996**, *118*, 100.

15) Stumpf, A. W.; Saive, E.; Demonceau, A.; Noels, A. F. *J. Chem. Soc., Chem. Commun.* **1995**, 1127.

16) Dias, E. L.; Nguyen, S. T.; Grubbs, R. H. *J. Am. Chem. Soc.* **1997**, *119*, 3887.

17) Wilhelm, T. E.; Belderrain, T. R.; Brown, S. N.; Grubbs, R. H. *Organometallics* **1997**, *16*, 3867.

18) Chang, S.; Jones, L.; Wang, C.; Henling, L. M.; Grubbs, R. H. *Organometallics* **1998**, *17*, 3460.

19) Sanford, M. S.; Henling, L. M.; Grubbs, R. H. *Organometallics* **1998**, *17*, 5384.

20) Dias, E. L.; Grubbs, R. H. *Organometallics* **1998**, *17*, 2758.

21) Dias, E. L. ; California Institute of Technology, 1998.

22) Sanford, M. S.; Henling, L. M.; Day, M. W.; Grubbs, R. H. *Angew. Chem. Int. Ed. Engl.* **2000**, *39*, 3451.

23) Del Rio, I.; Van Koten, G. *Tetrahedron. Lett.* **1999**, *40*, 1401.

24) Leung, W.-H.; Lau, K.-K.; Zhang, Q.; Wong, W.-T.; Tang, B. *Organometallics* **2000**, *19*, 2084.

25) Amoroso, D.; Fogg, D. E. *Macromolecules* **2000**, *33*, 2815.

26) Amoroso, D.; Yap, G. P. A.; Fogg, D. E. *Can. J. Chem.* **2001**, *79*, 958.

27) Hansen, S. M.; Rominger, F.; Metz, M.; Hofmann, P. *Chem. Eur. J.* **1999**, *5*, 557-566.

28) Hansen, S. M.; Volland, M. A. O.; Rominger, F.; Eisentrager, F.; Hofmann, P. *Angew. Chem. Int. Ed. Engl.* **1999**, *38*, 1273.

29) Hofmann, P.; Volland, M. A. O.; Hansen, S. M.; Eisentrager, F.; Gross, J. H. *J. Organomet. Chem.* **2000**, *606*, 88.

30) Volland, M. A. O.; Straub, B. F.; Gruber, I.; Rominger, F.; Hofmann, P. *J. Organomet. Chem.* **2001**, *617-618*, 288.

31) Werner, H.; Jung, S.; Gonzalez-Herrero, P.; Ilg, K.; Wolf, J. *Eur. J. Inorg. Chem.* **2001**, 1957.

32) Arduengo, A. J.; Dias, H. V. R.; Harlow, R. L.; Kline, M. *J. Am. Chem. Soc.* **1992**, *114*, 5530.

33) Huang, J.; Stevens, E. D.; Nolan, S. P.; Peterson, J. L. *J. Am. Chem. Soc* **1999**, *121*, 2674.

34) Scholl, M.; Trnka, T. M.; Morgan, J. P.; Grubbs, R. H. *Tetrahedron Lett.* **1999**, *40*, 2247.

35) Weskamp, T.; Kohl, F. J.; Hieringer, W.; Gleich, D.; Herrmann, W. A. *Angew. Chem. Int. Ed. Engl.* **1999**, *38*, 2416.

36) Weskamp, T.; Schattenmann, W. C.; Spiegler, M.; Herrmann, W. A. *Angew. Chem. Int. Ed. Engl.* **1998**, *37*, 2490.

37) Herrmann, W. A. *Angew. Chem. Int. Ed. Engl.* **1999**, *38*, 262.

CHAPTER 2

Experimental Procedures

2.1. Materials

2.1.1. Solvents

Reagent grade toluene, hexanes, diethyl ether and tetrahydrofuran (BDH) were dried and degassed using an Anhydrous Engineering solvent purification system. Other solvents were refluxed over and distilled from an appropriate drying agent under an atmosphere of N_2: benzene over sodium benzophenone ketyl; pentane over sodium; dichloromethane, pyridine and dimethylacetamide (DMA) over calcium hydride; methanol and 2-propanol over Mg/I_2; acetone over Drierite (anhydrous $CaSO_4$). All solvents (with the exception of methanol and 2-propanol) were stored over Linde 4Å molecular sieves under an atmosphere of N_2.

Deuterated solvents ($CDCl_3$, CD_2Cl_2, C_6D_6, D_2O and C_7D_8) were obtained from Cambridge Isotope Laboratories Ltd. $CDCl_3$ was refluxed over and distilled from Drierite under an atmosphere of N_2. C_6D_6 was deoxygenated by consecutive freeze/pump/thaw cycles and stored over Linde 4Å molecular sieves. Ampoules of CD_2Cl_2 and toluene-d_8 were used as received. All deuterated solvents were stored under N_2.

2.1.2. Gases

Hydrogen (Praxair U.H.P. Grade) was purified by passage through a Deoxo cartridge and an indicating column of Drierite in series. Carbon monoxide (Praxair, 99.5%) was passed through Drierite. Deuterium (Aldrich 99.8%) was used as received.

2.1.3. Phosphines

All phosphines, other than those independently synthesized, were of reagent grade and used as received. Triphenylphosphine (PPh_3), 1,4-bis(diphenylphosphino)butane (dppb), racemic 2,2'-bis(diphenylphosphino)-1,1'-binaphthyl (binap), and dicyclohexylphosphine ($HPCy_2$) were obtained from Strem Chemical Co. All phosphines (with the exception of dppb and PPh_3) were stored under an N_2 atmosphere.

2.1.4. Other Materials

Norbornene (Aldrich) was dried over and distilled from sodium. Cyclooctene (Aldrich) was degassed by consecutive freeze/pump/thaw cycles and stored under N_2. Benzaldehyde, *p*-toluenesulfonehydrazide, potassium hydride (KH), triethylene glycol, copper(I) chloride (CuCl), ammonium hexafluorophosphate (NH_4PF_6), 1,4-dibromobutane, *n*-butyllithium (2.5 M in hexanes), paraformaldehyde ($(CH_2O)_n$), potassium tri(*sec*-butyl)borohydride (1.0 M in Et_2O), 3,3-dimethyl-1-butyne, 3-chloro-3-methyl-1-butyne, 1,1-diphenyl-2-propyn-1-ol, *p*-$Bu^tC_6H_4OH$, and trimethylsilyl trifluoromethanesulfonate (TMS-OTf) were purchased from Aldrich and used as received.

Hydrated $RuCl_3$ (38-43% Ru), thallium(I)ethoxide (TlOEt) and silver hexafluorophosphate ($AgPF_6$) were obtained from Strem Chemical Co. and used as received.

The following materials were generously supplied by collaborators: 1,3-di-*tert*-butyl-1,3,2-diazasilol-2-ylidene ($SiLN_2$) by M. Haaf and Prof. R. West (Univ. of Wisconsin, Madison); dicyclohexylphosphinoxylene (dcpx; [1,3-$(Cy_2PCH_2)C_6H_4$]) and [RuCl(d'bpx)($C(CH_3)C_3H_7$)] (**29**) by Prof. D. Gusev (Wilfrid Laurier).

2.2. Instrumentation

Unless otherwise stated, all reactions were carried out at ambient temperatures (~ 22 C) under an inert atmosphere using standard Schlenk or drybox techniques.

Infrared spectra were recorded on a Bomem MB100 IR spectrometer. Nuclear magnetic resonance (NMR) spectra were recorded on a Varian Gemini 200 (200 MHz for ^1H), a Varian XL-300 (121 MHz for ^{31}P, 75 MHz for ^{13}C and 58 MHz for ^{29}Si), a Bruker Avance 300 (300 MHz for ^1H, 121 MHz for ^{31}P, 75 MHz for ^{13}C and 58 MHz for ^{29}Si) or a Bruker AMX-500 (500 MHz for ^1H, 202 MHz for ^{31}P, 125 MHz for ^{13}C and 99 MHz for ^{29}Si) FT-NMR spectrometer. For ^1H and ^{13}C NMR spectra the residual proton and carbon signals of the deuterated solvent were used as internal standards. ^{31}P NMR spectra were referenced externally against PPh_3 (δ -5.06, C_6D_6; -5.46, $CDCl_3$; -5.64, CD_2Cl_2); shifts are reported relative to 85% H_3PO_4. Downfield shifts are taken as positive for all nuclei. Solid state NMR spectra were recorded on a Bruker ASX-200 MHz spectrometer (81 MHz for ^{31}P). Variable temperature NMR spectra and 2D experiments (HMQC, HMBC and EXSY) were carried out on the Bruker Avance 300 or the Bruker AMX-500

instrument.

Elemental analyses were performed by V. Kuznetsov (of this department) using a Perkin Elmer Series II CHNS/O instrument, or by Guelph Chemical Laboratories. Dr. Glenn P. A. Yap of the departmental crystallographic service carried out single crystal X-ray diffraction studies.

Gel Permeation Chromatography (GPC) data were obtained with CH_2Cl_2 as eluent (flow rate 1.0 mL/min; samples 1-2 mg/mL) using a Wyatt DAWN light-scattering instrument equipped with an Optilab DSP refractometer, HPLC system with a Waters model 515 pump, Rheodyne model 7725i injector with a 200 μL injection loop, and Waters Styragel HR3 and HR4 columns in series.

Computational results were obtained using the Cerius[2]-DMol[3] molecular modeling suite from Molecular Simulations Inc.[1] Dynamics calculations were carried out with the Discover programs, using the OFF force field. Density functional theory (DFT) calculations were carried out with a Double Numerical basis set and Perdew-Wang local correlation using the default grid.

2.3. General Procedure for the Synthesis of Tosylhydrazones

The following tosylhydrazones were prepared according to literature procedures[2] and used as starting materials for the synthesis of corresponding diazoalkanes. All tosylhydrazones were prepared via similar procedures. The preparation of benzaldehyde tosylhydrazone is given as a representative procedure.

2.3.1. Benzaldehyde Tosylhydrazone

Solid *p*-toluenesulfonehydrazide (9.161 g, 49 mmol) was suspended in methanol, in air (20 mL) and the resulting slurry was stirred as 5 mL (49 mmol) of benzaldehyde was added. Upon addition of the aldehyde, the *p*-toluenesulfonehydrazide quickly dissolved and within a few minutes the tosylhydrazone product began to crystallize. The white product was collected on a Büchner funnel, washed with cold methanol and dried under vacuum for several hours. Yield 8.199 g (61%). NMR data agree with the values reported.[2] ^{1}H NMR ($CDCl_3$): δ 7.9-7.2 (m, 10H, Ar), 2.39 (s, 3H, C*H*$_3$). Melting point: 125.0-126.3 C (lit.: 124-125 C).[2]

2.3.2. 2-Naphthaldehyde Tosylhydrazone

p-Toluenesulfonehydrazide (1.190 g, 6.4 mmol); reaction carried out in methanol (5 mL) with addition of 2-naphthaldehyde (962 mg, 6.4 mmol). Yield 1.873 g (90%). NMR data agree with the values reported.[2] ^{1}H NMR ($CDCl_3$): δ 8.10 (s, 1H, N*H*S), 7.70-8.0 (m, 8H, Ar, C*H*N), 7.25-7.50 (m, 2H, Ar), 2.45 (s, 3H, C*H*$_3$). Melting Point: 168-170 C.

2.3.3. 1-Naphthaldehyde Tosylhydrazone

p-Toluenesulfonehydrazide (704 mg, 3.7 mmol); reaction carried out in methanol (5 mL) with addition of 1-naphthaldehyde (570 mg, 500 μL, 3.7 mmol). Yield 749 mg (63%). NMR data agree with the values reported.[2] ^{1}H NMR ($CDCl_3$): δ 9.24 (d, J = 16 Hz, 1H, C*H*N), 7.20-8.10 (m, 11H, Ar), 3.60 (s, 1H, N*H*S), 2.45 (s, 3H, C*H*$_3$). Melting

Point: 69.9-72.0 C.

2.3.4. β-Phenyl-Cinnamaldehyde Tosylhydrazone

This previously unreported tosylhydrazone was prepared as above. *p*-Toluenesulfonehydrazide (661 mg, 3.60 mmol); reaction carried out in methanol (20 mL) with addition of β-phenyl-cinnamaldehyde (739 mg, 3.60 mmol). Yield 670 mg (50%). ^{1}H NMR ($CDCl_3$): δ 7.8 (d, J = 8 Hz, 1H, C*H*N), 7.65 (s, 1H, N*H*S), 7.1-7.4 (m, 14H, Ar), 6.75 (d, J = 8 Hz, 1H, C*H*C), 2.43 (s, 3H, CH_3). Anal. Calcd. for $C_{22}H_{20}N_2O_2S$: C 70.18, H 5.37, N 7.44; Found: C 70.15, H 5.34, N 7.49.

2.4. Diazoalkane Syntheses

The following diazoalkanes were prepared by adaptation of literature procedures.[2]

2.4.1. Phenyldiazomethane

Triethylene glycol (40 mL) and NaOH (0.80 g, 20 mmol) in 5 mL distilled water were added to a 100 mL round bottom flask equipped with a stirbar. The flask was evacuated and back-filled with N_2, and the mixture heated at 70 C until the NaOH had completely dissolved. Benzaldehyde tosylhydrazone (2.393 g, 8.7 mmol) was rapidly added, causing a colour change from pale yellow to deep red within 1 minute. After 5 minutes, the reaction was quenched with ice-cold water (20 mL), and extracted with ice-cold hexanes (4 × 15 mL). The combined organic layers were washed with ice-cold distilled water (1 × 20 mL), and dried over $MgSO_4$. The solvent was removed on a rotary

evaporator and the resulting red oil was immediately transferred to the drybox freezer. Yield 0.58 g (68%). NMR data agree with the values reported.[2] ^{1}H NMR (C_6D_6): δ 7.0-6.9 (m, 2H, Ar), 6.8-6.7 (m, 1H, Ar), 6.55-6.45 (m, 2H, Ar), 4.05 (s, 1H, -C*H*N_2).

2.4.2. 2-Naphthyldiazomethane

Triethylene glycol (15 mL) and Na (0.257 g, 9.2 mmol) were placed in a 100 mL round bottom flask equipped with a stirbar. The flask was evacuated and back-filled with N_2, and the mixture heated at 70 C until the Na had completely dissolved. 2-Naphthaldehyde tosylhydrazone (0.996 g, 3.1 mmol) was rapidly added, causing a colour change from pale yellow to deep red within 1 minute. After 5 minutes, the reaction was quenched with ice-cold water (20 mL), and extracted with ice-cold hexanes (4 × 15 mL). The combined organic layers were washed with ice-cold distilled water (1 × 20 mL), and dried over $MgSO_4$. The solvent was removed on the vacuum line and the resulting pale red solid was immediately transferred to the drybox freezer. Yield 0.258 g (51%). NMR data agree with the values reported.[2] ^{1}H NMR ($CDCl_3$): δ 7.0-7.8 (m, 7H, Ar), 5.1 (s, 1H, -C*H*N_2).

2.4.3. 1-Naphthyldiazomethane

Triethylene glycol (40 mL) and NaOH (0.302 g, 7.6 mmol) were placed in a 100 mL round bottom flask equipped with a stirbar. The flask was evacuated and back-filled (3x) with N_2, and the mixture heated at 70 C until the Na had completely dissolved. 2-Naphthaldehyde tosylhydrazone (0.104 g, 0.31 mmol) was rapidly added, causing a

colour change from pale yellow to deep red within 1 minute. After 5 minutes, the reaction was quenched with ice-cold water (20 mL), and extracted with ice-cold hexanes (4 × 15 mL). The combined organic layers were washed with ice-cold distilled water (1 × 20 mL), and dried over $MgSO_4$. The solvent was removed on the vacuum line and the resulting red oil was immediately transferred to the drybox freezer. Yield 0.021 g (40%). NMR data agree with the values reported.[2] ^{1}H NMR ($CDCl_3$): δ 7.05-8.35 (m, 7H, Ar), 5.55 (s, 1H, -C*H*N_2).

2.4.4. 1,1-Diphenyl-2-Diazomethyl-Ethene

This previously unreported compound was prepared in manner analogous to those above.[2] Triethylene glycol (40 mL) and NaOH (0.677 g, 16.9 mmol) were placed in a 100 mL round bottom flask equipped with a stirbar. The flask was evacuated and back-filled with N_2, and the mixture heated at 70 C until the NaOH had completely dissolved. β-Phenyl-cinnamaldehyde tosylhydrazone (2.546 g, 6.8 mmol) was rapidly added to the solution, which was then stirred for 5 minutes over which time the solution changed from pale yellow to deep red in colour. The reaction was quenched with ice-cold water (20 mL), and extracted with ice-cold hexanes (4 × 15 mL). The combined organic layers were washed with ice-cold distilled water (1 × 20 mL), and dried over $MgSO_4$. The solvent was removed on the vacuum line and the resulting yellow oil was immediately transferred to the drybox freezer. Yield 0.341 g (23%). ^{1}H NMR ($CDCl_3$): δ 6.9-7.7 (m, 10H, Ar), 6.45 (d, J = 14 Hz, 1H, C*H*N_2), 4.8 (d, J = 14 Hz, 1H, C*H*C).

2.5. Azine Synthesis

2.5.1. *t,t*-Benzaldehyde azine

To a stirring solution of sodium (0.420 g, 18.3 mmol) in triethylene glycol (23 mL) at 65°C was added solid benzaldehyde tosylhydrazone (0.25 g, 9.1 mmol). The solution was stirred for 24 h. Addition of 20 mL of cold distilled water afforded a yellow precipitate, which was filtered and recrystallized from hot methanol. Yield 0.30 g (31%). NMR data agree with the values reported.[3] ^{1}H NMR (200 MHz, $CDCl_3$): 7.30-7.35 (m, Ar, 3H), 7.80-7.85 (m, Ar, 2H), 8.65 (s, -C*H*N, 2H).

2.6. Phosphine Syntheses

2.6.1. 1,4-bis(dicyclohexylphosphino)butane (dcypb)

This compound was prepared by a modification of earlier procedures.[4,5] THF (20 mL) and $HPCy_2$ (2.0 mL, 11.4 mmol) were placed in a flask and cooled to -35 C in the drybox freezer. The solution was stirred as a -35 C solution of n-BuLi (5.0 mL, 2.5 M in hexane) was added dropwise via syringe. The clear solution turned yellow and a pale yellow precipitate formed. The suspension was allowed to warm to RT over 1 h with stirring, at which point 1,4-dibromobutane (681 μL, 5.7 mmol) was added dropwise via syringe. The suspension immediately became homogeneous and colourless. The solution was stirred for 1 h, then reduced to dryness. Extraction with hot hexanes, as in the reported procedures, did not effect complete exclusion of LiBr from the isolated product. The white residue was therefore suspended in methanol (10 mL) and stirred for 10

minutes to extract LiBr. The solids were then filtered off, washed with methanol (3 × 10 mL) and dried under vacuum. Yield 2.255 g (88 %). ^{1}H NMR (C_6D_6): δ 1.0-2.0 (br, C*H*, C*H*$_2$). ^{31}P NMR (C_6D_6): δ -5.39 (s).

2.7. Aryloxide Salts

2.7.1. *p*-Bu^{t}C$_6$H$_4$O$^-$K$^+$

To a stirring THF solution (30 mL) of *p*-Bu^{t}C$_6$H$_4$OH (3.862 g, 25.7 mmol) was added dropwise (over the course of 30 minutes) a suspension of KH (1.031 g, 25.7 mmol) in THF (30 mL). Vigorous evolution of hydrogen gas ensued. The pale yellow solution was stirred for 30 minutes after addition of the KH suspension was completed and reduced to dryness leaving a white solid. The solids were washed with benzene (3 × 5 mL) and dried under vacuum. Yield 4.614 g (95 %). ^{1}H NMR (C_6D_6): δ 7.15 (br s, 2H, Ar), 6.63 (br s, 2H, Ar), 1.23 (s, 9H, C*H*$_3$).

2.8. Ruthenium Precursors

The following complexes were prepared by literature methods (unless otherwise indicated) for use as starting materials for the synthesis of derivatives of varied ligand frameworks and/or as precursors to metathesis-active alkylidene complexes.

2.8.1. $RuCl_2(PPh_3)_3$

A solution of $RuCl_3 \bullet xH_2O$ (0.970 g, 3.87 mmol) in MeOH (100 mL) was refluxed

under N_2 for 1 hour, then allowed to cool. Solid PPh_3 (6.097 g, 23.2 mmol) was added under a strong flow of N_2, and the mixture refluxed for an additional 3 hours. The resulting brown precipitate was filtered off, washed with MeOH (4 × 20 mL), then with hot hexanes (6 × 10 mL, or until the washings showed no trace of residual phosphine by tlc), and dried under vacuum. Yield 3.544 g (96%). ^1H and $^{31}P\{^1H\}$ NMR spectroscopic data have been previously reported.[6-8]

2.8.2. $RuCl_2(dppb)(PPh_3)$ (3a)

A dark green solution of $RuCl_2(PPh_3)_3$ (1.07 g, 1.12 mmol) and dppb (0.478 g, 1.12 mmol) in CH_2Cl_2 (20 mL) was stirred at RT for 2 h, then filtered to remove any $Ru_2Cl_4(dppb)_3$ formed. (None of this CH_2Cl_2-insoluble green precipitate[9] is obtained if the ruthenium precursor is free of residual PPh_3).[10] The solution was then concentrated to 5 mL and MeOH (10 mL) was added to precipitate the product. The mixture was stirred for 1 hour, after which the green solid was filtered off, washed with MeOH (2 × 5 mL) and hexanes (3 × 15 mL), and dried under vacuum. Yield 0.87 g (90%). ^1H and $^{31}P\{^1H\}$ NMR spectroscopic data have been previously reported.[11,12]

2.8.3. $RuCl_2(binap)(PPh_3)$ (3b)

The complex was prepared according to the published procedure,[11] but using racemic binap. An orange/brown solution formed by the addition of CH_2Cl_2 (15 mL) to a mixture of $RuCl_2(PPh_3)_3$ (0.251 g, 0.262 mmol) and binap (0.163 g, 0.262 mmol) was stirred for 24 h, then concentrated to 5 mL. Addition of Et_2O (10 mL) precipitated an orange product, which was filtered off, washed with hexanes (2 × 5 mL), and dried under

vacuum. Yield 0.23 g (83%). ^{1}H and $^{31}P\{^{1}H\}$ NMR spectroscopic data have been previously reported.[11,12]

2.8.4. $[RuCl(dppb)]_2(\mu\text{-}Cl)_2(\mu\text{-}H_2O)$ (4)

The complex was prepared according to the published procedure.[13] A C_6H_6 solution (20 mL) of $RuCl_2(dppb)(PPh_3)$ (0.336 g, 0.39 mmol) with added H_2O (5 mL) was refluxed under N_2 for 2.5 h. Addition of hexanes (25 mL) precipitated the orange solid. Stirring was continued for 30 min, after which the product was filtered off, washed with MeOH (1 × 10 mL) and hexanes (8 × 10 mL), and dried under vacuum. Yield 0.219 g (93%). ^{1}H and $^{31}P\{^{1}H\}$ NMR spectroscopic data have been reported previously.[13]

2.8.5. $Ru_2Cl_4(dcypb)_2(N_2)$ (5)

A green solution of $RuCl_2(PPh_3)_3$ (0.398 g, 0.415 mmol) and dcypb (0.190 g, 0.422 mmol) in C_6H_6 (5 mL) was stirred under N_2. Within 30 minutes the solution had become orange in colour and an orange precipitate had formed. After 16 h hexanes (5 mL) was added, precipitating more of the orange solid, which was filtered off, washed with hexanes (3 × 2 mL) and dried under a flow of N_2 for 16 h. (Note that drying under vacuum leads to decomposition.) Yield 0.257 g (97%). ^{1}H NMR ($CDCl_3$): δ 0.7-3.1 (br, C*H*, C*H*$_2$). $^{31}P\{^{1}H\}$ NMR ($CDCl_3$): δ 57.5 (d, $^{2}J_{PP}$ = 39 Hz), 45.0 (d, $^{2}J_{PP}$ = 27 Hz), 44.6 (d, $^{2}J_{PP}$ = 39 Hz), 42.3 (d, $^{2}J_{PP}$ = 27 Hz); (C_6D_6): δ 60.1 (d, $^{2}J_{PP}$ = 39 Hz), 49.1 (d, $^{2}J_{PP}$ = 26 Hz), 45.3 (d, $^{2}J_{PP}$ = 39 Hz), 37.4 (d, $^{2}J_{PP}$ = 26 Hz). Solid-state $^{31}P\{^{1}H\}$ CP/MAS NMR (80.9 MHz): 45-57 (br, unresolved), 43.6 (br), 41.2 (br). IR (Nujol, cm^{-1}): ν(N_2)

2124 (m). Anal. Calcd. for $C_{56}H_{104}N_2Cl_4P_4Ru_2$: C, 52.81; H, 8.25; N, 2.20%. Found: C, 52.90; H, 8.19; N, 1.90%. FAB-MS (m/z): 1245 (M - N_2).

2.8.6. $Ru(H)Cl(PPh_3)_3$

p-^{t}BuC$_6$H$_4$OK$^+$ (0.198 g, 1.12 mmol) in isopropanol (10 mL) was added to a C_6H_6 solution (40 mL) of $RuCl_2(PPh_3)_3$ (1.007 g, 1.05 mmol) and the solution was refluxed for 8 h. Concentration of the solution (~5 mL) afforded a purple solid. Addition of hexanes (10 mL) afforded more of the purple solid which was filtered off, washed with hexanes (4 × 5 mL) and methanol (4 × 3 mL) and dried under vacuum. Yield 0.940 g (97%). ^{1}H NMR ($CDCl_3$): δ 7.14-6.99 (br m, Ar, 18H), 6.83 (t, *m*-Ar, 12H, $^3J_{HH}$ = 7.5 Hz), -17.7 (q, Ru*H*, 1H, $^2J_{HP}$ = 26 Hz). $^{31}P\{^1H\}$ NMR (CH_2Cl_2): δ 57.5 (br s); resolves upon cooling to 183 K into the reported[7] AX_2 pattern: δ 94.2 (t, J_{PP} = 27 Hz, 1P), 38.4 (d, J_{PP} = 27 Hz, 2P). IR (Nujol, cm^{-1}): ν(Ru-H) 1929 (m).

2.8.7. $RuCl_2(PPh_3)_2(CHCHC(CH_3)_2$

To a purple solution of $Ru(H)Cl(PPh_3)_3$ (1.11 g, 1.2 mmol) in 10 mL CH_2Cl_2 was added 3-chloro-3-methyl-1-butyne (148 μL, 1.32 mmol). The solution immediately became brown in colour, stirring was continued for 1 h, after which time the solution was concentrated to ~1 mL and treated with hexanes (10 mL). The resulting brown solid was filtered off, washed with cold (-35 C) hexanes (5 × 3 mL) and dried under vacuum. The solid was reprecipitated from CH_2Cl_2/hexanes. Yield 0.762 g (83%). ^{1}H and $^{31}P\{^1H\}$ NMR spectroscopic data have been reported elsewhere.[14]

2.9. Reaction of Ruthenium Precursors with Diazoalkanes

2.9.1. Reaction of $RuCl_2(dppb)(PPh_3)$ (3a) with $PhCHN_2$

To a dark green suspension of **3a** (9.9 mg, 0.012 mmol) in C_6D_6 (0.75 mL) was added freshly prepared $PhCHN_2$ (48 μL, 0.48 mmol). Vigorous bubbling ensued, and all of the solids dissolved, forming a deep red/brown solution. The sample was immediately analyzed by NMR. ^1H NMR (200 MHz, C_6D_6): 18.91 (s, RuC*H*), 6.5-7.8 (br m, Ar), 0.8-1.8 (br, -CH_2). ^{31}P NMR (121.42 MHz, C_6D_6): 31.37 (d, 1P, $^2J_{PP}$ = 11 Hz), 36.70 (d, 1P, $^2J_{PP}$ = 11 Hz), -5.04 (s, PPh_3).

2.10. Polymerization of Norbornene via Ruthenium Precursors

2.10.1. General Procedure for the *in situ* Polymerization of Norbornene.

A freshly prepared solution of **3a** (9.0 mg, 10.6 μmol Ru) and $PhCHN_2$ (5.3 μL, 53 μmol) in $CDCl_3$ (2 mL) was added to a vigorously stirred solution of norbornene (200 mg, 2.1 mmol) in $CDCl_3$ (5 mL). The reaction was stirred at RT, and monitored by removing aliquots (0.5 mL) for NMR analysis. Each run was carried out in triplicate to ensure reproducibility.

2.10.2. Effect of CuCl

Reactions with **3a**/$PhCHN_2$ or **4**/$PhCHN_2$ were carried out as above, adding the freshly prepared catalyst solution to norbornene in $CDCl_3$ containing 1 or 10 equivalents

of CuCl per Ru (1 equiv: 1.0 mg, 10.6 μmol; 10 equiv: 10.5 mg, 0.11 mmol).

2.10.3. Effect of PPh_3

Reactions with **4** (6.4 mg, 5.3 μmol)/$PhCHN_2$ were carried out as above, adding the freshly prepared catalyst solution to norbornene (200 mg, 2.1 mmol) in $CDCl_3$ (5 mL). A single aliquot was taken for NMR analysis, then returned to the solution, at which point a solution of PPh_3 (2.8 mg, 10.6 μmol) in $CDCl_3$ (1 mL) was added. The solution was stirred at RT, and monitored by removing aliquots for NMR analysis.

2.10.4. Effect of $PhCHN_2$

Reactions with **2** or **4** were carried out as above, adding 0, 0.5, 1, or 5 equivalents of $PhCHN_2$ per Ru. Conversion at 48h for **2** in the absence of $PhCHN_2$: 12%.

2.10.5. Effect of Azine

Reactions with **4** (6.4 mg, 5.3 μmol)/$PhCHN_2$ were carried out as above, adding the freshly prepared catalyst solution to a rapidly stirring solution of norbornene (200 mg, 2.1 mmol) in $CDCl_3$ (5 mL) containing *t,t*-benzaldehyde azine (1.1 mg, 5.3 μmol).

2.11. N_2-Displacement Reactions of $Ru_2Cl_4(dcypb)_2(N_2)$

2.11.1. Isolation of $Ru_2Cl_5(dcypb)_2$ (6)

Complex **5** (40 mg, 0.04 mmol) was dissolved in $CDCl_3$ (0.5 mL), and the solution was monitored by $^{31}P\{^1H\}$ NMR. Resolution degraded perceptibly over ~30 min, and a broad singlet emerged at 50 ppm. On further reaction, S/N values decreased, and many new peaks could be discerned (46-63, 15-32 ppm). Slow evaporation deposited red crystals of **6**.

2.11.2. Decomposition of $Ru_2Cl_4(dcypb)_2(N_2)$ in vacuo

(a) NMR-scale. A solution of **5** (3.0 mg, 4.7 μmol Ru) in C_6D_6, with *t*-$RuCl_2(dppe)_2$ (2.3 mg, 2.35 μmol) as internal standard, was freeze-pump-thaw degassed in a round-bottom Schlenk flask. $^{31}P\{^1H\}$ NMR spectra were measured after every second cycle of degassing. No NMR signals were discerned after six degassing cycles, though gas evolution was sustained over three further cycles. (b) Large-scale. A suspension of **5** (20 mg, 0.016 mmol Ru_2) in benzene (10 mL) was freeze-pump-thaw degassed until no signals were evident by NMR. Concentration and addition of cold hexanes afforded a dark grey-green solid, which was filtered off, washed with cold hexanes, and dried under a flow of Ar. Yield 16 mg. IR (Nujol, cm^{-1}): ν(Ru-H) 1944 (m-w), ν(C=C) 1629 (m-w). (c) Prolonged exposure of solid **5** to vacuum at 50 C resulted in a mixture of diamagnetic products (multiple ^{31}P NMR signals in the region 75 to -15 ppm).

2.11.3. NMR-Scale Preparation of $Ru_2Cl_4(dcypb)_2(H_2)$ (7)

Stirring a suspension of **5** (4 mg, 3 μmol Ru_2) in C_6D_6 (0.5 mL) under H_2 at RT afforded a homogeneous orange solution within 15 min. No starting material was spectroscopically observable after 30 min. $^{31}P\{^1H\}$ NMR (C_6D_6): δ 65.1 (d, $^2J_{PP}$ = 25 Hz), 59.2 (d, $^2J_{PP}$ = 40 Hz), 45.9 (d, $^2J_{PP}$ = 25 Hz), 43.9 (d, $^2J_{PP}$ = 40 Hz). ^1H NMR (C_6D_6): δ 0.6-3.0 (br, CH_2, Cy of dcypb), -11.8 (br s, H_2). Hydride T_1 (min) 26 msec (300 K, 500 MHz).

2.11.4. $RuCl_2(dcypb)(CO)_2$ (*ccc*, **8**; *tcc*, **9**)

A suspension of **5** (27 mg, 39 μmol Ru_2) in THF (5 mL) was stirred under CO for 24 h, affording a clear yellow solution. The solution was concentrated and hexanes added to coprecipitate **8** and **9** as a yellow powder (1:4). Yield 23 mg (88%). $^{31}P\{^1H\}$ NMR (C_6D_6): δ 39.4 (d, $^2J_{PP}$ = 22 Hz, **8**), 17.1 (d, $^2J_{PP}$ = 22 Hz, **8**); 13.8 (s, **9**). ^1H NMR (C_6D_6): δ 0.8-2.4 (br, CH_2, Cy of dcypb). $^{13}C\{^1H\}$ NMR (C_6D_6): δ 198.7 (t, $^2J_{CP}$ (cis) = 12 Hz, **8**); 193.5 (dd, $^2J_{CP}$ (trans) = 113 Hz, $^2J_{CP}$ (cis) = 11 Hz, **8**); 193.8 (dd, $^2J_{CP}$ (trans) = 109 Hz, $^2J_{CP}$ (cis) = 23 Hz, **9**). IR (Nujol; cm^{-1}): ν(CO) 2052 (s, **8**), 2038 (s, **9**), 1976 (s, **9**), 1962 (s, **8**). Anal. Calcd. for $C_{30}H_{52}Cl_2O_2P_2Ru$: C, 53.09; H, 7.72%. Found: C, 53.39; H, 7.93%. X-ray quality crystals of **8** were obtained by slow evaporation of a benzene solution.

2.11.5. Isolation of $Ru_2Cl_4(dcypb)_2(CO)_2$ (10)

X-ray quality crystals of **10** were isolated by slow evaporation (~ 1 month) of a

benzene solution containing principally **8** and **9**, in which small peaks at δ 20.4 (s) and 23 (m) were also evident by $^{31}P\{^{1}H\}$ NMR. Amounts of **10** obtained were insufficient for NMR analysis. Subsequent efforts to prepare solely **10** via quantitative transfer of CO met with no success; the only products observed were **11** and/or **8**, **9**. The ^{31}P NMR signal at 23 was also sometimes observed, but no singlet corresponding to **10**.

2.11.6. $Ru_2Cl_4(dcypb)_2(CO)$ (11)

Gaseous formaldehyde, generated by heating paraformaldehyde at 180 Cunder a stream of N_2, was bubbled through a suspension of **5** (50 mg, 0.79 μmol) in C_6H_6 (10 mL). After 30 min, the supply of gaseous formaldehyde was stopped and the system was sealed. The suspension stirred for 24 h and concentrated to approximately 2 mL. Addition of hexanes (5 mL) afforded more orange/brown solid, which was filtered off, washed with hexanes (3 × 5 mL) and dried under vacuum. Yield 40 mg (80 %). ^{1}H NMR ($CDCl_3$): δ 0.7-3.1 (br, CH, CH_2 of dcypb). $^{31}P\{^{1}H\}$ NMR (C_6D_6): δ 59.6 (d, $^{2}J_{PP}$ = 40 Hz), 50.4 (d, $^{2}J_{PP}$ = 23 Hz), 43.7 (d, $^{2}J_{PP}$ = 40 Hz), 43.0 (d, $^{2}J_{PP}$ = 23 Hz). IR (Nujol, cm^{-1}): ν(CO) 1940 (m). Anal. Calcd. for $C_{57}H_{104}O_1Cl_4P_4Ru_2$: C, 53.77; H, 8.23%. Found: C, 53.21; H, 8.27%.

2.12. Ruthenium Silylene Chemistry

2.12.1. $RuCl(\eta^3\text{-dcypb})(SiL^N_2)$ (12)

Reaction of **5** (0.198 g, 0.314 mmol Ru) with SiL^N_2 (0.127 g, 0.647 mmol) in

C_6H_6 (10 mL) at 50 C gave a homogeneous deep red/brown solution over 4 h. Concentration and addition of cold hexanes afforded a yellow precipitate, which was reprecipitated from benzene-hexanes. Yield after drying under vacuum: 0.199 g (81%). ^{1}H NMR (C_6D_6): δ 6.33 (d, olefinic, 1H, $^2J_{HH}$ = 3.8 Hz), 6.17 (d, olefinic, 1H, $^2J_{HH}$ = 3.8 Hz), 3.2-3.4 (m, aliphatic, 2H), 2.8-3.0 (m, aliphatic, 2H), 1.0-2.7 (br m, aliphatic, 47H), 1.29 (s, Bu^t, 9H), 1.01 (s, Bu^t, 9H). ^{31}P{^{1}H} NMR (C_6D_6): δ 60.2 (d, CH_2CH_2P, $^2J_{PP}$ = 263 Hz), -10.3 (d, $CHCH_2P$, $^2J_{PP}$ = 263 Hz). Solid state ^{31}P NMR (80.9 MHz): δ 56.2 (d, CH_2CH_2P, $^2J_{PP}$ = 267 Hz), -11.6 (d, $CHCH_2P$, $^2J_{PP}$ = 267 Hz). ^{29}Si{^{1}H} NMR (C_6D_6): δ 105.7 ppm (t, $^2J_{PSi}$ = 32 Hz). IR (Nujol): ν(C-H) 2923, 2853, 2727, 2668 cm^{-1}; (benzene): 2924, 2851 cm^{-1}. The extreme air-sensitivity of the complex resulted in fuming and immediate decomposition to a dark brown powder on attempted combustion analysis, giving data consistently low in carbon. Crystals of **12** were obtained by slow evaporation of a benzene solution.

■

2.12.2. Reaction of RuCl(η^3-dcypb)(SiL$^N_2$) with H_2 at 50 C

A solution of **12** (62 mg, 0.08 mmol) in 5 mL of C_6H_6 was warmed at 50 C for 24 h under H_2. Conversion of SiL$^N_2$ to siloxane dimer [L$^N_2$Si(H)]$_2$O **13** was confirmed by detailed spectroscopic analysis (see text, Ch. 5), reinforced by comparison with literature values.[15] The inorganic product is spectroscopically identical to Ru species (Ru(dcypb)(H)(μ-Cl)$_2$(μ-H)Ru(dcypb)(H_2), **14**) prepared by reaction of **5** with potassium tri(*sec*-butyl)borohydride. Its isolation was thwarted by decomposition on stripping to a solid. Dehydrogenation processes are indicated by the appearance of olefinic signals and

a peak for dissolved H_2 by ^1H NMR (δ_H 4.2). Solution $^{31}P\{^1H\}$ NMR (C_6D_6): δ 65.1 (br s, **14**), 52.2 (br s, **14**), ratio 1:1. ^1H NMR (C_6D_6): δ 5.95 (s, Si*H*, **13**), 5.80 (s, olefinic, **13**), 0.6-3.0 (m, aliphatic, **14**), -13.8 (br s, Ru*H*, Ru(H_2), **14**).

2.12.3. Reaction of RuCl(η³-dcypb)(SiL$^N_2$) with D_2 at 50 C

Deuterium gas was bubbled through a solution of **12** (10 mg, 12.8 μmol) in C_6H_6 (1 mL) in a Teflon-lined screw-cap NMR tube (2 min). The sealed tube was warmed at 50 C for 24 h under D_2. ^2H NMR (C_6H_6): δ 5.95 (s, Si*D*, **13-d**), 0.5-3.0 (br m, aliphatic, **14-d**), -13.8 (br s, Ru*D*, Ru(D_2), **14-d**). ^{31}P NMR (C_6H_6): δ 65.1 (br s, **14-d**), 52.2 (br s, **14-d**); ratio 1:1.

2.12.4. Room Temperature Reaction of RuCl(η³-dcypb)(SiL$^N_2$) with D_2

Deuterium gas was bubbled through a solution of **12** (10 mg, 12.8 μmol) in C_6H_6 (1 mL) in a Teflon-lined screw-cap NMR tube (2 min). The sealed tube was stored at RT under D_2, and the reaction monitored by ^2H and ^{31}P NMR. After 48 h signals for **14-d** were visible, accompanying those for **12**. No incorporation of deuterium into the diphosphine backbone was observed prior to formation of **14-d**.

2.12.5. Reaction of RuCl(η³-dcypb)(SiL$^N_2$) with H_2O

To a solution of **12** (10 mg, 12.8 μmol) in C_6D_6 (1 mL) under N_2 in a Teflon-lined screw-cap NMR tube was added degassed H_2O (0.23 μL, 12.8 μmol). After 2 h at RT,

<20% of 12 remained (^{1}H, ^{31}P NMR); several new products were evident, of which only 15% of the integrated intensity could be ascribed to 14. The tube was then purged with H_2. After 4 h, no 12 remained and the major product (50% of integrated intensity) was 14. No further changes were observed over 24 h.

2.12.6. Reaction of RuCl(η^3-dcypb)(SiL$^N_2$) with H_2O and H_2

To a solution of 12 (10 mg, 12.8 μmol) in C_6D_6 (1 mL) in a Teflon-lined screw-cap NMR tube was added degassed H_2O (0.23 μL, 12.8 μmol). The sealed tube was immediately purged with H_2. Conversion to 14 and siloxane (13) was complete within 6 h at RT (^{1}H, ^{31}P NMR.)

2.12.7. Isolation of [(dcypb)(H)Ru(μ-Cl)$_3$Ru(dcypb)(N_2)] (15)

Complex 15 was serendipitously obtained on attempted isolation of 14 from the reaction of 12 with H_2. A benzene solution containing the reaction products was reduced to an orange residue under vacuum, washed with hexanes, and redissolved in benzene. ^{31}P NMR analysis revealed the presence of many products, including 14, characterized by resonances (many of which were broad) between 87 and 2 ppm. ^{1}H NMR, hydride region: δ -19.5 to -20.6 (overlapping multiplets), -13.8 (br s, 14), -11 to -12 (two broad singlets). Small crystals of 15 deposited on slow evaporation.

2.12.8. Reaction of RuCl(η^3-dcypb)(SiL^N_2) with CO

A suspension of **12** (86 mg, 0.11 mmol) in 0.75 mL of toluene-d_8 gave a homogeneous pale yellow solution on stirring under 1 atm CO. ^{1}H NMR showed complete loss of signals for bound silylene within 24 h, and a large singlet for free SiL^N_2. Three products evident by ^{31}P NMR were identified as isomeric Ru(η^3-dcypb)$(CO)_2$ species **16-18** (see text, Ch. 5). The high solubility of **16-18** in all solvents, including hexanes, precluded separation from free silylene. ^{1}H NMR (C_6D_6): δ 6.75 (s, olefinic, 2H), 0.8-3.4 (br, m, 51H), 1.40 (s, Bu^t, 18H). ^{31}P{^{1}H} NMR (C_6D_6): δ 77.6 (d, CH_2CH_2P, $^2J_{PP}$ = 249 Hz, **16** or **17**), 74.4 (d, CH_2CH_2P, $^2J_{PP}$ = 246 Hz, **16** or **17**), 72.9 (d, CH_2CH_2P, $^2J_{PP}$ = 164 Hz, **18**), -29.0 (d, $CHCH_2P$, $^2J_{PP}$ = 249 Hz, **16** or **17**), -29.9 (d, $CHCH_2P$, $^2J_{PP}$ = 246 Hz, **16** or **17**), -38.2 (d, $CHCH_2P$, $^2J_{PP}$ = 164 Hz, **18**). IR (Nujol, ν (CO), cm^{-1}): 2010, 1925, 1880.

2.12.9. Reaction of RuCl(η^3-dcypb)(SiL^N_2) with ^{13}CO

The reaction was carried out as above to afford the corresponding ^{13}C isotopomers, **16'-18'**. Peak doubling in the ^{31}P NMR spectrum due to ^{13}C-^{31}P coupling confirms the presence of two carbonyl ligands in each molecule, though second-order effects limit rigorous analysis of the ^{13}C NMR spectrum. ^{31}P{^{1}H} NMR (C_6D_6): δ 77.6 (ddd, CH_2CH_2P, $^2J_{PP}$ = 249 Hz, $^2J_{PC}$ = 12 Hz, $^2J_{PC}$ = 4.2 Hz, **16'** or **17'**), 74.4 (ddd, CH_2CH_2P, $^2J_{PP}$ = 246 Hz, $^2J_{PC}$ = 11.6 Hz, $^2J_{PC}$ = 4.6 Hz, **16'** or **17'**), 72.9 (dt, CH_2CH_2P, **18'**, $^2J_{PP}$ = 164 Hz, $^2J_{PC}$ = 13.2 Hz), -29.0 (ddd, CH_2CH_2P, $^2J_{PP}$ = 249 Hz, $^2J_{PC}$ = 13.4 Hz, $^2J_{PC}$ = 4.9 Hz, **16'** or **17'**), -29.9 (ddd, CH_2CH_2P, $^2J_{PP}$ = 246 Hz, $^2J_{PC}$ = 11.5 Hz, $^2J_{PC}$ =

3.6 Hz, 16' or 17'), -38.2 (dt, CH_2CH_2P, 18', $^2J_{PP}$ = 164 Hz, $^2J_{PC}$ = 13.4 Hz). $^{13}C\{^1H\}$ NMR (C_6D_6; CO region only): δ 214.6 (m), 210.4 (m), 205.9 (m), 202.3 (m), 201.7 (m), 198.9 (m), 198.2 (m).

2.13. Hydride Derivatives of dcypb

2.13.1. [Ru(H)(dcypb)(μ-Cl)$_2$(μ-H)Ru(dcypb)(H$_2$)] (14)

An orange suspension of **5** (20 mg, 31.4 μmol Ru) in C_6D_6 (1 mL) was stirred under H_2 atmosphere for 5 minutes, following which a C_6D_6 solution of KHB^{s}Bu$_3$ (32 μL of a 1.0 M solution in Et_2O) under H_2 was added by cannula. A clear, slightly darker orange solution formed within minutes. NMR analysis was carried out by transferring the solution by cannula into a Teflon-lined screw-cap NMR tube filled with H_2. Attempts to isolate these products resulted in substantial decomposition. Crystals of (**14**) suitable for X-ray analysis deposited over several days under H_2. ^1H NMR (C_6D_6): δ 0.6-3.0 (m, aliphatic **14**), -13.8 (s, *H*, *H*$_2$, **14**). ^{31}P NMR (C_6D_6): δ 65.1 (br s, **14**), 52.2 (br s, **14**). Hydride T_1 min (C_7D_8, H_2, 500 MHz, 284 K) 38 ms. IR (Nujol) ν(Ru-H) 2102 (m), 2066 (m) cm^{-1}.

2.13.2. D$_2$ Incorporation into [Ru(H)(dcypb)(μ-Cl)$_2$(μ-H)Ru(dcypb)(H$_2$)]

Deuterium gas was bubbled through a solution of **5** (10 mg, 12.8 μmol) in C_6D_6 (1 mL) in a Teflon-lined screw-cap NMR tube (2 min), following which KHB^{s}Bu$_3$ was added as before. ^2H NMR (C_6D_6): δ 0.5-3.0 (br m, aliphatic, **14-d**), -13.8 (s, *D*, *D*$_2$, **14-d**).

^{31}P NMR (C_6D_6): δ 65.1 (br s, **14-d**), 52.2 (br s, **14-d**); ratio ~1:1.

2.14. Alkylidene-, Vinylidene- and Allenylidene Derivatives

2.14.1. RuCl(dcypb)(μ-Cl)$_3$Ru(dcypb)[C=CH(Bu^t)] (19)

An orange suspension of **5** (180 mg, 0.14 mmol) in 5 mL benzene 5 mL was treated with 3,3-dimethyl-1-butyne (52.2 μL, 0.32 mmol). The mixture was stirred for 12 h, over which time it darkened slightly. Concentration and addition of pentane (2 mL) afforded more of the orange solid, which was filtered off, washed with pentane (3 × 1 mL) and dried under vacuum. Yield 161 mg (86%). ^1H NMR ($CDCl_3$): δ 3.1-3.2 (br, aliphatic, 2H), 3.06 (t, C=C*H*, $^4J_{HP}$ = 3.8 Hz, 1H), 1.24 (s, C(CH_3)$_3$, 9H), 1.0-3.2 (br, aliphatic, 102H). $^{31}P\{^1H\}$ NMR ($CDCl_3$): δ 50.6 (d, $^2J_{PP}$ = 37 Hz), 49.6 (d, $^2J_{PP}$ = 37 Hz), 45.9 (d, $^2J_{PP}$ = 23 Hz), 40.1 (d, $^2J_{PP}$ = 23 Hz). $^{13}C\{^1H\}$ NMR (C_6D_6): δ 352.1 (t, Ru*C*, $^2J_{CP}$ = 16 Hz), 119.2 (s, RuC:C), 15-45 (br, aliphatic). IR (Nujol): ν(C=C) 1633 cm^{-1}. Anal. Calcd. for $C_{62}H_{114}Cl_4P_4Ru_2$: C, 56.10; H, 8.66%. Found: C, 56.57; H, 9.05%.

2.14.2. RuCl(dcypb)(μ-Cl)$_3$Ru(dcypb)[C=CHC(OH)Ph$_2$] (20a)

An orange suspension of **5** (98 mg, 0.15 mmol Ru) and 1,1-diphenyl-2-propyn-1-ol (34 mg, 0.16 mmol) in 8 mL benzene was stirred for 12 h, over which time it darkened to brown. Hexanes (4 mL) was added, and the brown solid was filtered off, washed with hexanes (3 × 1 mL) and dried under vacuum. Yield 97 mg (88 %). ^1H NMR (C_6D_6): δ 7.51 (d, $^3J_{HH}$ = 6.5 Hz, 4H, *o*-C_6H_5), 7.28 (t, $^3J_{HH}$ = 7.5 Hz, 4H, *m*-C_6H_5), 7.18 (t, $^3J_{HH}$ =

7.1 Hz, 2H, *p*-C_6H_5), 4.38 (t, C=C*H*, $^4J_{HP}$ = 3.7 Hz, 1H), 3.99 (br, -O*H*, xch D_2O, 1H), 0.8-3.5 (br, aliphatic, 102H). $^{31}P\{^1H\}$ NMR (C_6D_6): δ 51.5 (d, $^2J_{PP}$ = 38 Hz), 50.1 (d, $^2J_{PP}$ = 38 Hz), 44.7 (d, unresolved), 40.9 (d, unresolved). $^{13}C\{^1H\}$ NMR ($CDCl_3$): δ 308.7 (t, Ru*C*, unresolved), 243.4 (s, RuC:*C*), 150.4 (s, RuC:C:*C*), 149.4-120.2 (Ar), 53.1-14.0 (aliphatic). IR (Nujol): ν(C=C) 1664 (s), ν(O-H) 3485 (m) cm^{-1}. Anal. Calcd. for $C_{71}H_{114}Cl_4P_4Ru_2$: C, 58.67; H, 8.04%. Found: C, 59.07; H, 8.34%.

2.14.3. NMR Scale Preparation of RuCl(dcypb)(μ-Cl)$_3$Ru(dcypb)[C=C=CPh$_2$] (20b)

A brown suspension of **20a** (20mg,) in C_6D_6 was heated at 70 C for 36 h, over which time the suspension cleared to a dark red solution. NMR analysis at this point showed quantitative conversion of the hydroxyvinylidene to allenylidene, **20b**. ^1H NMR (C_6D_6): δ 8.09 (d, $^3J_{HH}$ = 7.7 Hz, 4H, *o*-C_6H_5), 7.37 (t, $^3J_{HH}$ = 7.3 Hz, 4H, *m*-C_6H_5), 7.19 (t, $^3J_{HH}$ = 7.6 Hz, 2H, *p*-C_6H_5), 3.95 (br s, aliphatic, 1H), 3.58 (br s, aliphatic, 1H), 0.6-3.5 (br, aliphatic, 102H), 0.49 (s, H_2O, 2H). $^{31}P\{^1H\}$ NMR (C_6D_6): δ 57.6 (d, $^2J_{PP}$ = 39 Hz), 45.1 (d, $^2J_{PP}$ = 28 Hz), 44.5 (d, $^2J_{PP}$ = 39 Hz), 39.1 (d, unresolved). $^{13}C\{^1H\}$ NMR (C_6D_6): δ 308.7 (t, Ru*C*, $^2J_{PC}$ = 14 Hz), 244.4 (s, RuC:*C*), 146.0 (s, RuC:C:*C*), 147.4-129.2 (Ar), 43.9-14.4 (aliphatic). IR (Nujol): ν(C=C=C) 1914 (m) cm^{-1}.

2.14.4. RuCl(dcypb)(μ-Cl)$_3$Ru(dcypb)[CHCHC(CH$_3$)$_2$] (21,22)

To a stirring suspension of **5** (186 mg, 0.29 mmol Ru) in toluene (10 mL) under an atmosphere of H_2 was added KHB^sBu_3 (292 μL of a 1.0 M solution in Et_2O). The orange suspension was stirred at RT for 3 h, over which time it cleared to give a dark

orange solution. Subsequent addition of a solution of 3-chloro-3-methyl-1-butyne (66 μL, 0.58 mmol) in 2 mL toluene resulted in immediate darkening of the solution to green/brown. The solution was stirred for 14 h, filtered through Celite and the filtrate reduced to dryness. The resulting brown residue was suspended in pentane (2 mL) and the solids filtered off, washed with pentane (5 × 1 mL) and dried under vacuum. Two products are formed (ratio 4:1), the greater of which can be unambiguously identified as $Ru_2Cl_4(dcypb)_2(CHCHC(CH_3)_2)$ (**21**). The minor product (**22**) is proposed to be an isomer containing a bridging alkylidene (see text, Ch. 6). Yield (based on $C_{61}H_{112}Cl_4P_4Ru_2$) 158 mg (82%). Identical results were obtained on use of a larger excess of the alkyne (20 equiv), on shorter reaction times (1 h), or on carrying out the reaction at −35 C. ^1H NMR (C_6D_6): δ 16.92 (q, RuC*H*, $^3J_{HH}$ = 11.5 Hz, $^3J_{HP}$ = 11.5 Hz, **21**), 15.83 (q, RuC*H*, $^3J_{HH}$ = 12.0 Hz, $^3J_{HP}$ = 12.0 Hz, **22**), 9.1 (m, RuCHC*H*, **21** and **22**), 0.5-3.5 (br, aliphatic, **21** and **22**), -1.8 (br s), -7.9 (br s), -10.2 (br s). $^{31}P\{^1H\}$ NMR (C_6D_6): δ 54.0 (br s, **21**), 46.1 (br s, **21**), 45.1 (br s, **21**), 43.4 (s, **22**), 42.9 (br s, **21**); ($CDCl_3$) δ 59.0 (d, $^2J_{PP}$ = 39 Hz, **21**), 46.9 (d, $^2J_{PP}$ = 26 Hz, **21**), 46.4 (d, $^2J_{PP}$ = 35 Hz, **21**), 44.4 (s, **22**), 43.7 (d, $^2J_{PP}$ = 39 Hz, **21**), 42.6 (d, $^2J_{PP}$ = 35 Hz, **23**), 40.5 (d, $^2J_{PP}$ = 26 Hz, **21**). $^{13}C\{^1H\}$ NMR (C_6D_6): δ 308.6 (t, Ru*C*, $^2J_{PC}$ = 15 Hz), 292.7 (t, Ru*C*, $^2J_{PC}$ = 15 Hz). Solid-state $^{31}P\{^1H\}$ CP/MAS NMR (80.9 MHz): 61.5 (br, 1P), 55.8 (br, 1P), 51.2 (br, 2P), 49.2 (br, 2P), 41.5 (br, 1P), 37.0 (br, 1P). A new, unidentified species, **23**, (δ 46.4 (d, $^2J_{PP}$ = 35 Hz), 42.6 (d, $^2J_{PP}$ = 35 Hz)) is also present in $CDCl_3$, possibly owing to reaction with the solvent, as crystals of $Ru_2Cl_5(dcypb)_2$ (Chapter 3) form on prolonged reaction. IR (Nujol): ν(C=C) 1578 cm^{-1}. Anal. Calcd. for $C_{61}H_{112}Cl_4P_4Ru_2$ (**21**): C, 55.78; H, 8.60%. Found: C, 55.08; H, 8.33%. Crystals of **21** were obtained by layering a toluene solution with hexanes.

2.14.5. Decomposition of RuCl(dcypb)(μ-Cl)$_3$Ru(dcypb)[CHCHC(CH$_3$)$_2$] in $CDCl_3$

A sample containing a mixture of **21** and **22** (10 mg, 15.2 μmol Ru) was dissolved in $CDCl_3$ (0.75 mL) and the ^1H and $^{31}P\{^1H\}$ NMR spectra were recorded after 1 h which showed an approximate 1:1 ratio of **21**:**22**. The sample was heated to 60 C and the reaction monitored by ^1H and $^{31}P\{^1H\}$ NMR. Within 24 h, the ^{31}P NMR signals for **21** were no longer visible above the baseline, leaving only signals corresponding to **22** and **23**. ^1H NMR at this time showed the ratio of **21**:**22** to be 0.5:1. Also evident was an increase in intensity of the upfield peaks (at δ_H -1.8, -7.9 and -10.2) which at this point corresponded to approximately 10% of the total integrated intensity of the ^1H NMR spectrum (vs. < 5% immediately after dissolution). ^{31}P NMR analysis after 48 h showed a slight decrease in the amount of **23** (relative to **22**) while ^1H NMR showed the ratio of **21**:**22** to be 0.3:1. Slow evaporation deposited red crystals of **6**.

2.14.6. Loss in NMR signal for RuCl(dcypb)(μ-Cl)$_3$Ru(dcypb)[CHCHC(CH$_3$)$_2$]

An orange suspension of **5** (10.5 mg, 16.5 μmol) in THF (0.75 mL) was stirred under H_2 atmosphere for 5 minutes, following which KHB^{s}Bu$_3$ (16.5 μL of a 1.0 M solution in Et_2O) was added. A clear, slightly darker orange solution formed within minutes. NMR analysis after 1 h showed complete conversion to **14**. A solution of $RuCl_2(dmpe)_2$ in THF (0.75 mL of a 4.5 mM stock solution) was then added as internal standard; NMR analysis showed no reaction between the standard and **14**. Addition of 3-chloro-3-methyl-1-butyne (3.7 μL, 33 μmol) resulted in immediate darkening of the

solution to brown. NMR analysis showed complete conversion to **21/22**. $^{31}P\{^{1}H\}$ NMR showed a one-third loss of the original intensity for **21/22** after 48 h.

2.14.7. General Procedure for the Polymerization of Norbornene by 19, 20a, and 21/22

In a NMR tube was placed 201 μL of a stock solution of catalyst, prepared by dissolving 8.1 mmol of catalyst in 1 mL of the desired solvent. A solution of monomer, prepared by dissolving norbornene (34 mg, 225 equiv.) in 299 μL of solvent, was then added, and the reaction monitored by ^{1}H NMR.

2.14.8. Effect of Added TMSOTf

The polymerizations were carried out as above, with TMSOTf (1.6 μmol, 10 μL of a 0.16 M TMSOTf solution in the appropriate solvent) present in the solution of monomer. Final volume of monomer/TMSOTf solution: 299 μL.

2.14.9. Effect of Added $PhCHN_2$

The polymerizations were carried out as above, with $PhCHN_2$ (0.2 μL, 1.6 μmol) present in the solution of monomer. Final volume of monomer/$PhCHN_2$ solution: 299 μL.

2.15. Pincer Ligand Derivatives of Ruthenium

2.15.1. $RuCl(dcpx)PPh_3 \cdot PPh_3$ ($24 \cdot PPh_3$)

A green solution of $RuCl_2(PPh_3)_3$ (0.505 g, 0.53 mmol), dcpx (0.268 g, 0.54 mmol) and NEt_3 (1 mL, excess) in toluene (5 mL) was stirred for 18 h and then filtered through celite to remove precipitated $HNEt_3Cl$. Concentration to a green oil followed by addition of cold (-35 C) isopropanol (5 mL) afforded a green solid which was filtered off, washed with cold isopropanol (2 × 5 mL) and hexanes (3 × 5 mL) and dried under vacuum. Yield 0.478 g (79 %). The reaction is quantitative by $^{31}P\{^1H\}$ NMR however isolated yields are low owing to the high solubility of the complex. Both ^1H and $^{31}P\{^1H\}$ NMR show the presence of one equivalent of free triphenylphosphine, thus, the complex is formulated as a PPh_3 solvate (which is supported by repeated elemental analyses). ^1H NMR ($CDCl_3$): δ 7.0-8.2 (m, Ar, 30H), 6.79 (d, $CH_{meta}PCP$, $^3J_{HH}$ = 7.1 Hz, 2H), 6.68 (t, $CH_{para}PCP$, $^3J_{HH}$ = 7.2 Hz, 1H), 2.90 (dvt, ArC*H*HP, $^2J_{HH}$ = 16.7 Hz, $^v J_{HP}$ = 5.2 Hz, 2H), 2.55 (br d, ArCH*H*P, $^2J_{HH}$ = 12.2 Hz, 2H), 0.7-2.2 (br, Cy, 40H). $^{31}P\{^1H\}$ NMR ($CDCl_3$): δ 80.9 (t, PPh_3 bound, $^2J_{PP}$ = 32 Hz), 35.7 (d, dcpx, $^2J_{PP}$ = 32 Hz), -5.46 (s, PPh_3 solvate). Solid-state $^{31}P\{^1H\}$ CP/MAS NMR (80.9 MHz): 82.7 (br s, bound PPh_3), 34.1 (br s, dcpx), -6.1 (s, free PPh_3). Anal. Calcd. for $C_{68}H_{81}ClP_4Ru$ (i.e. $RuCl(dcpx)PPh_3 \cdot PPh_3$): C, 70.48; H, 7.05%. Found: C, 70.37, 70.94, 70.32; H, 7.02, 7.14, 7.11%. X-ray quality crystals of **24** were obtained by slow evaporation of an ether solution.

2.15.2. RuCl(dcpx)$(CO)_2$ (25)

A green solution of **24**•PPh_3 (0.083 g, 0.093 mmol) in benzene (5 mL) was placed under an atmosphere of CO and stirred. Within ~15 minutes the solution had become pale green to yellow in colour. After 24 h, the pale yellow solution was reduced to dryness. The yellow residue was redissolved in CH_2Cl_2 (~0.25 mL) and cooled to -35 C. Addition of cold Et_2O (-35 C, 1 mL) afforded a pale yellow solid which was filtered off, washed with cold Et_2O (-35 C, 3 × 1 mL) and dried under vacuum. Yield 0.056 g (88%). ^1H NMR ($CDCl_3$): δ 7.0 (m, Ar, 2H), 6.85 (m, Ar, 1H), 3.65 (m, CH_2, 2H), 3.35 (m, CH_2, 2H), 2.5 (m, aliphatic, 2H), 1.1-2.2 (br, aliphatic, 42H). $^{31}P\{^1H\}$ NMR ($CDCl_3$): δ 62.4 (s). $^{13}C\{^1H\}$ NMR ($CDCl_3$): δ 199.8 (t, $^2J_{CP}$ = 12 Hz, CO), 198.2 (t, $^2J_{CP}$ = 7 Hz, CO). IR (Nujol, cm^{-1}): ν(CO) 2018 (s), 1945 (s). Anal. Calcd. for $C_{56}H_{104}N_2Cl_4P_4Ru_2$: C, 59.04; H, 7.44%. Found: C, 59.16; H, 7.45%. X-ray quality crystals of **25** were obtained by slow evaporation of a benzene solution.

2.15.3. Reaction of RuCl(dcpx)PPh_3•PPh_3 with $PhCHN_2$ or terminal alkynes

A deep green solution of **24**•PPh_3 (10 mg, 8.6 μmol) in C_6D_6 was stirred as $PhCHN_2$ (1.2 μL, 12 μmol) or the desired acetylene was added (3,3-dimethyl-1-butyne: 5.3 μL, 43 μmol; 1,1-diphenyl-2-propyn-1-ol: 9 mg, 43 μmol). ^1H and $^{31}P\{^1H\}$ NMR analysis after 24 h showed only peaks due to starting materials. In the case of the reaction with $PhCHN_2$, both cis- and trans-stilbene were also evident by ^1H NMR.

2.15.4. RuH(dcpx)(PPh$_3$)(N$_2$) (26a/26b)

To a stirring, green solution of **24**•PPh$_3$ (150 mg, 0.13 mmol) in toluene (4 mL) was added KHB^{s}Bu$_3$ (135.9 μL of a 1.0 M solution in Et$_2$O). After 24 h, the solution had become red/brown in colour. Concentration to a red oil, followed by addition of isopropanol (3 mL), afforded a purple solid, which was filtered off, washed with isopropanol (3 × 1ml), and recrystallized from hexanes/isopropanol. Yield 100 mg (87%). ^{1}H NMR (C$_6$D$_6$): δ 7.96 (t, Ar, J_{HH} = 7.5 Hz, 3H), 7.50 (t, Ar, J_{HH} = 7.0 Hz, 3H), 7.34 (d, CH$_{meta}$PCP, $^3J_{HH}$ = 6.9 Hz, 2H), 7.24 (t, CH$_{para}$PCP, $^3J_{HH}$ = 6.9 Hz, 1H), 7.15 (t, Ar, J_{HH} = 7.2 Hz, 3H), 7.04 (m, Ar, 6H), 3.48 (d, ArC*H*HP, $^2J_{HH}$ = 14.9 Hz, 1H), 3.33 (d, ArC*H*HP, $^2J_{HH}$ = 14.9 Hz, 1H), 3.01 (br d, $^2J_{HH}$ = 16 Hz, 1H), 0.9-2.5 (br, Cy, 45H), -8.05 (dt, Ru*H*, **26a**, $^2J_{HP}$ = 21.8 Hz, $^2J_{HP}$ = 90 Hz). -12.2 (br s, Ru*H*, **26b**). ^{1}H NMR (C$_7$D$_8$, 253 K, partial): δ -12.2 (q, Ru*H*, **26b**, $^2J_{HP}$ = 19.5 Hz). Hydride T_1 (min) 333 msec (**26a**, 282 K, 500 MHz), 359 msec (**26b**, 278 K, 500 MHz). ^{31}P{^{1}H} NMR (C$_6$D$_6$): δ 59.6 (br s, dcpx, **26b**), 54.6 (d, dcpx, **26a**, $^2J_{PP}$ = 14 Hz), 45.0 (t, PPh$_3$, **26b**, $^2J_{PP}$ = 17 Hz), 28.8 (t, PPh$_3$, **26a**, $^2J_{PP}$ = 14 Hz). ^{31}P{^{1}H} NMR (C$_7$D$_8$, 253 K, partial): δ 59.2 (d, dcpx, **26b**, $^2J_{PP}$ = 17 Hz). IR (Nujol): ν(N$_2$) 2134 (m), ν(RuH) 2114 (m) cm^{-1}. Anal. Calcd. for C$_{50}$H$_{67}$N$_2$P$_3$Ru: C, 67.47; H, 7.59; N, 3.15%. Found: C, 67.56; H, 7.77; N, 0.14%. X-ray quality crystals of **27** were obtained by slow evaporation of a diethyl ether solution.

2.15.5. NMR-Scale Preparation of RuH(dcpx)(PPh$_3$)(H$_2$) (27a/27b)

A solution of **26a** and **26b**, generated by treating a C$_6$D$_6$ solution (~1 mL) of **24** (25 mg, 0.22 μmol) with KHB^{s}Bu$_3$ (43.1 μL of a 1.0 M solution in Et$_2$O), was placed

under an atmosphere of H_2. Within minutes, the originally red/brown solution had become yellow in colour and no starting material was spectroscopically observable. ^{1}H NMR (C_6D_6): δ -4.34 (br s, Ru*H*$_2$, **27b**), -7.08 (br s, Ru*H*$_2$, **27a**), -8.70 (q, Ru*H*, **27b**, $^2J_{HP}$ = 18.9 Hz), -10.64 (dt, Ru*H*, **27a**, $^2J_{HP,cis}$ = 21.7 Hz, $^2J_{HP,trans}$ = 80.1 Hz.) ^{31}P{^{1}H} NMR (C_6D_6): δ 71.1 (d, dcpx, $^2J_{PP}$ = 15 Hz, **27a**), 68.1 (d, dcpx, **27b**, $^2J_{PP}$ = 18 Hz), 56.6 (t, PPh_3, **27b**, $^2J_{PP}$ = 18 Hz), 37.1 (t, PPh_3, **27a**, $^2J_{PP}$ = 14 Hz). X-ray quality crystals of **27** were obtained by slow evaporation of a benzene solution.

2.15.6. Reaction of RuH(dcpx)(PPh_3)(N_2) with 3-chloro-3-methyl-1-butyne

To a stirring solution of **26a/b** (15 mg, 0.17 μmol) in C_6D_6 (0.75 mL), was added 3-chloro-3-methyl-1-butyne (19 μL, 1.7 μmol). The initially purple solution immediately became dark green. Both ^{1}H and ^{31}P{^{1}H} NMR analysis confirmed the quantitative conversion to RuCl(dcpx)(PPh_3) **24**.

2.15.7. $RuCl_2$(dcpx')(CHCHC(CH_3)$_2$) (28)

A brown suspension of $RuCl_2(PPh_3)_2$(CHCHC(CH_3)$_2$) (300 mg, 0.39 mmol) and dcpx (197 mg, 0.39 mmol) in benzene (10 mL) was stirred for 12 h over which time the solution phase became green in colour and a pink solid formed. The mixture was reduced to dryness leaving a dark green residue, which upon addition of ether (3 mL) afforded a pink solid suspended in a green supernatant. The solids were filtered off, washed with ether (5 × 1 mL) and hexanes (5 × 1 mL) and dried under vacuum. Yield 155 mg (54%). ^{1}H NMR ($CDCl_3$): δ 19.4 (d, RuC*H*, $^2J_{HH}$ = 11.6 Hz, 1H), 9.48 (s, agostic *ArH*, 1H), 8.13

(d, RuCHC*H*, $^2J_{HH}$ = 11.6 Hz, 1H), 7.42 (t, CH_{para}PCP, $^3J_{HH}$ = 7.6 Hz, 1H), 6.84 (d, CH_{meta}PCP, $^3J_{HH}$ = 5.7 Hz, 2H), 3.50 (br m, ArC*H*HP, 2H), 3.11 (br d, ArCH*H*P, $^2J_{HH}$ = 14.3 Hz, 2H), 1.30 (s, CH_3, 6H), 0.9-2.6 (br, Cy, 44H). $^{31}P\{^1H\}$ NMR ($CDCl_3$): δ 19.5 (s). $^{13}C\{^1H\}$ NMR ($CDCl_3$): δ. 301.3 (t, unresolved, Ru*C*). Anal. Calcd. for $C_{37}H_{60}Cl_2P_2Ru$: C, 60.15; H, 8.19%. Found: C, 59.79; H, 7.96%. X-ray quality crystals of **27** were obtained by slow evaporation of a toluene solution.

2.15.8. General Procedure for the Polymerization of Norbornene by 28 and 29

In a NMR tube was placed 201 μL of a stock solution of catalyst, prepared by dissolving 8.1 mmol of catalyst in 1 mL of the desired solvent. A solution of monomer, prepared by dissolving norbornene (34 mg, 225 equiv.) in 299 μL of solvent, was then added, and the reaction monitored by ^1H NMR.

2.15.9. Effect of Added TMSOTf

The polymerizations were carried out as above, with TMS-OTf (1.6 μmol, 10 μL of a 0.16 M TMSOTf solution in the appropriate solvent) present in the solution of monomer. Final volume of monomer/TMS-OTf solution: 299 μL.

2.15.10. General Procedure for Transfer Hydrogenation via Pincer Complexes

A suspension of catalyst (0.02 mmol) and KOH (2 mL, 0.2M *i*PrOH solution) in *i*PrOH (3 mL) was heated to reflux for 1 hour. To the resulting solution was added

benzophenenone (3.64 g, 20 mmol) in *i*PrOH (17 mL), and the mixture was then heated to reflux. The acetone formed was not distilled off. The reaction progress was monitored by removing aliquots for ^{1}H NMR analysis. When no pretreatment with KOH was performed, the catalyst and ketone were suspended in *i*PrOH (20 mL) and heated to reflux.

2.16. References

1) Molecular Simulations, I. *Cerius^2 Property Prediction*: San Diego, 1999.

2) Creary, X. *Organic Syntheses*; Wiley & Sons: Toronto, 1990; Vol. VII, pp 438.

3) Pouchert, C. J.; Behnke, J. *Aldrich Library of NMR Data*; 1 ed., 1993; Vol. 3.

4) Chau, D. E. K. Y. *M. Sc. Thesis*; University of British Columbia, 1992.

5) Priemer, H. *Ph. D. Thesis*; der Ruhr-Universitat Bochum, 1987.

6) Hallman, P. S.; Stephenson, T. A.; Wilkinson, G. *Inorg. Synth.* **1970**, *12*, 237.

7) Hoffman, P. R.; Caulton, K. G. *J. Am. Chem. Soc.* **1975**, *97*, 237.

8) Stephenson, T. A.; Wilkinson, G. *J. Inorg. Nuclear Chem.* **1966**, *28*, 945.

9) Bressan, M.; Rigo, P. *Inorg. Chem* **1975**, *14*, 2286.

10) Fogg, D. E.; Ph. D. Thesis, University of British Columbia: Vancouver, 1994.

11) Joshi, A. M.; Thorburn, I. S.; Rettig, S. J.; James, B. R. *Inorg. Chim. Acta* **1992**, *198-200*, 283.

12) Jung, C. W.; Garrou, P. E.; Hoffman, P. R.; Caulton, K. G. *Inorg. Chem.* **1984**, *23*, 726.

13) MacFarlane, K. S.; Thorburn, I. S.; Cyr, P. W.; Chau, D. E. K. Y.; Rettig, S. J.; James, B. R. *Inorg. Chim. Acta* **1998**, *270*, 130.

14) Snelgrove, J. L.; Fogg, D. E. *Unpublished results*.

15) Haaf, M.; Schmiedl, A.; Schmedake, T. A.; Powell, D. R.; Millevolte, A. J.; Denk, M.; West, R. *J. Am. Chem. Soc.* **1998**, *120*, 12714.

CHAPTER 3

Chlororuthenium Complexes of the Bulky, Electron-Rich Ligand Bis(dicyclohexyl)-1,4-phosphinobutane

3.1. Introduction

Enhanced catalytic activity is associated with use of electron-rich phosphine ligands in a range of reactions promoted by late transition metal complexes, including metathesis[1,2] and hydrogenation[3,4] catalysis. Efforts to date have focused on monodentate alkylphosphine derivatives:[1,2,5] despite the greater catalyst robustness commonly associated with chelating diphosphines, complexes of chelating alkylphosphines remain little explored in such chemistry, especially relative to the ubiquitous arylphosphine derivatives. With the intention of developing metathesis catalysts of general form $RuCl_2(PP)(CHR)$ (PP = chelating diphosphine), containing a sterically-defined coordination wedge at the metal, we pursued the synthesis of complexes containing large (seven-membered) chelate rings. 1,4-Bis(dicyclohexylphosphino)butane (dcypb) was chosen as a preliminary target, in view of the established correlation between phosphine basicity and increased catalyst activity.[1] This ligand system provides a convenient mimic for the monodentate PCy_3 ligands employed in the highly successful Grubbs catalyst systems. Throughout this thesis, the chemistry of this and related achiral phosphines was explored as a means of establishing

their behaviour, with incorporation of chirality being deferred to a later stage.

At the outset of this work, a single report had appeared in the literature on the use of this electron-rich, sterically demanding phosphine ligand (Figure 3. 1).[6] Highly insoluble, diphosphine-bridged $RuCl_2$(dcypb)(μ-dcypb)$RuCl_2$(dcypb) was obtained by treating $RuCl_2(PPh_3)_3$ with two equivalents of the diphosphine under an atmosphere of argon. Owing to its insolubility in all common organic solvents, the complex was not characterized by NMR methods. The mixed-phosphine complex $RuCl_2$(dcypb)(PPh_3) **3c** was observed on use of one equivalent of dcypb (CD_2Cl_2, Ar, -70 C),[6] but its very high solubility prevented isolation.

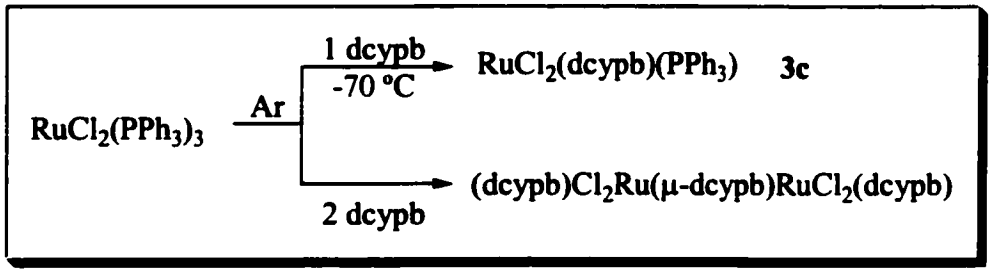

Figure 3. 1. Reaction of $RuCl_2(PPh_3)_3$ with dcypb in an Ar atmosphere.

Concurrent with this work, the Ru-allyl complex [κ^2P,P'-{(η^3-C_6H_8)CyP(CH_2)$_4$PCy_2}Ru(η^3-C_8H_{13})] was described. Multiple C-H activation results in a terdentate binding mode for the dcypb ligand, in which one of the cyclohexyl rings of the dcypb ligand functions as an η^3-allyl ligand.[7] Low yields (~30%), coupled with the limited reactivity of these allyl complexes precluded further exploration of this chemistry. In neither of the literature reports, therefore, is a precursor attained that provides a general, convenient entry point into dcypb chemistry. This chapter describes a high-yield route to such a precursor, the PPh_3-free system RuCl(dcypb)(μ-Cl)$_3$Ru(dcypb)(N_2). Also

described are insights into the decomposition pathways that have until now hindered the broader deployment of such systems.

3.2. Preparation and Characterization of $Ru_2Cl_4(dcypb)_2(N_2)$ (5)

In contrast to the reaction of $RuCl_2(PPh_3)_3$ with dcypb under Ar (vide supra), we found that reaction under a *nitrogen* atmosphere affords an efficient, high-yield route to $RuCl(dcypb)(\mu\text{-}Cl)_3Ru(dcypb)(N_2)$ **5** (Figure 3. 2). This net displacement of triphenylphosphine ligand by N_2 has no precedent in the corresponding aryldiphosphine chemistry, and is presumably driven by the low solubility of **5**. The identity of this species is confirmed by NMR and IR spectroscopy, and microanalysis. ^{31}P NMR analysis reveals four doublets for the inequivalent phosphine groups within **5**, in a pattern similar to that earlier reported[8,9] for dppb analogue **4a**. The ^{1}H NMR spectrum of **5** is less informative, consisting only of a series of overlapping multiplets between 0.7 and 3.1 ppm arising from the cyclohexyl protons and the methylene protons of the dcypb backbone. A strong infrared band for $\nu(N{\equiv}N)$ is evident at 2124 cm^{-1}.

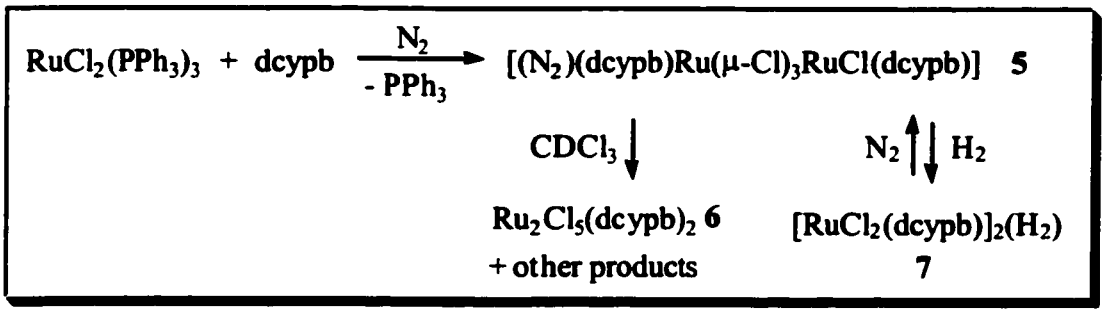

Figure 3. 2. Preparation of $[(N_2)Ru(dcypb)(\mu\text{-}Cl)_3RuCl(dcypb)]$ **5** and its reaction with $CDCl_3$ and H_2.

3.3. Reaction of 5 with Halogenated Solvents

Complex **5** shows low solubility in aromatic solvents (i.e. toluene and benzene) and non-halogenated solvents such as THF and diethyl ether, with limiting concentrations of ca. 1 mg/ml. Solubility is slightly improved in halogenated solvents such as CH_2Cl_2 or $CDCl_3$, but decomposition occurs in these solvents within hours of dissolution. Several distinct species are formed prior to conversion to Ru(III) products, as indicated by in situ ^{31}P NMR analysis prior to complete loss of the diamagnetic signals. One of the products, isolated by slow evaporation of $CDCl_3$ solutions under N_2, is identified (XRD) as the mixed-valence dimer RuCl(dcypb)(μ-Cl)$_3$RuCl(dcypb) **6**. Analogous arylphosphine species have been prepared in unrelated chemistry, involving reaction of chelating diphosphines with $RuCl_3(PR_3)_2$ (R = Ph, *p*-tolyl).[10] The molecular structure of **6** is shown in Figure 3. 3, with selected structural parameters in Table 3. 1.

3.3.1. Molecular Structure of RuCl(dcypb)(μ-Cl)$_3$RuCl(dcypb) (6)

Complex **6** adopts a triply chloride-bridged diruthenium structure, in which the coordination geometry at each metal center is distorted octahedral. The structure is unsymmetrical, with one of the octahedra being rotated by 120 about the Ru-Ru vector. A similar structure was earlier reported for $Ru_2Cl_5(P^nBu_3)_4$[8], whereas the only previous crystal structure of a chelating diphosphine derivative, $Ru_2Cl_5(chiraphos)_2$, exhibits a symmetrical ligand arrangement.[10] Ruthenium-phosphorus and -chloride distances fall within the ranges reported, as do angles within the Ru-P-Cl skeleton. Chloride atoms

trans to phosphorus display distinctly longer Ru-Cl bond distances (av 2.49 Å) compared to those trans to Cl (av 2.38 Å), as expected from the stronger trans influence of phosphine. The average bridging angle in **6** (83.7) is nearly 15 larger than the ideal value of 70.5 for two regular face-sharing octahedra[8], indicating that the Ru centers are further apart than expected for a regular cofacial bioctahedron. The Ru-Ru distance of 3.278 Å is considerably longer than the upper limit associated with the presence of a metal-metal bond (2.95 Å).[9] As with the chiraphos and the P^nBu_3 complexes, the crystallographic data do not permit assignment of formal oxidation states to the ruthenium atoms.

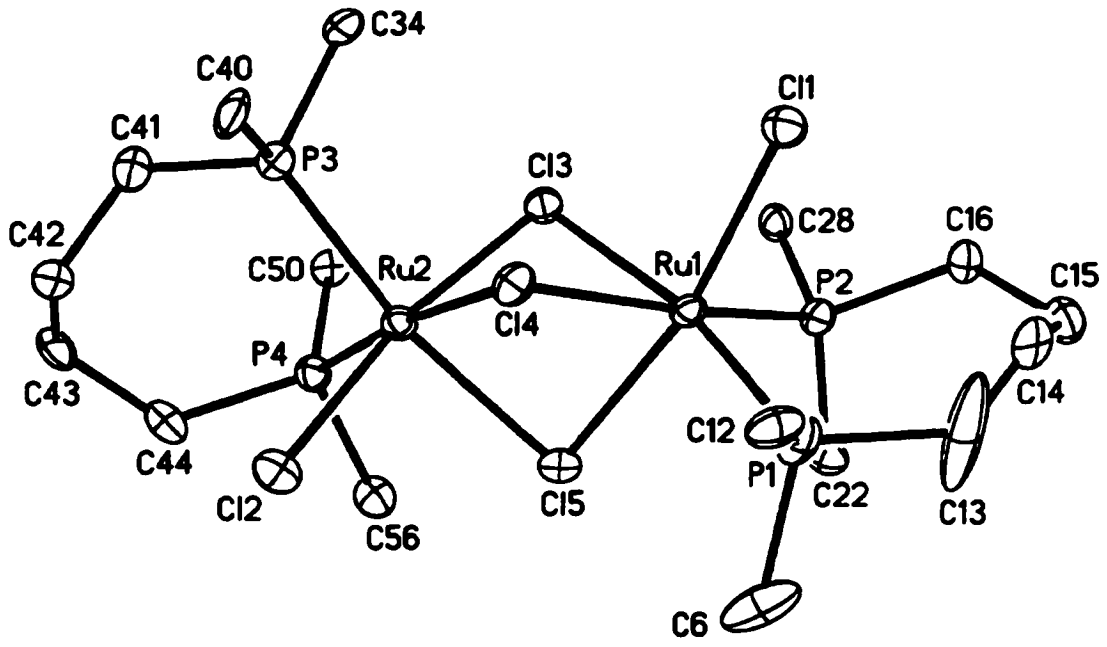

Figure 3. 3. ORTEP drawing of RuCl(dcypb)(μ-Cl)$_3$RuCl(dcypb) (**6**). Thermal ellipsoids depicted at 30% probability level; cyclohexyl rings (excluding C-*ipso*), hydrogen atoms, and solvent molecules omitted for clarity.

Table 3. 1. Selected Bond Lengths (Å) and Angles (deg) for **6**.

Ru(1)-P(1)	2.309(3)	Ru(2)-P(3)	2.323(2)
Ru(1)-P(2)	2.325(3)	Ru(2)-P(4)	2.348(3)
Ru(1)-Cl(5)	2.395(2)	Ru(2)-Cl(2)	2.360(3)
Ru(1)-Cl(1)	2.387(2)	Ru(2)-Cl(3)	2.373(2)
Ru(1)-Cl(3)	2.495(2)	Ru(2)-Cl(4)	2.466(2)
Ru(1)-Cl(4)	2.504(2)	Ru(2)-Cl(5)	2.505(2)
P(1)-Ru(1)-P(2)	95.14(9)	P(3)-Ru(2)-P(4)	93.75(9)
Cl(5)-Ru(1)-Cl(1)	168.81(8)	Cl(2)-Ru(2)-Cl(3)	168.58(9)
P(1)-Ru(1)-Cl(3)	169.32(9)	P(3)-Ru(2)-Cl(5)	168.60(9)
P(2)-Ru(1)-Cl(4)	172.19(9)	P(4)-Ru(2)-Cl(4)	173.97(9)

3.4. L-donor Exchange Reactions

In aromatic solvents, **5** is stable for weeks in solution under N_2. In contrast with $Ru_2Cl_4(dppb)_2(N_2)$, which exists in equilibrium with the "naked" dimer $[RuCl_2(dppb)]_2$ under N_2 (Figure 3. 4)[11] no peaks for $[RuCl_2(dcypb)]_2$ are observed.

$$Ru_2Cl_4(PP)_2(N_2) \rightleftharpoons Ru_2Cl_4(PP)_2 + N_2$$

Figure 3. 4. Equilibrium between N_2-coordinated dimers and "naked" dimers.

The lability of the dinitrogen ligand is indicated, however, by its facile replacement under H_2 or CO atmosphere, or in the presence of formaldehyde. Displacement of N_2 by dihydrogen is complete within 10 min at 1 atm H_2. The

transformation is accompanied by a 10-15 ppm downfield shift in the location of the ^{31}P NMR doublets associated with the "L-end" of the complex (Table 3. 2). ^{1}H NMR reveals a singlet for bound H_2 at -11.8 ppm; the T_1 (min) value of 26 msec (300 K, 500 MHz) corresponds to an H-H distance of 0.89 Å, assuming rapid rotation of the dihydrogen ligand. This compares well with the value of 0.86 Å reported for $Ru_2Cl_4(dppb)_2(H_2)$.[9] H_2-coordination is readily reversed within minutes of exposure to an N_2 atmosphere.

Table 3. 2. $^{31}P\{^{1}H\}$ NMR data for $Ru_2Cl_4(PP)_2(L)$ complexes.

Complex	Chemical shifts, δ (ppm)[a]	$^{2}J_{PP}$ (Hz)[a]
RuCl(dcypb)(μ-Cl)$_3$Ru(dcypb)(N_2) (**5**)	60.1 (d), 45.3 (d)	40
	49.1 (d), 37.4 (d)	26
RuCl(dppb)(μ-Cl)$_3$Ru(dppb)(N_2)[9]	54.4 (d), 53.5 (d)	45
	46.6 (d), 36.8 (d)	32
RuCl(dcypb)(μ-Cl)$_3$Ru(dcypb)(H_2) (**7**)	59.2 (d), 43.9 (d)	40
	65.1 (d), 45.9 (d)	25
RuCl(dcypb)(μ-Cl)$_3$Ru(dcypb)(CO) (**11**)	59.6 (d), 43.7 (d)	40
	50.4 (d), 43.0 (d)	23

[a] Measured at RT in C_6D_6; 121 MHz.

Reaction of **5** with gaseous formaldehyde, generated by heating paraformaldehyde at 180 C, affords monocarbonyl species RuCl(dcypb)(μ-Cl)$_3$Ru(dcypb)(CO) (**11**). Again, the transformation is readily monitored by $^{31}P\{^{1}H\}$ NMR. The IR spectrum of **11** exhibits a single ν(CO) band at 1940 cm^{-1} for terminally-bound CO. This is shifted to lower energy relative to the corresponding band in the dppb analog[12] (1977 cm^{-1}), as expected from the increased basicity of the dcypb ligand. Its

formulation as a monocarbonyl dimer is also supported by microanalysis.

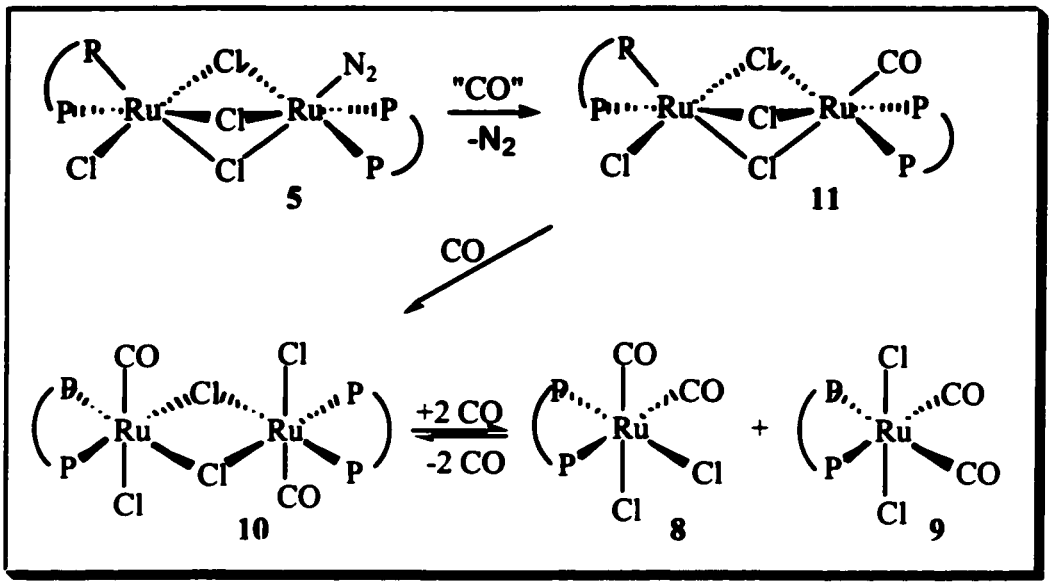

Figure 3. 5. Reaction of **5** with CO.

Under an atmosphere of CO, mononuclear $RuCl_2(dcypb)(CO)_2$ is formed as a mixture of *ccc* and *tcc* isomers (**8** and **9**, respectively; see Figure 3. 5). The two are readily distinguished by $^{31}P\{^1H\}$ NMR: the phosphine groups of all-cis **8** appear as a pair of doublets, whereas a singlet is found for *tcc*-**9**. Consistent with the proposed structures is the carbonyl region of the $^{13}C\{^1H\}$ NMR spectrum, which shows a triplet and a doublet of doublets for **8**, but only a doublet of doublets for **9**. Two infrared ν(CO) bands are seen for each complex.

X-ray quality crystals of **8** were obtained by slow evaporation of a benzene solution consisting almost entirely of **8** and **9**. More surprisingly, crystals of dinuclear, edge-bridged $RuCl(dcypb)(CO)(\mu\text{-}Cl)_2RuCl(dcypb)(CO)$ **10** (Figure 3. 5), were obtained from the same solution, over a period of about one month. Formation of **8** and **9** is thus

presumed to occur via this doubly-chloride bridged species. Attempts to access **10** in larger amounts via reaction of **5** with stoichiometric amounts of CO yielded only starting material and **8/9**. Our inability to arrest the reaction at the stage of **10**, or indeed to observe this species, suggests that formation and crystallization of this species may have been due to decarbonylation of **8/9** on prolonged storage. Consistent with this, symmetric dimers of the type $[RuX_2L_2(CO)]_2$ (X = Cl, Br, or I and L = PMe_2Ph) have been obtained via irradiation or degassing of solutions of all-*cis*-$[Ru(CO)_2X_2L_2]$.[13] These products are formed in a side reaction during isomerization of $RuX_2L_2(CO)_2$ via $RuX_2L_2(CO)$: where CO is lost from solution, the five-coordinate species readily dimerizes. The isomerization process was found to involve the dissociation of one CO molecule (for each mononuclear bis-CO complex). Partial loss of CO from solution was attributed to the formation of the highly insoluble symmetric dimers whose identities where assigned on the basis of elemental analyses (establishing an empirical formula of $[RuX_2L_2(CO)]$) and molecular weight determinations (which supported a dinuclear formulation). The dimers could also be prepared by bubbling N_2 through solutions of the all-cis mononuclear isomers. Loss of CO can also be induced by thermolysis, as suggested by a recent report[13] describing isolation of $[RuCl_2(dtbpe)(CO)]_2$ on refluxing $[RuCl_2(CO)_2]_2$ with dtbpe in ethanol. This species was also formed on heating mononuclear $RuCl_2(dtbpe)(CO)_2$ (mixture of *all*-cis and trans-CO isomers).

3.4.1. Molecular Structure of *ccc*-$RuCl_2(dcypb)(CO)_2$ (8)

The solid-state structure of *ccc*-$RuCl_2(dcypb)(CO)_2$ (**8**) is shown in Figure 3. 6, with relevant bond lengths and angles in Table 3. 3. The geometry at ruthenium is

distorted octahedral. Complex **8** represents a relatively rare example of a ruthenium(II) *bis*-carbonyl compound with cis-phosphines,[13] and only the second complex of this type to be characterized crystallographically.[13] The Ru-P distances within **8** are comparable to those reported for $[RuH(CO)_2(dtbpe)]^+BAr^F{}_4$.[13] The P-Ru-P angles are ca. 15 larger for **8** (100.50(3) , vs. an average of 86.21(7) for $[RuH(CO)_2(dtbpe)]^+BAr^F{}_4$), a manifestation of the increased flexibility of the four-carbon bridge. This flexibility also plays a part in the reaction chemistry of dcypb complexes (see Chapters 4, 5 and 6). The Ru-Cl(2) distance in **8** is similar to those reported for the bis-monophosphine complexes *cct*-$[RuCl_2(CO)_2(BzlPPh_2)_2]$ and all-*trans* $[RuCl_2(CO)_2(PBzl_3)_2]$.[14]

Bond lengths and angles involving Ru-Cl(1) and both Ru-CO moieties in **8** are meaningless, owing to disorder between Cl(1) and CO. A similar effect was observed in the related dichlorocarbonyl complex $[HP^tBu_2Me][Ru_2Cl_5(CO)_2(P^tBu_2Me)_2]$.[15] In the site identified as belonging to Cl(1) in Figure 3.5, the true occupancy is 66%, with the remaining electron density being found at the sites labeled CO(1') (18%) and CO(2') (16%). The presence of Cl(1) in the CO(1') position (i.e. trans to Cl(2), which is not disordered) implies that the *cct*-isomer is also represented in this structure.

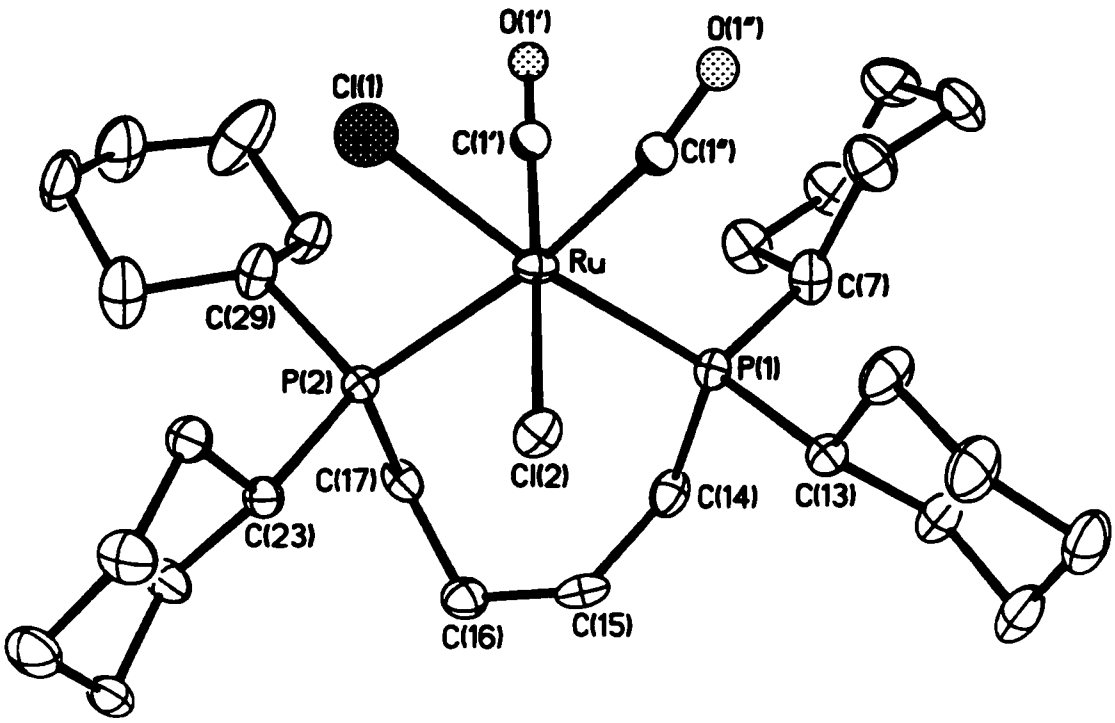

Figure 3. 6. ORTEP diagram for *ccc*-$RuCl_2(dcypb)(CO)_2$ (**8**). Thermal ellipsoids shown at 30% probability level. Solvate molecules and hydrogen atoms omitted for clarity.

Table 3. 3. Selected Bond Lengths (Å) and Angles (deg) for **8**.

Ru-P(1)	2.4101(9)	C(1)-O(1)	1.149(2)
Ru-P(2)	2.4825(9)	C(1')-O(1')	1.1347(19)
Ru-C(1)	1.901(2)	C(1")-O(1")	1.1437(19)
Ru-C(1')	1.8837(19)	Ru-Cl(1)	2.3948(16)
Ru-C(1")	1.8977(19)	Ru-Cl(2)	2.4360(9)
P(1)-Ru-Cl(1)	171.92(5)	C(1')-Ru-C(1")	87.7(3)
P(2)-Ru-C(1")	170.7(2)	Cl(1)-Ru-Cl(2)	90.87(5)
Cl(2)-Ru-C(1')	175.44(19)	Ru-C(1')-O(1')	174.3(5)
P(1)-Ru-P(2)	100.52(3)	Ru-C(1")-O(1")	170.5(6)

3.4.2. Molecular Structure of $Ru_2Cl_4(dcypb)_2(CO)_2$ (10)

The molecular structure of the symmetrical, doubly-chloride-bridged dimer $RuCl(dcypb)(CO)(\mu\text{-}Cl)_2RuCl(dcypb)(CO)$ (**10**) is shown in Figure 3. 7, with relevant bond lengths and angles in Table 3. 4. This edge-bridged motif is far less common than the ubiquitous face-sharing bioctahedral geometry.[16] Examples of other such crystallographically characterized structures include $Ru_2Cl_4(CO)_2L_2$ (L = 1, 10-phenanthroline or di(2-pyridyl) ketone).[7,17] Bridging Ru-Cl bond distances in all three structures are comparable, although the steric pressure exerted by the bulky dcypb ligand increases bridging Ru-Cl-Ru angles in **10** (99.09(4) , vs. 96.6(1) for the phenanthroline complex, and 94.89(4) for the di(2-pyridyl) ketone derivative). The average bridging angle in the trichloro-bridged structure of **6** (section 4.3.1) is much more acute 83.71(7) . This approximate 15 difference reflects the more compact nature of the face-sharing structure. Disorder between carbonyl and terminal chloride (CO, Cl(1)) in **10** is again present, as noted above for **8**, and no quantitative information can be gleaned from the bond lengths or angles of these fragments. The predominantly chloride site shown in Figure 3.6 has a true occupancy of 70% Cl.

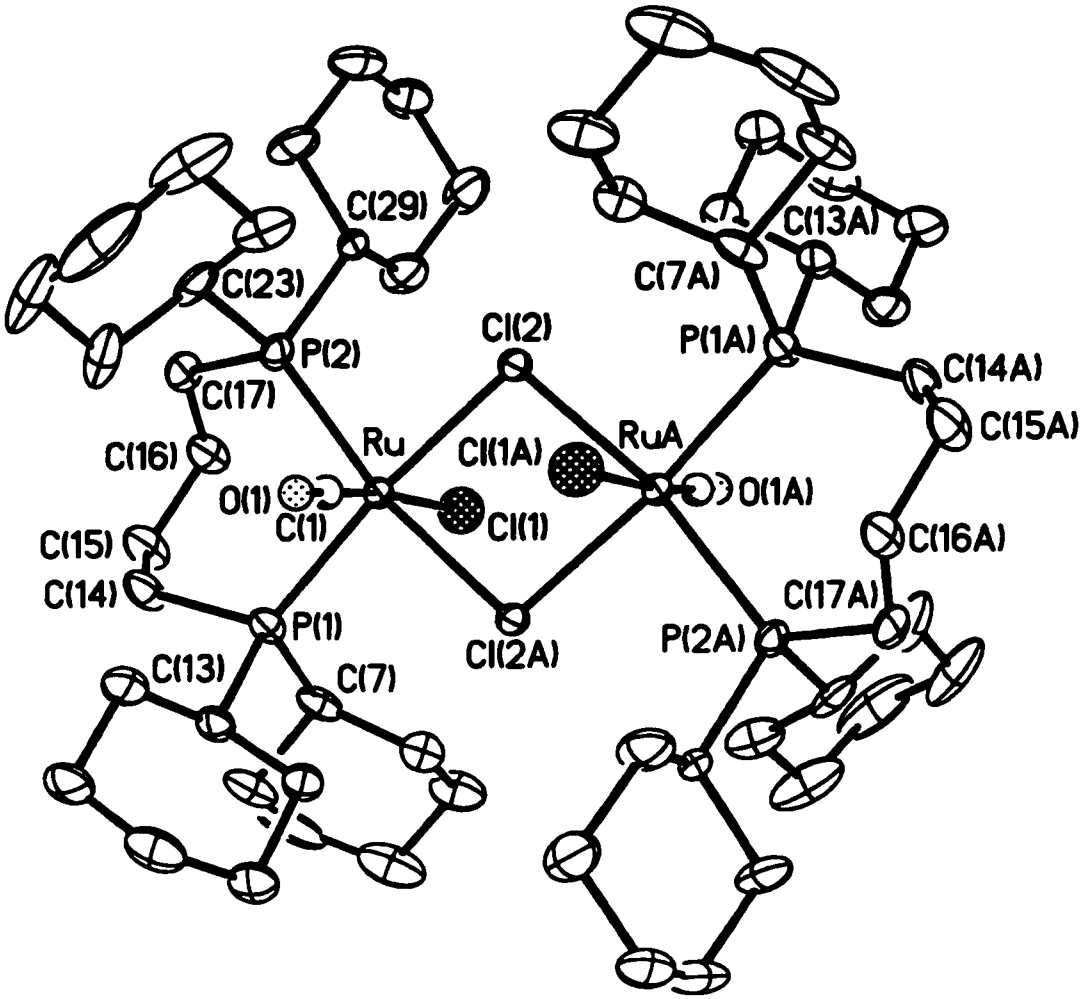

Figure 3. 7. ORTEP diagram for RuCl(dcypb)(CO)(μ-Cl)$_2$RuCl(dcypb)(CO) (**10**). Thermal ellipsoids shown at 30% probability level. Hydrogen atoms omitted for clarity.

Noteworthy in the structure of **10** is the proximity of C(16) to the metal center (Ru(1)-C(16) = 3.827(6) Å). This "folding-in" of the backbone toward the metal illustrates the flexibility of the four-carbon bridged dcypb ligand, and the mutual access between the diphosphine backbone and the metal center. Backbone activation has been observed in related silylene species (Chapter 5); for more subtle consequences of this

flexibility, see Chapter 6.

Table 3. 4. Selected Bond Lengths (Å) and Angles (deg) for **10**.

Ru-P(1)	2.3330(14)	Ru-Cl(2)	2.4630(12)
Ru-P(2)	2.3648(13)	Ru-C(1)	1.789(5)
Ru-Cl(1)	2.4741(19)	C(1)-O(1)	1.146(4)
P(1)-Ru-Cl(2)	173.27(5)	Cl(2)-Ru-Cl(2A)	80.88(4)
P(2)-Ru-Cl(2A)	168.79(4)	Ru-Cl(2)-Ru(A)	99.12(4)
Cl(1)-Ru-C(1)	172.6(2)	Ru-C(1)-O(1)	175.9(6)
P(1)-Ru-P(2)	98.63(5)		

3.5. Decomposition of 5 *in vacuo*

Surprisingly, in view of the observed lability of the dinitrogen ligand in **5**, no signals for a "naked" dimer were evident even under Ar atmosphere, or following freeze-pump-thaw (FPT) experiments carried out to shift the presumed equilibrium (Figure 3. 4) to the right. Sustained gas evolution was observed in NMR tubes (C_6D_6) subjected to successive FPT cycles (> 20), but no new peaks were evident by $^{31}P\{^1H\}$ NMR, even at low temperature (183 K). Degassing experiments using *trans*-$RuCl_2(dppe)_2$ as internal standard were carried out in Schlenk vessels, in which the higher surface area permitted more efficient removal of dissolved gas. A steady decrease in concentration of **5** is measured with increasing number of FPT cycles (Figure 3. 8), signifying conversion of **5** to a paramagnetic Ru product. Gas evolution is sustained after complete loss of the NMR signals, probably owing to paramagnetic broadening of signals for remaining **5**.

Observation of a large ^1H NMR singlet for dissolved H_2 at 4.2 ppm after each FPT cycle is consistent with Ru-promoted dehydrogenation of the cyclohexyl rings and/or the dcypb backbone (catalytic dehydrogenation of the solvent itself is excluded by observation of this behavior in benzene solvent). A C=C stretching band appears at 1629 cm^{-1} in the infrared spectrum, as well as a signal at 1944 cm^{-1} assigned to Ru-H. No HCl was detected by GC-MS, and no precipitate formed on forcing the effluent gas through concentrated ammonia or NH_4PF_6 solutions, suggesting that HCl is not evolved in the reaction.

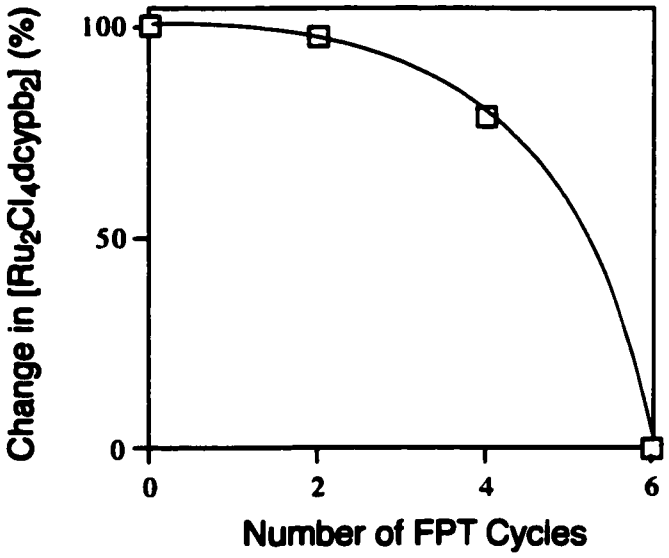

Figure 3. 8. Plot of % Change in **5** (relative to internal standard) versus number of FPT Cycles (when carried out in a Schlenk Flask).

The utility of closely related Ru complexes in catalytic dehydrogenation of sp^3 C-H bonds has been established by Leitner and coworkers.[18-20] While forcing conditions were required for activation of cyclooctane, dehydrogenation of the cyclohexyl rings

within complexes containing chelating $Cy_2P(CH_2)_nPCy_2$ (n = 3, 4) was induced at 50 C, resulting in diamagnetic η^3-cyclohexenyl derivatives. Chaudret has likewise described intramolecular dehydrogenation of cyclohexyl rings within Ru-PCy_3 complexes at RT, affording Ru(II) complexes containing η^3- and/or η^2-cyclohexenyl rings.[21] A related process is almost certainly involved in dehydrogenation of **5**, in which retention of both chloride ligands may be responsible for formation of a Ru(III) product. The possibility of concomitant attack on the four-carbon backbone cannot be excluded; agostic interactions between Ru and bound dppb, culminating in deuterium incorporation into the backbone methylene groups, have been noted[9], while Chapter 5 describes C-H bond activation within the dcypb backbone in related silylene chemistry. Confirmation of the identity of the dehydrogenation product(s) is hampered by paramagnetism and poor crystallinity. Attempts to probe the reaction by thermal gravimetric analysis are complicated by the observation of other, diamagnetic, products in solid-state degassing experiments. The high activity of these species toward activation of saturated C-H bonds under exceptionally mild conditions is notable, however. Facile intramolecular attack may be attributed to the combination of steric bulk and high basicity in the dcypb ligand. The ease of such reactions in the absence of stabilizing donor ligands accounts for prior difficulties in gaining access to this chemistry under Ar atmosphere. Use of N_2 as a labile donor to inhibit intramolecular attack opens up a potentially rich catalytic and coordination chemistry.

3.6. Conclusions

The foregoing describes the first general route into the chemistry of chlororuthenium phosphine complexes containing the basic, bulky diphosphine dcypb. Use of N_2 as a stabilizing ligand overcomes the problems of solubility and stability that previously limited development of this chemistry. Dinitrogen is unique as a placeholder ligand in providing a labile, innocuous donor that does not permit undesired reaction pathways, and does not contaminate the product. Dinuclear RuCl(dcypb)(μ-Cl)$_3$Ru(dcypb)(N_2) **5** thus provides an attractive entry point into dcypb chemistry. The H_2 adduct is analogous to that described for dppb and binap,[22] with significantly amplified ligand basicity, which has been exploited by Samantha Drouin of this group to develop highly active hydrogenation catalysts. The CO reaction chemistry, in comparison, yields dinuclear species unattainable in the corresponding aryl-diphosphine systems.[22] While steric pressure allied with high electron density renders these species susceptible to decomposition by attack on solvent or on the dcypb ligands, restraint of such process permits us to redirect this heightened reactivity and exploit it in catalysis, as exemplified in the potent ROMP activity of the alkylidene derivative (Chapter 4).

3.7. References

1) Dias, E. L.; Nguyen, S. T.; Grubbs, R. H. *J. Am. Chem. Soc.* **1997**, *119*, 3887.

2) Schwab, P.; Grubbs, R. H.; Ziller, J. W. *J. Am. Chem. Soc.* **1996**, *118*, 100.

3) McManus, N. T.; Rempel, G. L. *J. Macromol. Sci., Rev. Macromol. Chem. Phys.* **1995**, *C35*, 239.

4) Burk, M.; Martinez, J. P.; Feaster, J. E.; Cosford, N. *Tetrahedron* **1994**, *50*, 4399.

5) Dias, E. L.; Grubbs, R. H. *Organometallics* **1998**, *17*, 2758.

6) MacFarlane, K. S.; Joshi, A. M.; Rettig, S. J.; James, B. R. *Inorg. Chem.* **1996**, *35*, 7304-7310.

7) Six, C.; Gabor, B.; Gorls, H.; Mynott, R.; Philipps, P.; Leitner, W. *Organometallics* **1999**, *18*, 3316.

8) Thorburn, I. S.; Rettig, S. J.; James, B. R. *Inorg. Chem.* **1986**, *25*, 234, and references therein.

9) Joshi, A. M.; Thorburn, I. S.; Rettig, S. J.; James, B. R. *Inorg. Chim. Acta* **1992**, *198-200*, 283.

10) Chioccala, G.; Daly, J. J. *J. Chem. Soc. A* **1968**, 1981.

11) Joshi, A. M.; James, B. R. *J. Chem. Soc., Chem. Commun.* **1989**, 1785.

12) Barnard, C. F. J.; Daniels, J. A.; Jeffery, J.; Mawby, R. J. *J. Chem. Soc. Dalton Trans.* **1976**, 953.

13) Gottschalk-Gaudig, T.; Folting, K.; Caulton, K. G. *Inorg. Chem.* **1999**, *38*, 5241.

14) Wilkes, L. M.; Nelson, J. H.; Mitchener, J. P.; Babich, M. W.; Riley, W. C.; Helland, B. J.; Jacobson, R. A.; Cheng, M. Y.; Seff, K.; McCusker, L. *Inorg. Chem.* **1982**, *21*, 1376.

15) Huang, D.; Folting, K.; Caulton, K. G. *Inorg. Chem.* **1996**, 7035.

16) Deacon, G. B.; Kepert, C. M.; Sahely, N.; Skelton, B. W.; Spiccia, L.; Thomas, N. C.; White, A. H. *J. Chem. Soc. Dalton Trans.* **1999**, 275.

17) Leitner, W.; Six, C. *Chem. Ber.* **1997**, *130*, 555.

18) Sabo-Etienne, S.; Chaudret, B. *Coord. Chem. Rev.* **1998**, *178-180*, 381.

19) Chaudret, B.; Dagnac, P.; Labroue, D.; Sabo-Etienne, S. *New J. Chem.* **1996**, *20*, 1137.

20) Christ, M. L.; Sabo-Etienne, S.; Chaudret, B. *Organometallics* **1995**, *14*, 1082.

21) Ogasawara, M.; Saburi, M. *Organometallics* **1994**, *13*, 1911.

22) MacFarlane, K. S.; Ph. D. Thesis, University of British Columbia: Vancouver, 1995.

CHAPTER 4

Ring-Opening Metathesis Polymerization via Ruthenium Precursors

4.1. Introduction

Among the catalysts in use for olefin metathesis, ruthenium complexes of monodentate phosphines have attained a high profile, owing to their robustness and functional group tolerance. Recent efforts directed at diversifying the Ru ligand scaffold have led to complexes containing bidentate Schiff base ligands,[1] allylic groups,[2] Wanzlick-Arduengo carbenes,[3-6] hydridotris(pyrazolyl)borate, Cp and Cp*.[7] Wholly neglected, at the time this work commenced, were Ru alkylidene catalysts containing chelating diphosphine ligands. The potential scope of such systems, which afford a direct extension of the exceptionally diverse metathesis chemistry of Grubbs' catalyst $RuCl_2(PR_3)_2(CHR')$ (**1a**, R=Cy; **1b**, R=Ph),[8] is underlined by the plethora of readily accessible chelating diphosphines, including chiral versions, that have been used to remarkable effect in asymmetric catalysis. Ru ROMP lags far behind Mo-catalyzed ROMP in terms of definition of the active site (the ultimate expression of which is stereocontrolled ROMP or asymmetric RCM). By incorporating chelating diphosphines into the ligand set of Ru-alkylidene complexes, we hoped to develop routes into catalysts that integrated high catalyst selectivity with the functional-group tolerance of late-metal systems.

Prior neglect of this potentially rich area stems in part from the well-established requirement for phosphine loss in ROMP via catalysts of type **1**,[9] reinforced in the early stages of our investigations by a report describing the complete inactivity of $R_2P(CH_2)_2PR_2$ (R = Ph, Pr^i) ligands[10] within the $Ru_2Cl_4(arene)_2$/$TMSCHN_2$ system. The latter result, however, is almost certainly an artifact of the in situ catalyst synthesis. The overwhelming tendency of phosphines affording five-membered Ru chelates to disproportionate into well-characterized, very unreactive $RuCl_2(PP)_2$ species, has been described in exchange reactions with $RuCl_2(PPh_3)_3$[11] and $Ru_2Cl_4(arene)_2$.[12]

This Chapter describes the in situ synthesis and deployment of a family of highly active ROMP catalysts of the type $RuCl_2(PP)(CHR)$ **2**, in which the diphosphine ligand forms a seven-membered chelate ring (PP = dppb, **2a**; binap, **2b**; dcypb, **2c**). These complexes exhibit high polymerization activity without phosphine or halide abstraction, and afford polymers characterized by very low polydispersities. Their high reactivity prevents isolation, and hampers in situ observation, owing to the facility of decomposition pathways elucidated in Chapter 6. In closely related systems concurrently developed by Hofmann et al.[13-16] (see also later work by Werner[17]) the diphosphine ligands contain one- or two-carbon backbones (PP = bis(di-*tert*-butylphosphino)methane, dtbpm, **2d**; bis(di-*tert*-butylphosphino)ethane, dtbpe). Crystallographic analysis of these rigid chelate complexes reveals that the alkylidene ligand occupies the axial position within a square pyramidal geometry (Figure 4. 1). This geometry is characteristic of five-coordinate ruthenium alkylidene complexes, and is attributed to the high trans influence of the alkylidene ligand.[18-20] This orientation constrains incoming monomer to bind trans to alkylidene, and ligand abstraction is therefore required for high activity. The higher

flexibility of the seven-membered chelates **2a-c**, which affords access to the rare "apical phosphine" isomer, emerges as key to their activity in the absence of ligand abstraction.

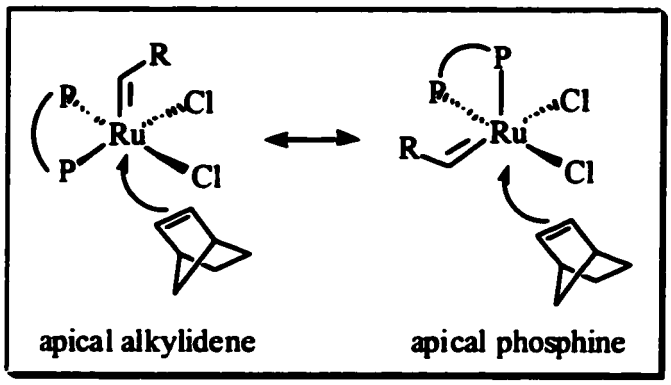

Figure 4. 1. Possible orientations for alkylidene moiety in square pyramidal geometry.

4.2. Synthesis of Diazoalkanes

A common method for installation of alkylidene at ruthenium involves the reaction of suitable precursor complexes with diazoalkanes.[8] Liberation of dinitrogen is accompanied by formation of the ruthenium alkylidene (Figure 4. 4). The preferred diazoalkane for catalyst systems of ruthenium is phenyldiazomethane, because of the increased rate of initiation of benzylidene relative to other alkylidenes.[8] The preparation of phenyldiazomethane, following established procedures, was thus undertaken.[21] It was found that while the yields were in accord with those reported (50 - 60%), the inclusion of an impurity in the product could not be avoided. The impurity, determined to be *t,t*-benzaldehyde azine (Ph(H)C=N-N=C(H)Ph), could not be removed owing to the instability of the diazoalkane. It should also be noted that decomposition of phenyldiazomethane to the olefin coupling products cis- or trans-stilbene is appreciable

with several days of storage and as a result, the diazoalkane was only used when freshly prepared.

In an effort to circumvent the instability of the benzylidene derivatives **2a-c** (vide infra), other diazoalkanes were also prepared, in the hope that these would afford less reactive alkylidene entities. Figure 4. 2 summarizes the various diazoalkanes examined (other than phenyldiazomethane), which we sought to incorporate into systems of type **2**. Others[8] have examined in detail the effects of the alkylidene moiety on metathesis and it was found that while none compared with the benzylidene derivative in terms of activity, the diphenyl-substituted vinylalkylidene (derived from **i**) gave rise to more stable alkylidene complexes. In light of this, the diphenyl-substituted vinyldiazoalkane **i** was prepared. The 1- and 2-naphthyldiazoalkanes (**ii** and **iii** respectively) were also prepared, with the intention of evaluating the effect of increased alkylidene bulk. Trimethylsilyldiazomethane, **iv**, was also examined as an alkylidene source, as some success has been reported on use of this reagent.[22]

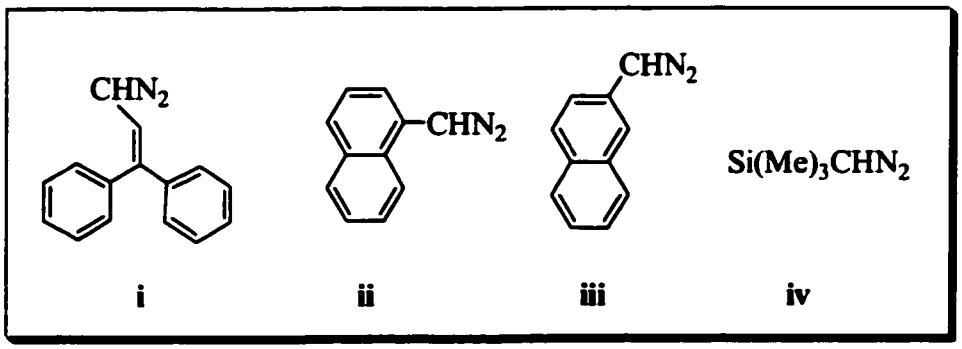

Figure 4. 2. Structures of the diazoalkanes employed.

Following established procedures, 1-napthaldehyde, 2-napthaldehyde, and β-phenylcinnamaldehyde ($(C_6H_5)_2C$=CHCHO) were converted into diazoalkane derivatives via the corresponding aldehydes (Figure 4. 3).[21] Use of **i** according to this chemistry proves a much more efficient route to diphenylvinylalkylidene than that previously reported[23] via 3,3-diphenylcyclopropene, the synthesis of which requires several difficult steps.[24] Trimethylsilyldiazomethane was not prepared, but was used as the commercially available solution in hexanes.

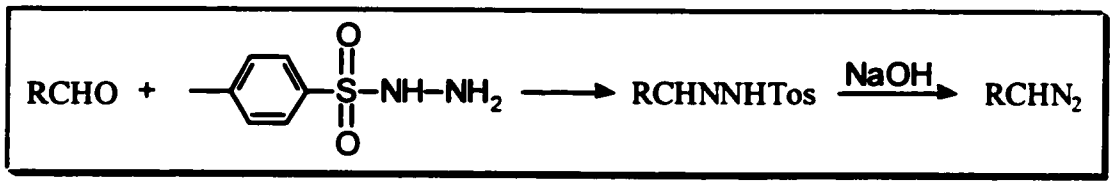

Figure 4. 3. General scheme for the preparation of diazoalkanes.

Despite the variations in the steric and electronic nature of the diazoalkanes, stable ruthenium-alkylidenes could not be derived from any of these compounds. Evidently the instability of the alkylidene complexes formed is such that a minor change in the steric or electronic nature of the alkylidene fragment can not curb their decomposition. Very likely, the same flexibility of these systems which allows for high ROMP activity without ligand abstraction, also results in a decreased stability. Use of a ruthenium-hydride species as a synthon for hydride provides access to more stable vinylalkylidene derivatives. Given the instability of the diphenylvinylalkylidene derivatives discussed above, the stability of the vinylalkylidenes (Chapter 6) may in fact be due to the greater stabilty of the alkyne precursors (used to install the alkylidene) versus diazoalkanes. These reactions are discussed in Chapter 6.

4.3. In situ Generation of Ruthenium Alkylidene Complexes

Probe experiments carried out with dppb complex $RuCl_2(dppb)(PPh_3)$ (**3a**) in the absence of monomer exhibit immediate and vigorous evolution of N_2 on addition of $PhCHN_2$, and ^1H NMR analysis shows an alkylidene signal at ca. 19 ppm, as expected for a complex of type $RuCl_2(PP)(CHPh)$ **2** (Figure 4. 4).[13,14]

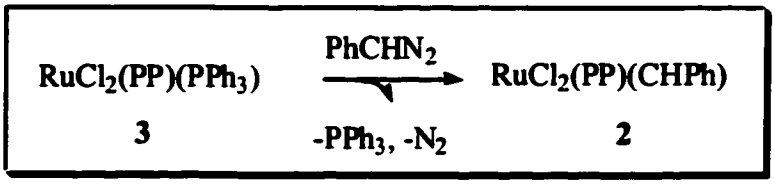

Figure 4. 4. General reaction of mixed-phosphine complexes with phenyldiazomethane.

In contrast to both **1** and **2d**, the phosphine ligands are unsymmetrically disposed about the metal center, as evidenced by the appearance of two doublets in the ^{31}P NMR spectrum, in place of the usual singlet.[8,13,14] This pattern is consistent with structure **2a** (Figure 4. 5). While crystallographic confirmation was frustrated by decomposition of the samples in solution, the MSI Cerius^2 (OFF optimized geometry)[25] structure supports this model for both dppb and dcypb: a distorted square-pyramidal geometry is found, with the alkylidene occupying a site trans to chloride, and one end of the diphosphine ligand in the axial position. An alternative structure with axial chloride is ca. 10 kcal/mol higher in energy, consistent with the higher trans effect of phosphine vs. chloride. Computationally and crystallographically-derived structures for **2d**, in comparison, place the alkylidene in the axial site (Figure 4. 5), consistent with both crystallographic and ^{31}P NMR

evidence.[13-15] The difference in orientation of the diphosphines is attributed to the differing flexibility of the four-carbon bridge relative to the single-carbon bridge.

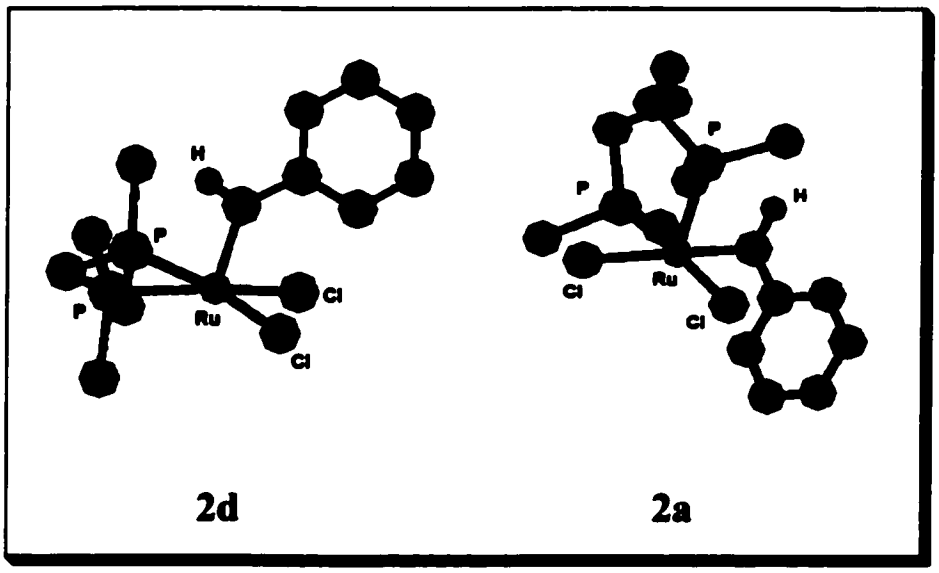

Figure 4. 5 Minimum energy structures of $RuCl_2(PP)(CHR)$ (**2d** PP = dtbpm; **2a**, PP = dppb), calculated using MSI Cerius[2] (OFF optimized geometry).[25] Phosphine phenyl and *tert*-butyl groups are abbreviated to a single carbon for clarity.

4.4. ROMP via Alkylidene Complexes Generated in situ

Complexes **2a-c** act as highly efficient ROMP initiators for the polymerization of norbornene in $CDCl_3$ (Figure 4. 6. and 4. 7). The turnover frequency of 2400 h^{-1} observed for dcypb system **5**/$PhCHN_2$ compares with figures of 60 h^{-1} for **2d**,[13] and 150 h^{-1} for **1b**,[8] while ROMP of norbornene (100 equiv.) by **1a** is complete within seconds.[8] The higher activity observed for the seven membered chelate complexes (**2a-c**) relative to **2d** is certainly due to the orientation of the alkylidene (Figure 4. 1 and 4. 5) which, in **2a-**

c, provides substrate direct access to the alkylidene moiety without ligand abstraction. In the case of **2d**, chloride abstraction is required to achieve high activity.

Initially erratic kinetic behavior observed for in situ NMR experiments with **2a-c** was traced to problems of diffusion control introduced by rapid increases in viscosity: removal of the NMR tube from the probe and shaking the sample results in temporary increases in the rate curve, which drop off again as ROMP is continued without agitation. Reproducible, well-behaved kinetics were obtained on carrying out polymerizations with continual stirring in the drybox, and monitoring the progress of the reaction by removing aliquots for NMR analysis.

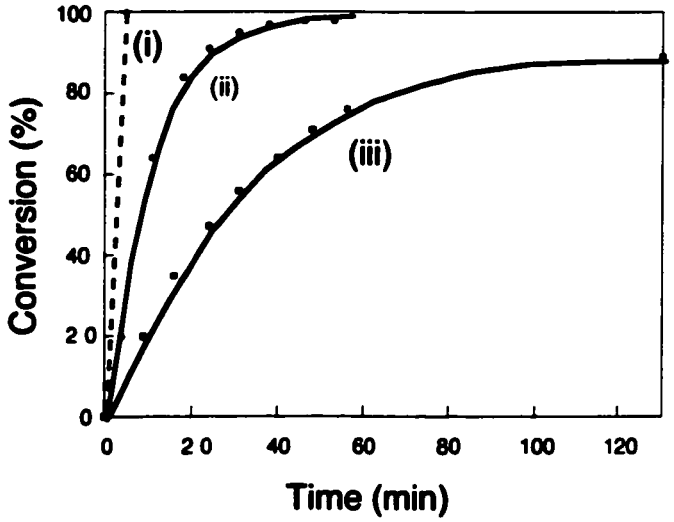

Figure 4. 6. ROMP activity of dcypb complexes. (i) **5** + 2eq $PhCHN_2$; $CDCl_3$-C_6D_6, (ii) **3c** + 2eq $PhCHN_2$; $CDCl_3$-C_6D_6, (iii) **5** + 2eq $PhCHN_2$; C_6D_6.

4.4.1. Effect of Solvent on ROMP Activity

The susceptibility of RuCl(dcypb)(μ-Cl)$_3$Ru(dcypb)(N_2) (**5**) to decomposition by chlorinated solvent was discussed in Chapter 3. Despite the probable reactivity of the electron-rich dcypb complex **2c** toward $CDCl_3$, the low ROMP activity found in C_6D_6 (Figure 4. 6) prompted us to investigate the utility of mixed solvent systems. With the intention of minimizing catalyst decomposition prior to metathesis, the catalyts were generated in C_6D_6 and subsequently added to a $CDCl_3$ solution of norbornene. ROMP activity increased dramatically, consistent with previously noted correlations between metathesis activity and solvent polarity.[9] Polymer polydispersities for reactions in benzene were also significantly higher than those observed in the mixed solvent systems (PDI 3.8, vs. 1.2-1.4), possibly because the slow rate of metathesis in neat benzene permits competing decomposition. In contrast, the very rapid rate of polymerization evident in $CDCl_3$ (curve (i)) indicates that decomposition of **2c** cannot compete with norbornene metathesis in this solvent, and this is supported by the low polydispersity obtained. Decomposition via extrusion of the alkylidene as stilbene is characteristic of all Ru alkylidene complexes, including Grubbs' catalyst **1a**. Observation of a bimodal molecular weight distribution for the reaction in benzene is consistent with the presence of more than one ROMP-active species, perhaps indicating that decomposition occurs in a two-step process, via a metathesis-active alkylidene intermediate. Indeed, this is consistent with our investigations of catalyst decomposition processes, described in Chapter 6.

4.4.2. Effect of Phosphine Bulk and Basicity on ROMP Activity

Rates of polymerization via **2a-c** are strongly dependent on phosphine bulk and basicity as in the monodentate systems of type **1** (Figure 4. 7.).[8,9] Thus, the strongly basic dcypb catalyst systems were most active in the series examined. The decreased reactivity of the binap system (**3b**/$PhCHN_2$) is expected on the basis of the greater bulk and rigidity of this ligand. This result was of particular interest for its potential control over polymer microstructure. It yields a notably low proportion of trans-olefinic linkages for Ru-catalyzed ROMP: the found value of 68% is the lowest in the systems under investigation, and represents a drop of 22% relative to that obtained with **1b** (R=Ph).[8] (It should be noted that systems of Os have recently been described which produce polynorbornene with a ca. 60% cis olefin content.[26]) Unlike early-metal catalysts, which give preferentially cis-olefins, virtually all Ru ROMP systems yield *principally* trans-linkages (though at least 10% cis-olefin is invariably obtained). We attribute this phenomenon to the larger size of the late metal, and the low degree of steric definition characteristic of existing Ru catalysts, which accommodates expression of the steric preference of the growing chain. The lower proportion of trans-olefin in poly(norbornene) prepared via $RuCl_2$(binap)(PPh_3) **3b** is consistent with increased spatial definition of the active site, which, until now, has not been achieved in well-defined ruthenium metathesis catalyst systems.

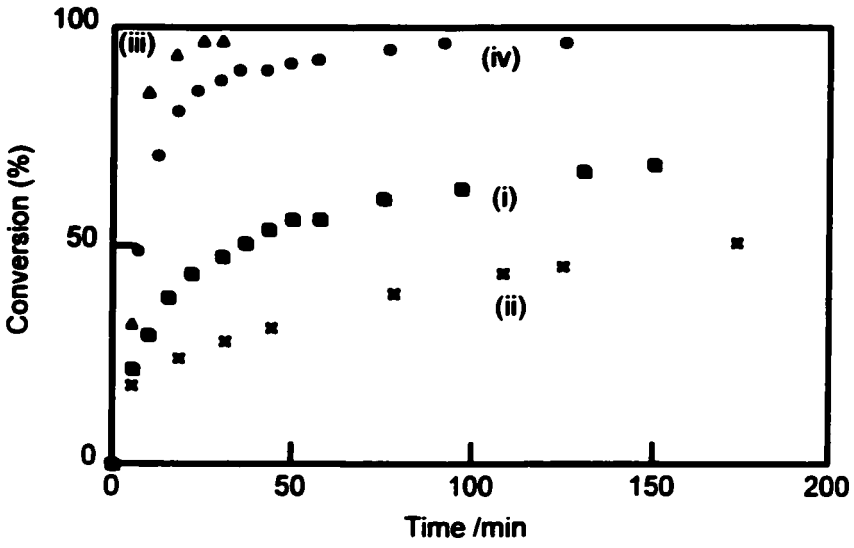

Figure 4. 7. ROMP activity of catalysts prepared by addition of $PhCHN_2$ (5 eq) to the following Ru diphosphine precursors: (i) $RuCl_2(dppb)(PPh_3)$, **3a**; (ii) $RuCl_2(binap)(PPh_3)$, **3b**; (iii) "$RuCl_2(dcypb)(PPh_3)$", **3c**; (iv) $[RuCl_2(dppb)]_2$, **4**.

4.4.3. Effect of Phosphine Scavenger on ROMP Activity

ROMP catalysts $RuCl_2(PR_3)_2(CHR')$ **1** and $RuCl_2(dtbpm)(CHCHC(CH_3)_2)$ **2d**, despite their coordinative unsaturation, require ligand loss in order to attain high polymerization activity. Indeed, rate accelerations have been reported for polymerization via **1a** following addition of CuCl as a phosphine scavenger (though catalyst lifetimes were decreased),[9] and for ROMP via **2d** on addition of trimethylsilyl triflate as a halide scavenger.[13] In sharp contrast, addition of halide or phosphine scavengers ($AgPF_6$ and CuCl, respectively) results in a five-fold rate decrease for ROMP via $[RuCl(dppb)]_2(\mu\text{-}Cl)_2(\mu\text{-}H_2O)/PhCHN_2$ ($\mathbf{4}/PhCHN_2$). Addition of *one* equivalent of CuCl to the

$RuCl_2(dppb)(PPh_3)/PhCHN_2$ catalyst system has a marked accelerating effect, consistent with removal of free PPh_3 generated via the equilibrium shown in Figure 4. 8.[11] As expected, the rate curve is virtually identical to that observed for ROMP via isolated[27] $[RuCl(dppb)]_2(\mu\text{-}Cl)_2(\mu\text{-}H_2O)$ (4) + $PhCHN_2$. The absence of any rate acceleration in this experiment suggests that ROMP is not mediated in our systems by a complex containing a "dangling" dppb ligand, which would compete with free PPh_3 for complexation of CuCl.

$$2\ RuCl_2(PP)(PPh_3) \rightleftharpoons [RuCl_2(PP)]_2 + 2\ PPh_3$$

Figure 4. 8. Equilibrium between mixed phosphine complexes and 'naked' dimers.

The broad polydispersities found for the rigid chelate complex **2d** (M_w/M_n=2.75), a function of the higher rate of propagation than initiation,[14] are consistent with a preequilibrium involving halide loss. In comparison, the seven-membered chelate complexes **2a-c** afford polymers with markedly low polydispersities (Table 4. 1). Consistent with placement of alkylidene in a basal site, this indicates that no preequilibrium - whether dechelation to give a "dangling" phosphine, or loss of halide - is required to generate the catalytically active species. While it does not exclude the possibility of a *rapid* preequilium to form spectroscopically unobservable amounts of a highly active alkylidene complex, related pincer chemistry (Chapter 7) suggests that such preequilibria are rather slow, resulting in low catalyst activity and high-PDI polymers. In addition, dechelation of one end of the dcypb ligand should generate a catalyst system

that reproduced the broader polydispersities of the $RuCl_2(PCy_3)_2(CHPh)$ system.[8]

Table 4. 1. Ru-catalyzed ROMP of norbornene[a]

Precursor	Diphosphine	M_n	Yield (%)	M_w/M_n	trans (%)
2d	dtbpm	n/a	55	2.75	71
3a	dppb	90,900	100	1.05	81
3b	binap	102,000	96	1.06	68
3c	dcypb	188,300	100	1.16	83
4	dppb	80,000	100	1.11	75

[a] *Reaction conditions:* norbornene/Ru = 200, $PhCHN_2$/Ru = 5, [Ru] = 0.0015 M, 24h; GPC measured by viscometry *vs.* polystyrene standards.

4.4.4. Effect of Dissociated PPh_3 on ROMP Activity

The convenience of in situ catalyst generation is frequently undermined by unanticipated side-reactions. Potential interference by "contaminating" PPh_3 was therefore assessed.

Dimers $[RuCl_2(PP)]_2$ exist in spectroscopically observable equilibrium[11] with their mixed phosphine counterpart (Figure 4.8), much of the chemistry of which they mediate. The results of Section 4.4.3 (above) suggest that PPh_3 functions as a catalyst poison in these systems. With the intention of evaluating the extent of this effect, we evaluated the relative ROMP activity of catalysts generated from mixed-phosphine precursor $RuCl_2(dppb)(PPh_3)$ (**3a**) and the "naked", PPh_3-free dimer $[RuCl(dppb)]_2(\mu\text{-}Cl)_2(\mu\text{-}H_2O)$ (**4**). Use of $[RuCl(dppb)]_2(\mu\text{-}Cl)_2(\mu\text{-}H_2O)$[27] permits evaluation of the activity of $RuCl_2(dppb)(CHR)$ (**2a**) unperturbed by PPh_3. The **4**/$PhCHN_2$ catalyst system

is approximately five times more active than $RuCl_2(dppb)(PPh_3)/PhCHN_2$ (**3a**/$PhCHN_2$, Figure 4. 7.). Addition of PPh_3 (2 equiv.) to solutions of **4** and norbornene after ROMP has been initiated with $PhCHN_2$ reduces the rate of polymerization by more than an order of magnitude, implying that poisoning of **2a** by free PPh_3[9] is implicated in the lower activity of **3a**/$PhCHN_2$. Competition of free PPh_3 with diazoalkane for the metal center is improbable: despite the fact that equilibrium in Figure 4. 8 lies strongly in favor of the mixed-phosphine complex, the active catalyst is rapidly formed, as evidenced by the absence of an induction period in Figure 4. 7. The amplified metathesis activity of systems derived directly from $[RuCl_2(PP)]_2$ is of particular interest given the popularity of in situ methods in Ru ROMP and RCM.

4.4.5. Effect of $PhCHN_2$ Concentration on ROMP Activity

Also relevant to in situ methods in ROMP is the often-overlooked effect of diazoalkane concentration (especially given the dificulties encountered in obtaining pure material; see Section 4.2). Decreasing the $PhCHN_2$:Ru ratio from 5:1 to 1:1 in ROMP via **4** causes a sharp increase in activity, effecting complete polymerization within less than ten minutes. The implied attack of phenyldiazomethane on the Ru-alkylidene unit is supported by the appearance of an increased proportion of stilbene in the ^1H NMR spectrum. The rate of reaction of **4** with $PhCHN_2$ must be slower than attack of norbornene itself, however, as the 5:1 system still shows high ROMP activity (Figure 4. 9). A similar inverse dependence on diazoalkane concentration was reported for the allylruthenium(IV)/$EtCO_2CHN_2$ system.[2] This is unsurprising given the relative bulk of

$PhCHN_2$ and the monomer itself; competing attack of diazoalkane on the [Ru=CHR] moiety is likely to be a complicating factor whenever diazoalkane is used in excess. Finally, use of half an equivalent of $PhCHN_2$ per Ru causes a rate decrease relative to a 1:1 ratio, supporting the formulation **2** versus a Ru_2-monoalkylidene alternative.[28] It should be noted that while $PhCHN_2$ can in principle act as a phosphine scavenger via ylide formation, this reaction is very slow relative to the rate of polymerization.

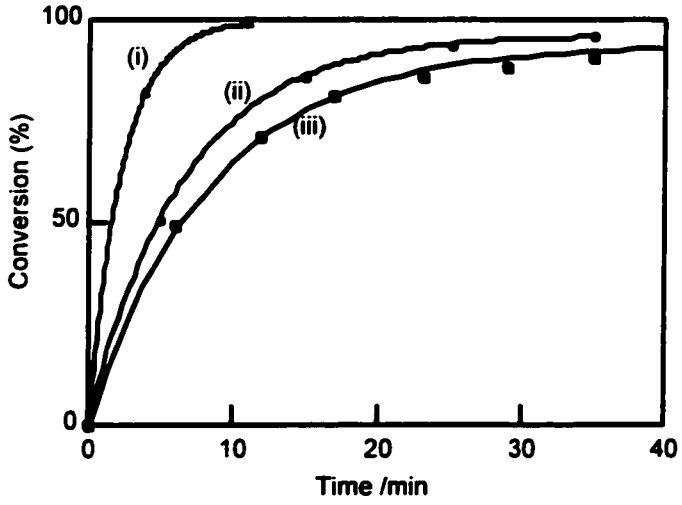

Figure 4. 9. Dependence of ROMP activity of **4**/$PhCHN_2$ on diazoalkane:Ru ratio (i) 1 equiv. $PhCHN_2$ per Ru; (ii) 0.5 equiv. $PhCHN_2$ per Ru; (iii) 5 equiv. $PhCHN_2$ per Ru.

4.4.6. Effect of *t,t*-Benzaldehyde Azine on ROMP Activity

Azine poisoning studies were undertaken to assess the effect of this potentially coordinating ligand (Section 4.2). Reaction of **4** with isolated azine is very slow: no reaction is observed at RT over 24 h in solution, even at equimolar concentrations. Consistent with this, ROMP via **3a** or **4** in the presence of azine (1 equiv. per Ru) shows

no deterioration in rate. Interference by this common contaminant may be problematic for less active catalysts, or unreactive monomers, where more forcing conditions are required. Thus, gentle thermolysis (50°C) of **4** with one equivalent of azine generates a complex ^{31}P NMR pattern, and a benzonitrile derivative of ruthenium has been crystallographically analyzed. Details of the coordination chemistry will be discussed separately.[29]

4.5. Conclusions

This Chapter describes the first example of ROMP via Ru-diphosphine complexes that do not require ligand abstraction in order to achieve high activity. The ruthenium alkylidene complexes generated via reaction of the ruthenium precursors with various diazoalkanes decompose rapidly in solution. Despite this, exceptionally narrow polydispersities are obtained, as well as, in the case of the binap derivative, a high proportion of cis-olefin linkages. Triphenylphosphine and excess diazoalkane emerge as potent catalyst poisons in these systems while increased phosphine bulk and basicity result in amplified metathesis activity.

The results described above serve as proof of principle for our initial beliefs that high activity *and* selectivity can be realized in ruthenium-catalysed metathesis reactions given judicious choice of the ligand framework. In order to improve upon the systems discussed above, a greater understanding of the deactivation/decomposition pathways is necessary. The incorporation of incipient donor ligands in order to curb bimolecular decomposition processes has been explored and is discussed in the following chapter. An intermediate along the decomposition pathway has also been identified (Chapter 6). The

identification of dimerization via formation of chloride bridged dimers as a deactiviation pathway also prompted the exploration of ligands which incorporate an anionic site into a tridentate chelating ligand (Chapter 7) eliminating one chloride and thereby minimizing the decomposition pathways.

4.6. References

1) Chang, S.; Jones, L.; Wang, C.; Henling, L. M.; Grubbs, R. H. *Organometallics* **1998**, *17*, 3460.

2) Herrmann, W. A.; Schattenmann, W. C.; Nuyken, O.; Glander, S. C. *Angew. Chem. Int. Ed. Engl.* **1996**, *35*, 1087-1088.

3) Weskamp, T.; Schattenmann, W. C.; Spiegler, M.; Herrmann, W. A. *Angew. Chem. Int. Ed. Engl.* **1998**, *37*, 2490.

4) Huang, J.; Stevens, E. D.; Nolan, S. P.; Peterson, J. L. *J. Am. Chem. Soc* **1999**, *121*, 2674.

5) Scholl, M.; Ding, S.; Lee, C. W.; Grubbs, R. H. *Org. Lett.* **1999**, *1*, 953.

6) Scholl, M.; Trnka, T. M.; Morgan, J. P.; Grubbs, R. H. *Tetrahedron Lett.* **1999**, *40*, 2247.

7) Katayama, H.; Yoshida, T.; Ozawa, F. *J. Organomet. Chem.* **1998**, *562*, 203-206.

8) Schwab, P.; Grubbs, R. H.; Ziller, J. W. *J. Am. Chem. Soc.* **1996**, *118*, 100.

9) Dias, E. L.; Nguyen, S. T.; Grubbs, R. H. *J. Am. Chem. Soc.* **1997**, *119*, 3887.

10) Demonceau, A.; Stumpf, A. W.; Saive, E.; Noels, A. F. *Macromolecules* **1997**, *30*, 3127.

11) Jung, C. W.; Garrou, P. E.; Hoffman, P. R.; Caulton, K. G. *Inorg. Chem.* **1984**, *23*, 726.

12) Fogg, D. E.; James, B. R. *J. Organomet. Chem.* **1993**, *462*, C21.

13) Hansen, S. M.; Volland, M. A. O.; Rominger, F.; Eisentrager, F.; Hofmann, P. *Angew. Chem. Int. Ed. Engl.* **1999**, *38*, 1273.

14) Hansen, S. M.; Rominger, F.; Metz, M.; Hofmann, P. *Chem. Eur. J.* **1999**, *5*, 557-566.

15) Volland, M. A. O.; Straub, B. F.; Gruber, I.; Rominger, F.; Hofmann, P. *J. Organomet. Chem.* **2001**, *617-618*, 288.

16) Hofmann, P.; Volland, M. A. O.; Hansen, S. M.; Eisentrager, F.; Gross, J. H. *J. Organomet. Chem.* **2000**, *606*, 88.

17) Werner, H.; Jung, S.; Gonzalez-Herrero, P.; Ilg, K.; Wolf, J. *Eur. J. Inorg. Chem.* **2001**, 1957.

18) Huang, D.; Streib, W. E.; Bollinger, J. C.; Caulton, K. G.; Winter, R. F.; Scheiring, T. *J. Am. Chem. Soc.* **1999**, *121*, 8087.

19) Su, M.-D.; Chu, S.-Y. *J. Am. Chem. Soc* **1997**, *119*, 10178.

20) Cundari, T. R. *J. Am. Chem. Soc* **1994**, *116*, 340.

21) Creary, X. *Organic Syntheses*; Wiley & Sons: Toronto, 1990; Vol. VII, pp 438.

22) Stumpf, A. W.; Saive, E.; Demonceau, A.; Noels, A. F. *J. Chem. Soc., Chem. Commun.* **1995**, 1127.

23) Nguyen, S. T.; Johnson, L. K.; Grubbs, R. H.; Ziller, J. W. *J. Am. Chem. Soc.* **1992**, *114*, 3974.

24) Binger, P. *Synthesis* **1974**, 190.

25) Molecular Simulations, I. *Cerius^2 Property Prediction*: San Diego, 1999.

26) Brumaghim, J. L.; Girolami, G. S. *Organometallics* **1999**, *18*, 1923.

27) Joshi, A. M.; Thorburn, I. S.; Rettig, S. J.; James, B. R. *Inorg. Chim. Acta* **1992**, *198-200*, 283.

28) Dias, E. L.; Grubbs, R. H. *Organometallics* **1998**, *17*, 2758.

29) Snelgrove, J. L.; Fogg, D. E. *Independent work* .

CHAPTER 5

Synthesis and Reaction Chemistry of a Coordinatively Unsaturated Ru-Dcypb Complex Containing a Stable Silylene Ligand

5.1. Introduction

Transition-metal derivatives of silylenes have been the target of considerable attention owing to their potential relevance to a range of organosilicon transformations, and development of routes to such complexes has provided a rich area of inquiry. Synthetic strategies focus on reactions of coordinatively unsaturated precursors with a stable silylene,[1-7] or generation and installation of the silylene in situ,[8-14] including by 1,2-migration from silyl hydrides.[15] Particularly well developed is the coordination chemistry[1-5,7] of 1,3-di-*tert*-butyl-1,3,2-diazasilol-2-ylidene (SiL^N_2), the first-isolated example of a stable silylene, reported by Denk and West in 1994.[16] This compound can be recognized as a silicon analog of the stable N-heterocyclic carbene ligands ("Arduengo carbenes")[17], which have recently attained a high profile in Ru-catalyzed metathesis reactions. Irrespective of installation route, the stability of the *bound* silylene is typically ensured by use of "innocent" ligands, noncoordinating anions, and a coordinatively saturated metal. With few exceptions,[4,6,7,18] common catalytically-relevant ligands such as chloride, hydride or phosphine have been neglected.

Given the apparent susceptibility of complexes of type $RuCl_2(PP)(CHR)$ to bimolecular decomposition (Chapter 4), we were interested in the stabilizing effects

potentially conferred by bulky, neutral donor ligands such as silylene. A target structural motif is shown in Figure 5. 1. Enhanced selectivity in metathesis might also be anticipated from the functioning of such a ligand as a steric wedge to amplify the steric effects of the coordination pocket. In order to offset decreases in catalyst activity arising from steric constraints on access to the active site, we chose to focus on complexes containing electron-rich alkylphosphines, the activating effect of which in metathesis was noted in Chapter 4. Building on the synthetic accessibility of $[RuCl_2(dcypb)]_2$ complexes (Chapter 3), we sought to incorporate a bulky, stable silylene ligand into this coordinatively unsaturated metal environment, for subsequent conversion into an alkylidene derivative.

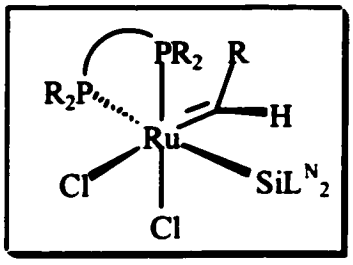

Figure 5. 1. Target silylene/alkylidene complex.

5.2. Preparation and Characterization of RuCl(η^3-dcypb)(SiL$^N_2$) (12)

A suspension of RuCl(dcypb)(μ-Cl)$_3$Ru(dcypb)(N_2) **5** in benzene reacts with SiL$^N_2$ within 4 h at 50 C, yielding a homogeneous orange solution in which RuCl(η^3-dcypb)(SiL$^N_2$) **12** is the sole Ru-containing product (Figure 5. 2). Also evident by ^{1}H NMR analysis is HClSiL$^N_2$, identified by comparison to an authentic sample.

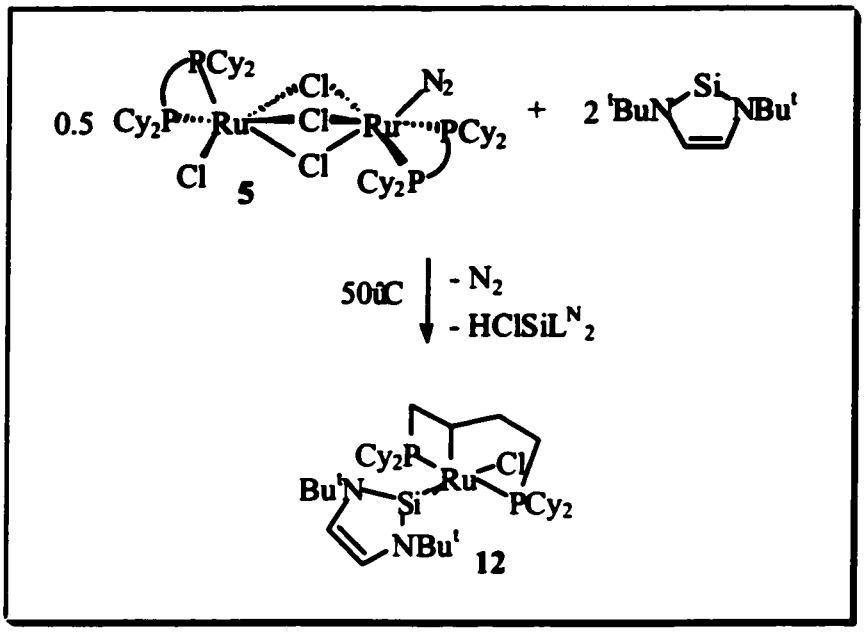

Figure 5. 2. Reaction of **5** with SiL^N_2.

Use of one equivalent of silylene resulted in 50% conversion of **5**. With two equivalents, quantitative reaction is effected, and **12** can be isolated as an air-sensitive yellow precipitate in >80% yield. $^{29}Si\{^1H\}$ NMR analysis of **12** reveals a triplet at 105.7 ppm, supporting identification as a Ru-silylene species containing two phosphine ligands. The relatively small coordination shift (cf. δ_{Si} 78 for the free ligand) is in keeping with values previously reported for complexes of these stable silylenes.[3-5,7] The characteristic singlet at 6.75 ppm for the equivalent aromatic protons in free SiL^N_2 is replaced in **12** by an AB quartet (δ_H 6.33, 6.17; J_{HH} = 3.8 Hz), indicating an unsymmetrical coordination environment for the silylene ligand within **12**. $^{31}P\{^1H\}$ NMR reveals a pair of doublets separated by ca. 80 ppm, with an unprecedentedly large coupling constant for a chelating diphosphine containing a four-carbon backbone (δ 60.2, -10.3; J_{PP} = 263 Hz). The strong

P-P coupling implies an unexpected trans disposition of inequivalent phosphorus atoms, while the large peak separation indicates the presence of two different ring sizes. Phosphine ligands within four-membered chelate rings normally resonate 50-100 ppm upfield of those in five- and seven-membered chelates, or monodentate phosphines.[19] The observed pattern finds precedent in bis(phosphine) systems in which one (i.e.) PPh_3 ligand is ortho-metallated to give a four-membered Ru-P-C-C ring at ~0 ppm, and a second, trans, PPh_3 is a simple η^1-donor ligand at a "normal" chemical shift value of ~50 ppm.[19] The presence of both four- and five-membered rings in **12** was confirmed by X-ray crystallographic analysis, which reveals an unprecedented attack of the metal on the four-carbon backbone of the dcypb ligand. The potential for this type of interaction was noted in Chapter 3, in context of the crystal structure of RuCl(dcypb)(CO)(μ-Cl)$_2$RuCl(dcypb)(CO) **10**. Other researchers have previously noted[20-22] a tendency within ruthenium cyclohexylphosphine systems toward activation of the cyclohexyl rings. In systems of both monodentate[20] (PCy_3) and bidentate[21,22] ($Cy_2P(CH_2)_nPCy_2$, n = 3, 4) cyclohexylphosphines, multiple C-H activations gave rise to an η^3-allyl binding mode for one of the cyclohexyl rings. In the case of the monodentate systems, activation of another cyclohexyl ring (from a second ligated PCy_3) resulted in its coordination as an η^2-alkene.

Formation of **12** clearly shows that for diphosphines forming flexible chelate rings, attack on the carbon backbone is also possible. Agostic interactions between Ru and α-methylene groups of bound $Ph_2P(CH_2)_4PPh_2$ (bis(diphenyl)phosphinobutane, dppb) have been described within a sterically congested bis(dppb) complex, resulting in deuterium incorporation into the four-carbon backbone on treatment with D_2.[23] Interception of the oxidative-addition product in **12** may result from facile abstraction of

HCl by the basic silylene moiety.

Low-temperature NMR analysis of **12** suggests the presence of an equilibrium that is masked in the RT spectrum. At 185 K, the downfield ^{31}P NMR signal for **12** resolves into two distinct doublets of approximately equal intensity (δ 62.2, J_{PP} = 274 Hz; δ 54.3, J_{PP} = 260 Hz), while the upfield doublet broadens into two poorly resolved, overlapping doublets centered at -10 ppm (Figure 5. 3). The corresponding solid state spectrum shows only one of these sets of doublets (δ 56.1, -11.6; J = 267 Hz; the <2 ppm chemical shift difference between the solid-state and low-temperature data is not considered significant[24]). These observations are consistent with a weak agostic interaction between Ru and a Bu^t C-H bond, observable in the solid state, but favored only at low temperature in solution. An agostic ν(C-H) band is found in the solid state IR spectrum, but not in solution; X-ray evidence for such an interaction is presented below. An alternative silyl-silylene equilibrium process[6] involving reversible migration of chloride ligand to Si may be discounted on the basis of the near-identity of the ^{31}P NMR values for the two species.

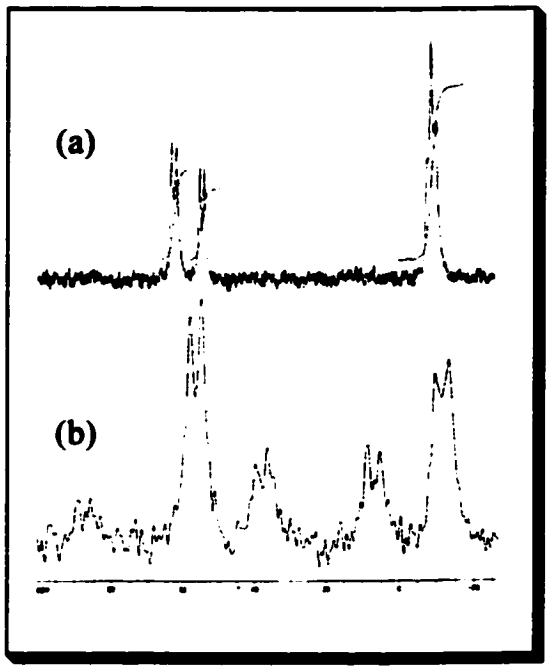

Figure 5. 3. (a) $^{31}P\{^{1}H\}$ NMR at 185 K and (b) Solid State ^{31}P CP/MAS NMR.

5.2.1. Mechanism

The observed requirement for two equivalents of SiL^{N}_{2} per Ru in the synthesis of **12** results from consumption of one equivalent of the basic silylene ligand as $HClSiL^{N}_{2}$, as noted above. Coordination of SiL^{N}_{2} as a simple donor ligand (Figure 5. 4, path A) may generate sufficient steric pressure to trigger oxidative addition of a diphosphine C-H bond to the electron-rich metal center, accompanied by insertion of silylene into the Ru-Cl bond. Reductive elimination of $HClSiL^{N}_{2}$ from Ru(IV) intermediate **A**, with coordination of a second silylene, would afford **12**. The Ru(IV) oxidation state is readily accessible in species containing strongly basic donor ligands. Examples include Cp*Ru silyl hydrides[4,13,14,25-28] as well as alkylphosphine complexes.[29,30] Precedent also exists, however, for direct insertion of SiL^{N}_{2} into a M-Cl bond (path B).[6] In view of the bulk of

the phosphine and silyl ligands, intermediate **B** may be more likely than six-coordinate **A**. Crystallographic evidence for four-coordinate Ru within a sterically encumbered ligand environment was recently reported.[31]

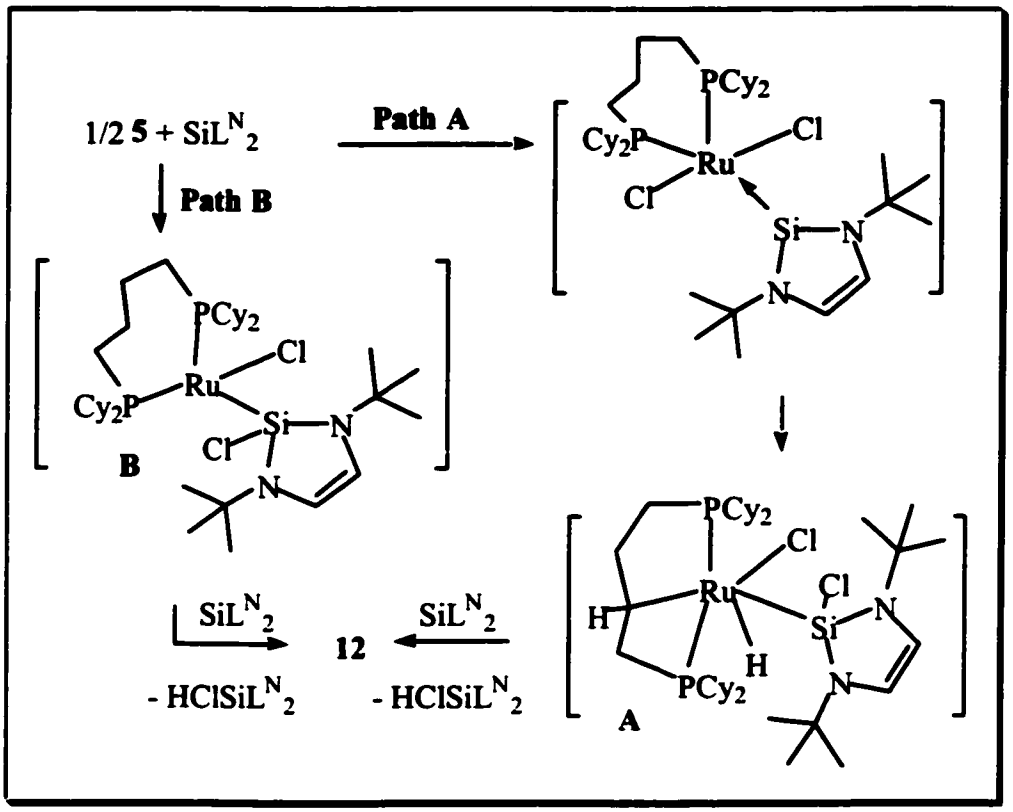

Figure 5. 4. Possible mechanisms for the formation of **12**.

5.2.2. Molecular Structure of RuCl(η^3-dcypb)(SiL^N_2) (12)

X-ray quality crystals of **12** were obtained by slow evaporation of a benzene solution. An ORTEP representation is given in Figure 5.5, with relevant bond lengths and angles in Table 5. 1. The complex exists as two crystallographically equivalent mirror images (a representation of the mirror image appears in the Appendices). The short non-

bonding distance between the Ru centre and a methyl carbon of one of the Bu^t groups (2.899(7) Å) suggests an agostic interaction between the C-H bond and the Ru centre. The solid-state geometry about the Ru center is thus best described as distorted octahedral, with the dcypb ligand functioning as a meridional η^3-donor. The activated carbon of the C_4 backbone is trans to the agostic interaction, while the SiL^N_2 ligand is trans to the remaining chloride ligand (Si-Ru-Cl ~160), and is planar at silicon (sum of bond angles = 359.81 , ~360). The Ru-Si bond distance of 2.2264(11) Å is the shortest such value currently on record, being slightly less than the value of 2.238(2) Å reported for $[Cp^*(Me_3P)_2Ru{=}SiMe_2][B(C_6F_5)_4]$.[14] However, π-bonding between the metal and silicon centers is improbable, as discussed in more detail below.

Of note in the structure are the Ru-Si-N angles, which differ by nearly 40 . This difference reflects a 20 "tipping" of the SiL^N_2 ligand from an axis drawn from Ru through Si and the centroid of the silylene ring. Like the 20 deviation from linearity in the Cl-Ru-Si angle, this distortion minimizes steric interactions between the Bu^t group on N(2) and the cyclohexyl substituents, while promoting development of the Ru/C-H agostic interaction.

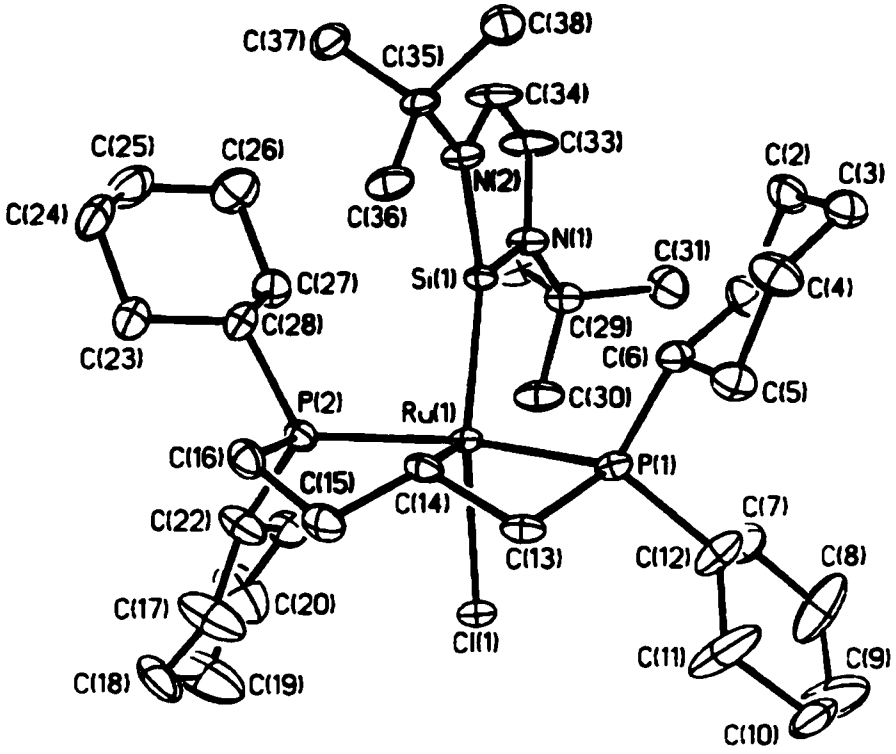

Figure 5. 5. ORTEP diagram of $RuCl(\eta^3\text{-dcypb})(SiL^N_2)$ (**12**). Thermal ellipsoids shown at 30% probability level. Hydrogen atoms, solvent molecules and mirror image complex omitted for clarity.

Table 5. 1. Selected Bond Lengths (Å) and Angles (deg) for **12**.[a]

Ru(1)-Si(1)	2.2264(11), 2.2293(12)	Si(1)-N(1)	1.732(3), 1.725(3)
Ru(1)-C(14)	2.110(4), 2.114(4)	Si(1)-N(2)	1.734(3), 1.741(3)
Ru(1)-P(2)	2.3373(12), 2.3279(12)	N(1)-C(33)	1.388(5), 1.377(6)
Ru(1)-P(1)	2.3389(12), 2.3422(11)	N(2)-C(34)	1.399(6), 1.411(6)
Ru(1)-Cl(1)	2.4713(11), 2.4738(10)	C(33)-C(34)	1.336(6), 1.329(6)
N(1)-Si(1)-N(2)	90.60(17), 90.61(17)	C(14)-Ru(1)-Si(1)	104.45(12), 103.76(12)
N(1)-Si(1)-Ru(1)	116.06(12),116.42(12)	C(14)-Ru(1)-P(1)	69.21(13), 69.50(12)
N(2)-Si(1)-Ru(1)	153.15(13), 152.97(13)	C(14)-Ru(1)-P(2)	83.05(13), 83.68(12)
P(2)-Ru(1)-P(1)	152.11(4), 152.91(4)	C(14)-Ru(1)-Cl(1)	95.16(12), 95.87(12)

[a] The second value is the corresponding value for the mirror image complex.

5.2.3. Frontier Orbital Analysis

The emerging picture of the SiL^N_2 moiety is of a predominantly σ-donor ligand, in which internal stabilization of the silylene is effected by donation of electron density from the lone pairs on nitrogen into the empty Si p orbital.[32,33] Consistent with minimal electronic perturbation of the ligand within **12**, relative to free SiL^N_2, is the small ^{29}Si NMR coordination shift. The observed value of δ 106 is well within the δ 97.5-146.9 range described for complexes containing primarily σ-donor silylenes.[3-7,14] Furthermore, despite the very short Ru-Si bond distance, the bond lengths within the SiL^N_2 fragment itself are very slightly shorter than those of the free silylene.[16] Examination of the frontier molecular orbitals supports this analysis. For complex **12**, assuming an octahedral solid-state geometry, a dxy, dxz or dyz orbital must constitute the HOMO. Ruthenium-silylene back-bonding requires localization of the HOMO on dxy, and the LUMO on a vacant Si p orbital (the dxz and dyz orbitals are orthogonal to the Si p-orbital, precluding overlap). Density functional theory calculations[34] carried out on intact **12** suggest that while the HOMO has the appropriate symmetry, the LUMO is localized not on Si but on Ru and, in part, on the Ru-C bond. The HOMO-LUMO gap is approximately 4 eV. The cumulative evidence thus supports identification of the silylene ligand as a σ-donor to Ru, the very short Ru-Si distance likely resulting from the strong electrostatic interaction between this electrophilic ligand and the electron-rich metal center.

5.2.4. Attempted Installation of Alkylidene

While activation of the dcypb ligand to generate a novel "pincer" species was unexpected, this does not in principle preclude conversion of **12** into a novel silylene-containing pincer alkylidene complex (Figure 5.6). However, treatment of a C_6D_6 solution of **12** with $PhCHN_2$ under the conditions of Chapter 3 showed no reaction, possibly owing to the steric bulk at Ru associated with the presence of both silylene and cyclohexyl rings . Treatment of **12** with $AgPF_6$ to abstract halide prior to addition of diazoalkane caused considerable decomposition, as indicated by the loss of peaks for coordinated silylene (^1H NMR) and the complete disappearance of ^{31}P NMR signals (other than the septet associated with the PF_6^- anion). Formation of paramagnetic products is suggested, supported by the observation of black solids forming in the NMR tube.

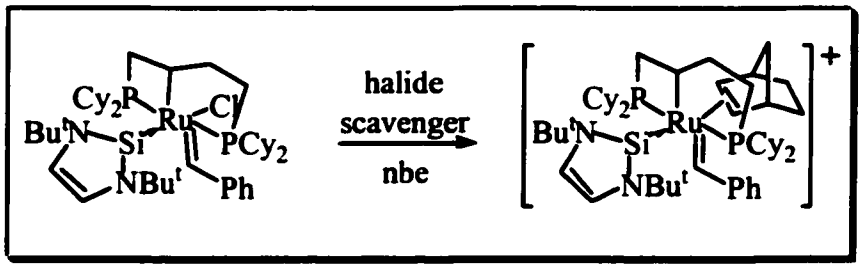

Figure 5. 6. Proposed silylene/alkylidene complex.

5.3. Reaction of Silylene Complex with Hydrogen

It was unclear whether the high reactivity of **12** noted in the experiments above was a function of attack of Ru on the dcypb moiety, or whether the silylene ligand was implicated. Reactivity studies on **12** were thus of considerable interest, especially given the dearth of such data for coordinatively unsaturated transition metal-silylene complexes. A recent study involving treatment of $Cp^*Ru(SiX_2)(PMe_3)_2]^+$ (X = SMe_2, Me) with nonpolar, unsaturated substrates (such as ethylene, acetylene and 2-butyne)[28] showed no reaction. Slow decomposition to several unidentified Ru hydride species was observed upon reaction with H_2. The potential reactivity of the silylene ligand under such conditions may be limited, however, by the coordinative saturation of the parent complex. Reactions of **12** with simple donors such as CO and H_2 were therefore undertaken, with the intention of probing the capacity of the SiL^N_2 ligand to function as an "innocent", neutral, two-electron donor (i.e. a phosphine mimic.[3,5])

Reaction of **12** under 1 atm H_2 is slow at room temperature, with <50% conversion after 1 week, but can be driven to completion within 24 h at 50 C. No intermediates are evident by ^{31}P NMR analysis. The Ru product is spectroscopically identical (^1H and ^{31}P NMR) to hydridochloro species **14** (Figure 5. 7.) obtained by treating **5** with potassium tri(*sec*-butyl)borohydride under H_2 (Chapter 6). Loss of the silicon ligand is further supported by X-ray crystallographic analysis of a decomposition product serendipitously obtained on attempted isolation of **14** from the reaction mixture (vide infra). ^1H, ^{13}C, and ^{29}Si NMR analysis of the sole Si-containing product permit its identification as $[L^N_2Si(H)]_2O$ **13**,[35] suggesting that reaction involves both

hydrogenolysis and, more unexpectedly, hydrolysis. (The latter may occur, despite the use of standard "anhydrous" Schlenk techniques, from use of a Deoxo cartridge to scavenge trace oxygen from the H_2 stream by catalytic conversion to water; no evidence of hydrolysis was observed under N_2 atmosphere.) Implication of water in this transformation is confirmed by complete conversion of **12** to **14** and siloxane **13**, without heating, on addition of stoichiometric quantities of H_2O under H_2. Other side-products form on use of water alone; these are partially converted to **14** and siloxane on subsequent exposure to H_2. Reaction with both water and H_2 is thus required to generate the observed hydride and siloxane products. The overall reaction of **12** is indicated in Figure 5. 7.

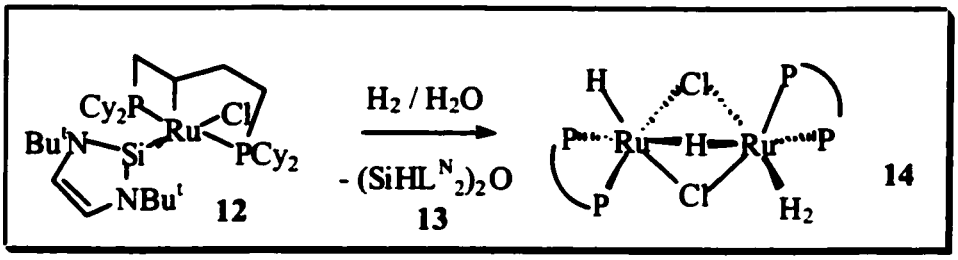

Figure 5. 7. Reaction of $RuCl(\eta^3\text{-dcypb})(SiL^N_2)$ **(12)** with H_2/H_2O.

The silylene-siloxane transformation is indicated by replacement of the olefinic doublets for **12** by two new signals in the olefinic/silyl region of the ^1H NMR spectrum. A singlet at 5.95 ppm is assigned to a silyl proton on the basis of its correlation with the ^{29}Si peak (^1H-^{29}Si HMQC; $^1J_{SiH}$ = 278 Hz), supported by the absence of an H-C correlation in the corresponding ^1H-^{13}C HMQC experiment. Also evident in this region (5.80 ppm) is one olefinic signal, which at 500 MHz is resolved into a doublet with long-

range coupling to silicon (J_{SiH} = 2 Hz; $^{1}H/^{29}Si$ HMBC). This resonance correlates with a ^{13}C methine signal at δ 111.8, itself assigned by ^{13}C DEPT. ^{29}Si INEPT analysis of the product mixture reveals one ^{29}Si resonance (δ -57.6), confirming identification of this species as siloxane dimer $[L^{N}_{2}Si(H)]_2O$.[35]

Jutzi and coworkers recently described the synthesis of metallosilanol species $Cp_2Mo(H)(SiL^{N}_{2}OH)$, via controlled hydrolysis of $Cp_2Mo(SiL^{N}_{2})$.[7] An analogous silyl hydride complex, $Cp_2Mo(H)(SiHL^{N}_{2})$, was obtained by insertion of SiL^{N}_{2} into an M-H bond of Cp_2MH_2 (M = Mo, W).[7] Interestingly, **12** appears to be stable toward hydrogenolysis alone, despite the presence of the Ru-C and silylene entities and the coordinative unsaturation of the metal. Thus, no products are evident that can be attributed to reaction with H_2 alone: while this might in principle be accounted for by a $(RuCl(\eta^3\text{-dcypb})(SiL^{N}_{2}) + H_2)$ equilibrium that lies far to the left, reaction with D_2 would then be expected to effect incorporation of D into the dcypb backbone (via reductive elimination of the activated C-H bond). However, labelling studies carried out with D_2 show no ^{2}H aliphatic signals prior to emergence of ^{31}P NMR signals for **14-d**. In conjunction with the stoichiometric reactions with H_2O/H_2 described above, this implies that reaction of **12** with water *precedes* reaction with D_2 (or H_2). ^{2}H NMR analysis indicates that the siloxane product formed in these reactions, whether at RT or by thermolyis, is solely $[L^{N}_{2}Si(D)]_2O$ **13-d**. Consistent with these observations is the mechanism of Figure 5.8, in which evolution of siloxane results from successive reaction of **12** with H_2O and D_2 (H_2). Nucleophilic attack of water on bound silylene may afford a η^1-silanol hydride intermediate,[7] which reductively eliminates to yield a silanol species

containing a simple η^2-diphosphine ligand. Reaction with H_2 would then liberate $L^N{}_2SiD(OH)$ (which can then condense to form the siloxane[35]) and a hydride species. Dimerization of the latter and reaction with D_2 would give **14**. Not indicated in the Figure are miscellaneous reactions involving scrambling of the deuterium label into the Cy rings and/or dcypb backbone. Exchange of Ru-D into phosphine cyclohexyl C-H bonds is common,[20-22](see also Chapter 6) while exchange with C_4-methylene backbones in a dppb complex[23] was noted above.

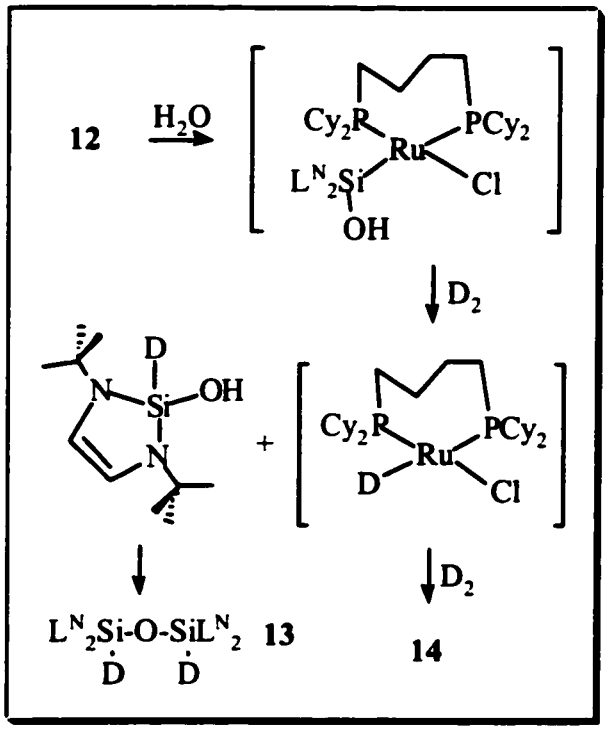

Figure 5. 8. Proposed mechanism for reaction of **12** with H_2/H_2O.

5.3.1. Molecular Structure of [(dcypb)(H)Ru(μ-Cl)$_3$Ru(dcypb)(N_2)] (15)

The susceptibility of the parent dcypb complex **5** to intramolecular

dehydrogenation on removal of H_2 atmosphere or concentration to dryness was noted in Chapter 3. Dehydrogenation likewise results from attempted isolation of **14**, as indicated by the emergence of olefinic signals and a singlet for dissolved H_2. Such processes may thus be a general characteristic of Ru-dcypb complexes in coordinatively unsaturated environments (see, for example, Sections 3.5 and 6.5.1). That other, intermolecular, processes are involved, at least in decomposition of **14**, is suggested by the presence of an additional chloride ligand in [(dcypb)(H)Ru(μ-Cl)$_3$Ru(dcypb)(N_2)] **15**. The latter species, identified by X-ray crystallography, crystallized on attempted isolation of **14** following reaction of **12** with H_2 /H_2O. A benzene solution containing the products was stripped to dryness, and the residue was washed with a few drops of hexanes, then redissolved in benzene. Crystals of **15** deposited on slow evaporation under N_2. Many other species are also present in solution, as judged by ^{31}P and ^{1}H NMR. An ORTEP representation of **15** (accompanied by a line drawing) appears in Figure 5.9 with selected bond lengths and angles in Table 5. 2.

Table 5. 2. Selected Bond Lengths (Å) and Angles (deg) for **15**.

N(1)-N(2)	1.110(5)	Ru(1)-Cl(1)	2.4840(10)
Ru(1)-N(1)	1.898(6)	Ru(1)-Cl(2)	2.4793(10)
Ru(1)-P(1)	2.3225(11)	Ru(1)-Cl(3)	2.4636(10)
Ru(1)-P(2)	2.3369(11)	Ru(2)-Cl(1)	2.6092(10)
Ru(2)-P(3)	2.2352(11)	Ru(2)-Cl(2)	2.5403(10)
Ru(2)-P(4)	2.2419(12)	Ru(2)-Cl(3)	2.5107(11)
N(2)-N(1)-Ru(1)	173.0(4)	P(3)-Ru(2)-P(4)	96.67(4)
N(1)-Ru(1)-P(1)	92.46(13)	Ru(1)-Cl(1)-Ru(2)	83.41(3)
N(1)-Ru(1)-P(2)	94.82(12)	Ru(1)-Cl(2)-Ru(2)	84.95(3)
P(1)-Ru(1)-P(2)	93.46(4)	Ru(1)-Cl(3)-Ru(2)	85.91(3)

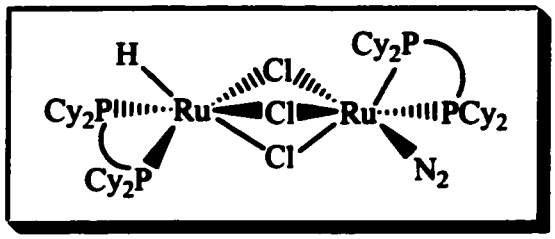

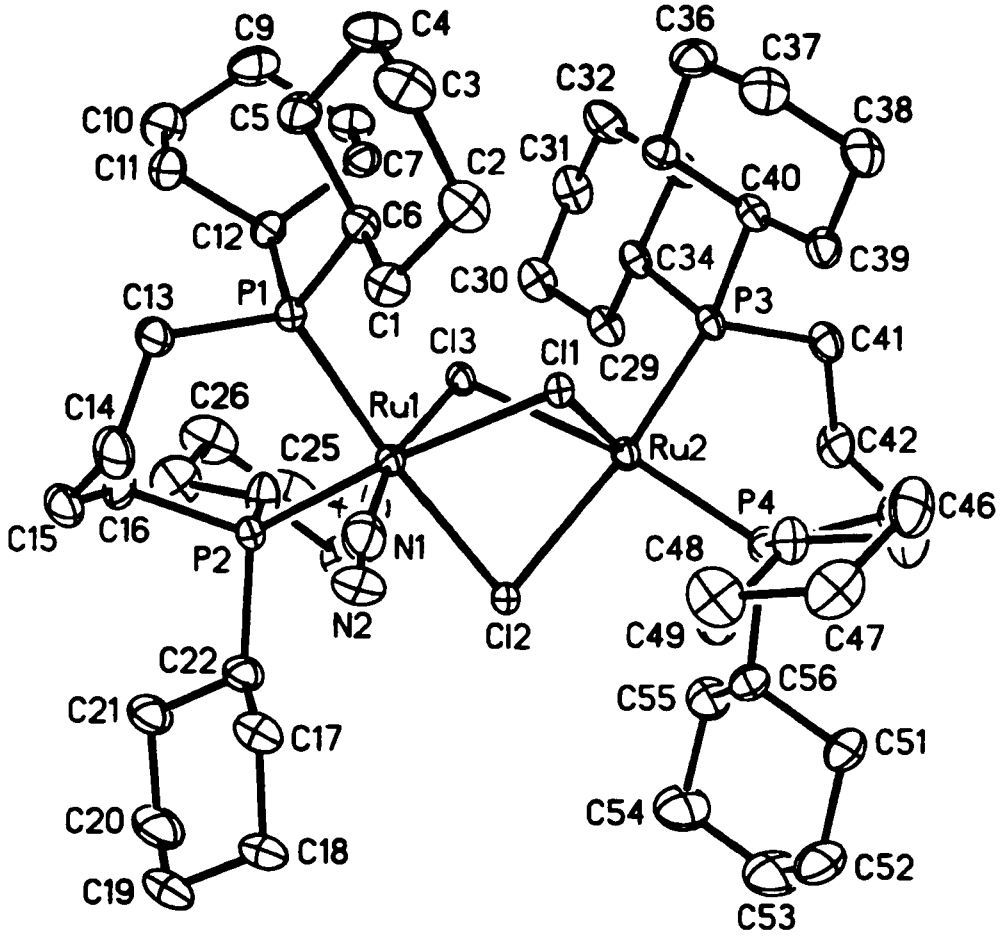

Figure 5. 9. ORTEP diagram of [(dcypb)(H)Ru(μ-Cl)$_3$Ru(dcypb)(N$_2$)] (**15**) with thermal ellipsoids shown at 30% probability level. Hydrogen atoms and solvent molecule omitted for clarity. Line diagram shows position of hydride (not located crystallographically).

Complex **15** adopts a triply chloride-bridged diruthenium structure, in which the coordination geometry at each metal center is distorted octahedral, taking into consideration the presence of a hydride ligand on Ru(2). The structure is unsymmetrical, with Ru(1) bearing an end-bound dinitrogen ligand. Location of the hydride ligand on Ru(2) is inferred from the very long Ru(2)-Cl(1) bond distance (2.6092(10) Å, vs. the average Ru-Cl bond length of 2.496(10) Å). The presence of this sterically undemanding ligand permits a larger bite angle of the diphosphine ligand subtended at Ru(2), vs. the more sterically crowded Ru(1) (96.7 , vs. 93.5). ^{1}H NMR analysis of the isolated solid shows several hydridic resonances. While a search of the Cambridge Crystallographic Database reveals no direct analogues of the "Ru(μ-Cl)$_3$Ru(H)" framework, the structural parameters for **15** are very similar to data reported for the closely related complex [(η^2-H_2)(dppb)Ru(μ-Cl)$_3$RuCl(dppb)].[36] Ruthenium-phosphorus, -nitrogen and -chloride distances (other than for the chloride trans to hydride) tally closely with the values reported, as do angles within the Ru-P-Cl skeleton.

5.4. Reaction with Carbon Monoxide

Suspensions of **12** react with CO within hours to give a clear pale yellow solution containing free SiL^N_2 and three isomeric ruthenium carbonyl derivatives **16-18**. The high solubility of the Ru products hampered their separation from each other and from free silylene. Displacement of SiL^N_2 is indicated by the complete disappearance (^{1}H NMR) of the AB quartet for the bound ligand, and emergence of a prominent singlet for free silylene (6.75 ppm). Retention of the η^3-dcypb framework in **16-18** is indicated by the

presence of three pairs of doublets with characteristically large $^{31}P\{^{1}H\}$ NMR peak separations (77.6, -29.0 ($^{2}J_{PP}$ = 249 Hz, **16** or **17**), 74.4, -29.9 ($^{2}J_{PP}$ = 246 Hz, **16** or **17**), 72.9, -38.2 ($^{2}J_{PP}$ = 164 Hz, **18**); $\Delta\delta_{P}$ ~ 100 ppm). Unambiguous identification of all three as isomeric bis(CO) derivatives (Figure 5. 10) is provided by ^{31}P NMR analysis of their ^{13}CO isotopomers. ^{31}P-^{13}C splitting results in transformation of each doublet present in the original ^{31}P NMR spectrum into a doublet of doublets of doublets (**16**, **17**) or a doublet of triplets (**18**). Isomers **16** and **17** contain trans-disposed phosphorus ligands, as indicated by their large $^{2}J_{PP}$ values (~250 Hz). Distortion from the idealized structures represented in Eqn. 3 is indicated by the observation of four inequivalent ^{13}CO resonances for **16** + **17** (as well as two for **18**). Consequently, **16** and **17** cannot be distinguished by spectroscopic data.

A structural distinction between these products and isomer **18** is indicated by the much smaller $^{2}J_{PP}$ value for the latter (164 Hz), which implies a smaller P-Ru-P dihedral angle. That the angle is still much larger than 90 is indicated, however, by comparison of this coupling constant to "normal" cis $^{2}J_{PP}$ values of 11-50 Hz.[19] A highly distorted octahedral arrangement, with the diphosphine ligand taking up a geometry intermediate between the meridional extreme of **16/17** and a true facial arrangement, is thus suggested.

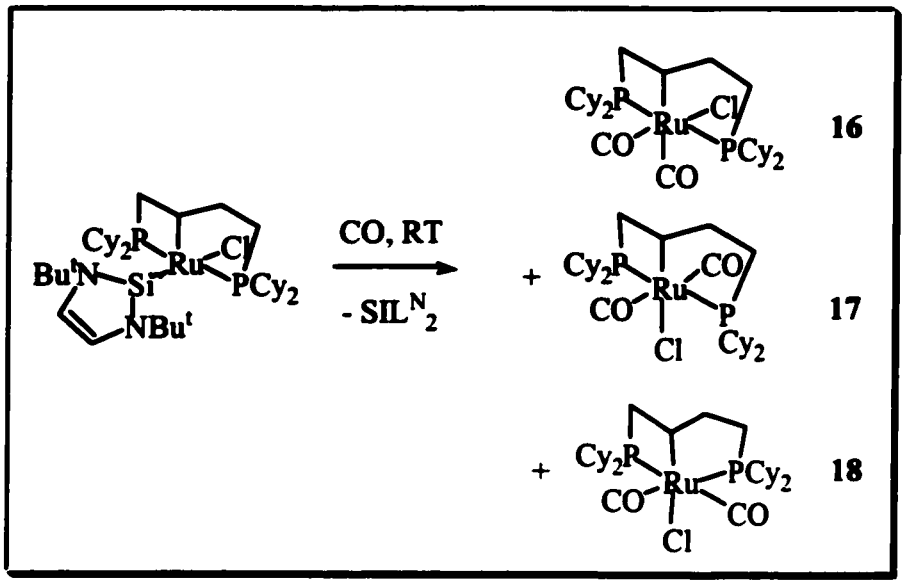

Figure 5. 10 Reaction of **12** with CO.

5.5. Conclusions

The foregoing describes an unusual example of a silylene moiety found within a coordinatively unsaturated ligand environment containing chloride and phosphine ligands, in which a novel η^3-coordination mode for the chelating diphosphine results from activation of an sp^3 C-H bond within the tetramethylene backbone. Solid-state and low-temperature NMR data, supported by crystallographic analysis, suggest a coordinatively saturated structure, in which an agostic interaction occupies the sixth coordination site. Confirmation of the accessibility of this site in solution, and clear indication of the non-innocent behaviour of the silylene ligand, comes from the observed reactivity toward both H_2/H_2O and CO. Displacement of silylene by CO is facile at room temperature, giving access to novel η^3-dcypb carbonyl complexes. Hydrolysis and

hydrogenolysis affords a simple η^2-dcypb complex, with elimination of bound silylene as siloxane. Attempts to introduce alkylidene at the metal were limited by unreactivity toward diazoalkane, and by the susceptibility of the silylene to decomposition. These results join several recent examples in suggesting that - in contrast to current views of the analogous, Arduengo-type carbenes - the SiL^N_2 ligand can readily participate in reactions at transition-metal centers.

5.6. References

1) Haaf, M.; Schmedake, T. A.; West, R. *Acc. Chem. Res.* **2000**, *33*, 704.

2) Schmedake, T. A.; Haaf, M.; Paradise, B. J.; Millevolte, A. J.; Powell, D. R.; West, R. *J. Organomet. Chem.* **2001**, *636*, 17.

3) Schmedake, T. A.; Haaf, M.; Paradise, B. J.; Powell, D.; West, R. *Organometallics* **2000**, *19*, 3263.

4) Dysard, J. M.; Tilley, T. D. *Organometallics* **2000**, *19*, 4726.

5) Denk, M.; Hayashi, R. K.; West, R. *J. Chem. Soc. Chem. Comm.* **1994**, 33.

6) Gehrhus, B.; Hitchcock, P. B.; Lappert, M. F.; Maciejewski, H. *Organometallics* **1998**, *17*, 5599.

7) Petri, S. H. A.; Eikenberg, D.; Neumann, B.; Stammler, H. G.; Jutzi, P. *Organometallics* **1999**, *18*, 2615.

8) Tilley, T. D. *The Silicon-Heteroatom Bond*; Patai, S. and Rappoport, Z., Ed.; Wiley: New York, 1991, pp Chapters 9 and 10, pp 245 and 309.

9) Tilley, T. D. *The Chemistry of Organic-Silicon Compounds*; Patai, S. and Rappoport, Z., Ed.; Wiley: New York, 1989; Vol. 2, pp Ch. 24, p 1415.

10) Wanandi, P. W.; Glaser, P. B.; Tilley, T. D. *J. Am. Chem. Soc.* **2000**, *122*, 972.

11) Grumbine, S. K.; Tilley, T. D.; Arnold, F. P.; Rheingold, A. L. *J. Am. Chem. Soc.* **1994**, *116*, 5495.

12) Straus, D. A.; Tilley, T. D. *J. Am. Chem. Soc.* **1987**, *109*, 5872.

13) Straus, D. A.; Grumbine, S. D.; Tilley, T. D. *J. Am. Chem. Soc.* **1990**, *112*, 7801.

14) Grumbine, S. K.; Mitchell, G. P.; Straus, D. A.; Tilley, T. D.; Rheingold, A. L. *Organometallics* **1998**, *17*, 5607.

15) Mitchell, G. P.; Tilley, T. D. *Angew. Chem. Int. Ed. Engl.* **1998**, *37*, 2524.

16) Denk, M.; Lennon, R.; Hayashi, R.; West, R.; Belyakov, A. V.; Verne, H. P.; Haaland, A.; Wagner, M.; Metzler, N. *J. Am. Chem. Soc.* **1994**, *116*, 2691.

17) Arduengo, A. J.; Dias, H. V. R.; Harlow, R. L.; Kline, M. *J. Am. Chem. Soc.* **1992**, *114*, 5530.

18) Jutzi, P.; Mohrke, A. *Angew. Chem. Int. Ed. Engl.* **1990**, *29*, 893.

19) Garrou, P. E. *Chem. Rev.* **1981**, *81*, 229.

20) Chaudret, B.; Dagnac, P.; Labroue, D.; Sabo-Etienne, S. *New J. Chem.* **1996**, *20*, 1137.

21) Leitner, W.; Six, C. *Chem. Ber.* **1997**, *130*, 555.

22) Six, C.; Gabor, B.; Gorls, H.; Mynott, R.; Philipps, P.; Leitner, W. *Organometallics* **1999**, *18*, 3316.

23) Ogasawara, M.; Saburi, M. *Organometallics* **1994**, *13*, 1911.

24) Bemi, L.; Clark, H. C.; Davies, J. A.; Fyfe, C. A.; Wasylishen, R. E. *J. Am. Chem. Soc.* **1982**, *104*, 438.

25) Djurovich, P. I.; Carroll, P. J.; Berry, D. H. *Organometallics* **1994**, *13*, 2551.

26) Wada, H.; Tobita, H.; Ogino, H. *Organometallics* **1997**, *16*, 3870.

27) Wada, H.; Tobita, H.; Ogino, H. *Organometallics* **1997**, *16*, 2200.

28) Mitchell, G. P.; Tilley, T. D. *J. Am. Chem. Soc.* **1997**, *119*, 11236.

29) Rodriguez, V.; Sabo-Etienne, S.; Chaudret, B.; Thorburn, J.; Ulrich, S.; Limbach, H.-H.; Eckert, J.; Barthelat, J.-C.; Hussein, K.; Marsden, C. J. *Inorg. Chem.* **1998**, *37*, 3475.

30) Drouin, S. D.; Yap, G. P. A.; Fogg, D. E. *Inorg. Chem.* **2000**, *39*, 5412.

31) Sanford, M. S.; Henling, L. M.; Day, M. W.; Grubbs, R. H. *Angew. Chem. Int. Ed. Engl.* **2000**, *39*, 3451.

32) Denk, M.; Green, J. C.; Metzler, N.; Wagner, M. J. *J. Chem. Soc. Dalton Trans.* **1994**, 2405.

33) West, R.; Denk, M. *Pure Appl. Chem.* **1996**, *68*, 785.

34) Molecular Simulations, I. *Cerius^2 Property Prediction*: San Diego, 1999.

35) Haaf, M.; Schmiedl, A.; Schmedake, T. A.; Powell, D. R.; Millevolte, A. J.; Denk, M.; West, R. *J. Am. Chem. Soc.* **1998**, *120*, 12714.

36) MacFarlane, K. S.; Thorburn, I. S.; Cyr, P. W.; Chau, D. E. K. Y.; Rettig, S. J.; James, B. R. *Inorg. Chim. Acta* **1998**, *270*, 130.

CHAPTER 6

Elucidation of Deactivation Pathways in Chlororuthenium Metathesis Catalysts

6.1. Introduction

Offsetting the high ROMP activity of benzylidene derivatives $RuCl_2(PP)(CHPh)$ described in Chapter 4 was an instability that precluded isolation, prompting us to undertake installation of alternative, more stable[1] alkylidenes for the purposes of ligand tuning and characterization. An attractive point of entry into such species involves use of hydride as a synthon for alkylidene, via reaction of hydridochlororuthenium complexes with 3-chloro-3-methyl-1-butyne to form complexes containing the $[Ru=CHCH=CMe_2]$ functionality.[2] Likewise, while extraordinary success has accrued to catalysts of the type $RuCl_2LL'(CHPh)$ ($L = PCy_3$; $L' = PCy_3$, imidazol-2-ylidene),[3] the instability of both the benzylidene functionality itself and its phenyldiazomethane precursor has focused recent attention on less reactive metal-carbon functionalities.[4,5] Rather stable vinylidene species can be accessed from chlororuthenium precursors, via treatment with *tert*-butylacetylene, while allenylidenes are accessible via the corresponding reaction with 1,1-diphenyl-2-propyn-1-ol. A number of Ru allenylidene or vinylidene complexes have shown promising metathesis activity in ring-closing or ring-opening metathesis reactions.[6] While the greater stability of the Ru=C entity, vs. Ru-benzylidene, can be anticipated to increase polymer polydispersity in ROMP, this should be manifested only as a latency

period in RCM or cross-metathesis.

Complex **5** $[Ru_2Cl_4(dcypb)_2(N_2)]$ is attractive as an incipient source of the mononuclear fragment "$RuCl_2(dcypb)$", unencumbered by extraneous, potentially interfering ligands such as phosphine or amine. This chapter describes the synthesis of a novel hydridochloro dimer (**14**) containing the chelating diphosphine dcypb, and the conversion of the hydridochloro and dichloro dimers into alkylidene, vinylidene, hydroxy-vinylidene and allenylidene derivatives.

6.2. Vinylidene Derivative

Vinylidene complexes, the simplest class of metallocumulenylidenes $M=(C=)_nCR_2$ (n = 1), are readily accessible via reactions of transition-metal precursors with 1-alkynes.[4,5,7] Reaction of **5** with excess 3,3-dimethyl-1-butyne cleanly forms dinuclear monovinylidene $RuCl(dcypb)(\mu\text{-}Cl)_3Ru(dcypb)(L)$ (L = :C=CH^{t}Bu, **19**), with evolution of N_2 gas. The identity of **19** is established by detailed spectroscopic analysis and microanalytical data. Installation of vinylidene proceeds smoothly at RT (22 C) despite the insolubility of both starting material and product. Thus, while addition of the alkyne reagent (0.5-4 equiv) to a stirred orange suspension of **5** in benzene did not effect dissolution, an aliquot removed after 12 h showed no remaining ^{31}P NMR signals for **5**. Concentration of the solution and addition of pentane permitted isolation of orange **19** in 86% yield. The proposed structure is supported by observation of a sharp, medium intensity infrared band at 1633 cm^{-1}, a location characteristic of the vinylidene $\nu_{C=C}$ vibration.[4,5,7] ^1H NMR analysis reveals a triplet for the vinylidene proton (δ_H 3.06, $^4J_{HP}$ =

3.8 Hz), accompanied by a peak for the *tert*-butyl protons at δ_H 1.24, visible as a sharp singlet above the broad, unresolved dcypb resonances (1.0-3.2 ppm). A diagnostic downfield triplet for the vinylidene α-carbon appears in the $^{13}C\{^1H\}$ NMR spectrum (δ_C 352.1, $^2J_{CP}$ = 16 Hz), accompanied by a singlet for C_β at δ_C 119.2. $^{31}P\{^1H\}$ NMR data provide unequivocal evidence for the dinuclear, monovinylidene structure. Four distinct sets of resonances are observed, signifying the presence of four inequivalent phosphorus nuclei within a dinuclear structure devoid of symmetry (δ_P 50.6, 49.6 (ABq, $^2J_{PP}$ = 37 Hz); 45.9, 40.1 (AB, $^2J_{PP}$ = 23 Hz)).

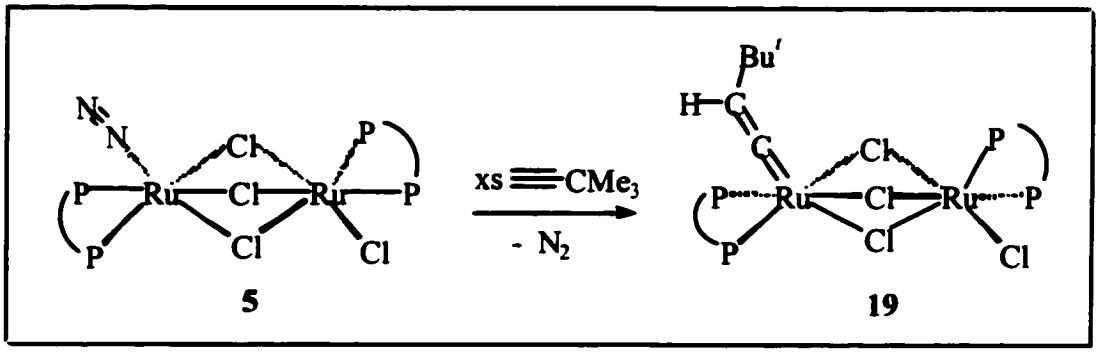

Figure 6. 1. Reaction of $Ru_2Cl_4(dcypb)_2(N_2)$ (**5**) with *tert*-butylacetylene.

Microanalytical data are in good agreement with the proposed structure, although low solubility precluded reprecipitation of **19** from THF or aromatic (benzene, toluene) solvents. Purification by reprecipitation from chlorocarbon solvents, in which solubility is higher, is thwarted by decomposition in such solvents. Dcypb complexes frequently undergo chlorination in chloroform or methylene chloride, and mixed-valence $Ru_2Cl_5(dcypb)_2$ has been crystallographically identified among the products (Chapter 3). A new ^{31}P NMR singlet (δ 46.8; ~2-5%) emerges immediately after dissolving **19** in

$CDCl_3$. Complete decomposition is comparatively slow, however (^{31}P NMR signals for **19** remain evident after 3 weeks in solution), permitting NMR analysis in $CDCl_3$.

6.3. Allenylidene/hydroxyvinylidene Derivative

Spontaneous dehydration of propyn-1-ols by transition-metal complexes provides an important route to allenylidene derivatives,[4,8] and in some cases their indenylidene rearrangement products.[9-12] The reaction proceeds via isomerization of a 3-hydroxyalkynyl-metal hydride[13,14] to a 3-hydroxyvinylidene species, which on loss of water yields the allenylidene complex.[4] Addition of 1,1-diphenyl-2-propyn-1-ol (2 equiv) to a stirred suspension of **5** at RT caused a colour change from orange to brown without dissolution; the ^{31}P NMR signals for starting **5** disappeared completely within 12 h. The light brown product was isolated in 88% yield by diluting the suspension with hexanes, filtering, and washing the powder with hexanes. As with **19**, the insolubility of the complex precluded reprecipitation, and purification was effected by trituration with hexanes.

$^{31}P\{^1H\}$ NMR analysis of the product reveals four sets of resonances of equal intensity, in a pattern closely analogous to that of **19** (51.5, 50.1 (ABq, $^2J_{PP}$ = 38 Hz); 44.7 (d, unresolved), 40.9 (d, unresolved)), indicating formation of a complex of the type RuCl(dcypb)(μ-Cl)$_3$Ru(dcypb)(L). The infrared spectrum, however, does not show the diagnostic, strong allenylidene $\nu_{C=C=C}$ band between 1870 and 1970 cm^{-1}.[4] Indeed, this region of the spectrum is featureless: instead, a sharp, medium-intensity band is found at much lower energy (1644 cm^{-1}), suggesting the presence of a vinylidene or indenylidene

ligand. The aromatic region of the ^{1}H NMR spectrum contains only a first-order splitting pattern for two equivalent, monosubstituted benzene rings, ruling out the possibility of isomerization of the allenylidene ligand to form a 3-phenyl-1-indenylidene[10] derivative (Figure 6. 2). The remainder of the spectrum contains the expected envelope for the dcypb protons from 0.8-3.5 ppm, as well as a triplet at 4.38 ($^4J_{HP}$ = 3.7 Hz) and a singlet at 3.99 ppm, each integrating to 1H. ^{1}H-^{13}C HMQC experiments correlate the signal at δ_H 4.38 with an sp^2 carbon at 120 ppm. The signal at δ_H 3.99 does not correlate with any carbon nucleus; its identity as a hydroxyl proton is confirmed by exchange with D_2O, as well as observation of a medium-intensity IR band at 3483 cm^{-1} (ν(OH)) for the protio-derivative.

These data imply that installation of the allenylidene ligand has halted at the stage of hydroxyvinylidene **20a**.[4,13,14] The resistance of electron-rich hydroxyvinylidene species to dehydration has been noted.[13,14] The ^{1}H NMR data, as well as the ^{13}C NMR shift position for C_β deduced from ^{1}H-detected HMQC experiments, are in excellent agreement with values reported for the related species [Cp*Ru{C=CHC(OH)Ph$_2$}(P^{i}Pr$_2$CH$_2$CH$_2$P^{i}Pr$_2$)][BPh$_4$].[14] Attempts to confirm the assignment by direct measurement of the ^{13}C{^{1}H} NMR spectrum were thwarted by the poor solubility of **20a** in benzene. The spectrum in $CDCl_3$, though complicated by competing decomposition over the 24 h timescale required for good signal-to-noise ratios (vide supra), reveals the diagnostic downfield signals for the allenylidene moiety (C_α, δ 308.7, unresolved t; C_β, 243.4, s; C_γ, 150.4, s). Dissolution-triggered tautomerization of related hydroxyvinylidene species was recently described.[14] This indirect evidence, with the cumulative weight of the ^{1}H NMR, HMQC, and infrared data, provides strong support

for hydroxyvinylidene structure **20a**. Microanalytical data are in good agreement with this formulation.

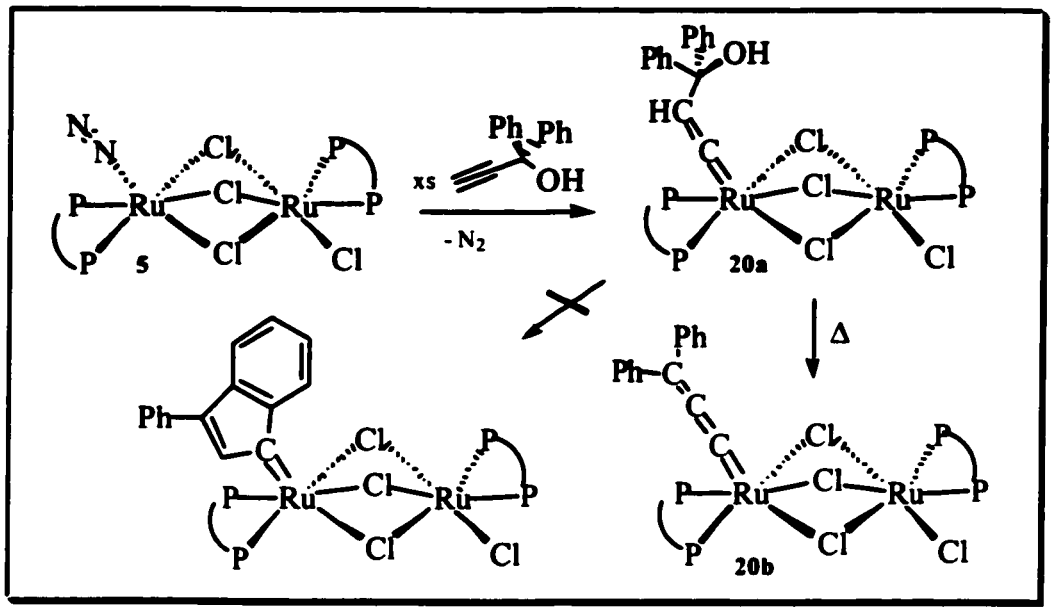

Figure 6. 2. Reaction of $Ru_2Cl_4(dcypb)_2(N_2)$ (**5**) with 1,1-diphenyl-2-propyn-1-ol.

In view of the partial transformation of hydroxyvinylidene **20a** to allenylidene in $CDCl_3$, the former complex was subjected to more forcing conditions in the hope of effecting quantitative dehydration. Indeed, NMR-scale thermolysis of a C_6D_6 suspension of **20a** (70 C, 48 h) gave quantitative conversion to allenylidene **20b**. The identity of **20b** is established on the basis of ^1H and $^{31}P\{^1H\}$ NMR and IR spectroscopy. $^{31}P\{^1H\}$ NMR analysis reveals four new sets of resonances of equal intensity, in a pattern closely analogous to that of **20a** (δ_P 57.6 (d, $^2J_{PP}$ = 39 Hz), 45.1 (d, $^2J_{PP}$ = 28 Hz), 44.5 (d, $^2J_{PP}$ = 39 Hz), 39.1 (d, unresolved)), indicating retention of the RuCl(dcypb)(μ-$Cl)_3$Ru(dcypb)(L) motif. Disappearance of the ^1H NMR triplet at 4.38 and singlet at 3.99 ppm (for the hydroxyvinylidene β-H and the hydroxy proton, respectively) provides

evidence for dehydration, as does emergence of a singlet at δ_H 0.49, integrating to 2H, and assigned to H_2O (one equivalent). As with **20a**, the aromatic region of the ^1H NMR spectrum contains only a first-order splitting pattern for two equivalent, monosubstituted benzene rings, ruling out the possibility of isomerization of the allenylidene ligand to form a 3-phenyl-1-indenylidene[10] derivative (Figure 6. 2). Consistent with the NMR data, IR analysis of the residue shows the diagnostic[4] allenylidene ν(C=C=C) band as a medium-intensity signal at 1914 cm^{-1}.

6.4. Origin of Dinuclear Products

In principle, the dinuclear vinylidene products may arise from decomposition of initially-formed $RuCl_2(PP)(L)$ (L = :C=CRR') via homodimerization (Figure 6. 3, path i), or via cross-dimerization[15] with unreacted **5** (path ii). In view of the poor solubility of both **5** and **19**, however, we cannot rule out the alternative possibility that reaction takes place within the dinuclear framework, at a site vacated by N_2 (path iii).

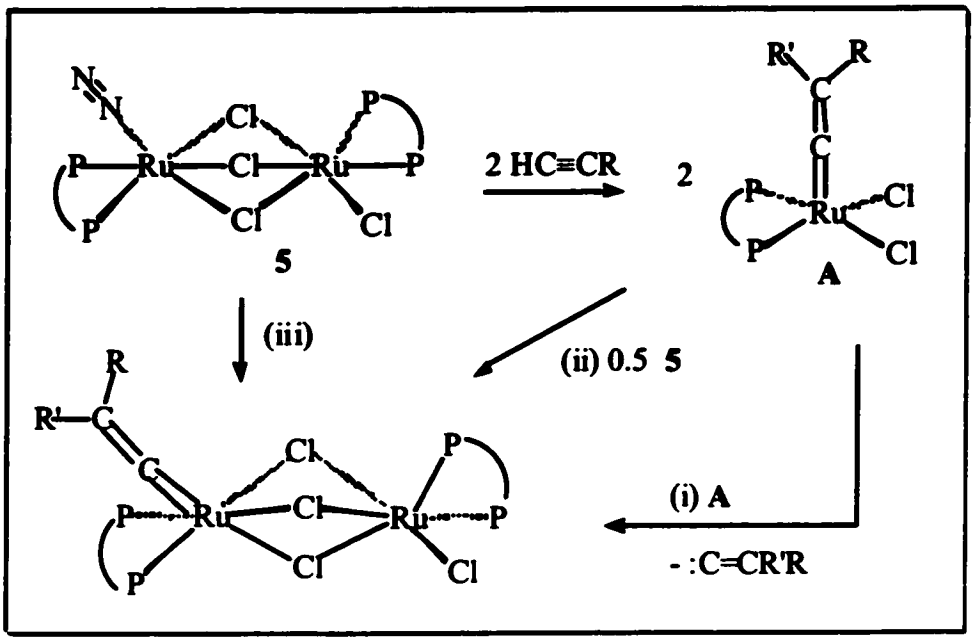

Figure 6. 3. Possible routes to formation of dinuclear vinylidene complexes.

In this context, installation of an alkylidene ligand via treatment of "RuHCl(dcypb)"[16] with the propargyl chloride derivative 3-chloro-3-methyl-1-butyne[2] (Figure 6. 4) is attractive for its mechanistic unambiguity. The extent of replacement of hydride by chloride offers direct insight into the probability of decomposition via homodimerization (path (i)) vs. paths (ii) and (iii). Furthermore, installation of one alkylidene concomitant with each chloride ligand means that formation of monoalkylidene **21** ($RuCl(dcypb)(\mu\text{-}Cl)_3Ru(dcypb)(L)$; L = $:CHCH=CMe_2$) would *necessarily* implicate homodimerization. Conversely, if formation of **20a/19** occurs via path (iii) (Figure 6. 3) and dimerization is disfavoured (as indeed suggested by the stability[17] of **2d**), the propargyl chloride route could potentially afford access to mononuclear $RuCl_2(dcypb)(CHCH=CMe_2)$ **2e** (Figure 6. 4).

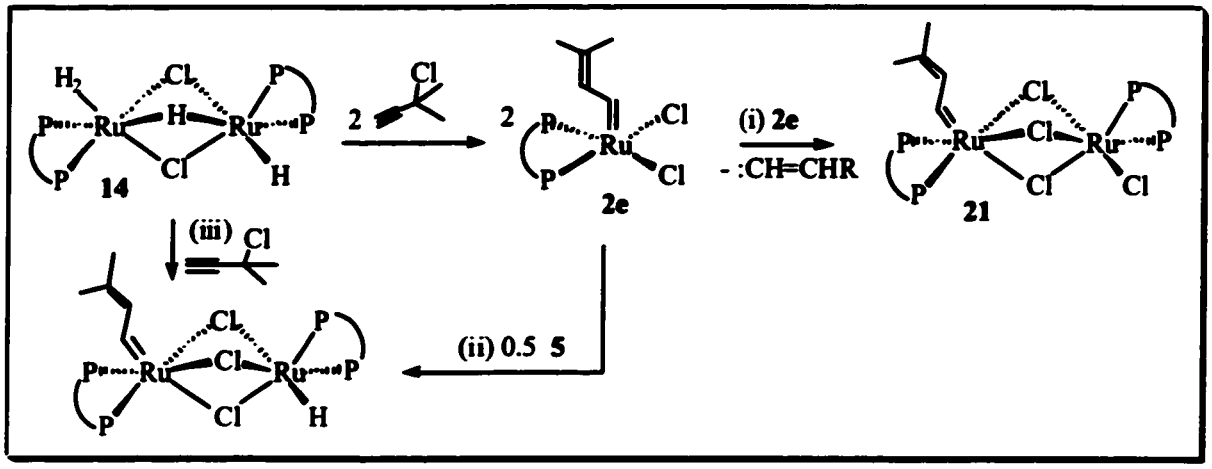

Figure 6. 4. Dimerization pathways for the mononuclear alkylidene complex $RuCl_2(dcpb)(CHCHC(CH_3)_2)$ **2e**.

6.5. Hydridochloro Derivatives

Exploration of the propargyl chloride route requires prior synthesis of hydridochloro dimer **14**, $Ru(\eta^2\text{-}H_2)(dcypb)(\mu\text{-}Cl)_2(\mu\text{-}H)Ru(H)(dcypb)$. The latter is cleanly obtained by reaction of **5** with KHB^sBu_3 (Figure 6. 5); disproportionation to a polyhydride does not occur, in contrast to the behaviour of dichlorocarbonyl species $[RuCl_2(dcypb)(CO)]_2$.[18] Suspensions of **5** react rapidly with two equivalents of KHB^sBu_3 in benzene under 1 atm H_2 (RT, < 5 min), yielding a homogeneous orange solution. Detailed NMR studies, supported by X-ray crystallography, confirm the identity of the product.

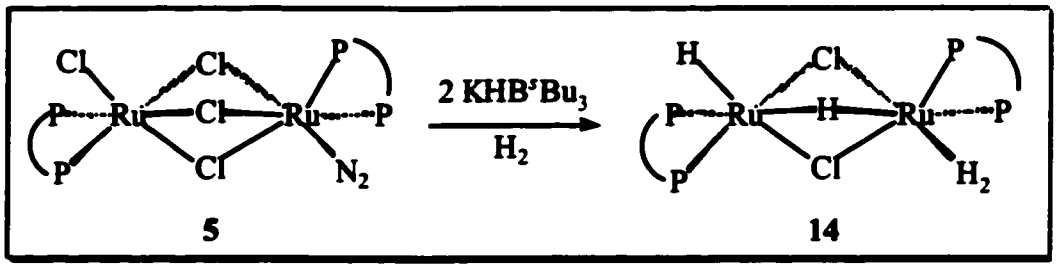

5 14

Figure 6. 5. Reaction of $Ru_2Cl_4(dcypb)_2(N_2)$ (**5**) with KHB^sBu_3.

^{31}P NMR analysis of **14** (C_6D_6, 22 C) reveals two broad singlets, at 65 and 52 ppm (1:1 ratio; $\omega_{1/2}$ 57.8 Hz, 173.7 Hz, respectively). These signals do not couple to each other (^{31}P-^{31}P COSY), but correlate by ^{31}P EXSY-NMR. The upfield resonance broadens into the baseline on cooling to 276 K, while the signal at δ_P 65 sharpens. Little further change occurs down to 180 K, at which temperature two broad signals (δ_P 78 and 21) emerge, each integrating to approximately half the intensity of the resonance still apparent at 63 ppm. This behaviour is characteristic of $Ru(\eta^2\text{-}H_2)(PP)(\mu\text{-}Cl)_2(\mu\text{-}H)Ru(H)(PP)$ species: directly analogous spectra have been described for triphenylphosphine and tri(p-tolyl)phosphine complexes.[19,20] The broad upfield peak in these species is assigned to the "Ru-H_2" end of the molecule, at which the terminal dihydrogen ligand undergoes rapid exchange with bridging hydride. Owing to the breadth of this signal, we are unable to observe a hydride correlation in ^1H-^{31}P HMQC experiments.[21] ^1H NMR analysis of **14** (C_7D_8, 22 C) is likewise in excellent agreement with the literature reports.[19,20] A single hydride resonance appears (δ_H -13.8, br s), which on cooling to 194 K coalesces into three broad resonances (Table 6. 1). No improvement in resolution occurs down to 170 K. Integration and T_1 values are consistent with the presence of two hydride ligands and a single $Ru(\eta^2\text{-}H_2)$ moiety.

Table 6. 1. Properties of Hydride Signals for 14 at 194 K, 500 MHz.

δ_H	-9.8	-12.6	-20.3
integration	1H	2H	1H
T_1	200 msec	60 msec	450 msec
assignment	Ru(μ,η^1-H)	Ru(η^2-H_2)	Ru(η^1-H)

6.5.1. Molecular Structure of [RuH(dcypb)](μ-H)(μ-Cl)$_2$[Ru(H_2)(dcypb)] (14)

Several small crystals of **14** formed at the gas-solution interface of a benzene solution of **14** on storage under H_2, one of which was found suitable for X-ray analysis. An ORTEP representation appears in Figure 6. 6, with crystallographic and selected bond lengths and angles in Table 6. 2. All hydride ligands were located and refined with a riding model.

Complex **14** adopts a diruthenium structure, in which the two metal centers have a distorted octahedral geometry, bridged by two chloride and one hydride ligand. The diffraction data indicate 50% site occupancy of two terminal sites by hydride and η^2-H_2. The "Ru-H" (terminal) distances (ca. 1.57(2) Å) are thus intermediate between values expected for Ru-H and Ru-H_2: cf. values of 1.75(3) Å for the Ru-(η^2-H_2) distance in chloride-bridged dimer in Ru(η^2-H_2)(dppb)(μ-Cl)$_3$RuCl(dppb),[22] and 1.50(4) Å for the terminal Ru-H distance in Ru(η^2-H_2)(L_2)(μ-Cl)$_2$(μ-H)Ru(H)(PPh_3)$_2$ (L_2 = Fe(η^5-C_5H_3(CHMeNMe$_2$)P^{i}Pr)$_2$-1,2)(η^5-C_5H_5)[19]), in which no such disorder exists. Likewise, the strong trans effect of hydride, relative to η^2-H_2, will normally cause lengthening of the Ru-Cl bond trans to the hydride ligand. However, the presence in **14** of a statistical

distribution of hydride and dihydrogen ligands trans to μ-Cl results in a narrower range in bond lengths relative to those in $Ru(\eta^2\text{-}H_2)(L_2)(\mu\text{-}Cl)_2(\mu\text{-}H)Ru(H)(PPh_3)_2$; cf. values of 2.4298(5) - 2.5531(5) Å in **14**, vs. 2.435(2) - 2.620(2) Å in the literature complex.

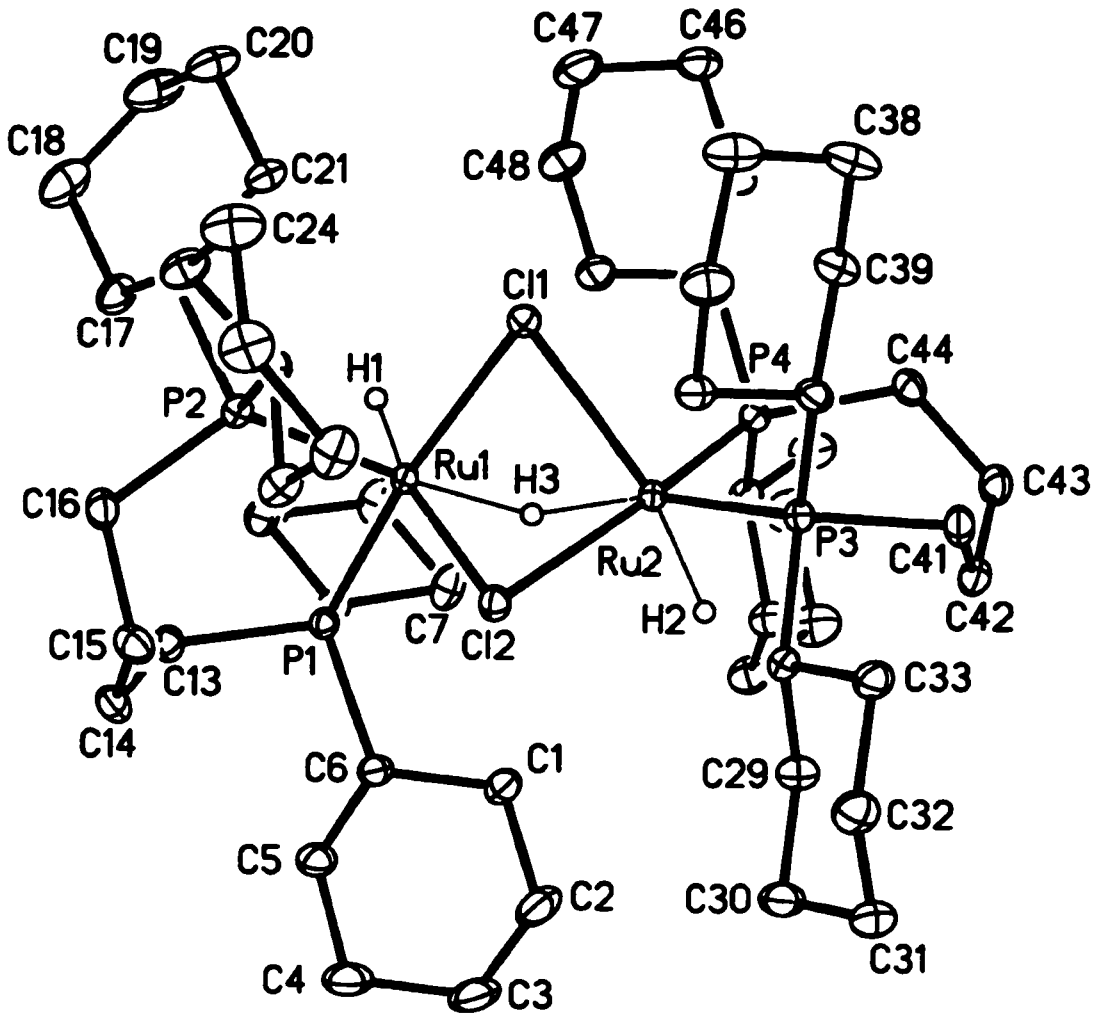

Figure 6. 6. ORTEP diagram of $Ru(H)(dcypb)(\mu\text{-}Cl)_2(\mu\text{-}H)Ru(H_2)(dcypb)$ **14** with thermal ellipsoids shown at 30% probability level. Non-hydridic hydrogen atoms and solvent molecules omitted for clarity.

Table 6. 2. Selected Bond Lengths (Å) and Angles (deg) for **14**.

Ru(1)-P(1)	2.2681(5)	Ru(2)-P(3)	2.2543(5)
Ru(1)-P(2)	2.3854(5)	Ru(2)-P(4)	2.2453(5)
Ru(1)-H(1)	1.573(13)	Ru(2)-H(2)	1.559(12)
Ru(1)-H(3)	1.768(18)	Ru(2)-H(3)	1.84(2)
Ru(1)-Cl(1)	2.4725(5)	Ru(2)-Cl(1)	2.5531(5)
Ru(1)-Cl(2)	2.4298(5)	Ru(2)-Cl(2)	2.5034(5)
Ru(1)-Ru(2)	2.8595(3)		
P(1)-Ru(1)-P(2)	100.384(17)	P(4)-Ru(2)-P(3)	98.762(19)
Ru(1)-Cl(1)-Ru(2)	69.337(12)	Ru(1)-Cl(2)-Ru(2)	70.832(14)
P(1)-Ru(1)-Cl(1)	171.687(17)	P(4)-Ru(2)-Cl(2)	166.667(19)
P(2)-Ru(1)-H(3)	173.2	P(3)-Ru(2)-H(3)	167.1
H(1)-Ru(1)-Cl(2)	168.3	H(2)-Ru(2)-Cl(1)	169.5
Ru(1)-H(3)-Ru(2)	104.6(9)		

Despite formation of a few small crystals of **14** as described above, repeated efforts to isolate this species proved unsuccessful. Its high solubility inhibited precipitation from all solvents investigated, including cold (-35 C) pentane. As with other dcypb complexes, concentration to dryness results in decomposition. We have described the susceptibility of the parent complex **5** to intramolecular dehydrogenation under vacuum or argon (Chapter 3). Intramolecular decomposition also occurs on stripping solutions containing **14** to dryness, as indicated by the serendipitous crystallization of [Ru(H)(dcypb)(μ-Cl)$_3$Ru(dcypb)(N_2)] **13**, containing an additional chloride ligand, from the large number of species formed. The crystal structure of **13** was described in Chapter 5. Attempts to circumvent dehydrogenation by drying **14** under a stream of H_2 were unsuccessful, decomposition to many products again being indicated

by NMR analysis. Microanalysis carried out on the solid products, on the possibility that decomposition ensues on redissolution, gave results consistently low in carbon. As with complex **5**, however, **14** can be synthesized and handled without difficulty in solutions saturated with an appropriate, stabilizing donor ligand. For all subsequent synthetic efforts, **14** was therefore prepared and reacted in situ under H_2.

6.6. Alkylidene Derivatives

Reaction of a homogeneous, orange solution of [Ru(H)(dcypb)(μ-Cl)$_2$(μ-H)Ru(dcypb)(H_2)] with 3-chloro-3-methyl-1-butyne resulted in immediate formation of dinuclear monoalkylidene RuCl(dcypb)(μ-Cl)$_3$Ru(dcypb)(CHCH=CMe$_2$) (**21**, Figure 6. 4), the identity of which is confirmed by NMR and crystallographic analysis. In contrast to **20a/19**, the complex exhibits good solubility, aiding its spectroscopic characterization. It is isolated in ca. 80% yield on reprecipitation from benzene-hexanes, though contaminated with ca. 20% of coproduct **22** (vide infra) which could not be separated by reprecipitation or washing. No other products are spectroscopically evident. ^{1}H NMR analysis of the mixture in C_6D_6 reveals two quartets, in a ratio of 4:1, due to H_α of two distinct alkylidene ligands (**21**, δ_H 16.92; q, $^3J_{HH}$ = 11.5 Hz, $^3J_{HP}$ = 11.5 Hz; **22**, 15.83 (q, RuC*H*, $^3J_{HH}$ = 12.0 Hz, $^3J_{HP}$ = 12.0 Hz). The multiplicity of this signal indicates coupling to two phosphorus nuclei and H_β with coincident $^3J_{HH}$ and $^3J_{HP}$ values (as earlier found[17] for RuCl$_2$(dtbpm)(CHCH=CMe$_2$), **2d**). Four ^{31}P{^{1}H} NMR resonances, of equal integrated intensity, are found for **21**, signifying the presence of four inequivalent phosphorus nuclei within a dinuclear complex devoid of symmetry. At RT in C_6D_6, these

resonances are broad, unresolved singlets (δ 54.0, 46.1, 45.1, 42.9). On cooling to 273 K (C_7D_8), the signal at ca. 43 ppm sharpens to a doublet ($^2J_{PP}$ = 32 Hz), but the others remain unresolved: on cooling further, all four signals broaden until (245 K) they are nearly lost in the baseline. All four resonances are resolved into doublets in $CDCl_3$ (δ 59.0, 43.7 ($^2J_{PP}$ = 39 Hz); 46.9, 40.5 ($^2J_{PP}$ = 26 Hz)); in a pattern closely similar (including *J* values) to those found for **20/19**, particularly for the upfield pair of doublets. The latter signals are therefore assigned to the "Cl-end" of the dimer. Reaction with solvent also occurs, however, affording an unidentified product (**23**) characterized by a pair of doublets at δ_P 46.4, 42.6 (^2J = 35 Hz) (vide infra).

Complex **21** is much more susceptible to chlorination by $CDCl_3$ than was the case for **19**, as indicated by complete disappearance of signals due to **21**, accompanied by crystallization of paramagnetic $Ru_2Cl_5(dcypb)_2$ (identified by comparison of the unit cell to that established in Chapter 3) within 48 h of dissolution. The nature of the reaction with $CDCl_3$ is probed in more detail in Section 6.6.2. Complex **21** is observed irrespective of reaction time, stoichiometry (2-20 equiv), or temperature (-35 C or RT), providing strong evidence for facile homodimerization of initially-formed **2e** (Figure 6. 4). Formation of triene $Me_2C{=}CHCH{=}CHCH{=}CMe_2$, the anticipated product of alkylidene elimination and coupling, is confirmed by ^1H NMR.

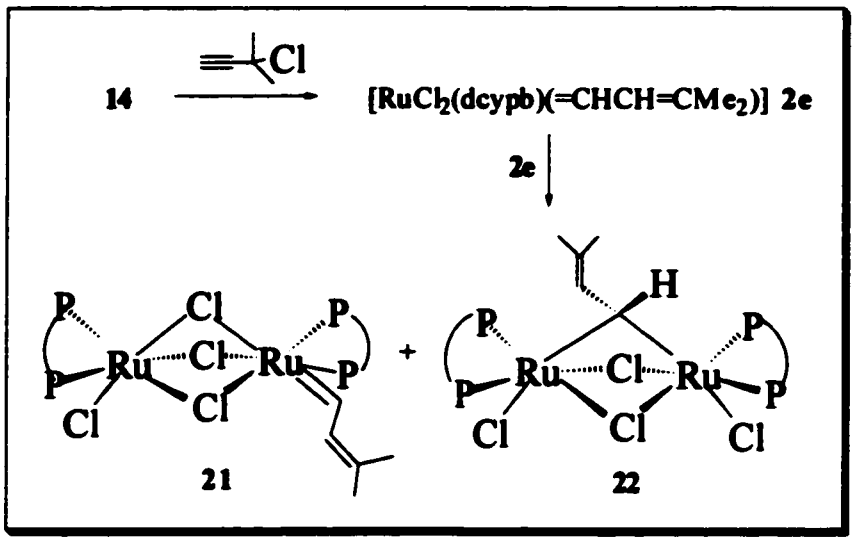

Figure 6. 7. Reaction of **14** with propargyl chloride.

Byproduct **22** also contains an Ru(dcypb)(CHCH=CMe_2) entity, as indicated by observation of a $^{31}P\{^1H\}$ NMR singlet at δ_P 43.4, which correlates in ^1H-^{31}P NMR HMQC experiments with the alkylidene quartet at δ_H 15.83 ppm. The equivalence of the phosphorus nuclei indicates a higher degree of symmetry than in the dinuclear terminal alkylidene complex **21**; this does not appear to be due to averaging of environments through a fluxional process, as low-temperature ^{31}P NMR studies show no change (other than moderate peak broadening) from 333-203K. The NMR data are consistent with square pyramidal **2e** (Figure 6. 4; cf. **2d**[17]), containing apical alkylidene and equivalent, cis phosphine ligands. However, this formulation is difficult to reconcile with the instability of **2e** suggested by formation of **21**, especially given the persistence of signals for the former in NMR spectra recorded over 7 days in solution. The latter evidence strongly suggests that **22** is not on the reaction path leading to **21**, but that both arise from decomposition of **2e**.

A possible alternative structure is a species isomeric with **21**, containing a bridging alkylidene ligand (**22**, Figure 6. 7), potentially formed by nucleophilic attack of the electron-rich metal at C_α. Precedent for such an alkylidene binding mode is found in crystallographically characterized $(Cp^*Ru)_2(\mu\text{-}Cl)_2(\mu\text{-}CHCH{=}CPh_2)$, in which the bridging alkylidene lies perpendicular to the Ru-Ru vector.[23] Observation of a quartet for H_α in **22** implies a similar geometry: the plane containing C_α and the two terminal chloride ligands bisects the P-Ru-P vector, and a near-zero dihedral angle exists between H_α and one ^{31}P nucleus of each dcypb ligand.[24] Attempts to confirm this structure by $^{13}C\{^1H\}$ NMR analysis are hampered by the limited solubility of **22**, but observation of a poorly resolved multiplet containing five principal lines at δ_C 308.6 for C_α (cf. a well-resolved triplet for the corresponding carbon nucleus in **22**) is consistent with an A_2B_2X spin system, in which $J_{P(A)\text{-}C} \neq J_{P(B)\text{-}C}$.

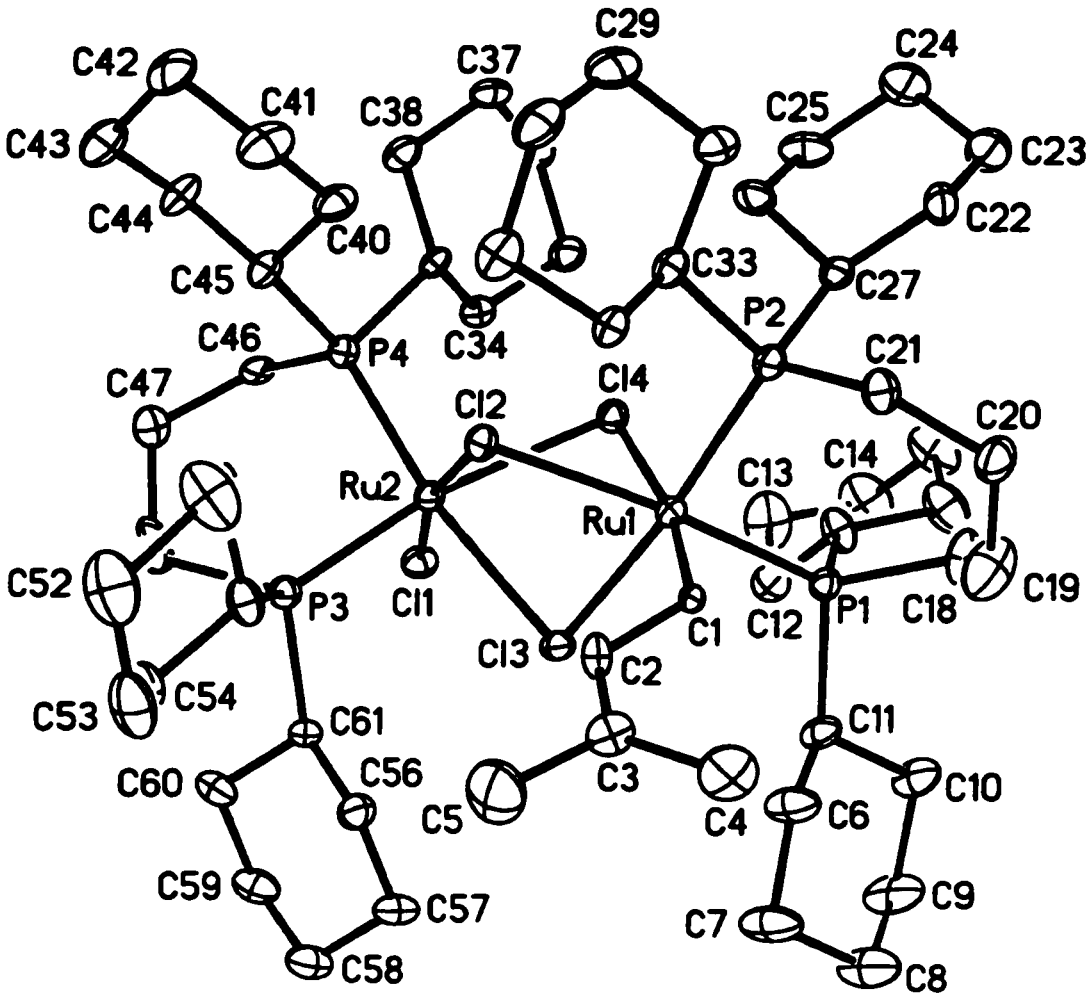

Figure 6. 8. ORTEP diagram of RuCl(dcypb)(μ-Cl)$_3$Ru(dcypb)[:CHCH:C(CH$_3$)$_2$] **21** with thermal ellipsoids shown at 30% probability level. Hydrogen atoms and solvent molecule omitted for clarity.

6.6.1. Molecular Structure of $Ru_2Cl_4(dcypb)_2(CHCHC(CH_3)_2)$ (21)

Crystals of **21** were obtained by slow evaporation of toluene solutions layered with hexanes. An ORTEP drawing is shown in Figure 6. 8, with key bond lengths and angles in Table 6. 3. Complex **21** adopts a triply chloride-bridged diruthenium structure, in which the coordination geometry at each metal center is distorted octahedral. The

structure is unsymmetrical, with Ru(1) bearing an alkylidene functionality, and Ru(2) a chloride ligand. Complex **21** represents the first crystallographically characterized example of a dinuclear Ru phosphine complex containing a single, terminal alkylidene moiety. The Ru-C distance is similar to that in dtbpm complex **2d**[17] (1.888 Å for **21**, vs. 1.858 Å for **2a**). The most significant difference between the two structures appears in the P-Ru-P angles, which are ca. 20 greater in **21**, in keeping with the increased flexibility associated with the four-carbon, vs. one-carbon, diphosphine backbone. Non-alkylidene bond lengths and angles within the $RuCl(PP)(\mu\text{-}Cl)_3Ru(PP)(L)$ skeleton compare well with those reported for $[RuCl(dppb)(\mu\text{-}Cl)_3Ru(dppb)(dmso)]$ (dppb = bis(diphenyl)-1,4-phosphinobutane).[25] Ru-P bond lengths are very slightly longer for **21** (average 2.29 Å, vs. 2.28 Å); $Ru(\mu\text{-}Cl)_3Ru$ angles are ca. 3 larger (average 86.20), reflecting the higher steric demand of the bis(dicyclohexyl)phosphinobutane entity.

Table 6. 3. Selected Bond Lengths (Å) and Angles (deg) for **21**.

Ru(1)-C(1)	1.888(8)	Ru(1)-Cl(3)	2.451(2)
Ru(1)-P(1)	2.304(3)	Ru(1)-Cl(4)	2.543(2)
Ru(1)-P(2)	2.320(2)	Ru(2)-Cl(1)	2.398(2)
Ru(2)-P(3)	2.257(3)	Ru(2)-Cl(2)	2.400(2)
Ru(2)-P(4)	2.277(2)	Ru(2)-Cl(3)	2.525(2)
Ru(1)-Cl(2)	2.471(2)	Ru(2)-Cl(4)	2.532(2)
C(1)-Ru(1)-Cl(4)	170.0(3)	P(4)-Ru(2)-Cl(3)	170.33(9)
P(2)-Ru(1)-Cl(3)	173.33(8)	P(3)-Ru(2)-P(4)	96.95(9)
P(1)-Ru(1)-Cl(2)	169.43(8)	Ru(2)-Cl(2)-Ru(1)	88.43(8)
P(1)-Ru(1)-P(2)	94.31(9)	Ru(1)-Cl(3)-Ru(2)	86.12(7)
Cl(1)-Ru(2)-Cl(2)	166.89(8)	Ru(2)-Cl(4)-Ru(1)	84.04(7)
P(3)-Ru(2)-Cl(4)	167.92(7)		

6.6.2. Decomposition of 21/22 in Halogenated Solvents

Dcypb complexes show a tendency to undergo chlorination by methylene chloride or chloroform (see above; also transformation of **5** to $Ru_2Cl_5(dcypb)_2$ **6**, Chapter 3). Such solvents are preferred, however, for investigation of metathesis activity, which is dramatically slower in benzene or THF (Chapter 4).[26] We were therefore prompted to investigate the reaction of the alkylidene complex(es) with $CDCl_3$.

^1H and $^{31}P\{^1H\}$ NMR run 1 h after dissolution of a NMR sample containing **21/22** in $CDCl_3$ showed an approximate 1:1 ratio of **21**:**22**. Within 24 h of heating at 60 C, ^{31}P NMR signals for **21** were no longer visible above the baseline, leaving only signals corresponding to **22** and unknown species **23** (Section 6.6). The alkylidene α-proton of **21** was still observable, but in a ratio of 0.5:1 relative to the signal for **22**. Prominent features of the spectrum are several broad, upfield resonances, also present (though weaker) in the RT spectrum (δ_H -1.8, -7.9, and -10.2). While the location of the two upfield signals is consistent with one or more hydride species (possibly arising from attack on the dcypb ligand, see Section 6.5.1), the signal intensities argue against assignment to hydride. These peaks may instead be due to paramagnetic shifting of the dcypb alkyl resonances within a mixed-valence species. A possible reaction scheme is shown in Figure 6. 9, in which Ru(II,III) alkylidene species **A** represents an intermediate en route to mixed-valence dimer **6**. Decreases in signal intensity for **21** (and **22**) on standing for 48 h (measured against an unreactive internal standard) relative to the intensity measured immediately after formation supports the eventual decomposition to paramagnetic products.

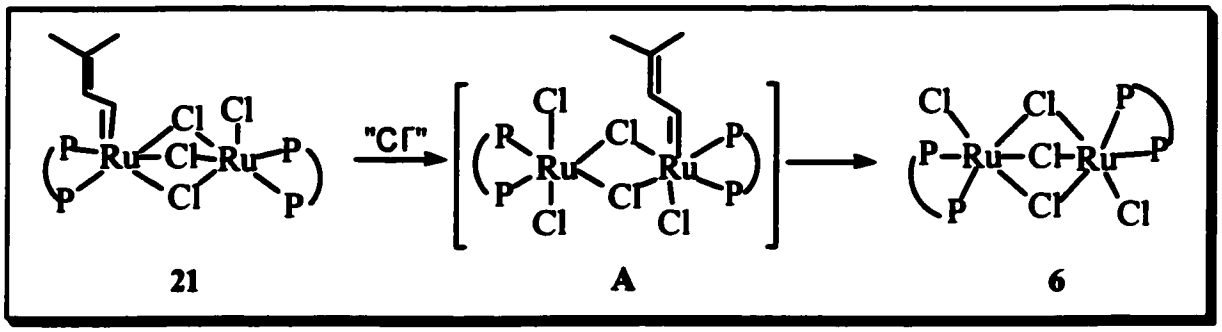

Figure 6. 9. Decomposition of **21** in halogenated solvents.

6.7. ROMP via Alkylidene and Vinylidene Derivatives

In preliminary catalytic studies, complexes **21/22** (as a mixture) showed low activity in ROMP of norbornene (Table 6. 4). A turnover number of 180 h^{-1} is calculated (cf. a TON of 2400 h^{-1} for $RuCl_2$(dcypb)(CHPh) **2a** generated in situ from **5** + 2 $PhCHN_2$ (Chapter 4)). Activity could be restored by addition of 1.0 equiv $PhCHN_2$ per dimer, in which case $CDCl_3$-induced decomposition does not compete with metathesis as indicated by the rapid and quantitative polymerization of norbornene. ROMP in C_6D_6 (in which **21/22** are stable) occurs much more slowly. Such a solvent effect was previously noted (Chapter 4). Abstraction of chloride from **21/22** with trimethylsilyl triflate (TMS-OTf; 1 equiv per dimer) improves activity to a limited extent, presumably via liberation of a coordination site cis to the Ru=C bond. The activity of the hydroxyvinylidene complex **20a** is considerably greater than that of vinylidene **19**, although both are considerably less active than **21/22** (Entries 1, 4 and 6). An improvement in activity is observed upon abstraction of chloride from **19**. In the case of **20a**, TMS-OTf decreases activity, possibly owing to catalyst decomposition. A potential culprit is triflic acid, generated via

deprotonation of the hydroxyvinylidene. In all cases, however, solutions became highly viscous as the reaction progressed, and the polymers were insoluble once isolated, precluding molecular weight determination. This is consistent with slow rates of initiation relative to propagation, which effectively results in a low concentration of catalytically-active species, and formation of very high molecular weight polymers.

The low metathesis activity of these dimers can be attributed in part to their coordinative saturation (in the absence of added triflate or $PhCHN_2$), coupled with the stability of the $Ru_2(\mu\text{-}Cl)_3$ entity. This reaction barrier is exacerbated by the lower reactivity of the [Ru=C=CRR'] entity in the vinylidene derivatives,[27,28] relative to benzylidene[1] (Chapter 4). The higher reactivity of hydroxyvinylidene than vinylidene in this series is worthy of note.

Table 6. 4. Ru-Catalyzed ROMP of norbornene[a]

Entry	Catalyst	Initiating Ligand	Additive[b]	Conversion (%)	Time (min)
1	**21/22**	$CHCHC(CH_3)_2$	-	81	60
2	**21/22**	$CHCHC(CH_3)_2$	TMS-OTf	87	5
3	**21/22**	$CHCHC(CH_3)_2$	$PhCHN_2$	100	5
4	**19**	C=CH(Bu^t)	-	27	1140
5	**19**	C=CH(Bu^t)	TMS-OTf	90	1200
6	**20a**	$C=CHC(OH)Ph_2$	-	99	478
7	**20a**	$C=CHC(OH)Ph_2$	TMS-OTf	92	1353

[a] Reaction conditions: $CDCl_3$ solvent, [norbornene] : [Ru=C] = 225, [Ru=C] = 3.2 mM, RT. [b] Additives: 3.2 mM TMS-OTf or $PhCHN_2$.

6.8. Conclusions

The foregoing describes the synthesis of new ruthenium hydrides that provide an atom-efficient entry point into metathesis chemistry. Dinuclear monoalkylidene, monovinylidene, and monoallenylidene derivatives of $Ru_2Cl_4(dcypb)_2$ are isolated on reactions of the parent dimer with an excess of the appropriate alkyne. In no case are the bis(Ru=CHR) derivatives obtained. While formation of vinylidene and hydroxyvinylidene species of the form $RuCl(dcypb)(\mu\text{-}Cl)_3Ru(dcypb)(L)$ may be an artifact of the poor solubility of both the starting dimer and these products, formation of the analogous alkylidene complex from the soluble hydridochloro precursor indicates a strong driving force for homodimerization of initially-formed $RuCl_2(dcypb)(CHR)$. The low metathesis activity of the face-bridged alkylidene products, in conjunction with the facility with which such dimers are formed, affords a key insight into deactivation pathways incurred by catalysts of type 1 containing non-rigid donor ligands. Related dimerization pathways involving monophosphine species are potentially operative in the Grubbs systems.

6.9. References

1) Schwab, P.; Grubbs, R. H.; Ziller, J. W. *J. Am. Chem. Soc.* **1996**, *118*, 100.

2) Wilhelm, T. E.; Belderrain, T. R.; Brown, S. N.; Grubbs, R. H. *Organometallics* **1997**, *16*, 3867.

3) Recent reviews: (a) Trnka, T. M.; Grubbs, R. H. *Acc. Chem. Res.* **2001**, 34, 18. (b) Jørgensen, M.; Hadwiger, P.; Madsen, R.; Stütz, A. E.; Wrodnigg, T. M. *Curr. Org. Chem.* **2000**, 4, 565. (c) Roy, R.; Das, S. K. *J. Chem. Soc., Chem. Commun.* **2000**, 519. (d) Buchmeiser, M. R. *Chem. Rev.* **2000**, 100, 1565. (e) Fürstner, A. *Angew. Chem. Int. Ed. Engl.* **2000**, 39, 3012. (f) Wright, D. *Org. Chem.* **1999**, 3, 211. (g) Randall, M. L.; Snapper, M. L. *J. Mol. Catal.* **1998**, 133, 29. (h) Ivin, K. J. *J. Mol. Catal.* **1998**, 133, 1. (i) Armstrong, S. K. *Perkin Trans. 1* **1998**, 371. (j) Grubbs, R. H.; Chang, S. *Tetrahedron* **1998**, 54, 4413. (k) Schuster, M.; Blechert, S. *Angew. Chem., Int. Ed. Engl.* **1997**, 36, 2036.

4) Bruce, M. I. *Chem. Rev.* **1998**, *98*, 2797.

5) Bruneau, C.; Dixneuf, P. H. *Acc. Chem. Res.* **1999**, *32*, 311.

6) For representative examples in ROMP, see: (a) Katayama, H.; Ozawa, F. *Chem. Lett.* **1998**, 67. (b) Katayama, H.; Yoshida, T.; Ozawa, F. *J. Organomet. Chem.* **1998**, *562*, 203. (c) Del Rio, I.; Van Koten, G. *Tetrahedron. Lett.* **1999**, *40*, 1401. (d) Saoud, M.; Romerosa, A.; Peruzzini, M. *Organometallics* **2000**, *19*, 4005. (e) Louie, J.; Grubbs, R. H. *Angew. Chem. Int. Ed. Engl.* **2001**, *40*, 1. In RCM: Ref (e). (f) Schanz, H.-J.; Jafarpour, L.; Stevens, E. D.; Nolan, S. P. *Organometallics* **1999**, *18*, 5187. (g) Fürstner, A.; Liebl, M.; Lehmann, C. W.; Picquet, M.; Kunz, R.; Bruneau, C.; Touchard, D.;

Dixneuf, P. H. *Chem. Eur. J.* **2000**, *6*, 1847. (h) Cetinkaya, B.; Demir, S.; Ozdemir, I.; Toupet, L.; Semeril, D.; Bruneau, C.; Dixneuf, P. H. *New J. Chem.* **2001**, *25*, 519. Indenylidene complexes have also proved metathesis-active in RCM: See Ref (f); also (i) Fürstner, A.; Hill, A. F..; Liebl, M.; Wilton-Ely, J. D. E. T. *J. Chem. Soc., Chem. Commun.*. **1999**, 601, and references therein. (j) Jafarpour, L.; Schanz, H.-J.; Stevens, E. D.; Nolan, S. P. *Organometallics* **1999**, *18*, 5416.

7) Bruce, M. I. *Chem. Rev.* **1991**, *91*, 197.

8) Selegue, J. *Organometallics* **1982**, *1*, 217.

9) Bruce, M. I.; Skelton, B. W.; White, A. H.; Zaitseva, N. N. *Inorg. Chem. Commun.* **1999**, *2*, 17.

10) Jafarpour, L.; Schanz, H.-J.; Stevens, E. D.; Nolan, S. P. *Organometallics* **1999**, *18*, 5416.

11) Pirio, N.; Touchard, D.; Toupet, L.; Dixneuf, P. H. *J. Chem. Soc., Chem. Commun.* **1991**, 980.

12) Touchard, D.; Pirio, N.; Toupet, L.; Fettouhi, M.; Ouahab, L.; Dixneuf, P. H. *Organometallics* **1995**, *14*, 5263.

13) Touchard, D.; Dixneuf, P. H. *Coord. Chem. Rev.* **1998**, *178-180*, 409.

14) Bustelo, E.; Jiménez-Tenorio, M.; Puerta, M. C.; Valerga, P. *Eur. J. Inorg. Chem.* **2001**, 2391.

15) Ohm, M.; Schulz, A.; Severin, K. *Eur. J. Inorg. Chem.* **2000**, 2623.

16) Neither the 14-electron, mononuclear species nor the 16-electron dimer is attainable, but the H_2-stabilized dimer (cf. **5**) provided a suitable alternative; vide infra.

17) Hofmann has described related systems based on four- and five-membered chelate rings, which are activated upon abstraction of halide. See: (a) Hansen, S. M.; Rominger, F.; Metz, M.; Hofmann, P. *Chem. Eur. J.* **1999**, *5*, 557. (b) Hansen, S. M.; Volland, M. A. O.; Rominger, F.; Eisentrager, F.; Hofmann, P. *Angew. Chem. Int. Ed. Engl.* **1999**, *38*, 1273. (c) Volland, M. A. O.; Straub, B. F.; Gruber, I.; Rominger, F.; Hofmann, P. *J. Organomet. Chem.* **2001**, 617, 288.

18) Drouin, S. D.; Amoroso, D.; Yap, G. P. A.; Fogg, D. E. *Organometallics* , accepted.

19) Hampton, C.; Cullen, W. R.; James, B. R.; Charland, J.-P. *J. Am. Chem. Soc.* **1988**, *110*, 6918; (b) Hampton, C. R. S. M.; Butler, I. R.; Cullen, W. R.; James, B. R.; Charland, J.-P.; Simpson, J. *Inorg. Chem.* **1992**, *31*, 5509.

20) Hampton, C.; Dekleva, T. W.; James, B. R.; Cullen, W. R. *Inorg. Chim. Acta* **1988**, *145*, 165.

21) For successful correlation by HMQC experiments, the peak width in Hz must be less than the value of the heteronuclear coupling constant. While exchange masks the 1H-31P coupling within **14**, the expected $^{2}J_{HP}$ value of 2-4 Hz is very small relative to the peak width of 40 Hz.

22) MacFarlane, K. S.; Thorburn, I. S.; Cyr, P. W.; Chau, D. E. K. Y.; Rettig, S. J.; James, B. R. *Inorg. Chim. Acta* **1998**, *270*, 130.

23) Gagné, M. R.; Grubbs, R. H.; Feldman, J.; Ziller, J. W. *Organometallics* **1992**, *11*, 3933.

24) The alkylidene resonance for $RuCl_2(PCy_3)_2(CHCH{=}CMe_2)$ likewise appears as a singlet, rather than the triplet found for the PPh_3 analogue.

25) Joshi, A. M.; Thorburn, I. S.; Rettig, S. J.; James, B. R. *Inorg. Chim. Acta* **1992**, *198-200*, 283.

26) Dias, E. L.; Nguyen, S. T.; Grubbs, R. H. *J. Am. Chem. Soc.* **1997**, *119*, 3887.

27) Louie, J.; Grubbs, R. H. *Angew. Chem. Int. Ed. Engl.* **2001**, *40*, 1.

28) Schanz, H.-J.; Jafarpour, L.; Stevens, E. D.; Nolan, S. P. *Organometallics* **1999**, *18*, 5187.

CHAPTER 7

Synthesis and Catalytic Chemistry of Ruthenium Complexes Containing Bulky, Basic Pincer Ligands

7.1. Introduction

Chapters 3 and 4 of this thesis describe diversification of the ligand scaffold in Ru alkylidene complexes to incorporate chelating diphosphine ligands, the promising metathesis activity of such systems, and preliminary indicators of selectivity. The metathesis activity of these systems overturned views prevailing at the outset of this work that suggested that such complexes would be too sterically encumbered to induce metathesis. With the intention of further increasing selectivity, and of circumventing deactivation via dimerization pathways (Chapter 6), we sought to replace the chloride ligands with alternative anionic donors.

Other groups have undertaken replacement of the chloride ligand of Grubbs' catalyst with aryloxide[1-3] or alkoxide[4] ligands, cyclopentadienes,[5] hydridotris(pyrazolyl)borate),[5,6] allyl groups,[7] sulfur-based ligands (such as $K[N(PPh_2S)_2]$, [9]aneS_3 and $K[PS_2(OR)_2]$, where R = Et or *i*-Pr),[8] and amidinates.[9] We were interested, however, in incorporating the anionic donor into a diphosphine-containing scaffold, with the intention of restricting the number of stereochemically identical sites presented to incoming monomer. Our attention thus focused on PCP-type

pincer ligands. The versatility of this ligand system, indicated by use of closely related $RuX(dppx)PPh_3$ (X = Cl or OTf, dppx = $[2,6\text{-}(Ph_2PCH_2)C_6H_3]^-$) catalysts in transfer hydrogenation[10] (including via a chiral version of the dppx system[11]), Heck coupling,[12] Kharasch addition and atom transfer radical polymerization[13,14] is promising from the perspective of ultimately developing tandem catalyses. Such processes, coupling metathesis with hydrogenation or other catalytic manifolds, are attractive for their power and efficiency. Samantha Drouin of this laboratory has developed highly efficient tandem ROMP-hydrogenation protocols, as a powerful route to saturated polymer blends.[15]

The first example of a metathesis-active pincer complex was recently reported. $[Ru(NN'N)(PPh_3)(C{=}CPh_2)][BF_4]_2$ (NN'N = 2,6-bis[(dimethylamino)methyl]pyridine displayed modest activity in ROMP of norbornene.[16] This is unsurprising in view of the accompanying structural data, which described a square pyramidal complex with alkylidene located in the apical site. In keeping with the geometric analysis presented in Chapter 4, we anticipate that high activity in these systems will require abstraction of a chloride ligand to open up a site cis to alkylidene. Refinement of the ligand design may thus ultimately require steric compensation in order to maintain a well-defined coordination wedge at the metal. Pincer systems are attractive for the ease with which phosphine substituents can be modified, as well as the central donor site, which may be anionic or neutral. This modularity lends itself readily to steric and electronic tuning.[17] These systems appeared well adapted to addressing issues of decomposition and selectivity identified in Chapters 4 and 6, while offering the potential for improved definition of the active site (including, ultimately, through derivatives containing chiral pincer ligands). The PCP-type pincer alkylidene complex shown in Figure 7. 1 was thus

identified as a target. This chapter describes the preparation and characterization of a series of ruthenium complexes of the cyclohexyl-substituted pincer ligand dicyclohexylphosphinoxylene (dcpx). Chloride, hydride, carbonyl, and alkylidene derivatives are described, as well as the utility of dcpx systems in both transfer hydrogenation and olefin metathesis.

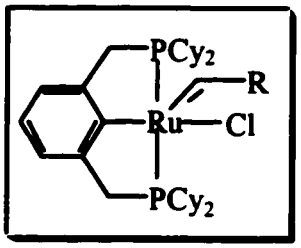

Figure 7. 1. Target pincer alkylidene complex.

The ruthenium chemistry of ^{t}Bu[18-20] and ^{i}Pr[21] pincer ligands derived from m-xylene is now well developed. In comparison, the corresponding cyclohexyl-pincer ligand (dcpx, Fig. 7.1) remains largely unexplored. Hampering development of dcpx chemistry is the tendency of the ligand to form PP-bridged, rather than chelated species. Bridged products are formed in reactions of dcpx with $RuCl_2(dmso)_4$, $[RuCl_2(cod)]_n$ and $[RuCl_2(p\text{-cymene})]_2$).[22] We felt that use of a mononuclear precursor with good solubility (and thus improved stoichiometric precision) might be more likely to yield chelated products. We therefore sought to establish a route from $RuCl_2(PPh_3)$ into ruthenium complexes incorporating the basic, cyclohexyl-substituted pincer ligand dcpx.

7.2. Preparation of a Pincer Precursor Complex

Treatment of $RuCl_2(PPh_3)_3$ with dcpx and NEt_3 in benzene at RT effects quantitative conversion ($^{31}P\{^1H\}$ NMR) to deep green $RuCl(dcpx)(PPh_3)\bullet PPh_3$ (**24**$\bullet PPh_3$, Figure 7. 2). The complex is isolated in ca. 80% yield. It displays high solubility in common organic solvents, with the exception of isopropanol, in which it is only slightly soluble at ambient temperature. In contrast to the complexes of dcypb described in earlier Chapters 3 and 4, it shows no tendency to chlorination by dichloromethane or chloroform as evidenced by the stability of this complex in such solvents over several weeks in solution (^1H and $^{31}P\{^1H\}$ NMR). Formulation of **24** as a PPh_3 solvate is based on $^{31}P\{^1H\}$ and ^1H NMR analysis, supported by microanalysis. The $^{31}P\{^1H\}$ NMR spectrum reveals the expected A_2B pattern for **24** (δ_P 80.9 (t, 1P, $^2J_{PP}$ = 32 Hz, Ru-PPh_3), 35.7 (d, 2P, $^2J_{PP}$ = 32 Hz, dcpx), accompanied by a singlet at δ_P -5.46 for the PPh_3 solvate. The excellent agreement with solid state $^{31}P\{^1H\}$ CP/MAS NMR data (δ_P 82.7, 34.1, -6.1) indicates that the solvating PPh_3 ligand is not bound in the solid state. All analytical methods consistently reveal the presence of one equivalent of "free" PPh_3, even after exhaustive trituration, or multiple reprecipitation from (for example) benzene, toluene, dichloromethane, chloroform, methanol, THF, or ether solvent, by addition of pentane, hexanes or isopropanol. Low yields were incurred on use of hexanes or pentane as a precipitating agent, owing to the partial solubility of **24**$\bullet PPh_3$ in these solvents.

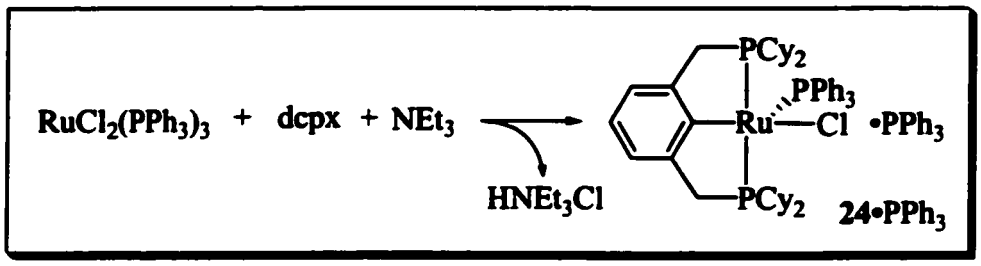

Figure 7. 2. Preparation of $RuCl(dcpx)PPh_3 \bullet PPh_3$ ($24 \bullet PPh_3$).

7.2.1. Molecular Structure of $RuCl(dcpx)(PPh_3)$ ($24 \bullet PPh_3$)

X-ray quality crystals of **24** were obtained by slow evaporation of an ether solution. An ORTEP representation appears in Figure 7. 3, with selected structural parameters in Table 7. 1. Surprisingly, the solvating PPh_3 is not present in the unit cell, which reveals only a distorted square pyramidal ruthenium-dcpx species, with a single, coordinated PPh_3 ligand occupying the apical site. That no PPh_3 solvate was detected, despite the persistence of one equivalent of "free" PPh_3 in solids, implies that this structure is not representative of the bulk.

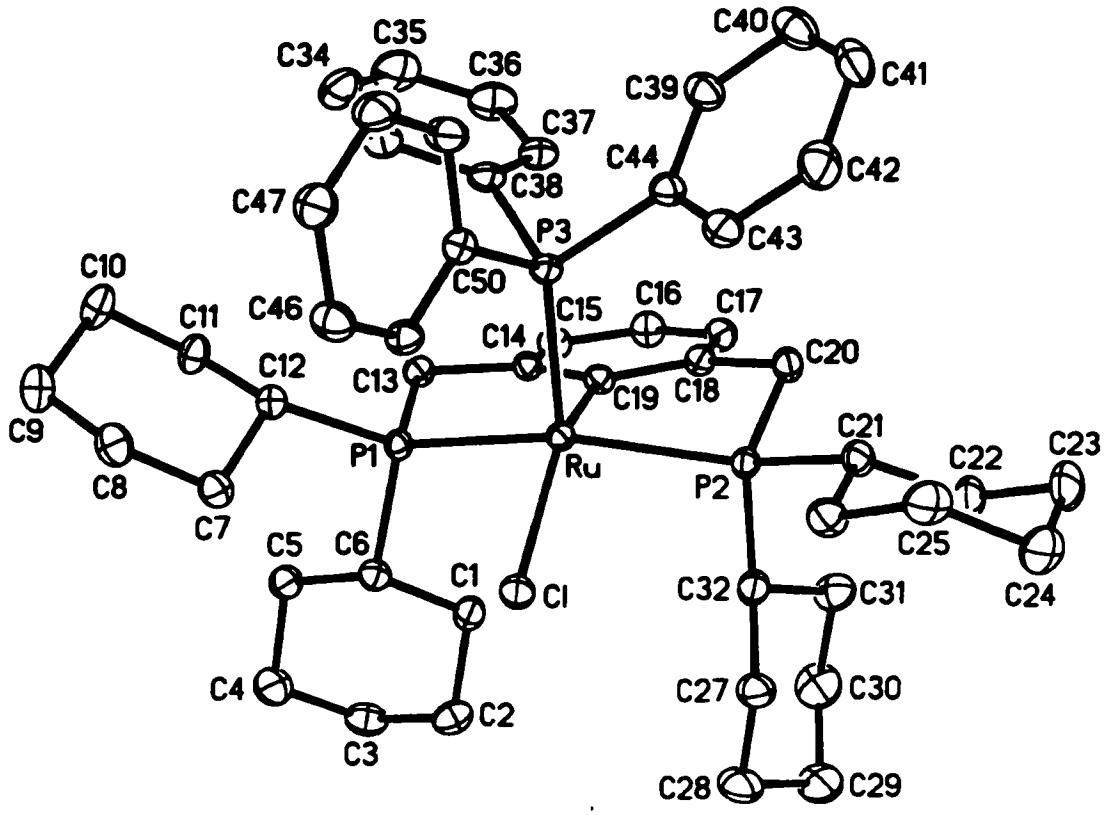

Figure 7. 3. ORTEP diagram of RuCl(dcpx)(PPh_3) (**24**). Thermal ellipsoids shown at 30% probability level. Hydrogen atoms and solvent molecule omitted for clarity.

In both **24** and the closely related diphenylphosphinoxylene complex, RuCl(dppx)(PPh_3) (dppx = [2,6-(Ph_2PCH_2)C_6H_3]$^-$),[23] the PPh_3 ligand occupies the apical site in the square pyramid, consistent with its stronger trans effect vs. the aryl carbon. The P(1)-Ru-P(2) angle in the latter complex is 4 larger than that in **24** (150.4(1) , vs. (154.21(4)). The chloride ligand in **24** is also displaced further from the P-Ru-P plane, and its C(19)-Ru-Cl angle is contracted by 10 (151.42(11)) relative to the dppx complex. These features are a consequence of the increased P(3)-Ru-C(19) and P(3)-Ru-Cl angles (cf. values of 88.13(11) and 120.31(4) , respectively, in **24**, vs. values of 84.8(1) and 113.6(1) in the dppx complex). This difference is a manifestation of the

greater steric pressure exerted by the cyclohexyl substituents relative to phenyl. Ru-C distances for the activated aromatic carbon are very similar (2.061(4) Å in **24**, vs. 2.070(4) Å in the dppx species). Ruthenium-phosphorus and -chloride bonds compare closely, as does the Ru-PPh_3 bond distance (Ru-P(3) in **24**), which is notably shorter than the mutually trans Ru-P(1) and Ru-P(2) bonds.

Table 7. 1. Selected Bond Lengths (Å) and Angles (deg) for RuCl(dcpx)PPh_3 (**24**).

Ru(1)-C(19)	2.061(4)	Ru(1)-P(3)	2.1996(10)
Ru(1)-P(1)	2.3247(10)	Ru(1)-Cl(1)	2.4520(10)
Ru(1)-P(2)	2.3522(10)		
P(1)-Ru-P(2)	154.21(4)	Cl(1)-Ru-P(3)	120.31(4)
C(19)-Ru-Cl(1)	151.42(11)	P(3)-Ru-P(1)	95.60(4)
C(19)-Ru-P(1)	82.26(11)	P(3)-Ru-P(2)	102.63(4)
C(19)-Ru-P(2)	80.29(11)	P(1)-Ru-Cl(1)	91.43(3)
C(19)-Ru-P(3)	88.13(11)	P(2)-Ru-Cl(1)	94.87(3)

7.3. Reaction of RuCl(dcpx)PPh_3•PPh_3 with $PhCHN_2$ and Terminal Acetylenes

Complex **24**•PPh_3 can be regarded as a pincer analogue of $RuCl_2(PPh_3)_3$, and thus a potentially valuable synthetic precursor. Unlike $RuCl_2(PPh_3)_3$, however, which reacts rapidly with $PhCHN_2$ to yield metathesis-active $RuCl_2(PPh_3)_2$(CHPh) (**1b**),[24] complex **24**•PPh_3 undergoes no apparent reaction under the same conditions. Significant quantities of stilbene (cis- and trans-PhCH=CHPh) are formed, probably via independent decomposition of $PhCHN_2$.

$RuCl_2(PPh_3)_3$ reacts rapidly with terminal alkynes such as phenylacetylene at RT, affording vinylidene products.[25] The corresponding reactions of $RuCl(dppx)(PPh_3)$ yields unexpected coupling products of the type $RuCl(PPh_3)(\eta^4\text{-}PhCH{=}C\text{-}2,6\text{-}(PPh_2CH_2)_2C_6H_3)$.[26,27] With the intention of exploring the generality of the latter reaction, and in the hope of gaining access to vinylidene or allenylidene products, **24**•PPh_3 was treated with (respectively) 3,3-dimethyl-1-butyne[28] and 1,1-diphenyl-2-propyn-1-ol.[29] No reaction was observed (^1H, ^{31}P NMR) over 24 h in solution at ambient temperature. The implied non-lability of the PPh_3 ligand in **24**•PPh_3 is consistent with NMR data, which show no evidence of phosphine loss (Figure 7. 4). In contrast, $RuCl_2(PPh_3)_3$ exists in equilibrium with dimeric $[RuCl_2(PPh_3)]_2$ (+ 2 PPh_3) in solution. The dimerization pathway may be precluded for **24** by the steric encumbrance at Ru (evident from the deviation from ideal square pyramidal geometry in Figure 7. 3. Indeed, the resistance to dimerization offered by the bulky dcpx ligand is one of the attractive features of this system.

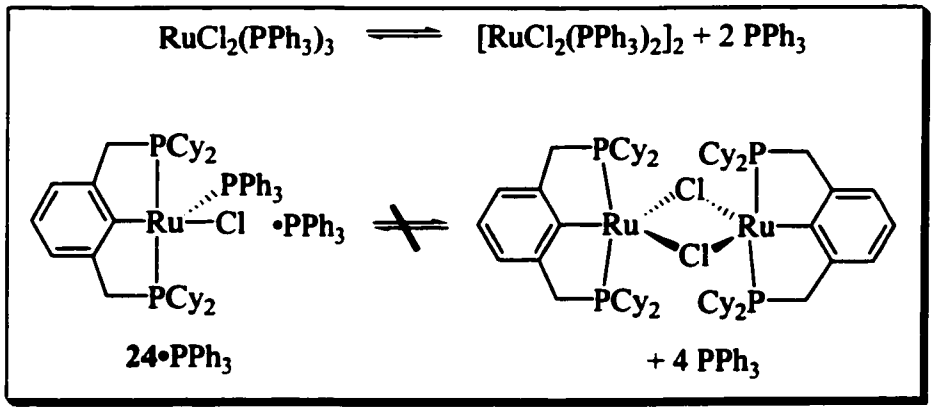

Figure 7. 4. Dimerization pathways of chlororuthenium complexes.

7.4. Reaction of RuCl(dcpx)PPh_3 with CO

The lability of the PPh_3 ligand in **24** was probed by exposure to carbon monoxide. The deep green colour of **24**•PPh_3 dissipates within minutes on exposure to 1 atm CO (RT, benzene), giving a pale yellow solution. Displacement of PPh_3 and formation of RuCl(dcpx)$(CO)_2$ **25** (Figure 7. 5) is unequivocally indicated by infrared, $^{31}P\{^1H\}$ and $^{13}C\{^1H\}$ NMR data. In situ $^{31}P\{^1H\}$ NMR analysis reveals a singlet for (free) PPh_3, and another singlet, of equal integrated intensity, for the equivalent phosphorus nuclei of the dcpx ligand (δ_P 62.4). The PPh_3 signal disappears on reprecipitation of the product from dichloromethane/diethyl ether, and **25** is isolated in 88% yield. The inequivalence of the two carbonyl groups is evident by $^{13}C\{^1H\}$ NMR analysis: two downfield triplets are apparent, each split by the equivalent ^{31}P nuclei of the dcpx ligand (δ_C 199.8, t, $^2J_{CP}$ = 12 Hz; 198.2, t, $^2J_{CP}$ = 7 Hz). The IR spectrum reveals two strong ν(CO) bands (2018, 1945 cm^{-1}), confirming the cis disposition of the carbonyl ligands. The identity of the product is supported by microanalytical and X-ray crystallographic data.

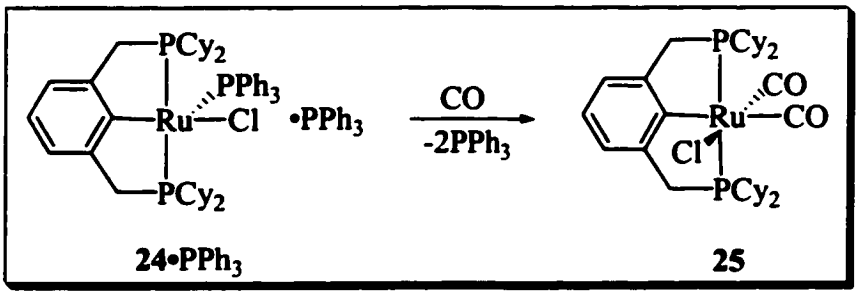

24•PPh_3 **25**

Figure 7. 5. Reaction of RuCl(dcpx)PPh_3•PPh_3 with CO.

7.4.1. Molecular Structure of RuCl(dcpx)$(CO)_2$ (25)

X-ray quality crystals of **25** were obtained by slow evaporation of a benzene solution. The structure is shown in Figure 7. 6, with significant bond lengths and angles in Table 7. 2. The geometry at ruthenium is octahedral, with the dcpx ligand occupying one meridian, a CO ligand occupying the site trans to the activated ring carbon, and the remaining carbonyl and chloride ligands, which are disordered with respect to each other, completing the coordination sphere. The electron density is smeared over C(34), O(2) and Cl(1) and their positions are arbitrarily assigned. The excess of electron density at C(34) results in an unusually small ellipsoid.

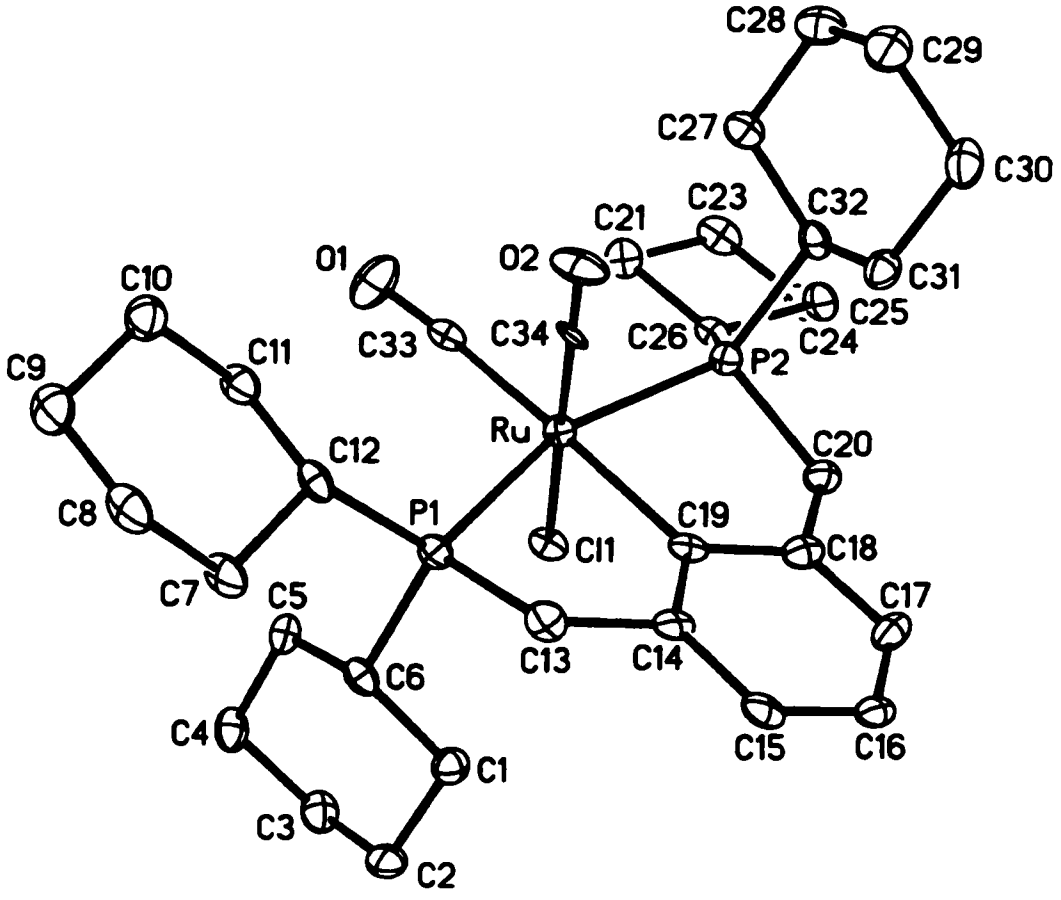

Figure 7. 6. ORTEP diagram of RuCl(dcpx)$(CO)_2$ (**25**). Thermal ellipsoids shown at 30% probability level. Hydrogen atoms omitted for clarity.

The Ru-C(19) distance for the activated ring position is slightly shorter in **25** than in precursor **24** (2.112(4) Å , vs. 2.061(4) Å), possibly owing to diminished electron density in the Ru-C bond of **25** (in which the bond lies trans to the π-acid CO ligand). While Ru-P and Ru-Cl bond lengths in the two molecules are comparable, a noteworthy difference is the "normal" pincer P-Ru-P bond angle in the latter (161.76(4)), vs. the highly compressed angle in **24** (154.21(4)). The value for **25** is very close to that in RuCl(dppx)(PPh_3) (161.6(1)),[23] a measure of the relief in steric pressure associated with displacement of PPh_3 from **24**. These data suggest that the unreactivity of **24**•PPh_3 is due to the steric inaccessibility of the metal, a consequence of the cumulative bulk of the dcpx and PPh_3 ligands.

Table 7. 2. Selected Bond Lengths (Å) and Angles (deg) for RuCl(dcpx)$(CO)_2$ (**25**).[a]

Ru(1)-C(34)	1.837(11), 1.859(11)	Ru(1)-P(2)	2.3698(13)
Ru(1)-C(33)	1.912(5)	Ru(1)-Cl(1)	2.447(4), 2.447(4)
Ru(1)-C(19)	2.112(4)	C(33)-O(1)	1.167(5)
Ru(1)-P(1)	2.3649(14)	C(34)-O(2)	1.187(11), 1.166(11)
P(1)-Ru-P(2)	160.76(4)	C(19)-Ru-P(2)	81.88(13)
C(33)-Ru-C(19)	177.7(2)	C(34)-Ru-C(33)	90.4(6), 88.3(6)
C(34)-Ru-Cl(1)	178.8(5), 178.6(7)	C(19)-Ru-Cl(1)	88.66(16), 89.12(16)
C(19)-Ru-P(1)	78.88(13)	C(34)-Ru-C(19)	91.4(6), 89.9(6)

[a] Where two values are given, the second is for the mirror image complex.

The two Ru-CO distances within **25** differ, with a bond length of 1.912(5) Å for the carbonyl ligand trans to the aryl carbon, vs. 1.837(11) Å for that trans to chloride

(1.859(11) Å for the CO ligand trans to chloride in the mirror image). This difference is ascribed to the greater trans influence of the aryl group relative to chloride. The C-O bond distances do not differ significantly, and are within the range reported for related ruthenium carbonyl complexes.[30-33]

7.5. Hydride Derivatives of dcpx

In view of the latent lability of PPh_3 within **24**•PPh_3 implied by formation of **25**, transformation of this species into a hydride derivative was undertaken. Introduction of a sterically undemanding hydride ligand offers the possibility of amplified reactivity vs. **24**•PPh_3, and a potential means of installing an alkylidene functionality via subsequent reaction with propargyl chloride (Chapter 6).[34] Treatment of a green solution of **24**•PPh_3 with 1 equivalent of KHB^sBu_3 at RT caused a colour change to deep red over 24 h. ^1H and $^{31}P\{^1H\}$ NMR analysis confirmed complete transformation to $RuH(dcpx)(PPh_3)(N_2)$, as a mixture of isomers (**26a** and **26b**, Figure 7. 7) present in approximately equal amounts. Identification of the two products as isomers is supported by microanalysis and by their observed correlation by ^{31}P EXSY-NMR, which indicates that the complexes interconvert on the NMR timescale.

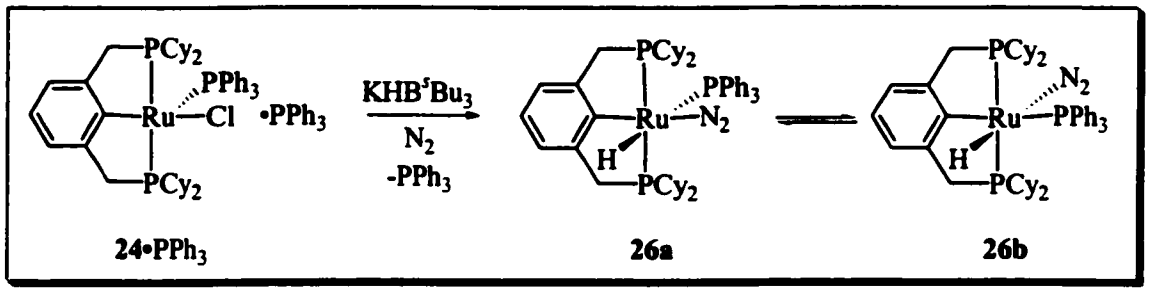

Figure 7. 7. Reaction of $RuCl(dcpx)PPh_3$•PPh_3 with KHB^sBu_3.

Structural assignments are made on the basis of ^{1}H and $^{31}P\{^{1}H\}$ NMR and infrared data, supported by X-ray data in the case of **26b**. Retention of PPh_3 in both products is indicated by observation of two A_2B patterns in the $^{31}P\{^{1}H\}$ NMR spectrum. The RT spectrum for **26a** is well resolved (δ_P 54.6 (d, 2P, $^{2}J_{PP}$ = 14 Hz, dcpx), 28.8 (t, 1P, $^{2}J_{PP}$ = 14 Hz, PPh_3)), while that for **26b** reveals the PPh_3 triplet (δ_P 45.0 (t, 2P, $^{2}J_{PP}$ = 17 Hz)), but only a broad singlet for the dcpx ligand (59.6 ppm). The latter signal resolves into a doublet at 253K ($^{2}J_{PP}$ = 17 Hz).

Trans-disposition of the hydride and PPh_3 ligands in **26a** is deduced from splitting of the hydride signal into a doublet of triplets, arising from two cis and one trans $^{2}J_{PH}$ couplings (δ_H -8.05; $^{2}J_{HP,\ cis}$ = 21.8 Hz; $^{2}J_{HP,\ trans}$ = 90 Hz). The strong trans-hydride coupling can likewise be observed in the ^{31}P NMR (^{1}H-coupled) spectrum, in which the PPh_3 resonance at δ_P 28.8 appears as a broad doublet ($^{2}J_{HP}$ = 90 Hz). The smaller cis-coupling is obscured by the breadth of this signal.

In contrast, the hydride signal for **26b** is a very broad resonance centered at -12 ppm, barely visible above the baseline at RT. The breadth of this peak may arise from the increased lability of the N_2 ligand in this isomer, consistent with its trans disposition with respect to the high trans effect, labilizing hydride ligand. This signal is resolved into a quartet at 253 K (δ_H -12.2; $^{2}J_{HP,\ cis}$ = 19.5 Hz), in which the magnitude of the coupling constant confirms the cis relationship between hydride and all three phosphorus nuclei. No splitting of this triplet is observed in the $^{31}P\{^{1}H\text{-coupled}\}$ NMR spectrum, presumably because the relatively small cis splitting is obscured by peak broadening.

The hydridic resonances of both isomers display long T_1(min) relaxation times characteristic of hydride ligands. Values of 333 msec for **26a** (282 K, 500 MHz) and 359 msec for **26b** (278 K, 500 MHz) are observed. Medium intensity infrared bands are observed for ν(Ru-H) at 2114 cm^{-1} and ν(N≡N) at 2134 cm^{-1} which suggests that only a single isomer is present in the solid state. This is also supported by the observation of only a single isomer in crystals isolated from a solution containing a mixture of both isomers (vide infra).

7.5.1. Molecular Structure of RuH(dcpx)(PPh_3)(N_2) (26b)

X-ray quality crystals of isomer **26b** were isolated by slow evaporation of an ether solution. Relevant bond lengths and angles are given in Table 7. 3. An ORTEP plot is shown in Figure 7. 8.

The coordination geometry about Ru in **26b** is distorted octahedral, with a pincer P(1)-Ru-P(2) angle of 154.95(5) Å. Comparable geometries and structural features (including Ru-P and Ru-C bond lengths) were found in RuCl(dcpx)(PPh_3) (**24**) and RuCl(dcpx)$(CO)_2$ (**25**) (vide supra). The P(1)-Ru-P(2) angle of 154.95(5) in **26b** is very close to the value of 154.21(4) in **24**, presumably because of the greater steric pressure exerted by the PPh_3 ligand present in both. The Ru-H distance of 1.60(4) Å, is shorter than the corresponding value of 1.73(7) Å observed for the related Ru/hydrido pincer complex RuH(dtbpx)(CO).[19] The difference may arise from positioning of the hydride in **26b** trans to dinitrogen, while that in the literature complex is trans to a vacant site. Ru-N (2.014(4) Å) and N-N (1.111(6) Å) distances correlate well with literature values for related pincer/dinitrogen complexes (avg. Ru-N = 2.10 Å; avg. N-N = 1.13 Å).[19]

Observation of only a single isomer is consistent with infrared evidence which suggests that only one isomer exists in the solid state.

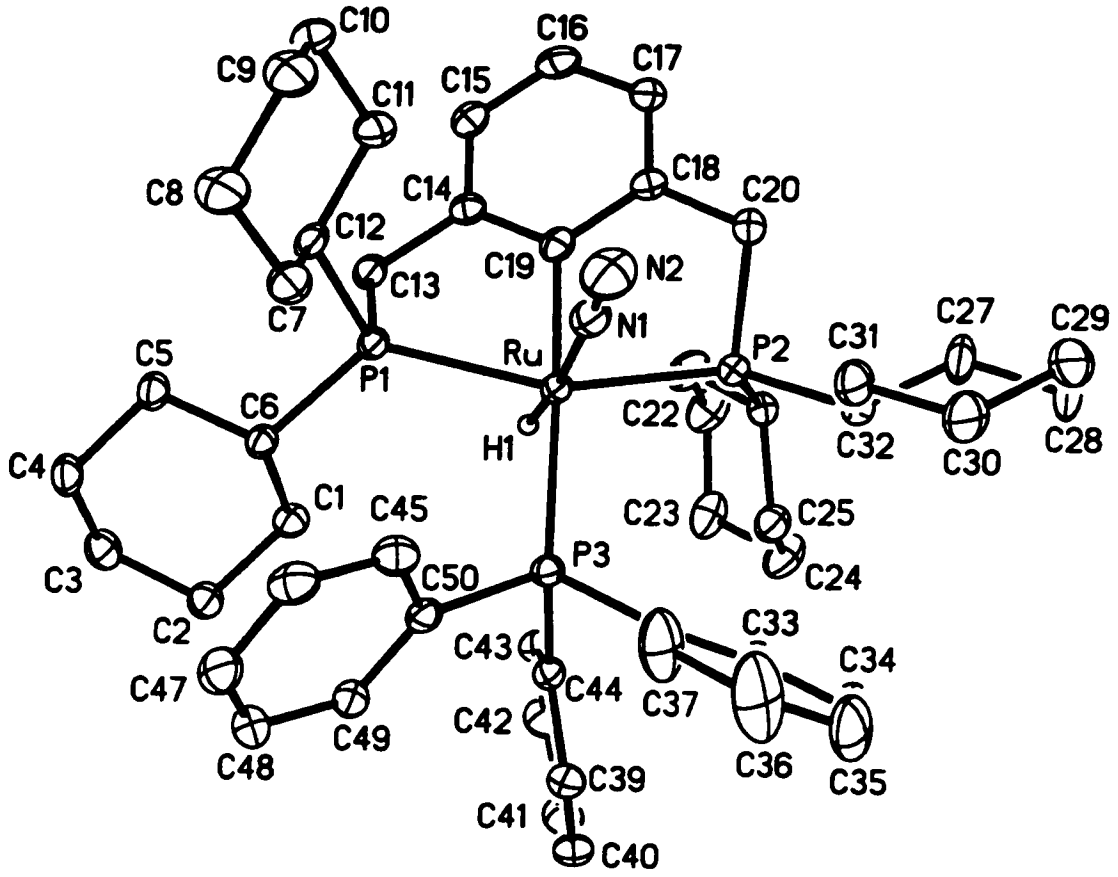

Figure 7. 8. Molecular structure of RuH(dcpx)(PPh_3)(N_2) (**26b**). Thermal ellipsoids shown at 30% probability level. Non-hydride H atoms and solvent molecules omitted for clarity.

Table 7. 3. Selected Bond Lengths (Å) and Angles (deg) for RuH(dcpx)(PPh_3)(N_2) (**26b**).

Ru-C(19)	2.129(5)	Ru-H(1)	1.60(4)
Ru-P(1)	2.3433(12)	Ru-N(1)	2.014(4)
Ru-P(2)	2.3578(12)	N(1)-N(2)	1.111(6)
Ru-P(3)	2.3655(12)		
C(19)-Ru-P(3)	198.96(12)	P(1)-Ru-C(19)	77.61(12)
P(1)-Ru-P(2)	154.95(5)	P(2)-Ru-C(19)	77.68(12)
H(1)-Ru-N(1)	173(1)	P(1)-Ru-P(3)	101.15(4)
Ru-N(1)-N(2)	178.3(4)	P(2)-Ru-P(3)	102.30(4)

7.5.2. Reaction of RuH(dcpx)(PPh_3)(N_2) with H_2

Upon exposure of a NMR sample (C_6D_6) to one atmosphere of hydrogen, **26a** and **26b** are cleanly transformed into the corresponding dihydrogen adducts RuH(dcpx)(PPh_3)(H_2) (**27a** and **27b**) (Figure 7. 9). The reaction can be monitored by ^1H and $^{31}P\{^1H\}$ NMR. Product ratios favor **27b** over **27a** by ca. 3:1. No correlation between the two was observed in ^{31}P EXSY-NMR experiments, indicating that exchange in this system is unobservable on the NMR timescale. All of the hydride ligands in the two isomers display distinct ^1H NMR resonances. That of **27a** gives rise to a doublet of triplets (δ_H -10.64; $^2J_{HP,cis}$ = 21.7 Hz, $^2J_{HP,trans}$ = 80.1 Hz), indicating coupling to one trans and two cis phosphines. The dihydrogen ligand within **27a** gives rise to a broad singlet at δ_H -7.08, and integrates to twice the intensity of the hydride ligand of the same complex. For **27b**, the hydride ligand gives rise to a quartet, consistent with placement cis to three phosphorus nuclei (δ_H -8.70; $^2J_{HP}$ = 18.9 Hz). The dihydrogen ligand, again of twice the integrated intensity, appears as a broad singlet at δ_H -4.34. Trans disposition of hydride and PPh_3 in **27a** is confirmed by ^1H-coupled ^{31}P NMR analysis, which shows splitting of

the triplet at δ_P 37.1 into a broad doublet by strong trans coupling to the hydride ligand; $^2J_{HP}$ = 80 Hz.

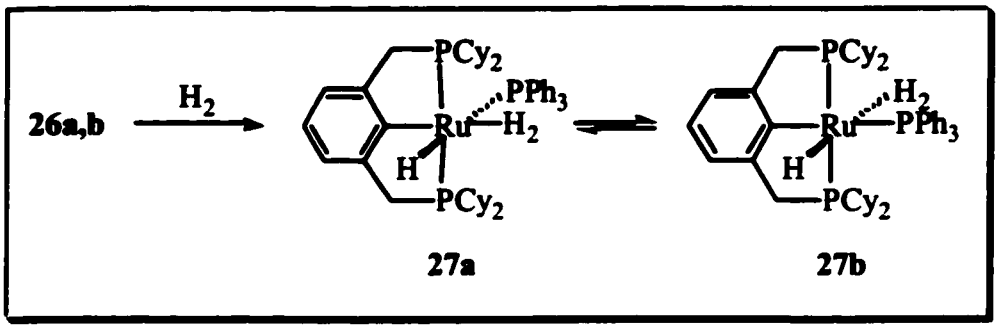

Figure 7. 9. Reaction of RuH(dcpx)(PPh_3)(N_2) with hydrogen.

7.5.3. Molecular Structure of RuH(dcpx)(PPh_3)(H_2) (27b)

The strength with which the H_2 ligand is bound in **27** is implied by isolation of crystals of **27b** from a benzene solution that was allowed to evaporate slowly in a N_2-filled drybox over a period of 2-3 days. While the quality of the crystals did not permit location of the hydride or dihydrogen ligands, the absence of bound N_2 suggests that H_2 is retained. An ORTEP diagram is given in Figure 7. 10, with relevant bond lengths and angles in Table 7. 4.

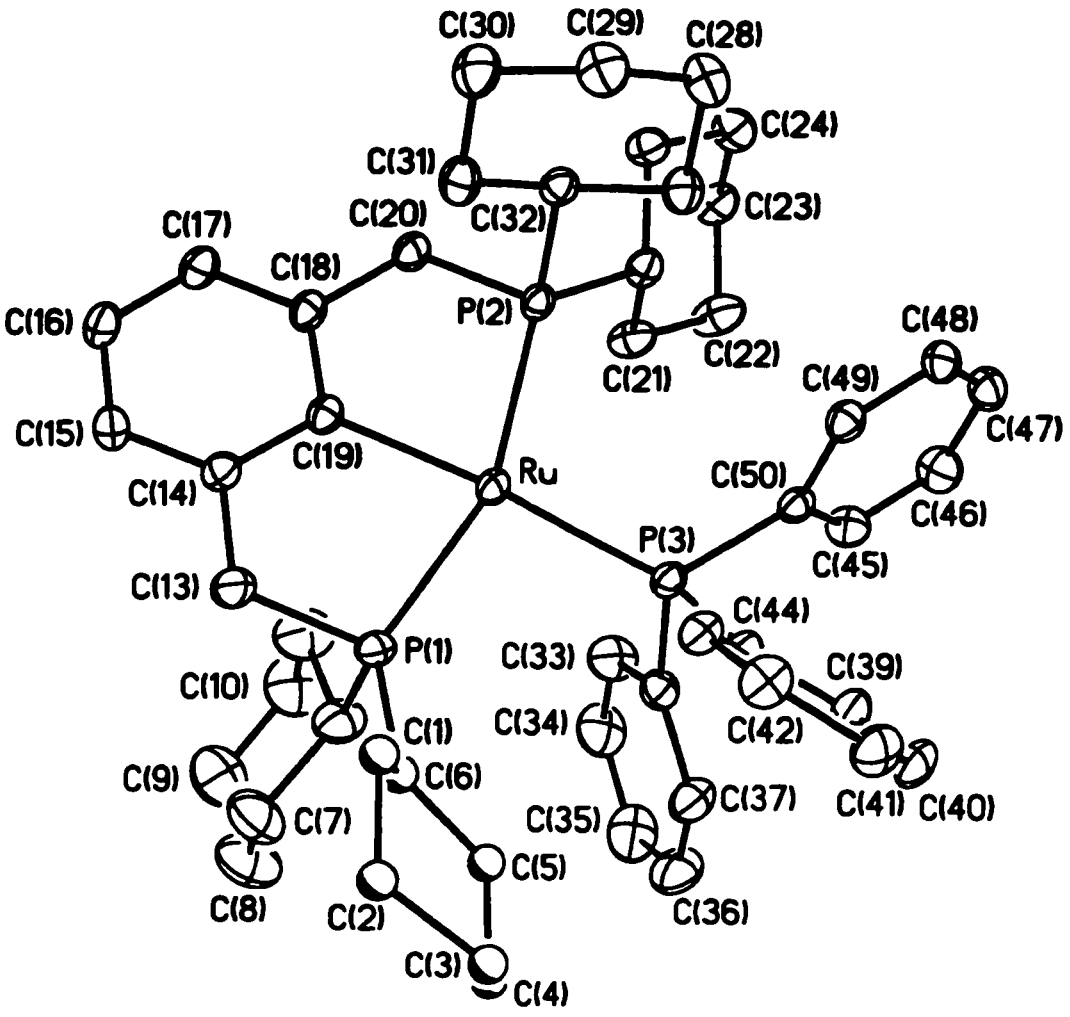

Figure 7. 10. Molecular structure of RuH(dcpx)(PPh_3)(H_2) (**27b**). Thermal ellipsoids shown at 30% probability level. Non-hydridic hydrogen atoms and solvent molecule omitted for clarity. Hydride and dihydrogen ligands not located.

Presuming the presence of hydride and dihydrogen ligands, the Ru center is six-coordinate. Ru-P and Ru-C bond distances in **27b** tally closely with those of dinitrogen analogue **26b**. Again, the P(1)-Ru-P(2) angle (158.36(4)°) deviates from linearity as a result of the steric pressure exerted by the PPh_3 ligand. Other angles within the P-Ru-C skeleton of **27b** do not differ significantly from those of dinitrogen analogue **26b**. One

cyclohexyl group was found to be conformationally disordered, with a 50/50 site occupancy distribution.

Table 7. 4. Selected Bond Lengths (Å) and Angles (deg) for RuH(dcpx)(PPh_3)(H_2) (**27b**).

Ru-C(19)	2.133(4)	Ru-P(2)	2.3148(10)
Ru-P(1)	2.3434(11)	Ru-P(3)	2.3617(10)
C(19)-Ru-P(3)	170.88(10)	P(2)-Ru-C(19)	79.31(11)
P(1)-Ru-P(2)	158.36(4)	P(1)-Ru-P(3)	98.06(4)
P(1)-Ru-C(19)	79.12(11)	P(2)-Ru-P(3)	103.02(4)

7.5.4. Reaction of RuH(dcpx)(PPh_3)(H_2) with 3-Chloro-3-methyl-1-butyne

Hydride derivatives **26a/b** were treated with 3-chloro-3-methyl-1-butyne, with the intention of installing the [Ru=CHCH=CMe_2] functionality (Figure 7. 11).[34] A purple solution of **26a/b** in C_6D_6 turned deep green immediately following addition of 10 equivalents of the alkyne. Unexpectedly, ^1H and $^{31}P\{^1H\}$ NMR spectroscopy reveal quantitative regeneration of RuCl(dcpx)(PPh_3) **24**. Given the quantitative formation of **24**, and use of a non-chlorinated solvent, the source of chloride must necessarily be 3-chloro-3-methyl-1-butyne. Particularly intriguing is the possibility that an initially-displaced PPh_3 ligand competes for recoordination to the metal, inducing elimination of the alkylidene. Arguing against this is the bulk of the PPh_3 ligand, which should impede recoordination, as well as the absence of signals for Me_2C=CHCH=CHCH=CMe_2, the expected alkylidene coupling product. Indeed, at least eight different olefinic resonances appear between 4.5 and 6.5 ppm

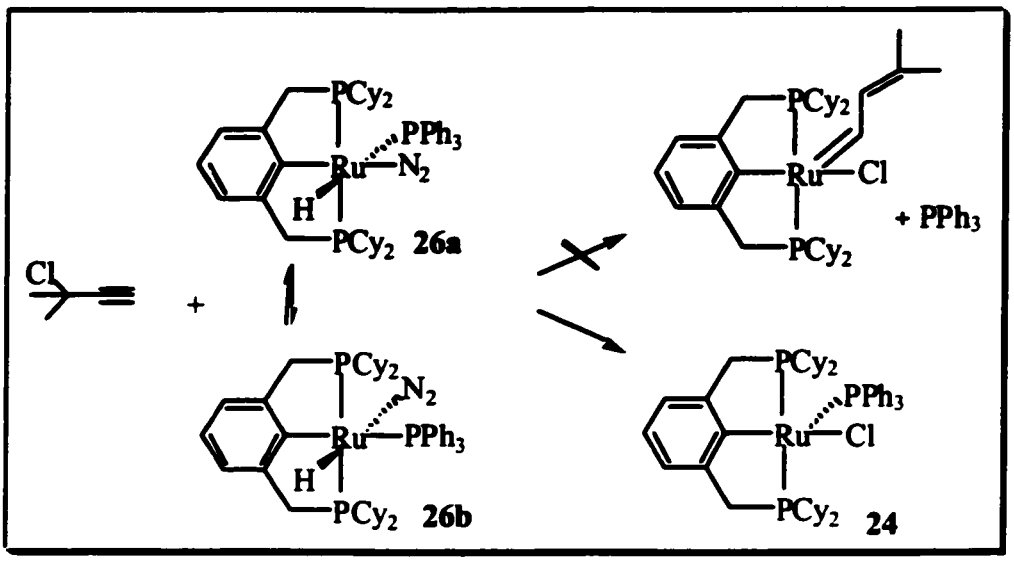

Figure 7. 11. Reaction of RuH(dcpx)(PPh_3)(H_2) (**26a/b**) with 3-chloro-3-methyl-1-butyne.

The chemical shift and coupling constant of one of the more prominent multiplets present (δ 4.5 ppm; sept, J = 3.1 Hz) are in excellent agreement with values calculated for the olefinic protons of 3-methyl-buta-1,2-diene. A possible mechanism for formation of **24** and this allene (Figure 7. 12) involves insertion of the alkyne into the Ru-H bond and formation of the vinyl derivative (**A**). Migration of chloride and elimination of the hydrocarbon ligand would generate **24** and the observed allene. A related reaction has been reported between a pincer hydride complex and phenylacetylene, in which a vinyl complex analogous to intermediate **A** was identified.[18]

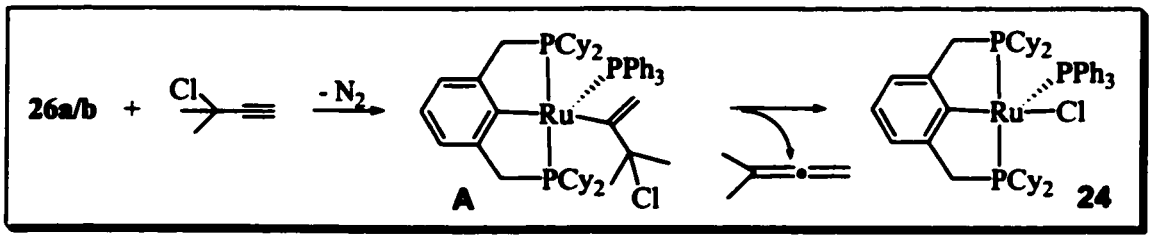

Figure 7. 12. Formation of allene in reaction of **26a/b** with 3-chloro-3-methyl-1-butyne.

7.6. Alkylidene Derivatives of dcpx

In view of the difficulty of installing the pincer ligand prior to alkylidene, the feasibility of the opposite approach was explored. Phosphine exchange between dcpx and $RuCl_2(PPh_3)_2(CHCHCMe_2)$ proceeds readily at RT in benzene to afford pink alkylidene derivative $RuCl_2(dcpx')(CHCH{=}C(CH_3)_2)$ (**28**; where dcpx' is $[1,3\text{-}(CH_2PCy_2)_2C_6H_4]$). Also formed is ca. 20% of dark green **24**•PPh_3 (Figure 7. 13). The two complexes can be separated by extraction of **24**•PPh_3 with diethyl ether. Analytically pure **28** is isolated in ~50% yield.

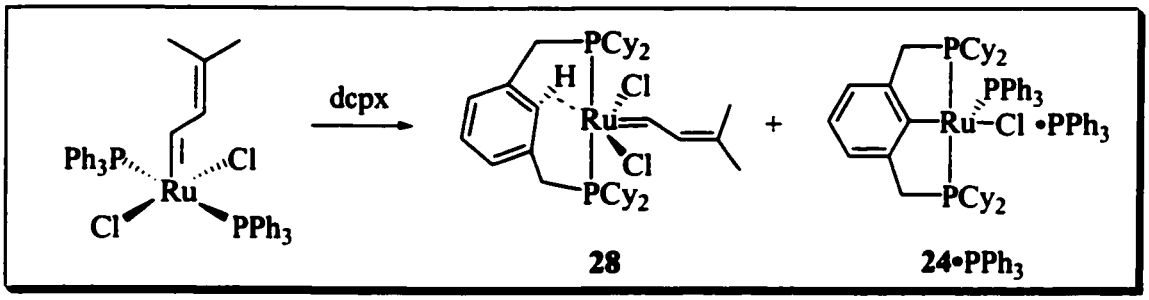

Figure 7. 13. Phosphine exchange reaction with $RuCl_2(PPh_3)_2(CHCHCMe_2)$ and dcpx.

Complex **28** is identified as the η^2-pincer structure shown in Figure 7. 13 on the basis of NMR data, supported by crystallographic analysis and microanalytical data. Its

$^{31}P\{^{1}H\}$ NMR spectrum consists of a singlet (δ_P 19.5) for the equivalent phosphorus nuclei of the dcpx' moiety. The α-proton of the alkylidene appears as a doublet at δ_H 19.4 ($^{2}J_{HH}$ = 11.6 Hz). Observation of a doublet for the alkylidene α-H, as opposed to a doublet of triplets (or higher order pattern) arising from coupling to the two phosphorus nuclei and the alkylidene β-proton, can be attributed to the orientation of the alkylidene relative to the dcpx ligand. In the solid state structure (vide infra) the H_α-C_α-Ru-P dihedral angle is approximately 90 ,[35] and poor orbital overlap thus precludes coupling between the alkylidene α-H and the phosphorus nuclei.

^{1}H NMR spectroscopy shows unequivocal evidence against C-H activation to generate an η^3-pincer ligand. The aromatic region contains the anticipated triplet and doublet for the *para*- and *ortho*-protons (respectively) of the aryl ring (δ_H 7.42, 1H; 6.84, 2H). In addition, however, a singlet is observed (δ_H 9.48 , 1H) for the isolated aromatic proton, in the site where bond activation is required. This bond interacts in an agostic fashion with the metal center, as indicated by X-ray crystallographic analysis.

7.6.1. Molecular Structure of $RuCl_2$(dcpx')(CHCHCMe$_2$) (28)

X-ray quality crystals of **28** were obtained on slow evaporation of a toluene solution. An ORTEP diagram is shown in Figure 7. 14, with relevant bond lengths and angles in Table 7. 5. The geometry about ruthenium is octahedral, with an agostic interaction between the metal and C(24) occupying the sixth coordination site, confirming the [1,3-(Cy_2PCH_2)C_6H_4] binding mode for the pincer ligand.

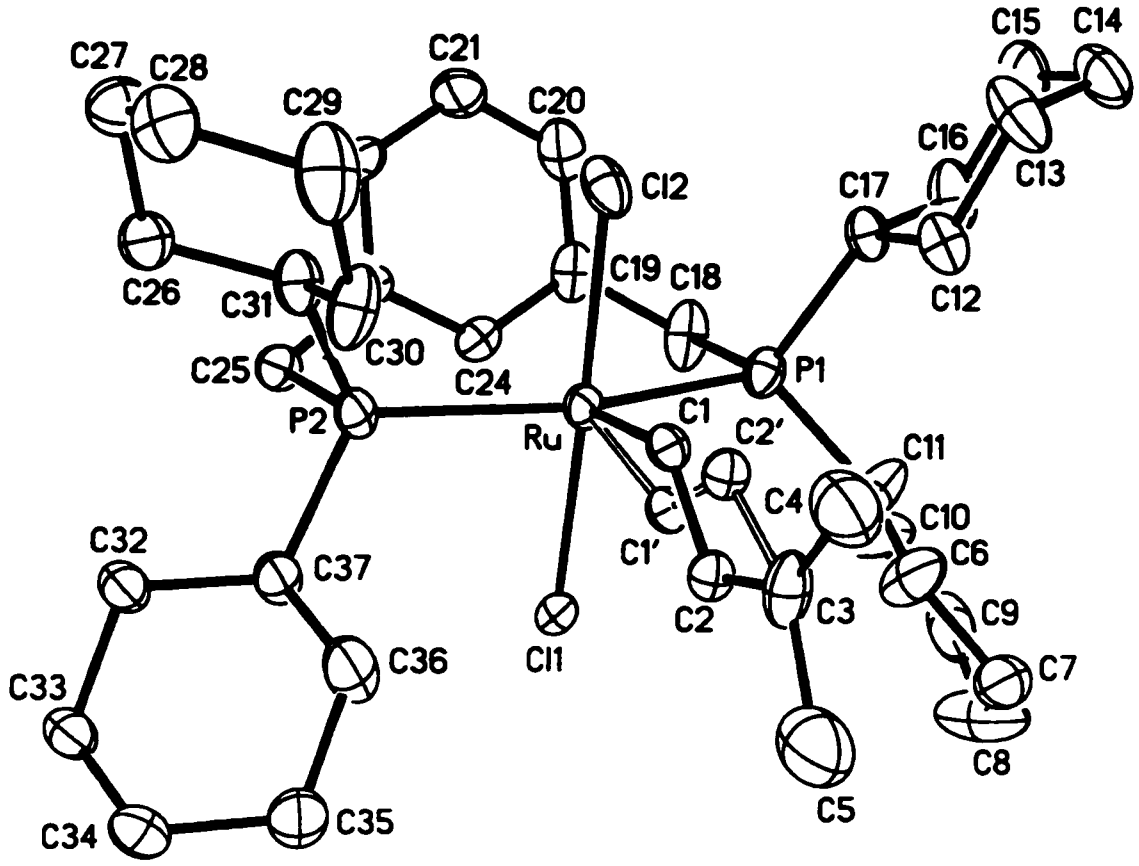

Figure 7. 14. Molecular structure of $RuCl_2(dcpx')(CHCHMe_2)$ (**28**). Thermal ellipsoids shown at the 30% probability level. Hydrogen atoms omitted for clarity.

The short non-bonding distance between the metal and C(24) of 2.606(8) Å is consistent with the presence of an agostic interaction between the C-H bond and the ruthenium center. Such interactions have been observed crystallographically in related ruthenium pincer complexes $RuHCl[1,3\text{-}(^tBu_2PCH_2)_2C_6H_4]$ and $RuHI[1,3\text{-}(^tBu_2PCH_2)_2C_6H_4]$.[20] The Ru-C distances in the reported complexes are much shorter than in **28** (2.115(3) Å for the hydridochloro complex and 2.135(4) Å for the hydridoiodo complex). It has been suggested that the extent of activation of the η^2 C-H bond is directly related to the π-donor abilities and inversely related to the trans effect of the

substituent oriented trans to the η^2 C-H bond.[20] The much larger distance in **28** suggests that the π-donor abilities of alkylidene are weak while the trans effect is strong. The latter is consistent with the overwhelming tendency of alkylidene to occupy the apical site in square pyramidal alkylidene complexes of ruthenium.[36] It has been established that the strongest trans effect ligand will occupy this site in square pyramidal five-coordinate d^6 metal complexes.[36] The only reported instance in which the alkylidene does not occupy this site is in a hydride complex reported by Coalter et al.[37] in which hydride (evidently a stronger trans effect ligand than alkylidene) occupies the apex.

Table 7. 5. Selected Bond Lengths (Å) and Angles (deg) for $RuCl_2(dcpx')(CHCHMe_2)$ (**28**).

Ru(1)-C(1)	1.919(8)	Ru(1)-Cl(2)	2.3845(12)
Ru(1)-C(1')	1.832(8)	C(1)-C(2)	1.407(11)
Ru(1)-C(24)	2.606(8)	C(1')-C(2')	1.442(11)
Ru(1)-P(1)	2.4000(12)	C(2)-C(3)	1.367(8)
Ru(1)-P(2)	2.4040(11)	C(2')-C(3)	1.454(9)
Ru(1)-Cl(1)	2.4307(13)		
P(1)-Ru-P(2)	159.80(3)	Cl(2)-Ru-C(1), C(1')	81.0(3), 103.8(3)
Cl(2)-Ru-Cl(1)	176.80(5)	Ru-C(1)-C(2)	129.4(6)
P(1)-Ru-C(1), C(1')	101.5(3), 97.1(3)	Ru-C(1')-C(2')	129.4(7)
P(2)-Ru-C(1), C(1')	98.5(3), 102.6(3)	C(1)-C(2)-C(3)	120.3(7)
C(1)-Ru-C(1')	23.1(3)	C(1')-C(2')-C(3)	117.8(7)
Cl(1)-Ru-C(1), C(1')	102.2(3), 79.4(3)		

The ruthenium-phosphorus distances in **28** (2.4000(12) and 2.4040(11) Å) are slightly longer than the average Ru-P bond length of 2.3529(12) Å observed in **24**•PPh_3 and **25**. The bond compression in the latter species is likely due to the presence of a true η^3-pincer ligand, which would tether the two phosphine arms more closely to the metal center. The two Ru-Cl distances in **28** differ by approximately 0.05 Å. Bond lengths and angles within the alkylidene moiety cannot be assessed, owing to a conformational disorder (as shown in Figure 7. 14) with a 50/50 site occupancy distribution.

7.6.2. Mechanism of Formation of $RuCl_2$(dcpx')(CHCHMe_2)

Formation of RuCl(dcpx)(PPh_3) **24** in the reaction of dcpx with $RuCl_2(PPh_3)_2$(CHCHCMe_2) was unexpected, this result suggesting that the lability of alkylidene is rather similar to that of PPh_3 in these complexes. It is unclear whether the alkylidene ligand is attacked by HCl generated in the course of the C-H activation of the dcpx ligand (i.e. as $H_2ClCCH{=}C(CH_3)_2$), or whether the alkylidene is displaced as :$CHCHC(CH_3)_2$ Attempts to probe the mechanism via in situ NMR experiments revealed no ^1H NMR signals for the expected alkylidene coupling product, $Me_2C{=}CHCH{=}CHCH{=}CMe_2$, or the chloroalkene, although several resonances are observed in the range of 3.5-6 ppm. These resonances do not coincide with any of those observed in the reaction of hydride derivatives **26a/b** with 3-chloro-3-methyl-1-butyne (section 7.5.4).

Attempts to induce C-H activation by adding NEt_3 or other bases, in the hope of curtailing side-reactions through abstraction of HCl, were unsuccessful. At high base strengths (Proton Sponge (pKa = 12.37), benzyl potassium (pKa = 35)) abstraction of the

alkylidene α-H occurred, as indicated by disappearance of this signal from the ^{1}H NMR spectrum. Conversion of alkylidene to carbyne species via proton abstraction has been reported elsewhere.[2]

7.6.3. ROMP via Pincer Alkylidene Complexes

η^2-Pincer species **28** exhibits only modest activity in ROMP of norbornene (TON_{max} = 220 h^{-1}; [Ru=C] = 3.2 mM; Table 7. 6). This is unsurprising, given that the coordinative saturation of **28** requires dechelation of one arm of the dcpx' ligand for productive metathesis. The polymer solutions obtained are highly viscous, and the polymers are completely insoluble once isolated (precluding molecular weight determinations). These observations are consistent with slow rates of initiation relative to propagation, which translates into a low concentration of the catalytically-active species, and formation of high molecular weight polymers.

Addition of a halide abstracting agent (trimethylsilyl trifluoromethanesulfonate, TMS-OTf) doubles metathesis activity at the 50% conversion point (compare Entry 1 vs. 2, Table 7. 6). Observation of comparable turnover numbers at maximum conversion (TON_{max}), however, suggested that in the later stages of polymerization, further reaction was limited by diffusion control. Accordingly, polymerizations were carried out at a four-fold dilution (still in the presence of halide scavenger). Under these conditions, ROMP was complete at four minutes (Entry 4). This figure translates into a minimum TON_{max} of 4275 h^{-1}. This catalyst system is the most active of all those examined in this thesis, significantly exceeding that of the highly active dcypb system $RuCl_2$(dcypb)(CHPh) (**2c**) described in Chapter 4. In contrast, the *tert*-butyl substituted pincer complex

RuCl(d'bpx)(C(CH$_3$)C$_3$H$_7$)] (**29**) is only moderately active under the same conditions (TON_{max} 30 h^{-1}). The difference may arise in part from the lower reactivity of the disubstituted alkylidene ligand in the latter.[38]

Table 7. 6. ROMP of norbornene via Ru pincer complexes.[a]

Entry	Catalyst	Additive[d]	Conversion (%)	Time (min)	TON_{max}[e]	TON_{50}[f]
1[b]	**28**	-	94	58	220	477
2[b]	**28**	TMS-OTf	95	57	225	911
3[c]	**28**	-	96	60	216	868
4[c]	**28**	TMS-OTf	95	3	4275	n/a
5[c]	**29**	TMS-OTf	87	390	30	270

[a] Reaction conditions: $CDCl_3$ solvent, [norbornene] : [Ru=C] = 225, RT. [b] [Ru=C] = 3.2 mM. [c] [Ru=C] = 0.8 mM. [d] Additive: 3.2[b] or 0.8[c] mM TMS-OTf. [e] TON at maximum observed conversion. [f] TON at 50% conversion.

7.7. Transfer Hydrogenation via dcpx Complexes

Recent interest in pincer complexes of ruthenium (eg. RuCl(dppx)PPh_3 and Ru(OTf)(dppx)PPh_3) as transfer hydrogenation catalysts[10,11] prompted us to examine the activity of **24**•PPh_3 in this application. We anticipated that the activity of the dcpx system would exceed that of the diphenylphosphine analogue, given the correlation between increased phosphine basicity and hydrogenation activity.[39-41] We therefore chose to focus on transfer hydrogenation of benzophenone, a notoriously challenging substrate. Reduction of diarylketones has received considerable interest owing to the value of the benzhydrol products as pharmaceutical intermediates.[42]

Catalyst **24•PPh$_3$** effects 92% reduction of Ph_2CO over 40 h in refluxing isopropanol. In comparison, the literature systems requires over 100 h to achieve comparable conversions[10] (compare Entry 1 vs. 5, Table 7. 7). When the hydrogenation is carried out under 1 atm H_2, the reaction time required for the **24•PPh$_3$** drops to 24 h, a fourfold increase in activity (Entry 2). Reduction thus proceeds via both H_2-hydrogenation and transfer hydrogenation pathways.

Table 7. 7. Transfer hydrogenation of benzophenone.[a]

Entry	Catalyst	Conversion (%)	Time (h)	TON[b]
1	**24•PPh$_3$**	92	40	23
2[d]	**24•PPh$_3$**	91	24	38
3[c]	**26**	88	96	9
4	**26**	90	24	38
5[10]	Ru(OTf)(dppx)PPh$_3$	98	108	9[e]

[a] The reactions were carried out on a 20-mmol scale in 20mL of *i*PrOH under N_2 with [KOH]/[Ru] = 20, [Ru] = 0.1 mol% at reflux. [b] Turnover number (moles of ketone converted to alcohol per mole of catalyst per hour) determined at ~90% conversion. [c] No pretreatment with KOH. [d] H_2 atmosphere. [e] Calculated at 98% conversion.

In their original report,[10] van Koten et al. identified an anionic ruthenium hydrido complex, $[RuH(O^iPr)(dppx)PPh_3]^-K^+$ as a potential catalyst resting state in catalysis, and speculated that the active catalyst was the neutral ruthenium hydride, presumably generated in their pretreatment with KOH. We therefore examined the activity of both chloro complex **24•PPh$_3$** and its isolated, neutral, hydrido analogue RuH(dcpx)(PPh$_3$)(N_2) **26**. Surprisingly, the activity of **26** was quite low in the absence of KOH, while pretreatment with KOH restored activity to the level of the chloride system (Entries 3 vs. 4). This result suggests that KOH is more intimately involved in these systems than

originally believed. Residual KOH may serve to scavenge acidic impurities which may be present. The sensitivity of the hydride complex toward such impurities *is* expected to be greater than its chloride counter part **24**•PPh_3.

7.8. Conclusions

The tricyclohexyl-substituted pincer ligand dcpx gave access to a series of ruthenium complexes which find use in both metathesis and hydrogenation chemistry. Triphenylphosphine can be displaced from the mixed-phosphine complex $RuCl(dcpx)PPh_3$•PPh_3 by CO, yielding $RuCl(dcpx)(CO)_2$, but this ligand is otherwise difficult to displace, and indeed appears to show an unexpected affinity for the Ru(dcpx) entity. Reaction of $RuCl(dcpx)PPh_3$•PPh_3 with tri(*sec*-butyl)borohydride gave isomeric hydride complexes $RuH(dcpx)(PPh_3)(N_2)$, the labile N_2 ligand of which was easily displaced under 1 atm of H_2 to afford the analogous dihydrogen isomers. Both the chloride and hydride derivatives are found to be highly active in the transfer hydrogenation of benzophenone.

In all of the above complexes, the dcpx ligand binds as an η^3-pincer, $[2,6\text{-}(Cy_2PCH_2)C_6H_3]^-$, accessed via C-H bond activation of the dcpx ligand. Such C-H activation does not occur when dcpx is allowed to react with the alkylidene complex, $RuCl_2(PPh_3)_2(CHCHC(CH_3)_2)$. In this case, the six-coordinate agostic complex, $RuCl_2(dcpx')(CHCHC(CH_3)_2)$ is isolated, wherein the dcpx ligand binds in a $[1,3\text{-}(CH_2PCy_2)_2C_6H_4]$ mode. While the metathesis activity of this alkylidene derivative is

modest, very high activity is observed in the presence of a halide abstracting agent. In fact, this system is the most active catalyst system examined in this thesis.

7.8. References

1) Chang, S.; Jones, L.; Wang, C.; Henling, L. M.; Grubbs, R. H. *Organometallics* **1998**, *17*, 3460.

2) Coalter, J. N.; Bollinger, J. C.; Eisenstein, O.; Caulton, K. G. *New. J. Chem.* **2000**, *24*, 925.

3) Coalter, J. N.; Huffman, J. C.; Caulton, K. G. *Chem. Commun.* **2001**, 1158.

4) Sanford, M. S.; Henling, L. M.; Day, M. W.; Grubbs, R. H. *Angew. Chem. Int. Ed. Engl.* **2000**, *39*, 3451.

5) Katayama, H.; Yoshida, T.; Ozawa, F. *J. Organomet. Chem.* **1998**, *562*, 203-206.

6) Sanford, M. S.; Henling, L. M.; Grubbs, R. H. *Organometallics* **1998**, *17*, 5384.

7) Six, C.; Beck, K.; Wegner, A.; Leitner, W. *Organometallics* **2000**, *19*, 4639.

8) Leung, W.-H.; Lau, K.-K.; Zhang, Q.; Wong, W.-T.; Tang, B. *Organometallics* **2000**, *19*, 2084.

9) Hayashida, T.; Nagashima, H. *Organometallics* **2001**, *20*, 4996.

10) Dani, P.; Karlen, T.; Gossage, R. A.; Gladiali, S.; Koten, G. v. *Angew. Chem. Int. Ed. Engl.* **2000**, *39*, 743.

11) Albrecht, M.; Kocks, B. M.; Spek, A. L.; Koten, G. v. *J. Organomet. Chem.* **2001**, *624*, 271.

12) Ohff, M.; Ohff, A.; Boom, M. E. v. d.; Milstein, D. *J. Am. Chem. Soc.* **1997**, *119*, 11687.

13) Kuil, L. A. v. d.; Grove, D. M.; Gossage, R. A.; Zwikker, J. W.; Koten, G. v. *Organometallics* **1997**, *16*, 4985.

14) Gossage, R. A.; Kuil, L. A. v. d.; Koten, G. v. *Acc. Chem. Res.* **1998**, *31*, 423, and refs. therein.

15) Drouin, S. D.; Zamanian, F.; Fogg, D. E. *Organometallics* , *20*, 5495. (b) Drouin, S. D.; Yap, G. P. A.; Fogg, D. E. *Inorg. Chem.* **2000**, *39*, 5412.

16) Del Rio, I.; Van Koten, G. *Tetrahedron. Lett.* **1999**, *40*, 1401.

17) Albrecht, M.; Koten, G. v. *Angew. Chem. Int. Ed. Engl.* **2001**, *40*, 3750.

18) Reinhart, B.; Gusev, D. G. *New J. Chem.* **1999**, 1.

19) Gusev, D. G.; Dolgushin, F. M.; Antipin, M. Y. *Organometallics* **2000**, *19*, 3429.

20) Gusev, D. G.; Madott, M.; Dolgushin, F. M.; Lyssenko, K. A.; Antipin, M. Y. *Organometallics* **2000**, *19*, 1734.

21) Boom, M. E. v. d.; Kraatz, H.-B.; Hassner, L.; Ben-David, Y.; Milstein, D. *Organometallics* **1999**, *18*, 3873.

22) Gusev, D. G., personal communication.

23) Jia, G.; Lee, H. M.; Williams, I. D. *J. Organomet. Chem.* **1997**, *534*, 173.

24) Schwab, P.; France, M. B.; Ziller, J. W.; Grubbs, R. H. *Angew. Chem. Int. Ed. Engl.* **1995**, *34*, 2039.

25) Wakatsuki, Y.; Yamazaki, H.; Kumegawa, N.; Satoh, T.; Satoh, J. Y. *J. Am. Chem. Soc.* **1991**, *113*, 9604.

26) Jia, G.; Lee, H. M.; Xia, H. P.; Williams, I. D. *Organometallics* **1996**, *15*, 5453.

27) Lee, H. M.; Xia, H. P.; Williams, I. D.; Jia, G. *Organometallics* **1997**, *16*, 3927.

28) Bruce, M. I. *Chem. Rev.* **1991**, *91*, 197.

29) Bruce, M. I. *Chem. Rev.* **1998**, *98*, 2797.

30) Maddock, S. M.; Rickard, C. E. F.; Roper, W. R.; Wright, L. J. *Organometallics* **1996**, *15*, 1793.

31) Gottschalk-Gaudig, T.; Folting, K.; Caulton, K. G. *Inorg. Chem.* **1999**, *38*, 5241.

32) Batista, A. A.; Zukerman-Schpector, J.; Porcu, O. M.; Queiroz, S. L.; Araujo, M. P.; Oliva, G.; Souza, D. H. F. *Polyhedron* **1994**, *13*, 689.

33) Wilkes, L. M.; Nelson, J. H.; Mitchener, J. P.; Babich, M. W.; Riley, W. C.; Helland, B. J.; Jacobson, R. A.; Cheng, M. Y.; Seff, K.; McCusker, L. *Inorg. Chem.* **1982**, *21*, 1376.

34) Wilhelm, T. E.; Belderrain, T. R.; Brown, S. N.; Grubbs, R. H. *Organometallics* **1997**, *16*, 3867.

35) Dias, E. L.; Nguyen, S. T.; Grubbs, R. H. *J. Am. Chem. Soc.* **1997**, *119*, 3887.

36) Huang, D.; Streib, W. E.; Bollinger, J. C.; Caulton, K. G.; Winter, R. F.; Scheiring, T. *J. Am. Chem. Soc.* **1999**, *121*, 8087.

37) Coalter, J. N.; Caulton, K. G. *New. J. Chem.* **2001**, *25*, 679.

38) Louie, J.; Grubbs, R. H. *Angew. Chem. Int. Ed. Engl.* **2001**, *40*, 1.

39) Drouin, S. D.; Amoroso, D.; Yap, G. P. A.; Fogg, D. E. *Organometallics* , accepted.

40) Burk, M.; Martinez, J. P.; Feaster, J. E.; Cosford, N. *Tetrahedron* **1994**, *50*, 4399.

41) Burk, M. J. *Acc. Chem. Res.* **2000**, *33*, 363.

42) Ohkuma, T.; Koizumi, M.; Ikehira, H.; Yokozawa, T.; Noyori, R. *Organic Letters* **2000**, *2*, 659.

CHAPTER 8

Conclusions and Recommendations for Future Work

The work summarized in this thesis has demonstrated that ruthenium alkylidene complexes containing chelating diphosphines could display high metathesis activity with enhanced control over product stereochemistry. Efforts to amplify steric pressure by use of the stable silylene 1,3-di-*tert*-butyl-1,3,2-diazasilol-2-ylidene was undermined by the hydrolytic sensitivity of the silylene. Also, the ease with which the silylene is displaced suggests its utility as a phosphine mimic is limited. A facile decomposition pathway in diphosphine catalyst systems has been identified with potential relevance to related catalysts of type $RuCl_2(PR_3)_2(CHR')$ **1**, including Grubbs' catalyst. A synthetic route to η^2-pincer alkylidene complexes was developed which demonstrated exceptionally high activity. In view of the difficulty associated with activation of the aromatic position, the ligand design must be adjusted to incorporate more readily activated donors. This approach holds much promise for the development of highly active and stereoselective metathesis catalysts.

Other interesting findings which emerge include a route to a suitable precursor complex which incorporates the flexible, electron-rich diphosphine 1,4-bis(dicyclohexylphosphino)butane (dcypb). The reaction of $RuCl_2(PPh_3)_3$ under an atmosphere of nitrogen was found to result in the formation of the dimeric complex $RuCl(dcypb)(\mu\text{-}Cl)_3Ru(dcypb)(N_2)$ (**5**) in high yields. Use of N_2 atmosphere was found to be critical to stabilization of this species: in the presence of argon or vacuum, extensive

decomposition occurred via dehydrogenation of the dcypb ligand. The coordinated N_2 ligand is easily displaced by other donors such as H_2 and CO. Thus, under an atmosphere of H_2, RuCl(dcypb)(μ-Cl)$_3$Ru(dcypb)(H_2) (**7**) is observed while direct reaction of **5** with one atmosphere of carbon monoxide gives access to a series of well-behaved mononuclear isomers *ccc*- (**8**) and *tcc*-$RuCl_2$(dcypb)$(CO)_2$ (**9**). Their formation proceeds through the symmetrical dimer RuCl(dcypb)(CO)(μ-Cl)$_2$RuCl(dcypb)(CO) (**10**).

Complex **5** is also susceptible to attack by halogenated solvents: sustained exposure to CH_2Cl_2 or $CDCl_3$ results in isolation of mixed-valence dimer RuCl(dcypb)(μ-Cl)$_3$RuCl(dcypb) (**6**). Such chlorination processes were common to all dcypb complexes and may indeed be general for such complexes of electron-rich phosphines. This raises the interesting possibility of harnessing this phenomenon. The activation of C-X bonds is an important area of research: *catalytic* activation of such bonds holds great potential as an efficient means of disposing of halogenated (particularly chlorinated) organic compounds (such as the notorious polychlorinated biphenyls). Reduction of mixed-valence Ru(II,III) species back to Ru(II,II) dimers is well established in aryldiphosphine chemistry.[1] Thus, one can envision a system which employs complexes of type **5** to dehalogenate a range of substrates under catalytic conditions.

Alkylidene complexes of general formula $RuCl_2$(PP)(CHR) (where PP can be: dppb, **2a**; binap, **2b**; or dcypb, **2c**) are generated by treatment of either mixed phosphine complexes (i.e. $RuCl_2$(PP)(PPh_3)) or chloro-bridged dimers (i.e. $Ru_2Cl_4PP_2$) of the corresponding diphosphine with phenyldiazomethane. The cyclohexyl derivative, **2c**, is

---

[1] Joshi, A. M.; Thorburn, I. S.; Rettig, S. J.; James, B. R. *Inorg. Chim. Acta* **1992**, *198-200*, 283.

found to be most active as turn-over frequencies in excess of 2400 h^{-1} are calculated, while the binap derivative (**2b**) is found to yield an unprecedentedly high percentage (~36%) of cis-olefin linkages in the resulting polymer. Catalyst systems generated in situ from the mixed phosphine precursors are less active than those derived from PPh_3-free dimers implying that dissociated PPh_3 functions as a catalyst poison. The addition of phosphine scavenger results in decomposition which suggests that diphosphine dechelation is not occurring. Addition of halogen scavenger also results in catalyst decomposition which implies that halogen dissociation is also not a factor in these systems. The absence of ligand dissociation in these systems is further corroborated by the exceptionally narrow polydispersities observed for the polymers produced. The systems reported here stand alone as the only systems based on chelating diphosphines (or more generally chelating ligands) which do not require ligand dissociation or abstraction to achieve high activity in metathesis. This is attributed to the greater flexibility of the four carbon bridged diphosphines employed here relative to the more rigid systems described in the literature. This flexibility makes stereoselectivity a possibility as steric delineation of the active site is not compromised by the requirement for ligand dissociation. Proof of this is found in the high cis content of polymers produced via system **2b**.

The greater flexibility of the four-carbon bridged diphosphines employed herein have allowed for high activity while maintaining a sterically delineated active site. Concurrent with the increased flexibility of these systems is an increased tendency toward bimolecular decomposition. In contrast, the rigidity of the one- and two-carbon bridged systems in the literature allows for their isolation. The possible deployment of

three-carbon bridged diphosphines as a potential compromise between the flexible four-carbon bridged systems and the more stable two-carbon bridged systems should be explored. Such systems may lead to isolable mononuclear ruthenium alkylidene complexes of type **2** which do not require ligand abstraction. The incorporation of chiral, three-carbon bridged diphosphines coupled with subsequent modification of the anionic ligands may yield potentially active and selective metathesis catalysts.

Reaction of **5** with 1,3-di-*tert*-butyl-1,3,2-diazasilol-2-ylidene (SiL^N_2) results in the formation of $RuCl(\eta^3\text{-dcypb})(SiL^N_2)$ (**12**). Activation of the methylene backbone gives rise to the novel η^3 coordination mode for the dcypb ligand. The silylene ligand was found incapable of tolerating the conditions required for metathesis chemistry as decomposition precluded its incorporation into the ligand framework of an active catalyst system. Exposing **12** to an atmosphere of CO results in displacement of the silylene ligand and formation of three isomeric, bis-CO adducts $RuCl(\eta^3\text{-dcypb})(CO)_2$ (**16-18**). The SiL^N_2 moiety of **12** was also found to be sensitive toward hydrolysis and subsequent hydrogenolysis when exposed to an atmosphere of H_2.

The hydridochloro dimer $[Ru(H)(dcypb)(\mu\text{-}Cl)_2(\mu\text{-}H)Ru(dcypb)(H_2)]$ **14** serves as a useful in situ precursor to alkylidene complexes of the type $RuCl(dcypb)(\mu\text{-}Cl)_3Ru(dcypb)[CHCHC(CH_3)_2]$ **21**. A structural isomer in which the alkylidene moiety bridges the two Ru centers along with two other chlorides ($RuCl(dcypb)(\mu\text{-}Cl)_2(\mu\text{-}CHCHC(CH_3)_2)RuCl(dcypb)$ (**22**)) is also observed. These complexes can be identified as products of the decomposition of mononuclear alkylidene complexes of the type $RuCl_2(dcypb)(CHCH(CH_3)_2)$ **2e**. This deactivation pathway may be extended to systems of the type $RuCl_2(PR_3)_2(CHR)$.

Dinuclear, terminal mono-vinylidene $RuCl(dcypb)(\mu\text{-}Cl)_3Ru(dcypb)[C{=}CH(Bu^t)]$ (19) and hydroxyvinylidene $RuCl(dcypb)(\mu\text{-}Cl)_3Ru(dcypb)[C{=}CHC(OH)Ph_2]$ (20a) complexes are obtained upon reaction of 5 with 3,3-dimethyl-1-butyne and 1,1-diphenyl-2-propyn-1-ol respectively. The alkylidene, vinylidene and hydroxyvinylidene derivatives are all found to catalyze the ROMP of norbornene however with only moderate activities. The decreased activity of these systems relative to the closely related systems of type 2 is attributed to the decreased lability of the trichlorobridge. Indeed, increased activity is observed upon addition of halogen scavenger in the dimeric alkylidene (21/22) and vinylidene (19) systems. The activity of vinylidene 20a does not improve upon addition of halogen scavenger. In all cases the polymers produced were insoluble which suggests that the rate of initiation is slow relative to propagation. This effectively results in a low concentration of catalytically-active species which ultimately leads to the formation of very high molecular weight polymers.

The reaction of the PCP-type pincer ligand dcpx with $RuCl_2(PPh_3)_3$ in the presence of NEt_3 affords the mixed phosphine complex $RuCl(dcpx)(PPh_3)\bullet(PPh_3)$ **24**$\bullet PPh_3$. The PPh_3 solvate can not be separated however it does not appear to affect the reactivity of the complex. Thus, **24**$\bullet PPh_3$ reacts with one atm of CO to give the bis-carbonyl adduct $RuCl(dcpx)(CO)_2$ **25**. Isomeric hydride complexes $RuH(dcpx)PPh_3(N_2)$ (**26a/b**), which differ in the position of the N_2 and PPh_3 ligands with respect to hydride, are isolated upon reaction of **24**$\bullet PPh_3$ with KHB^sBu_3. When placed in an H_2 atmosphere, the analogous H_2 complexes **27a/b** are observed. The activity of the chloro derivative **24**$\bullet PPh_3$, in the transfer hydrogenation of benzophenone, is found to be greater than that of the hydrido complex(es) **26a/b**.

APPENDICES

Appendix A. Crystallographic Information for RuCl(dcypb)(μ-Cl)$_3$RuCl(dcypb) (6).

Table A.1. Crystal data and structure refinement for RuCl(dcypb)(μ-Cl)$_3$RuCl(dcypb) (6).

Empirical formula	$C_{64}H_{112}Cl_{11}P_4Ru_2$
Formula weight	1597.51
Temperature	203(2) K
Wavelength	0.71073 Å
Crystal system, space group	Triclinic, *P*-1
Unit cell dimensions	a = 13.390(2) Å α = 77.325(2)°
	b = 15.726(2) Å β = 70.964(2)°
	c = 19.524(2) Å γ = 73.478(2)°
Volume	3689.3(8) Å^3
Z, Calculated density	2, 1.438 mg/m^3
Absorption coefficient	0.932 mm^{-1}
F(000)	1662
Crystal size	0.10 × 0.10 × 0.03 mm
Theta range for data collection	1.11 to 20.81°
Limiting indices	$-12 \le h \le 13, -15 \le k \le 15, 0 \le l \le 19$
Reflections collected / unique	29133 / 7712 [R(int) = 0.1237]
Completeness to θ = 28.83	99.7%
Absorption correction	Semi-empirical from equivalents
Max. and min. transmission	0.928077 and 0.637019
Refinement method	Full-matrix least-squares on F^2
Data / restraints / parameters	7712 / 0 / 722
Goodness-of-fit on F^2	1.025
R^a	0.0533
$R_w{}^b$	0.1009

$^aR = \sum||F_o| - |F_c||/\sum|F_o|$. $^bR_w = [\sum w\delta^2/\sum wF_o{}^2]^{1/2}$.

Table A.2. Bond lengths [Å] and angles [deg] for RuCl(dcypb)(μ-Cl)$_3$RuCl(dcypb) (**6**).

Ru(1)-P(1)	2.309(3)
Ru(1)-P(2)	2.325(3)
Ru(1)-Cl(5)	2.395(2)
Ru(1)-Cl(1)	2.387(2)
Ru(1)-Cl(3)	2.495(2)
Ru(1)-Cl(4)	2.504(2)
Ru(2)-P(3)	2.323(2)
Ru(2)-P(4)	2.348(3)
Ru(2)-Cl(2)	2.360(3)
Ru(2)-Cl(3)	2.373(2)
Ru(2)-Cl(4)	2.466(2)
Ru(2)-Cl(5)	2.505(2)
P(1)-C(13)	1.782(13)
P(1)-C(6)	1.859(12)
P(1)-C(12)	1.867(9)
P(2)-C(16)	1.846(8)
P(2)-C(28)	1.878(9)
P(2)-C(22)	1.865(9)
P(3)-C(40)	1.840(10)
P(3)-C(41)	1.843(9)
P(3)-C(34)	1.868(9)
P(4)-C(44)	1.823(8)
P(4)-C(56)	1.858(9)
P(4)-C(50)	1.844(9)

P(1)-Ru(1)-P(2)	95.14(9)
P(1)-Ru(1)-Cl(5)	93.29(9)
P(2)-Ru(1)-Cl(5)	97.85(9)
P(1)-Ru(1)-Cl(1)	94.84(10)
P(2)-Ru(1)-Cl(1)	89.09(9)
Cl(5)-Ru(1)-Cl(1)	168.81(8)
P(1)-Ru(1)-Cl(3)	169.32(9)
P(2)-Ru(1)-Cl(3)	92.55(8)
Cl(5)-Ru(1)-Cl(3)	78.30(8)
Cl(1)-Ru(1)-Cl(3)	92.69(8)
P(1)-Ru(1)-Cl(4)	92.67(9)
P(2)-Ru(1)-Cl(4)	172.19(9)
Cl(5)-Ru(1)-Cl(4)	81.96(8)
Cl(1)-Ru(1)-Cl(4)	89.97(8)
Cl(3)-Ru(1)-Cl(4)	79.74(8)
P(3)-Ru(2)-P(4)	93.75(9)
P(3)-Ru(2)-Cl(2)	97.39(9)

P(4)-Ru(2)-Cl(2)	88.71(9)
P(3)-Ru(2)-Cl(3)	91.90(9)
P(4)-Ru(2)-Cl(3)	97.33(9)
Cl(2)-Ru(2)-Cl(3)	168.58(9)
P(3)-Ru(2)-Cl(4)	92.26(8)
P(4)-Ru(2)-Cl(4)	173.97(9)
Cl(2)-Ru(2)-Cl(4)	90.04(9)
Cl(3)-Ru(2)-Cl(4)	82.95(8)
P(3)-Ru(2)-Cl(5)	168.60(9)
P(4)-Ru(2)-Cl(5)	93.57(8)
Cl(2)-Ru(2)-Cl(5)	91.50(8)
Cl(3)-Ru(2)-Cl(5)	78.50(8)
Cl(4)-Ru(2)-Cl(5)	80.56(7)
C(13)-P(1)-C(6)	104.1(8)
C(13)-P(1)-C(12)	103.1(6)
C(6)-P(1)-C(12)	104.2(5)
C(13)-P(1)-Ru(1)	117.3(5)
C(6)-P(1)-Ru(1)	111.3(4)
C(12)-P(1)-Ru(1)	115.5(3)
C(16)-P(2)-C(28)	98.8(4)
C(16)-P(2)-C(22)	108.1(4)
C(28)-P(2)-C(22)	105.3(4)
C(16)-P(2)-Ru(1)	116.8(3)
C(40)-P(3)-C(41)	104.4(4)
C(40)-P(3)-C(34)	105.8(5)
C(41)-P(3)-C(34)	101.2(4)
C(44)-P(4)-C(56)	98.0(4)
C(44)-P(4)-C(50)	109.7(4)
C(56)-P(4)-C(50)	105.2(4)
Ru(2)-Cl(3)-Ru(1)	84.63(8)
Ru(2)-Cl(4)-Ru(1)	82.54(7)
Ru(1)-Cl(5)-Ru(2)	83.97(7)

Symmetry transformations used to generate equivalent atoms:

Appendix B. Crystallographic Information for *ccc*-$RuCl_2(CO)_2$(dcypb) (9).

Table B.1. Crystal data and structure refinement for *ccc*-$RuCl_2(CO)_2$(dcypb) (9).

Empirical formula	C42 H64 Cl2 O2 P2 Ru
Formula weight	834.84
Temperature	203(2) K
Wavelength	0.71073 Å
Crystal system, space group	Orthorhombic, Pna2(1)
Unit cell dimensions	a = 15.560(1) Å α = 90°
	b = 11.522(1) Å β = 90°
	c = 23.213(2) Å γ = 90°
Volume	4161.9(6) $Å^3$
Z, Calculated density	4, 1.332 mg/m^3
Absorption coefficient	0.615 mm^{-1}
F(000)	1760
Crystal size	0.2 × 0.2 × 0.2 mm
Theta range for data collection	1.75 to 28.82°
Limiting indices	$0 \le h \le 20$, $0 \le k \le 15$, $-30 \le l \le 31$
Reflections collected / unique	32606 / 9930 [R(int) = 0.0506]
Completeness to θ = 28.82	94.8%
Absorption correction	Semi-empirical from equivalents
Max. and min. transmission	0.928076 and 0.731149
Refinement method	Full-matrix least-squares on F^2
Data / restraints / parameters	9930 / 8 / 430
Goodness-of-fit on F^2	1.005
R^a	0.0411
R_w^b	0.0544

$^aR = \sum||F_o| - |F_c||/\sum|F_o|$. $^bR_w = [\sum w\delta^2/\sum wF_o^2]^{1/2}$.

Table B.2. Bond lengths [Å] and angles [deg] for *ccc*-$RuCl_2(CO)_2$(dcypb) (**9**).

Ru-C(1')	1.8837(19)
Ru-C(1")	1.8977(19)
Ru-C(1)	1.901(2)
Ru-Cl(1")	2.300(8)
Ru-Cl(1)	2.3948(16)
Ru-P(1)	2.4101(9)
Ru-Cl(1')	2.417(6)
Ru-Cl(2)	2.4360(9)
Ru-P(2)	2.4825(9)
Cl(1)-C(1)	0.505(4)
Cl(1)-O(1)	0.681(4)
Cl(1')-C(1')	0.534(6)
Cl(1')-O(1')	0.603(6)
Cl(1")-O(1")	0.755(7)
C(1)-O(1)	1.149(2)
C(1')-O(1')	1.1347(19)
C(1")-O(1")	1.1437(19)
P(1)-C(14)	1.831(4)
P(1)-C(7)	1.851(4)
P(1)-C(13)	1.869(4)
P(2)-C(17)	1.842(3)
P(2)-C(29)	1.853(4)
P(2)-C(23)	1.857(3)
C(14)-C(15)	1.551(6)
C(15)-C(16)	1.503(6)
C(16)-C(17)	1.504(6)

C(1')-Ru-C(1")	87.7(3)
C(1')-Ru-C(1)	87.9(5)
C(1")-Ru-C(1)	83.9(5)
C(1')-Ru-Cl(1")	83.4(2)
C(1")-Ru-Cl(1")	7.6(3)
C(1)-Ru-Cl(1")	77.5(5)
C(1')-Ru-Cl(1)	85.08(19)
C(1")-Ru-Cl(1)	83.2(2)
C(1)-Ru-Cl(1)	2.8(5)
Cl(1")-Ru-Cl(1)	76.60(19)
C(1')-Ru-P(1)	94.16(19)
C(1")-Ru-P(1)	88.8(2)
C(1)-Ru-P(1)	172.3(5)
Cl(1")-Ru-P(1)	95.32(19)
Cl(1)-Ru-P(1)	171.92(5)

C(1')-Ru-Cl(1')	0.8(3)
C(1")-Ru-Cl(1')	87.5(2)
C(1)-Ru-Cl(1')	87.1(5)
Cl(1")-Ru-Cl(1')	83.2(2)
Cl(1)-Ru-Cl(1')	84.31(16)
P(1)-Ru-Cl(1')	94.92(15)
C(1')-Ru-Cl(2)	175.44(19)
C(1")-Ru-Cl(2)	89.78(19)
C(1)-Ru-Cl(2)	88.1(4)
Cl(1")-Ru-Cl(2)	93.64(16)
Cl(1)-Ru-Cl(2)	90.87(5)
P(1)-Ru-Cl(2)	89.56(3)
Cl(1')-Ru-Cl(2)	174.73(15)
C(1')-Ru-P(2)	92.01(18)
C(1")-Ru-P(2)	170.7(2)
C(1)-Ru-P(2)	86.8(5)
Cl(1")-Ru-P(2)	163.80(19)
Cl(1)-Ru-P(2)	87.55(5)
P(1)-Ru-P(2)	100.52(3)
Cl(1')-Ru-P(2)	92.01(15)
Cl(2)-Ru-P(2)	89.90(3)
C(1)-Cl(1)-O(1)	151(2)
C(1)-Cl(1)-Ru	10.8(17)
O(1)-Cl(1)-Ru	161.3(10)
C(1')-Cl(1')-O(1')	172.4(19)
C(1')-Cl(1')-Ru	2.7(10)
O(1')-Cl(1')-Ru	171.6(10)
O(1")-Cl(1")-Ru	163.4(9)
Cl(1)-C(1)-O(1)	16.9(12)
Cl(1)-C(1)-Ru	166(2)
O(1)-C(1)-Ru	176.5(13)
Cl(1)-O(1)-C(1)	12.5(9)
Cl(1')-C(1')-O(1')	4.0(10)
Cl(1')-C(1')-Ru	176.5(13)
O(1')-C(1')-Ru	174.3(5)
Cl(1')-O(1')-C(1')	3.6(9)
O(1")-C(1")-Ru	170.5(6)
Cl(1")-O(1")-C(1")	18.3(8)
C(14)-P(1)-C(7)	101.2(2)
C(14)-P(1)-C(13)	100.84(18)
C(7)-P(1)-C(13)	105.62(18)
C(14)-P(1)-Ru	114.86(13)
C(7)-P(1)-Ru	118.89(15)
C(13)-P(1)-Ru	113.24(12)
C(17)-P(2)-C(29)	102.6(2)
C(17)-P(2)-C(23)	102.18(15)

C(29)-P(2)-C(23)	110.51(18)
C(17)-P(2)-Ru	119.22(13)
C(29)-P(2)-Ru	108.73(16)
C(23)-P(2)-Ru	112.95(12)
C(12)-C(13)-P(1)	114.6(3)
C(8)-C(13)-P(1)	116.3(3)
C(15)-C(14)-P(1)	113.0(3)
C(16)-C(15)-C(14)	113.6(3)
C(15)-C(16)-C(17)	114.1(3)
C(16)-C(17)-P(2)	118.7(3)

Symmetry transformations used to generate equivalent atoms:

Appendix C. Crystallographic Information for RuCl(dcypb)(CO)(μ-Cl)$_2$RuCl(dcypb)(CO) (10).

Table C.1. Crystal data and structure refinement for RuCl(dcypb)(CO)(μ-Cl)$_2$RuCl(dcypb)(CO) (10).

Empirical formula	C58 H104 Cl4 O2 P4 Ru2
Formula weight	1301.23
Temperature	203(2) K
Wavelength	0.71073 Å
Crystal system, space group	Monoclinic, C2/c
Unit cell dimensions	a = 26.508(3) Å α = 90°
	b = 14.576(2) Å β = 109.078(2)°
	c = 17.037(2) Å γ = 90°
Volume	6221.2(14) Å^3
Z, Calculated density	4, 1.389 mg/m^3
Absorption coefficient	0.799 mm^{-1}
F(000)	2736
Crystal size	0.1 × 0.1 × 0.1 mm
Theta range for data collection	1.62 to 28.84°
Limiting indices	$-35 \le h \le 33, 0 \le k \le 19, 0 \le l \le 22$
Reflections collected / unique	24591 / 7487 [R(int) = 0.1291]
Completeness to θ = 28.84	91.9%
Absorption correction	Semi-empirical from equivalents
Max. and min. transmission	0.928077 and 0.742233
Refinement method	Full-matrix least-squares on F^2
Data / restraints / parameters	7487 / 4 / 311
Goodness-of-fit on F^2	1.015
R[a]	0.0529
R$_w$[b]	0.1280

[a] $R = \Sigma||F_o| - |F_c||/\Sigma|F_o|$. [b] $R_w = [\Sigma w\delta^2/\Sigma wF_o^2]^{1/2}$.

Table C.3. Bond lengths [Å] and angles [deg] for RuCl(dcypb)(CO)(μ-Cl)$_2$RuCl(dcypb)(CO) (**10**).

Ru-C(1')	1.775(10)
Ru-C(1)	1.789(5)
Ru-P(1)	2.3330(14)
Ru-P(2)	2.3648(13)
Ru-Cl(2)	2.4630(12)
Ru-Cl(1)	2.4741(19)
Ru-Cl(2)#1	2.4949(12)
Ru-Cl(1')	2.514(6)
P(1)-C(14)	1.825(5)
P(1)-C(7)	1.857(5)
P(1)-C(13)	1.862(5)
P(2)-C(17)	1.853(5)
P(2)-C(23)	1.873(6)
P(2)-C(29)	1.877(5)
O(1)-C(1)	1.146(4)
C(1')-O(1')	1.143(4)
Cl(2)-Ru#1	2.4949(12)
C(14)-C(15)	1.522(7)
C(15)-C(16)	1.538(7)
C(16)-C(17)	1.508(7)
C(1')-Ru-C(1)	178.6(6)
C(1')-Ru-P(1)	88.0(5)
C(1)-Ru-P(1)	90.6(2)
C(1')-Ru-P(2)	88.3(5)
C(1)-Ru-P(2)	92.3(2)
P(1)-Ru-P(2)	98.63(5)
C(1')-Ru-Cl(2)	91.3(5)
C(1)-Ru-Cl(2)	90.1(2)
P(1)-Ru-Cl(2)	173.27(5)
P(2)-Ru-Cl(2)	88.04(4)
C(1')-Ru-Cl(1)	7.3(5)
C(1)-Ru-Cl(1)	172.6(2)
P(1)-Ru-Cl(1)	90.41(6)
P(2)-Ru-Cl(1)	94.77(6)
Cl(2)-Ru-Cl(1)	88.11(5)
C(1')-Ru-Cl(2)#1	93.7(5)
C(1)-Ru-Cl(2)#1	86.0(2)
P(1)-Ru-Cl(2)#1	92.48(4)
P(2)-Ru-Cl(2)#1	168.79(4)
Cl(2)-Ru-Cl(2)#1	80.88(4)
Cl(1)-Ru-Cl(2)#1	86.66(6)

C(1')-Ru-Cl(1')	172.9(5)
C(1)-Ru-Cl(1')	7.7(3)
P(1)-Ru-Cl(1')	95.92(13)
P(2)-Ru-Cl(1')	96.94(13)
Cl(2)-Ru-Cl(1')	84.11(12)
Cl(1)-Ru-Cl(1')	165.69(13)
Cl(2)#1-Ru-Cl(1')	80.28(12)
C(14)-P(1)-C(7)	100.9(3)
C(14)-P(1)-C(13)	98.2(2)
C(7)-P(1)-C(13)	104.6(2)
C(14)-P(1)-Ru	118.02(18)
C(7)-P(1)-Ru	113.54(16)
C(13)-P(1)-Ru	118.82(17)
C(17)-P(2)-C(23)	102.7(3)
C(17)-P(2)-C(29)	101.2(2)
C(23)-P(2)-C(29)	101.5(2)
C(17)-P(2)-Ru	120.19(18)
C(23)-P(2)-Ru	115.22(16)
C(29)-P(2)-Ru	113.54(15)
O(1)-C(1)-Ru	175.9(6)
O(1')-C(1')-Ru	167.9(15)
Ru-Cl(2)-Ru#1	99.12(4)
C(14)-C(15)-C(16)	115.3(4)
C(17)-C(16)-C(15)	112.9(5)

Symmetry transformations used to generate equivalent atoms:
#1 -x+1/2,-y+3/2,-z

Appendix D. Crystallographic Information for RuCl(η^3-dcypb)(SiL^N_2) (12).

Figure D.1. ORTEP diagram of the mirror image complex of **12**. Thermal ellipsoids shown at 30% probability level. Hydrogen atoms and solvate molecules omitted for clarity.

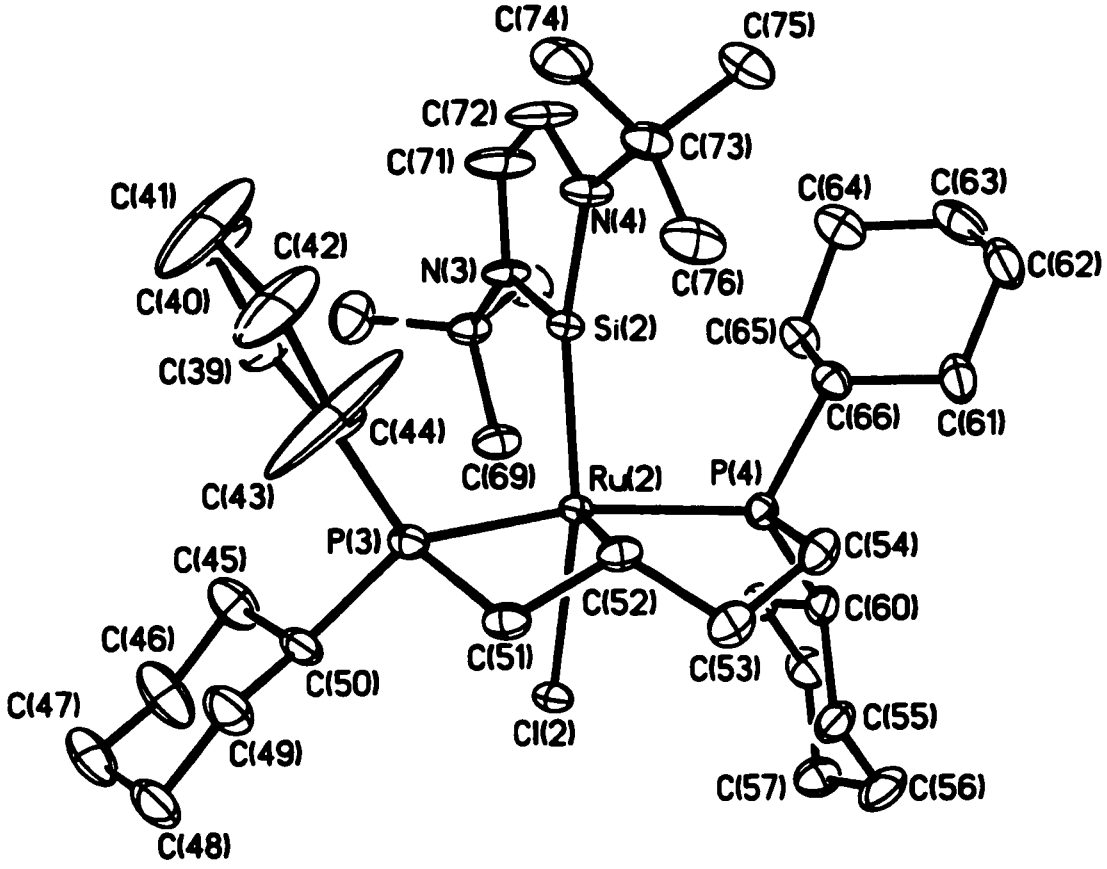

Table D.1. Crystal data and structure refinement for RuCl(η^3-dcypb)(SiL$^N_2$) (12).

Empirical formula	$C_{44}H_{77}ClN_2P_2RuSi$
Formula weight	860.63
Temperature	203(2) K
Wavelength	0.71073 Å
Crystal system, space group	Monoclinic, *Pc*
Unit cell dimensions	a = 13.503(1) Å $\alpha = 90^\circ$
	b = 17.697(2) Å $\beta = 105.742(2)^\circ$
	c = 20.110(2) Å $\gamma = 90^\circ$
Volume	4625.3(8) Å^3
Z, Calculated density	4, 1.236 mg/m^3
Absorption coefficient	0.522 mm^{-1}
F(000)	1840
Crystal size	0.2 × 0.2 × 0.1 mm
Theta range for data collection	1.15 to 28.83°
Limiting indices	$-17 \le h \le 18, 0 \le k \le 23, -26 \le l \le 25$
Reflections collected / unique	36492 / 17571 [R(int) = 0.0496]
Completeness to θ = 28.83	92.3%
Absorption correction	Semi-empirical from equivalents
Max. and min. transmission	0.928076 and 0.613589
Refinement method	Full-matrix least-squares on F^2
Data / restraints / parameters	17571 / 2 / 895
Goodness-of-fit on F^2	1.021
R^a	0.0388
$R_w{}^b$	0.0513

$^aR = \Sigma||F_o| - |F_c||/\Sigma|F_o|$. $^bR_w = [\Sigma w\delta^2/\Sigma wF_o{}^2]^{1/2}$

Table D.2. Bond lengths [Å] and angles [deg] for RuCl(η^3-dcypb)(SiL$^N_2$) (12).

Ru(1)-C(14)	2.110(4)
Ru(1)-Si(1)	2.2264(11)
Ru(1)-P(2)	2.3373(12)
Ru(1)-P(1)	2.3389(12)
Ru(1)-Cl(1)	2.4713(11)
Ru(2)-C(52)	2.114(4)
Ru(2)-Si(2)	2.2293(12)
Ru(2)-P(4)	2.3279(12)
Ru(2)-P(3)	2.3422(11)
Ru(2)-Cl(2)	2.4738(10)
Si(1)-N(1)	1.732(3)
Si(1)-N(2)	1.734(3)
Si(2)-N(3)	1.725(3)
Si(2)-N(4)	1.741(3)
N(1)-C(33)	1.388(5)
N(1)-C(29)	1.490(5)
N(2)-C(34)	1.400(6)
N(2)-C(35)	1.484(4)
N(3)-C(71)	1.377(6)
N(3)-C(67)	1.492(5)
N(4)-C(72)	1.411(6)
N(4)-C(73)	1.485(5)
P(1)-C(13)	1.826(4)
P(1)-C(6)	1.854(4)
P(1)-C(12)	1.854(5)
P(2)-C(16)	1.833(4)
P(2)-C(22)	1.841(5)
P(2)-C(28)	1.863(5)
P(3)-C(51)	1.840(5)
P(3)-C(50)	1.845(5)
P(3)-C(44)	1.856(5)
P(4)-C(54)	1.847(4)
P(4)-C(60)	1.867(4)
P(4)-C(66)	1.868(4)
C(13)-C(14)	1.541(6)
C(14)-C(15)	1.492(6)
C(15)-C(16)	1.530(7)

C(14)-Ru(1)-Si(1)	104.45(12)
C(14)-Ru(1)-P(2)	83.05(13)
Si(1)-Ru(1)-P(2)	92.85(4)
C(14)-Ru(1)-P(1)	69.21(13)

Si(1)-Ru(1)-P(1)	96.74(4)
P(2)-Ru(1)-P(1)	152.11(4)
C(14)-Ru(1)-Cl(1)	95.16(12)
Si(1)-Ru(1)-Cl(1)	160.03(4)
P(2)-Ru(1)-Cl(1)	93.23(4)
P(1)-Ru(1)-Cl(1)	86.61(4)
C(52)-Ru(2)-Si(2)	103.76(12)
C(52)-Ru(2)-P(4)	83.68(12)
Si(2)-Ru(2)-P(4)	94.42(4)
C(52)-Ru(2)-P(3)	69.50(12)
Si(2)-Ru(2)-P(3)	95.57(4)
P(4)-Ru(2)-P(3)	152.91(4)
C(52)-Ru(2)-Cl(2)	95.87(12)
Si(2)-Ru(2)-Cl(2)	159.57(4)
P(4)-Ru(2)-Cl(2)	93.30(4)
P(3)-Ru(2)-Cl(2)	85.93(4)
N(1)-Si(1)-N(2)	90.60(17)
N(1)-Si(1)-Ru(1)	116.06(12)
N(2)-Si(1)-Ru(1)	153.15(13)
N(3)-Si(2)-N(4)	90.61(17)
N(3)-Si(2)-Ru(2)	116.42(12)
N(4)-Si(2)-Ru(2)	152.97(13)
C(33)-N(1)-C(29)	119.6(3)
C(33)-N(1)-Si(1)	111.7(3)
C(29)-N(1)-Si(1)	128.7(3)
C(34)-N(2)-C(35)	116.8(3)
C(34)-N(2)-Si(1)	110.0(3)
C(35)-N(2)-Si(1)	133.3(3)
C(71)-N(3)-C(67)	119.3(3)
C(71)-N(3)-Si(2)	111.8(3)
C(67)-N(3)-Si(2)	128.8(3)
C(72)-N(4)-C(73)	117.2(3)
C(72)-N(4)-Si(2)	109.5(3)
C(73)-N(4)-Si(2)	133.3(3)
C(13)-P(1)-C(6)	104.36(19)
C(13)-P(1)-C(12)	109.9(2)
C(6)-P(1)-C(12)	105.1(3)
C(13)-P(1)-Ru(1)	83.77(14)
C(6)-P(1)-Ru(1)	119.86(14)
C(12)-P(1)-Ru(1)	128.20(19)
C(16)-P(2)-C(22)	103.9(2)
C(16)-P(2)-C(28)	101.4(2)
C(22)-P(2)-C(28)	103.8(3)
C(16)-P(2)-Ru(1)	101.30(16)
C(22)-P(2)-Ru(1)	122.0(2)
C(28)-P(2)-Ru(1)	121.00(17)

C(51)-P(3)-C(50)	105.7(2)
C(51)-P(3)-C(44)	106.9(2)
C(50)-P(3)-C(44)	107.9(3)
C(51)-P(3)-Ru(2)	83.15(14)
C(50)-P(3)-Ru(2)	123.01(16)
C(44)-P(3)-Ru(2)	123.4(2)
C(54)-P(4)-C(60)	105.1(2)
C(54)-P(4)-C(66)	102.4(2)
C(60)-P(4)-C(66)	102.9(2)
C(6)-C(1)-C(2)	110.9(4)
C(3)-C(2)-C(1)	112.0(4)
C(4)-C(3)-C(2)	112.0(4)
C(3)-C(4)-C(5)	112.1(4)
C(4)-C(5)-C(6)	110.6(4)
C(1)-C(6)-C(5)	111.4(4)
C(1)-C(6)-P(1)	111.3(3)
C(5)-C(6)-P(1)	116.2(3)
C(8)-C(7)-C(12)	115.2(4)
C(9)-C(8)-C(7)	119.5(6)
C(8)-C(9)-C(10)	118.1(6)
C(9)-C(10)-C(11)	112.6(6)
C(12)-C(11)-C(10)	118.1(6)
C(11)-C(12)-C(7)	115.2(5)
C(11)-C(12)-P(1)	120.7(5)
C(7)-C(12)-P(1)	112.3(3)
C(14)-C(13)-P(1)	97.3(3)
C(15)-C(14)-C(13)	117.0(4)
C(15)-C(14)-Ru(1)	112.1(3)
C(13)-C(14)-Ru(1)	99.3(2)
C(14)-C(15)-C(16)	108.9(4)
C(15)-C(16)-P(2)	107.7(3)

Symmetry transformations used to generate equivalent atoms:

Appendix E. Crystallographic Information for [Ru(H)(dcypb)(μ-Cl)$_2$(μ-H)Ru(dcypb)(H$_2$)] (14).

Table E.1. Crystal data and structure refinement for [Ru(H)(dcypb)(μ-Cl)$_2$(μ-H)Ru(dcypb)(H$_2$)] (14).

Empirical formula	$C_{68}H_{120}Cl_2P_4Ru_2$
Formula weight	1334.56
Temperature	203(2) K
Wavelength	0.71073 Å
Crystal system, space group	Triclinic, P-1
Unit cell dimensions	a = 11.2119(7) Å α = 77.5280(10)°
	b = 13.6190(9) Å β = 79.2950(10)°
	c = 24.6084(16) Å γ = 68.6670(10)°
Volume	3393.7(4) Å^3
Z, Calculated density	2, 1.306 mg/m^3
Absorption coefficient	0.656 mm^{-1}
F(000)	1420
Crystal size	0.30 × 0.12 × 0.07mm
Theta range for data collection	1.63 to 28.73°
Limiting indices	$-14 \le h \le 14, -17 \le k \le 18, 0 \le l \le 33$
Reflections collected / unique	26599 / 15369 [R(int) = 0.0187]
Completeness to θ = 28.73	87.3%
Absorption correction	Semi-empirical from equivalents
Max. and min. transmission	0.928074 and 0.861365
Refinement method	Full-matrix least-squares on F^2
Data / restraints / parameters	15369 / 0 / 694
Goodness-of-fit on F^2	1.012
R [a]	0.0273
R$_w$ [b]	0.0385

[a] $R = \sum||F_o| - |F_c||/\sum|F_o|$. [b] $R_w = [\sum w\delta^2/\sum wF_o^2]^{1/2}$.

Table E.2. Bond lengths [Å] and angles [deg] for [Ru(H)(dcypb)(μ-Cl)$_2$(μ-H)Ru(dcypb)(H$_2$)] (14).

Ru(1)-P(1)	2.2681(5)
Ru(1)-P(2)	2.3854(5)
Ru(1)-Cl(2)	2.4298(5)
Ru(1)-Cl(1)	2.4725(5)
Ru(1)-Ru(2)	2.8595(3)
Ru(1)-H(1)	1.573(13)
Ru(1)-H(3)	1.768(18)
Ru(2)-P(4)	2.2453(5)
Ru(2)-P(3)	2.2543(5)
Ru(2)-Cl(2)	2.5034(5)
Ru(2)-Cl(1)	2.5531(5)
Ru(2)-H(2)	1.559(12)
Ru(2)-H(3)	1.84(2)
P(1)-C(13)	1.848(2)
P(1)-C(6)	1.8586(19)
P(1)-C(12)	1.864(2)
P(2)-C(16)	1.8461(19)
P(2)-C(22)	1.860(2)
P(2)-C(28)	1.864(2)
P(3)-C(41)	1.8535(19)
P(3)-C(40)	1.8599(19)
P(3)-C(34)	1.8807(19)
P(4)-C(44)	1.857(2)
P(4)-C(56)	1.880(2)
P(4)-C(50)	1.887(2)

P(1)-Ru(1)-P(2)	100.384(17)
P(1)-Ru(1)-Cl(2)	96.284(18)
P(2)-Ru(1)-Cl(2)	97.169(17)
P(1)-Ru(1)-Cl(1)	171.687(17)
P(2)-Ru(1)-Cl(1)	87.929(16)
Cl(2)-Ru(1)-Cl(1)	82.543(16)
P(1)-Ru(1)-Ru(2)	115.973(14)
P(2)-Ru(1)-Ru(2)	135.354(14)
Cl(2)-Ru(1)-Ru(2)	55.787(11)
Cl(1)-Ru(1)-Ru(2)	56.659(11)
P(4)-Ru(2)-P(3)	98.762(19)
P(4)-Ru(2)-Cl(2)	166.667(19)
P(3)-Ru(2)-Cl(2)	93.689(17)
P(4)-Ru(2)-Cl(1)	101.339(17)
P(3)-Ru(2)-Cl(1)	106.416(17)

Cl(2)-Ru(2)-Cl(1)	79.509(15)
P(4)-Ru(2)-Ru(1)	116.328(15)
P(3)-Ru(2)-Ru(1)	141.660(14)
Cl(2)-Ru(2)-Ru(1)	53.381(12)
Cl(1)-Ru(2)-Ru(1)	54.004(11)
Ru(1)-Cl(1)-Ru(2)	69.337(12)
Ru(1)-Cl(2)-Ru(2)	70.832(14)
Ru(1)-H(3)-Ru(2)	104.6(9)
C(13)-P(1)-C(6)	101.33(9)
C(13)-P(1)-C(12)	98.24(9)
C(6)-P(1)-C(12)	104.88(9)
C(13)-P(1)-Ru(1)	117.40(6)
C(6)-P(1)-Ru(1)	117.01(6)
C(12)-P(1)-Ru(1)	115.35(6)
C(16)-P(2)-C(22)	102.50(9)
C(16)-P(2)-C(28)	101.62(9)
C(22)-P(2)-C(28)	103.44(9)
C(16)-P(2)-Ru(1)	121.08(6)
C(22)-P(2)-Ru(1)	113.74(6)
C(28)-P(2)-Ru(1)	112.35(6)
C(41)-P(3)-C(40)	99.95(9)
C(41)-P(3)-C(34)	100.50(9)
C(40)-P(3)-C(34)	101.52(9)
C(41)-P(3)-Ru(2)	122.15(7)
C(40)-P(3)-Ru(2)	117.59(7)
C(34)-P(3)-Ru(2)	111.97(6)
C(44)-P(4)-C(56)	102.42(9)
C(44)-P(4)-C(50)	96.34(9)
C(56)-P(4)-C(50)	100.24(9)
C(44)-P(4)-Ru(2)	121.76(7)
C(56)-P(4)-Ru(2)	114.39(6)
C(50)-P(4)-Ru(2)	118.05(6)

Symmetry transformations used to generate equivalent atoms:

Appendix F. Crystallographic Information for [Ru(H)(dcypb)(μ-Cl)$_3$Ru(dcypb)(N$_2$)] (15).

Table F.1. Crystal data and structure refinement for [Ru(H)(dcypb)(μ-Cl)$_3$Ru(dcypb)(N$_2$)] (15).

Empirical formula	C62 H109 Cl3 N2 P4 Ru2
Formula weight	1314.88
Temperature	203(2) K
Wavelength	0.71073 Å
Crystal system, space group	Triclinic, P-1
Unit cell dimensions	a = 11.6220(9) Å α = 89.7230(10) °
	b = 13.5699(10) Å β = 86.8370(10) °
	c = 22.7781(17) Å γ = 66.5080(10) °
Volume	3289.0(4) Å^3
Z, Calculated density	2, 1.328 mg/m^3
Absorption coefficient	0.716 mm^{-1}
F(000)	1388
Crystal size	0.20 × 0.10 × 0.05 mm
Theta range for data collection	1.64 to 28.71°
Limiting indices	-15 ≤ h ≤ 15, -17 ≤ k ≤ 17, 0 ≤ l ≤ 30
Reflections collected / unique	25795 / 14910 [R(int) = 0.0404]
Completeness to θ = 28.71	87.6%
Absorption correction	Semi-empirical from equivalents
Max. and min. transmission	0.928076 and 0.828149
Refinement method	Full-matrix least-squares on F^2
Data / restraints / parameters	14910 / 0 / 658
Goodness-of-fit on F^2	1.028
R[a]	0.0487
R_w[b]	0.0971

[a] $R = \sum||F_o| - |F_c||/\sum|F_o|$. [b] $R_w = [\sum w\delta^2/\sum wF_o^2]^{1/2}$

Table F.2. Bond lengths [Å] and angles [deg] for [Ru(H)(dcypb)(μ-Cl)$_3$Ru(dcypb)(N$_2$)] **(15)**.

Ru(1)-N(1)	1.898(6)
Ru(1)-P(1)	2.3225(11)
Ru(1)-P(2)	2.3369(11)
Ru(1)-Cl(3)	2.4636(10)
Ru(1)-Cl(2)	2.4793(10)
Ru(1)-Cl(1)	2.4840(10)
Ru(2)-P(3)	2.2352(11)
Ru(2)-P(4)	2.2419(12)
Ru(2)-Cl(3)	2.5107(11)
Ru(2)-Cl(2)	2.5403(10)
Ru(2)-Cl(1)	2.6092(10)
N(1)-N(2)	1.110(5)
P(1)-C(6)	1.852(4)
P(1)-C(13)	1.866(4)
P(1)-C(12)	1.875(4)
P(2)-C(16)	1.830(4)
P(2)-C(22)	1.832(4)
P(2)-C(28)	1.862(5)
P(3)-C(34)	1.866(4)
P(3)-C(40)	1.876(4)
P(3)-C(41)	1.868(4)
P(4)-C(44)	1.853(4)
P(4)-C(56)	1.856(4)
P(4)-C(50)	1.879(4)

N(1)-Ru(1)-P(1)	92.46(13)
N(1)-Ru(1)-P(2)	94.82(12)
P(1)-Ru(1)-P(2)	93.46(4)
N(1)-Ru(1)-Cl(3)	167.40(13)
P(1)-Ru(1)-Cl(3)	96.02(4)
P(2)-Ru(1)-Cl(3)	93.95(4)
N(1)-Ru(1)-Cl(2)	90.30(14)
P(1)-Ru(1)-Cl(2)	174.50(4)
P(2)-Ru(1)-Cl(2)	91.04(4)
Cl(3)-Ru(1)-Cl(2)	80.51(3)
N(1)-Ru(1)-Cl(1)	89.56(12)
P(1)-Ru(1)-Cl(1)	93.38(4)
P(2)-Ru(1)-Cl(1)	171.71(4)
Cl(3)-Ru(1)-Cl(1)	80.68(3)
Cl(2)-Ru(1)-Cl(1)	81.88(3)
P(3)-Ru(2)-P(4)	96.67(4)

P(3)-Ru(2)-Cl(3)	93.35(4)
P(4)-Ru(2)-Cl(3)	169.98(4)
P(3)-Ru(2)-Cl(2)	170.74(4)
P(4)-Ru(2)-Cl(2)	91.59(4)
Cl(3)-Ru(2)-Cl(2)	78.44(3)
P(3)-Ru(2)-Cl(1)	104.29(4)
P(4)-Ru(2)-Cl(1)	99.77(4)
Cl(3)-Ru(2)-Cl(1)	77.41(3)
Cl(2)-Ru(2)-Cl(1)	78.32(3)
Ru(1)-Cl(1)-Ru(2)	83.41(3)
Ru(1)-Cl(2)-Ru(2)	84.95(3)
Ru(1)-Cl(3)-Ru(2)	85.91(3)
N(2)-N(1)-Ru(1)	173.0(4)
C(6)-P(1)-C(13)	100.6(2)
C(6)-P(1)-C(12)	105.53(18)
C(13)-P(1)-C(12)	107.3(2)
C(6)-P(1)-Ru(1)	113.73(14)
C(13)-P(1)-Ru(1)	118.36(15)
C(12)-P(1)-Ru(1)	110.23(14)
C(16)-P(2)-C(22)	106.3(2)
C(16)-P(2)-C(28)	100.5(2)
C(22)-P(2)-C(28)	104.9(2)
C(16)-P(2)-Ru(1)	117.60(14)
C(22)-P(2)-Ru(1)	115.51(15)
C(28)-P(2)-Ru(1)	110.35(16)
C(34)-P(3)-C(40)	101.21(18)
C(34)-P(3)-C(41)	100.5(2)
C(40)-P(3)-C(41)	100.30(19)
C(34)-P(3)-Ru(2)	111.65(13)
C(40)-P(3)-Ru(2)	119.06(13)
C(41)-P(3)-Ru(2)	120.92(15)
C(44)-P(4)-C(56)	103.0(2)
C(44)-P(4)-C(50)	101.0(2)
C(56)-P(4)-C(50)	104.4(2)
C(44)-P(4)-Ru(2)	122.51(16)
C(56)-P(4)-Ru(2)	113.66(15)
C(50)-P(4)-Ru(2)	110.26(16)

Symmetry transformations used to generate equivalent atoms:

Appendix G. Crystallographic Information for RuCl(dcypb)(μ-Cl)$_3$Ru(dcypb)[CHCHC(CH$_3$)$_2$] (21).

Table G.1. Crystal data and structure refinement for RuCl(dcypb)(μ-Cl)$_3$Ru(dcypb)[CHCHC(CH$_3$)$_2$] (21).

Empirical formula	$C_{64}H_{119}Cl_4P_4Ru_2$
Formula weight	1356.41
Temperature	203(2) K
Wavelength	0.71073 Å
Crystal system, space group	Triclinic, P-1
Unit cell dimensions	a = 11.7069(16) Å α = 95.066(3)°
	b = 14.1411(19) Å β = 93.018(2)°
	c = 22.140(3) Å γ = 112.186(2)°
Volume	3365.9(8) Å^3
Z, Calculated density	2, 1.338 mg/m^3
Absorption coefficient	0.739 mm^{-1}
F(000)	1438
Crystal size	0.12 × 0.10 × 0.01 mm
Theta range for data collection	1.57 to 20.82°
Limiting indices	$-11 \le h \le 11, -14 \le k \le -14, 0 \le l \le 22$
Reflections collected / unique	26256 / 7055 [R(int) = 0.1233]
Completeness to θ = 20.82	99.8%
Absorption correction	Semi-empirical from equivalents
Max. and min. transmission	0.928076 and 0.598612
Refinement method	Full-matrix least-squares on F^2
Data / restraints / parameters	7055 / 579 / 667
Goodness-of-fit on F^2	1.038
R [a]	0.0540
R$_w$ [b]	0.1076

[a] $R = \sum ||F_o| - |F_c|| / \sum |F_o|$. [b] $R_w = [\sum w\delta^2 / \sum wF_o^2]^{1/2}$.

Table G.2. Bond lengths [Å] and angles [deg] for RuCl(dcypb)(μ-Cl)$_3$Ru(dcypb)[CHCHC(CH$_3$)$_2$] (**21**).

Ru(1)-C(1)	1.888(8)
Ru(1)-P(1)	2.304(3)
Ru(1)-P(2)	2.320(2)
Ru(1)-Cl(3)	2.451(2)
Ru(1)-Cl(2)	2.471(2)
Ru(1)-Cl(4)	2.543(2)
Ru(2)-P(3)	2.257(3)
Ru(2)-P(4)	2.277(2)
Ru(2)-Cl(1)	2.398(2)
Ru(2)-Cl(2)	2.400(2)
Ru(2)-Cl(3)	2.525(2)
Ru(2)-Cl(4)	2.532(2)
P(1)-C(18)	1.832(8)
P(1)-C(17)	1.858(9)
P(1)-C(11)	1.869(8)
P(2)-C(27)	1.834(9)
P(2)-C(33)	1.847(9)
P(2)-C(21)	1.849(7)
P(3)-C(49)	1.824(8)
P(3)-C(55)	1.871(9)
P(3)-C(61)	1.879(8)
P(4)-C(46)	1.830(7)
P(4)-C(39)	1.854(8)
P(4)-C(45)	1.867(9)
C(1)-C(2)	1.459(11)
C(2)-C(3)	1.362(11)
C(3)-C(4)	1.460(11)
C(3)-C(5)	1.489(13)

C(1)-Ru(1)-P(1)	91.5(3)
C(1)-Ru(1)-P(2)	89.0(2)
P(1)-Ru(1)-P(2)	94.31(9)
C(1)-Ru(1)-Cl(3)	95.1(2)
P(1)-Ru(1)-Cl(3)	90.87(9)
P(2)-Ru(1)-Cl(3)	173.33(8)
C(1)-Ru(1)-Cl(2)	95.0(3)
P(1)-Ru(1)-Cl(2)	169.43(8)
P(2)-Ru(1)-Cl(2)	94.14(8)

Cl(3)-Ru(1)-Cl(2)	80.26(8)
C(1)-Ru(1)-Cl(4)	170.0(3)
P(1)-Ru(1)-Cl(4)	95.37(8)
P(2)-Ru(1)-Cl(4)	97.76(8)
Cl(3)-Ru(1)-Cl(4)	77.53(7)
Cl(2)-Ru(1)-Cl(4)	77.20(7)
P(3)-Ru(2)-P(4)	96.95(9)
P(3)-Ru(2)-Cl(1)	91.58(9)
P(4)-Ru(2)-Cl(1)	89.95(8)
P(3)-Ru(2)-Cl(2)	94.77(9)
P(4)-Ru(2)-Cl(2)	100.62(8)
Cl(1)-Ru(2)-Cl(2)	166.89(8)
P(3)-Ru(2)-Cl(3)	92.56(8)
P(4)-Ru(2)-Cl(3)	170.33(9)
Cl(1)-Ru(2)-Cl(3)	88.11(8)
Cl(2)-Ru(2)-Cl(3)	80.17(7)
P(3)-Ru(2)-Cl(4)	167.92(7)
P(4)-Ru(2)-Cl(4)	94.25(8)
Cl(1)-Ru(2)-Cl(4)	92.93(8)
Cl(2)-Ru(2)-Cl(4)	78.69(7)
Cl(3)-Ru(2)-Cl(4)	76.40(7)
Ru(2)-Cl(2)-Ru(1)	88.43(8)
Ru(1)-Cl(3)-Ru(2)	86.12(7)
Ru(2)-Cl(4)-Ru(1)	84.04(7)

Symmetry transformations used to generate equivalent atoms:
#1 -x,-y+2,-z+1

Appendix H. Crystallographic Information for RuCl(dcpx)(PPh_3) (24).

Table H.1. Crystal data and structure refinement for RuCl(dcpx)(PPh_3) (24).

Empirical formula	$C_{54}\ H_{74}\ Cl\ O\ P_3\ Ru$
Formula weight	968.56
Temperature	203(2) K
Wavelength	0.71073 Å
Crystal system, space group	Triclinic, P-1
Unit cell dimensions	a = 12.9390(8) Å = 99.9870(10)°
	b = 14.2861(9) Å β = 100.7430(10)°
	c = 14.9545(9) Å γ = 93.3590(10)°
Volume	2662.9(3) $Å^3$
Z, Calculated density	2, 1.208 mg/m^3
Absorption coefficient	0.469 mm^{-1}
F(000)	1024
Crystal size	0.10 × 0.10 × 0.10 mm
Theta range for data collection	1.44 to 28.72°
Limiting indices	$-17 \le h \le 16, -19 \le k \le 18, 0 \le l \le 20$
Reflections collected / unique	20833 / 11993 [R(int) = 0.0299]
Completeness to θ = 28.72	86.8%
Absorption correction	Semi-empirical from equivalents
Max. and min. transmission	0.928075 and 0.843640
Refinement method	Full-matrix least-squares on F^2
Data / restraints / parameters	11993 / 0 / 518
Goodness-of-fit on F^2	1.027
R^a	0.0515
$R_w{}^b$	0.0766

$^aR = \sum||F_o| - |F_c||/\sum|F_o|$, $^bR_W = [\sum w\delta^2/\sum wF_o^2]^{1/2}$.

Table H.2. Bond lengths [Å] and angles [deg] for RuCl(dcpx)(PPh_3) (**24**).

Ru-C(19)	2.061(4)
Ru-P(3)	2.1996(10)
Ru-P(1)	2.3247(10)
Ru-P(2)	2.3522(10)
Ru-Cl	2.4520(10)
P(1)-C(13)	1.833(4)
P(1)-C(6)	1.854(4)
P(1)-C(12)	1.855(4)
P(2)-C(20)	1.837(4)
P(2)-C(21)	1.842(4)
P(2)-C(32)	1.862(4)
P(3)-C(50)	1.841(4)
P(3)-C(44)	1.848(4)
P(3)-C(38)	1.853(4)
C(1)-C(6)	1.529(6)
C(1)-C(2)	1.537(6)
C(2)-C(3)	1.514(6)
C(3)-C(4)	1.513(7)
C(4)-C(5)	1.528(6)
C(5)-C(6)	1.537(5)
C(7)-C(8)	1.516(6)
C(7)-C(12)	1.523(5)
C(8)-C(9)	1.522(6)
C(9)-C(10)	1.534(7)
C(10)-C(11)	1.531(6)
C(11)-C(12)	1.544(5)
C(13)-C(14)	1.506(5)
C(14)-C(15)	1.395(5)
C(14)-C(19)	1.419(5)
C(15)-C(16)	1.384(6)
C(16)-C(17)	1.389(6)
C(17)-C(18)	1.392(5)
C(18)-C(19)	1.429(5)
C(18)-C(20)	1.515(5)
C(19)-Ru-P(3)	88.13(11)
C(19)-Ru-P(1)	82.26(11)
P(3)-Ru-P(1)	95.60(4)
C(19)-Ru-P(2)	80.29(11)
P(3)-Ru-P(2)	102.63(4)
P(1)-Ru-P(2)	154.21(4)
C(19)-Ru-Cl	151.42(11)

P(3)-Ru-Cl	120.31(4)
P(1)-Ru-Cl	91.43(3)
P(2)-Ru-Cl	94.87(3)
C(13)-P(1)-C(6)	103.96(18)
C(13)-P(1)-C(12)	107.78(18)
C(6)-P(1)-C(12)	105.69(18)
C(13)-P(1)-Ru	103.54(13)
C(6)-P(1)-Ru	110.39(12)
C(12)-P(1)-Ru	123.83(13)
C(20)-P(2)-C(21)	103.66(18)
C(20)-P(2)-C(32)	104.40(19)
C(21)-P(2)-C(32)	108.94(18)
C(20)-P(2)-Ru	102.00(13)
C(21)-P(2)-Ru	132.94(15)
C(32)-P(2)-Ru	101.86(13)
C(50)-P(3)-C(44)	96.20(18)
C(50)-P(3)-C(38)	102.02(19)
C(44)-P(3)-C(38)	102.87(19)
C(50)-P(3)-Ru	113.86(13)
C(44)-P(3)-Ru	120.45(14)
C(38)-P(3)-Ru	117.91(13)
C(6)-C(1)-C(2)	111.8(4)
C(3)-C(2)-C(1)	112.1(4)
C(4)-C(3)-C(2)	110.6(4)
C(3)-C(4)-C(5)	111.6(4)
C(4)-C(5)-C(6)	112.1(3)
C(1)-C(6)-C(5)	110.0(3)
C(1)-C(6)-P(1)	110.2(3)
C(5)-C(6)-P(1)	115.0(3)
C(8)-C(7)-C(12)	110.5(3)
C(7)-C(8)-C(9)	113.7(4)
C(8)-C(9)-C(10)	111.1(4)
C(11)-C(10)-C(9)	112.0(4)
C(10)-C(11)-C(12)	109.8(3)
C(7)-C(12)-C(11)	111.3(3)
C(7)-C(12)-P(1)	112.1(3)
C(11)-C(12)-P(1)	117.1(3)
C(14)-C(13)-P(1)	108.9(2)
C(15)-C(14)-C(19)	121.2(4)
C(15)-C(14)-C(13)	119.4(3)
C(19)-C(14)-C(13)	119.3(3)
C(16)-C(15)-C(14)	121.1(4)
C(15)-C(16)-C(17)	119.2(4)
C(16)-C(17)-C(18)	120.8(4)
C(17)-C(18)-C(19)	121.3(4)
C(17)-C(18)-C(20)	120.4(4)

C(19)-C(18)-C(20)	118.3(3)
C(14)-C(19)-C(18)	116.3(3)
C(14)-C(19)-Ru	121.6(3)
C(18)-C(19)-Ru	122.0(3)
C(18)-C(20)-P(2)	106.1(3)
C(26)-C(21)-C(22)	111.4(3)
C(26)-C(21)-P(2)	112.5(3)
C(22)-C(21)-P(2)	115.2(3)

Symmetry transformations used to generate equivalent atoms:

Appendix I. Crystallographic Information for RuCl(dcpx)$(CO)_2$ (25).

Table I.1. Crystal data and structure refinement for RuCl(dcpx)$(CO)_2$ (25).

Empirical formula	$C_{34}\ H_{51}\ Cl\ O_2\ P_2\ Ru$
Formula weight	690.21
Temperature	203(2) K
Wavelength	0.71073 Å
Crystal system, space group	Triclinic, P-1
Unit cell dimensions	a = 11.082(2) Å = 94.222(2)°
	b = 11.568(2) Å β = 91.744(2)°
	c = 14.228(2) Å γ = 115.517(2)°
Volume	1637.8(4) $Å^3$
Z, Calculated density	2, 1.400 mg/m^3
Absorption coefficient	0.687 mm^{-1}
F(000)	724
Crystal size	0.10 × 0.07 × 0.02 mm
Theta range for data collection	1.44 to 28.74°
Limiting indices	$-14 \le h \le 14, -15 \le k \le 15, 0 \le l \le 18$
Reflections collected / unique	12803 / 7413 [R(int) = 0.0616]
Completeness to θ = 28.83	87.3%
Absorption correction	Semi-empirical from equivalents
Max. and min. transmission	0.928076 and 0.643412
Refinement method	Full-matrix least-squares on F^2
Data / restraints / parameters	7413 / 2 / 388
Goodness-of-fit on F^2	1.025
R^a	0.0530
$R_w{}^b$	0.0878

$^aR = \sum||F_o| - |F_c||/\sum|F_o|$, $^bR_w = [\sum w\delta^2/\sum wF_o{}^2]^{1/2}$.

Table I.2. Bond lengths [Å] and angles [deg] for $RuCl(dcpx)(CO)_2$ **(25).**

Ru-C(34)	1.837(11)
Ru-C(34')	1.859(11)
Ru-C(33)	1.912(5)
Ru-C(19)	2.112(4)
Ru-P(1)	2.3649(14)
Ru-P(2)	2.3698(13)
Ru-Cl(1)	2.447(4)
Ru-Cl(1')	2.447(4)
P(1)-C(13)	1.839(4)
P(1)-C(6)	1.847(5)
P(1)-C(12)	1.855(4)
P(2)-C(20)	1.830(4)
P(2)-C(26)	1.849(4)
P(2)-C(32)	1.853(5)
O(1)-C(33)	1.167(5)
O(2)-C(34)	1.187(11)
O(2')-C(34')	1.166(11)
C(1)-C(6)	1.533(6)
C(1)-C(2)	1.534(6)
C(2)-C(3)	1.515(6)
C(3)-C(4)	1.520(6)
C(4)-C(5)	1.526(7)
C(5)-C(6)	1.535(6)
C(7)-C(8)	1.532(6)
C(7)-C(12)	1.536(6)
C(8)-C(9)	1.511(7)
C(9)-C(10)	1.526(7)
C(10)-C(11)	1.529(6)
C(11)-C(12)	1.532(6)
C(13)-C(14)	1.535(7)
C(14)-C(19)	1.347(6)
C(14)-C(15)	1.384(6)
C(15)-C(16)	1.363(7)
C(16)-C(17)	1.388(7)
C(17)-C(18)	1.391(6)
C(18)-C(19)	1.462(6)
C(18)-C(20)	1.508(6)

C(34)-Ru-C(34')	178.6(9)
C(34)-Ru-C(33)	90.4(6)
C(34')-Ru-C(33)	88.3(6)
C(34)-Ru-C(19)	91.4(6)

C(34')-Ru-C(19)	89.9(6)
C(33)-Ru-C(19)	177.7(2)
C(34)-Ru-P(1)	84.3(5)
C(34')-Ru-P(1)	96.3(7)
C(33)-Ru-P(1)	99.95(14)
C(19)-Ru-P(1)	78.88(13)
C(34)-Ru-P(2)	96.2(5)
C(34')-Ru-P(2)	83.7(7)
C(33)-Ru-P(2)	99.28(14)
C(19)-Ru-P(2)	81.88(13)
P(1)-Ru-P(2)	160.76(4)
C(34)-Ru-Cl(1)	178.8(5)
C(34')-Ru-Cl(1)	1.5(7)
C(33)-Ru-Cl(1)	89.51(17)
C(19)-Ru-Cl(1)	88.66(16)
P(1)-Ru-Cl(1)	96.93(12)
P(2)-Ru-Cl(1)	82.64(12)
C(34)-Ru-Cl(1')	2.6(6)
C(34')-Ru-Cl(1')	178.6(7)
C(33)-Ru-Cl(1')	92.72(17)
C(19)-Ru-Cl(1')	89.12(16)
P(1)-Ru-Cl(1')	82.60(12)
P(2)-Ru-Cl(1')	97.08(11)
Cl(1)-Ru-Cl(1')	177.77(18)
C(13)-P(1)-C(6)	104.6(2)
C(13)-P(1)-C(12)	103.1(2)
C(6)-P(1)-C(12)	107.3(2)
C(13)-P(1)-Ru	101.76(17)
C(6)-P(1)-Ru	118.83(15)
C(12)-P(1)-Ru	118.86(16)
C(20)-P(2)-C(26)	101.9(2)
C(20)-P(2)-C(32)	104.5(2)
C(26)-P(2)-C(32)	106.5(2)
C(20)-P(2)-Ru	101.70(17)
C(26)-P(2)-Ru	119.77(16)
C(32)-P(2)-Ru	119.50(15)
C(6)-C(1)-C(2)	110.1(4)
C(3)-C(2)-C(1)	110.4(4)
C(2)-C(3)-C(4)	110.8(4)
C(3)-C(4)-C(5)	111.4(4)
C(4)-C(5)-C(6)	112.6(4)
C(1)-C(6)-C(5)	111.4(4)
C(1)-C(6)-P(1)	112.5(3)
C(5)-C(6)-P(1)	111.3(3)
C(8)-C(7)-C(12)	110.7(4)
C(9)-C(8)-C(7)	111.5(4)

C(8)-C(9)-C(10)	110.3(4)
C(9)-C(10)-C(11)	112.2(4)
C(10)-C(11)-C(12)	111.1(4)
C(11)-C(12)-C(7)	110.5(4)
C(11)-C(12)-P(1)	114.5(3)
C(7)-C(12)-P(1)	113.7(3)
C(14)-C(13)-P(1)	109.6(3)
C(19)-C(14)-C(15)	124.2(5)
C(19)-C(14)-C(13)	116.3(4)
C(15)-C(14)-C(13)	119.4(4)
C(16)-C(15)-C(14)	120.4(5)
C(15)-C(16)-C(17)	119.0(4)
C(16)-C(17)-C(18)	120.8(5)
C(17)-C(18)-C(19)	120.1(4)
C(17)-C(18)-C(20)	120.2(4)
C(19)-C(18)-C(20)	119.8(4)
C(14)-C(19)-C(18)	115.4(4)
C(14)-C(19)-Ru	125.7(4)
C(18)-C(19)-Ru	118.9(3)
C(18)-C(20)-P(2)	109.8(3)
C(26)-C(21)-C(22)	110.5(4)
C(23)-C(22)-C(21)	111.6(4)
C(24)-C(23)-C(22)	110.8(4)
C(23)-C(24)-C(25)	111.6(4)
C(24)-C(25)-C(26)	110.5(4)
C(21)-C(26)-C(25)	109.9(4)
C(21)-C(26)-P(2)	116.5(3)
C(25)-C(26)-P(2)	113.7(3)
C(28)-C(27)-C(32)	112.4(4)
C(27)-C(28)-C(29)	111.2(4)
C(28)-C(29)-C(30)	110.8(4)
C(31)-C(30)-C(29)	111.6(4)
C(30)-C(31)-C(32)	110.9(4)
C(27)-C(32)-C(31)	111.4(4)
C(27)-C(32)-P(2)	112.6(3)
C(31)-C(32)-P(2)	112.4(3)
O(1)-C(33)-Ru	176.0(4)
O(2)-C(34)-Ru	178.1(18)
O(2')-C(34')-Ru	178(2)

Symmetry transformations used to generate equivalent atoms:

Appendix J. Crystallographic Information for $RuCl_2(dcpx)(CHCHC(Me_2))$ (28).

Table J.1. Crystal data and structure refinement for $RuCl_2(dcpx)(CHCHC(Me_2))$ (28).

Empirical formula	$C_{37}\ H_{60}\ Cl_2\ P_2\ Ru$
Formula weight	738.81
Temperature	203(2) K
Wavelength	0.71073 Å
Crystal system, space group	Triclinic, P-1
Unit cell dimensions	a = 9.6092(10) Å = 72.382(2)°
	b = 13.4522(14) Å β = 82.512(2)°
	c = 15.4284(16) Å γ = 73.621(2)°
Volume	1821.5(3) $Å^3$
Z, Calculated density	2, 1.345 mg/m^3
Absorption coefficient	0.689 mm^{-1}
F(000)	778
Crystal size	0.10 × 0.10 × 0.03 mm
Theta range for data collection	1.39 to 28.85°
Limiting indices	$-12 \le h \le 12, -16 \le k \le 17, 0 \le l \le 20$
Reflections collected / unique	14324 / 8271 [R(int) = 0.0347]
Completeness to θ = 28.85	86.7%
Absorption correction	Semi-empirical from equivalents
Max. and min. transmission	0.928077 and 0.623334
Refinement method	Full-matrix least-squares on F^2
Data / restraints / parameters	8271 / 0 / 386
Goodness-of-fit on F^2	1.058
R^a	0.0534
$R_w{}^b$	0.0872

$^aR = \sum||F_o| - |F_c||/\sum|F_o|$, $^bR_W = [\sum w\delta^2/\sum wF_o^2]^{1/2}$.

Table J.2. Bond lengths [Å] and angles [deg] for $RuCl_2$(dcpx)(CHCHC(Me_2)) (**28**).

Ru-C(1')	1.832(8)
Ru-C(1)	1.919(8)
Ru-Cl(2)	2.3845(12)
Ru-P(1)	2.4000(12)
Ru-P(2)	2.4040(11)
Ru-Cl(1)	2.4307(13)
P(1)-C(17)	1.851(4)
P(1)-C(11)	1.852(5)
P(1)-C(18)	1.855(4)
P(2)-C(31)	1.845(4)
P(2)-C(37)	1.848(4)
P(2)-C(25)	1.855(3)
C(1)-C(2)	1.407(11)
C(2)-C(3)	1.367(8)
C(1')-C(2')	1.442(11)
C(2')-C(3)	1.454(9)
C(3)-C(4)	1.467(7)
C(3)-C(5)	1.469(8)
C(6)-C(11)	1.424(7)
C(6)-C(7)	1.550(8)
C(7)-C(8)	1.467(9)
C(8)-C(9)	1.402(9)
C(9)-C(10)	1.474(8)
C(10)-C(11)	1.428(7)
C(12)-C(13)	1.516(6)
C(12)-C(17)	1.522(5)
C(13)-C(14)	1.508(7)
C(14)-C(15)	1.518(7)
C(15)-C(16)	1.519(7)
C(16)-C(17)	1.521(6)
C(18)-C(19)	1.512(6)
C(19)-C(20)	1.376(7)
C(19)-C(24)	1.383(6)
C(20)-C(21)	1.373(7)
C(21)-C(22)	1.378(6)
C(22)-C(23)	1.383(5)
C(23)-C(24)	1.397(5)
C(23)-C(25)	1.495(5)
C(26)-C(31)	1.498(6)
C(26)-C(27)	1.533(6)
C(27)-C(28)	1.511(6)
C(28)-C(29)	1.487(7)
C(29)-C(30)	1.509(7)

C(30)-C(31)	1.526(5)
C(32)-C(37)	1.499(6)
C(32)-C(33)	1.528(6)
C(33)-C(34)	1.513(6)
C(34)-C(35)	1.494(7)
C(35)-C(36)	1.515(7)
C(36)-C(37)	1.528(5)

C(1')-Ru-C(1)	23.1(3)
C(1')-Ru-Cl(2)	103.8(3)
C(1)-Ru-Cl(2)	81.0(3)
C(1')-Ru-P(1)	97.1(3)
C(1)-Ru-P(1)	101.5(3)
Cl(2)-Ru-P(1)	89.99(4)
C(1')-Ru-P(2)	102.6(3)
C(1)-Ru-P(2)	98.5(3)
Cl(2)-Ru-P(2)	90.00(4)
P(1)-Ru-P(2)	159.80(3)
C(1')-Ru-Cl(1)	79.4(3)
C(1)-Ru-Cl(1)	102.2(3)
Cl(2)-Ru-Cl(1)	176.80(5)
P(1)-Ru-Cl(1)	89.68(5)
P(2)-Ru-Cl(1)	89.22(4)
C(17)-P(1)-C(11)	104.7(3)
C(17)-P(1)-C(18)	104.6(2)
C(11)-P(1)-C(18)	105.5(2)
C(17)-P(1)-Ru	115.40(14)
C(11)-P(1)-Ru	122.5(3)
C(18)-P(1)-Ru	102.43(15)
C(31)-P(2)-C(37)	111.6(2)
C(31)-P(2)-C(25)	104.27(18)
C(37)-P(2)-C(25)	102.49(17)
C(31)-P(2)-Ru	115.30(14)
C(37)-P(2)-Ru	117.72(15)
C(25)-P(2)-Ru	103.15(14)
C(2)-C(1)-Ru	129.4(6)
C(3)-C(2)-C(1)	120.3(7)
C(2')-C(1')-Ru	129.4(7)
C(1')-C(2')-C(3)	117.8(7)
C(2)-C(3)-C(2')	43.8(5)
C(2)-C(3)-C(4)	144.3(6)
C(2')-C(3)-C(4)	100.7(5)
C(2)-C(3)-C(5)	100.4(6)
C(2')-C(3)-C(5)	144.1(6)
C(4)-C(3)-C(5)	115.2(5)

C(11)-C(6)-C(7)	115.3(5)
C(8)-C(7)-C(6)	114.7(6)
C(9)-C(8)-C(7)	118.9(6)
C(8)-C(9)-C(10)	116.0(6)
C(11)-C(10)-C(9)	118.6(6)
C(6)-C(11)-C(10)	120.5(5)
C(6)-C(11)-P(1)	114.7(4)
C(10)-C(11)-P(1)	119.0(4)
C(13)-C(12)-C(17)	110.9(4)
C(14)-C(13)-C(12)	112.8(4)
C(13)-C(14)-C(15)	110.7(4)
C(14)-C(15)-C(16)	112.2(4)
C(15)-C(16)-C(17)	111.5(4)
C(16)-C(17)-C(12)	110.7(4)
C(16)-C(17)-P(1)	117.4(3)
C(12)-C(17)-P(1)	111.2(3)
C(19)-C(18)-P(1)	105.1(3)
C(20)-C(19)-C(24)	118.4(4)
C(20)-C(19)-C(18)	123.5(5)
C(24)-C(19)-C(18)	117.8(4)
C(21)-C(20)-C(19)	120.1(5)
C(20)-C(21)-C(22)	121.2(5)
C(21)-C(22)-C(23)	120.1(4)
C(22)-C(23)-C(24)	117.6(4)
C(22)-C(23)-C(25)	124.2(4)
C(24)-C(23)-C(25)	117.7(4)

Symmetry transformations used to generate equivalent atoms:

Appendix K. Crystallographic Information for RuH(dcpx)(PPh_3)(N_2) (26b).

Table K.1. Crystal data and structure refinement for RuH(dcpx)(PPh_3)(N_2) (**26b**).

Empirical formula	$C_{54}\ H_{77}\ N_2\ O\ P_3\ Ru$
Formula weight	964.16
Temperature	293(2) K
Wavelength	0.71073 Å
Crystal system, space group	Triclinic, P-1
Unit cell dimensions	a = 11.3988(10) Å α = 91.4430(10)°
	b = 11.4641(10) Å β = 92.0320(10)°
	c = 19.3073(16) Å γ = 99.1330(10)°
Volume	2488.3(4) $Å^3$
Z, Calculated density	2, 1.287 mg/m^3
Absorption coefficient	0.451 mm^{-1}
F(000)	1024
Crystal size	0. 10 × 0.10 × 0.05 mm
Theta range for data collection	1.06 to 26.37 °
Limiting indices	-14<=h<=14, -14<=k<=14, 0<=l<=24
Reflections collected / unique	22227 / 10024 [R(int) = 0.0657]
Completeness to θ = 26.37	98.3 %
Absorption correction	Semi-empirical from equivalents
Max. and min. transmission	0.928075 and 0.779621
Refinement method	Full-matrix least-squares on F^2
Data / restraints / parameters	10024 / 0 / 553
Goodness-of-fit on F^2	1.024
R^a	0.0565
$R_w{}^b$	0.0976

$^aR = \Sigma||F_o| - |F_c||/\Sigma|F_o|$. $^bR_w = [\Sigma w\delta^2/\Sigma wF_o{}^2]^{1/2}$.

Table K.2. Bond lengths [Å] and angles [deg] for RuH(dcpx)(PPh_3)(N_2) (**26b**).

Ru-N(1)	2.014(4)
Ru-C(19)	2.129(5)
Ru-P(1)	2.3433(12)
Ru-P(2)	2.3578(12)
Ru-P(3)	2.3655(12)
Ru-H(1)	1.60(4)
N(1)-N(2)	1.111(6)
P(1)-C(13)	1.833(5)
P(1)-C(6)	1.866(4)
P(1)-C(12)	1.869(4)
P(2)-C(20)	1.834(5)
P(2)-C(26)	1.863(5)
P(2)-C(32)	1.872(5)
P(3)-C(50)	1.844(5)
P(3)-C(44)	1.851(4)
P(3)-C(38)	1.860(5)
C(13)-C(14)	1.507(6)
C(14)-C(19)	1.400(6)
C(14)-C(15)	1.401(6)
C(15)-C(16)	1.377(7)
C(16)-C(17)	1.381(7)
C(17)-C(18)	1.388(6)
C(18)-C(19)	1.407(6)
C(18)-C(20)	1.508(6)

N(1)-Ru-C(19)	94.69(17)
N(1)-Ru-P(1)	95.41(12)
N(1)-Ru-H(1)	173(1)
P(1)-Ru-H(1)	81(2)
P(2)-Ru-H(1)	90(2)
P(3)-Ru-H(1)	91(1)
C(19)-Ru-H(1)	78(1)
C(19)-Ru-P(1)	77.61(12)
N(1)-Ru-P(2)	90.66(12)
C(19)-Ru-P(2)	77.68(12)
P(1)-Ru-P(2)	154.95(5)
N(1)-Ru-P(3)	96.35(12)
C(19)-Ru-P(3)	168.96(12)
P(1)-Ru-P(3)	101.15(4)
P(2)-Ru-P(3)	102.30(4)
N(2)-N(1)-Ru	178.3(4)
C(13)-P(1)-C(6)	103.4(2)

C(13)-P(1)-C(12)	101.0(2)
C(6)-P(1)-C(12)	101.6(2)
C(13)-P(1)-Ru	101.97(15)
C(6)-P(1)-Ru	124.77(14)
C(12)-P(1)-Ru	120.36(15)
C(20)-P(2)-C(26)	103.0(2)
C(20)-P(2)-C(32)	101.1(2)
C(26)-P(2)-C(32)	102.5(2)
C(20)-P(2)-Ru	101.42(16)
C(26)-P(2)-Ru	118.30(15)
C(32)-P(2)-Ru	126.74(17)
C(50)-P(3)-C(44)	101.2(2)
C(50)-P(3)-C(38)	100.3(2)
C(44)-P(3)-C(38)	96.9(2)
C(50)-P(3)-Ru	116.54(14)
C(44)-P(3)-Ru	119.25(15)
C(38)-P(3)-Ru	118.96(15)

Symmetry transformations used to generate equivalent atoms:

Appendix L. Crystallographic Information for RuH(dcpx)(PPh_3)(H_2) (27b).

Table L.1. Crystal data and structure refinement for RuH(dcpx)(PPh_3)(H_2) (**27b**).

Empirical formula	$C_{56}H_{74}P_3Ru$
Formula weight	941.13
Temperature	203(2) K
Wavelength	0.71073 Å
Crystal system, space group	Monoclinic, P2(1)/c
Unit cell dimensions	a = 18.886(3) Å $\alpha = 90^\circ$
	b = 14.2595(19) Å $\beta = 107.256(2)^\circ$
	c = 19.073(3) Å $\gamma = 90^\circ$
Volume	4905.4(11) $Å^3$
Z, Calculated density	4, 1.274 mg/m^3
Absorption coefficient	0.453 mm^{-1}
F(000)	1996
Crystal size	0.10 x 0.10 x 0.10
Theta range for data collection	1.13 to 28.71 °
Limiting indices	-25<=h<=24, 0<=k<=19, 0<=l<=25
Reflections collected / unique	43750 / 11732 [R(int) = 0.0480]
Completeness to $\theta = 28.71$	92.5 %
Absorption correction	Semi-empirical from equivalents
Max. and min. transmission	1.000000 and 0.925298
Refinement method	Full-matrix least-squares on F^2
Data / restraints / parameters	11732 / 36 / 527
Goodness-of-fit on F^2	1.028
R^a	0.0580
R_w^b	0.0965

$^aR = \Sigma||F_o| - |F_c||/\Sigma|F_o|$. $^bR_w = [\Sigma w\delta^2/\Sigma wF_o^2]^{1/2}$.

Table L.2. Bond lengths [Å] and angles [deg] for RuH(dcpx)(PPh_3)(H_2) (**27b**).

Ru-C(19)	2.133(4)
Ru-P(2)	2.3148(10)
Ru-P(1)	2.3434(11)
Ru-P(3)	2.3617(10)
P(1)-C(13)	1.834(5)
P(1)-C(6)	1.856(6)
P(1)-C(12)	1.869(5)
P(2)-C(20)	1.845(4)
P(2)-C(26)	1.864(4)
P(2)-C(32)	1.865(4)
P(3)-C(38)	1.848(4)
P(3)-C(50)	1.854(4)
P(3)-C(44)	1.857(4)
C(1)-C(6)	1.419(9)
C(1)-C(2)	1.545(11)
C(2)-C(3)	1.522(11)
C(3)-C(4)	1.515(11)
C(4)-C(5)	1.531(11)
C(5)-C(6)	1.498(10)
C(1')-C(2')	1.535(11)
C(2')-C(3')	1.525(12)
C(3')-C(4')	1.502(12)
C(4')-C(5')	1.523(11)
C(7)-C(12)	1.492(8)
C(7)-C(8)	1.573(9)
C(8)-C(9)	1.476(10)
C(9)-C(10)	1.477(9)
C(10)-C(11)	1.542(8)
C(11)-C(12)	1.567(8)
C(13)-C(14)	1.515(6)
C(14)-C(15)	1.387(6)
C(14)-C(19)	1.404(5)
C(15)-C(16)	1.387(6)
C(16)-C(17)	1.378(6)
C(17)-C(18)	1.400(5)
C(18)-C(19)	1.414(5)
C(18)-C(20)	1.506(6)
C(19)-Ru-P(2)	79.31(11)
C(19)-Ru-P(1)	79.12(11)
P(2)-Ru-P(1)	158.36(4)
C(19)-Ru-P(3)	170.88(10)

P(2)-Ru-P(3)	103.02(4)
P(1)-Ru-P(3)	98.06(4)
C(13)-P(1)-C(6)	101.2(2)
C(13)-P(1)-C(12)	105.7(3)
C(6)-P(1)-C(12)	104.0(2)
C(13)-P(1)-Ru	102.41(15)
C(6)-P(1)-Ru	125.79(18)
C(12)-P(1)-Ru	115.28(18)
C(20)-P(2)-C(26)	102.25(18)
C(20)-P(2)-C(32)	101.03(19)
C(26)-P(2)-C(32)	102.89(18)
C(20)-P(2)-Ru	103.94(13)
C(26)-P(2)-Ru	123.32(13)
C(32)-P(2)-Ru	119.81(12)
C(38)-P(3)-C(50)	100.32(19)
C(38)-P(3)-C(44)	104.59(19)
C(50)-P(3)-C(44)	94.33(17)
C(38)-P(3)-Ru	112.67(14)
C(50)-P(3)-Ru	122.32(12)
C(44)-P(3)-Ru	119.29(13)
C(14)-C(13)-P(1)	108.2(3)
C(15)-C(14)-C(19)	122.7(4)
C(15)-C(14)-C(13)	120.0(4)
C(19)-C(14)-C(13)	117.2(4)
C(16)-C(15)-C(14)	120.4(4)
C(17)-C(16)-C(15)	119.1(4)
C(16)-C(17)-C(18)	120.4(4)
C(17)-C(18)-C(19)	122.0(4)
C(17)-C(18)-C(20)	120.1(4)
C(19)-C(18)-C(20)	117.8(3)
C(14)-C(19)-C(18)	115.4(3)
C(14)-C(19)-Ru	122.3(3)
C(18)-C(19)-Ru	122.2(3)

Symmetry transformations used to generate equivalent atoms: